CSDL-R-1835

A HIGHLY ADAPTABLE STEERING/SELECTION
PROCEDURE FOR COMBINED CMG/RCS
SPACECRAFT CONTROL

DETAILED REPORT

by

J. Paradiso

March 1986

The Charles Stark Draper Laboratory, Inc.
Cambridge, Massachusetts 02139

CSDL-R-1835

A Highly Adaptable Steering/Selection Procedure
for Combined CMG/RCS Spacecraft Control

Detailed Report

by

Joseph A. Paradiso
March 1986

ABSTRACT

A linear optimal CMG steering law has been developed which
exhibits very high adaptability to hardware failures, variations in CMG
system definition, and changes in vehicle mass properties. The package
is also capable of performing fuel-optimal jet selections and
establishing control via a hybrid mixture of jets and CMGs. The
instantaneous output torque of each CMG gimbal is used to form a set of
activity vectors that are selected to answer input rate-change requests
via linear programming techniques. Each selection is performed to
optimize an objective function which encourages avoidance of gimbal
stops, minimization of inner gimbal excursions, and prevention of CMG
alignment in singular orientations. The linear selections are repeated
during CMG rotation to account for changes in CMG torques and objective
values. The solution incorporates upper bounds specifying the maximum
allowed CMG gimbal displacement; these limit CMG response to input
requests and provide a means of intrinsically incorporating gimbal stops
into the CMG selection process.

Activity vectors for jets are formed from their thrusts and
positions relative to the vehicle center of mass. Their objective values
are set to penalize fuel consumption and price jets out of solutions
unless they are needed due to limited CMG control authority or CMG
saturation.

This report describes the principles and operational detail behind
the hybrid steering/selection process. Performance is demonstrated by
driving a model of the Power Tower Space Station with simulated arrays of
both double and single gimballed CMGs.

TABLE OF CONTENTS

TABLE OF CONTENTS (CONT.)

CHAPTER 1

INTRODUCTION

Attitude control and momentum management of the space station will be realized primarily by two types of actuators. Control Moment Gyros (CMGs) will provide limited onboard storage of angular momentum. Since they require only electrical power, CMGs have the ability to torque a vehicle without expending consumables. Reaction Control System (RCS) jets are capable of delivering much larger torques (and also provide translational control) at the expense of fuel consumption.

The space station environment will be very dynamic; its characteristics will evolve drastically during buildup, and significant changes in mass properties and actuator response can be expected during routine operations. Control, steering, and actuator selection procedures must be able to provide an adaptive and flexible response in order to function effectively under such conditions. Existing strategies used to select and steer such actuators suffer from a variety of drawbacks which could prove significantly disadvantageous for space station application.

Present CMG steering laws are considerably calculation-intensive, and any attempts at simplification generally result in tight restrictions being placed upon the CMG system configuration and behavior. This reduces available degrees of freedom and greatly lowers the ability of the selection procedure to deal with device failures and changes in the CMG system definition.

CMG gimbal rates are generally calculated via a pseudo-inverse method, which requires an additional "Null Motion" procedure to compute gimbal commands that prevent the CMGs from being driven into stable singular states. Pseudo-inverse formulations are not conducive to changes in the number of available actuators; when adding or deleting

1

CMGs, the size of the pseudo-inverse and the dimension of related calculations and quantities must be correspondingly altered.

Peak limits on CMG output torque and stop constraints on gimbal excursion are not considered in most CMG steering procedures and must be enforced after the CMG selection has been performed.

Current spacecraft systems possessing both types of actuators employ independent jet selection and CMG steering procedures which do not allow for the possibility of coordinated CMG/RCS control. The space station environment, however, encourages a control scheme which addresses the possibility of mixed CMG/RCS response, particulatly in the cases of re-boost, desaturation, docking, or other maneuvers in which the CMGs are saturated or do not possess sufficent control authority to satisfy input requests without assistance from other actuators.

The effort discussed in this report has addressed the problems posed above and has resulted in the development of an efficent and extremely flexible CMG steering procedure which is also capable of performing optimal jet selections and establishing control via a hybrid mixture of jets and CMGs.
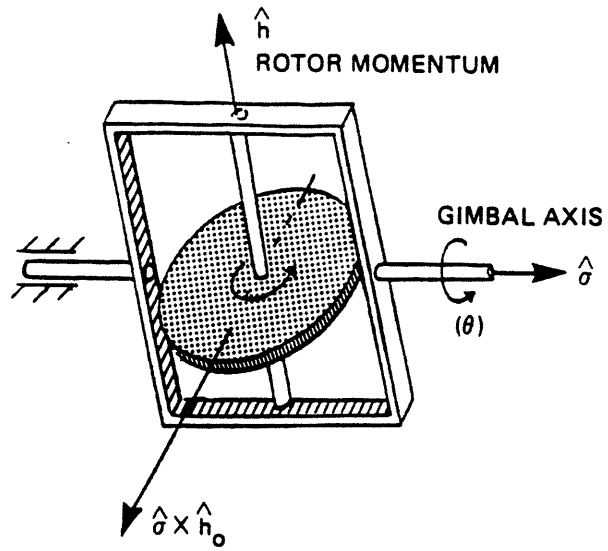
(a) SINGLE-GIMBALLED CMG
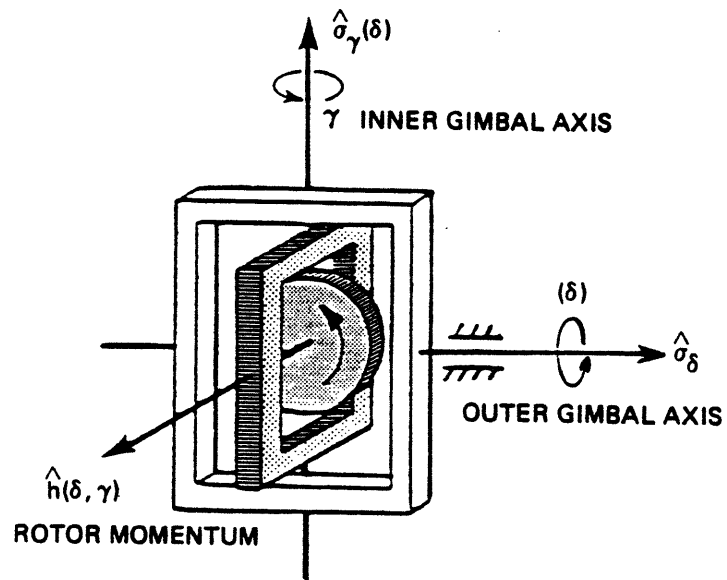
(b) DOUBLE-GIMBALLED CMG

FIGURE 1: SINGLE AND DOUBLE GIMBALLED CMGs

3

CHAPTER 2

FORMALISM

2.1)   CMG Fundamentals

Fig. 1 presents sketches of the basic CMG mechanical
configurations. A single gimballed device is drawn in Fig. 1a. This is
the simplest type of CMG, and the easiest to conceptualize. It consists
of a flywheel spinning at constant rate around an axis which can be
rotated about a gimbal mount. The CMG is a momentum exchange device
which achieves an output torque by altering the direction of the flywheel
angular momentum vector relative to inertial space. The flywheel rate
(ie. magnitude of angular momentum stored in the rotor) is held constant
in conventional CMG systems, which enables the design of rotor mechanics
to be optimized to minimize frictional losses, etc. Reaction wheels, in
contrast, are momentum exchange devices which keep the orientation of the
rotor fixed and transfer momentum by adjusting the flywheel rate. The
response time and bandwidth are typically much lower for a reaction wheel
system than for a group of CMGs. This is particularly relevant near
saturation, where the reaction wheel rotor drives become highly
nonlinear.

The output torque of a single gimballed CMG is always applied at
right angles to the gimbal axis. Since the gimbal is mounted rigidly to
the spacecraft structure, this configuration is capable of carrying high
torque levels. Single gimballed CMGs thus provide what is termed "torque
amplification", where the small input torque required to move the
flywheel about the gimbal results in a much larger resultant torque on
the vehicle as the rotor angular momentum vector changes its

orientation. These devices generally operate with large gimbal rates (units exist with peak gimbal rates in excess of 1 rad/sec) in order to exploit the amplification principle and couple large torques into the spacecraft. Single gimballed CMGs are thus often used in applications requiring rapid slewing or high bandwidth response. They are also applied in cases where their mechanical simplicity and low mass are advantageous.

Since single gimballed CMGs offer only one degree of freedom per device, at least three units are required for three axis control. Double gimballed CMGs (Fig. 1b) offer two degrees of freedom per device and allow the flywheel (in the absence of gimbal stops) to be oriented freely in 3-dimensional space. At least two units are needed for three axis control. The output torque created when gimbaling the flywheel must be supported by the gimbal drive system (there is no "hard mount" to the spacecraft as with single gimbal CMGs), thus the torque amplification advantage is limited in such devices. The excess degrees of freedom in double gimballed CMG systems generally aid in simplifying the associated control and steering procedures, and can increase tolerance to hardware failures. They tend to be somewhat heavier and considerably more mechan-ically complex than their single gimballed cousins, but are generally preferred in momentum management applications for large spacecraft (as in Skylab[1] and the proposed space station[2]). Double gimballed CMGs are commonly designed to have fairly large angular momentum storage in the flywheel (currently up to 4000 ft-lb-sec) and modest peak gimbal rates (ie. approximately 5 deg/sec per gimbal).

RCS jets are capable of delivering high torques and performing translational control (the only means of attaining the latter operation with a CMG is to throw it off the spacecraft, which is obviously an option not supported by most control packages). CMGS do not rely upon consumables for their operation; this is a major advantage of employing momentum exchange devices over RCS jets for attitude control. Jets expend fuel which must be periodically re-supplied, whereas CMGs require only electrical power, which is readily available from solar arrays.

The mechanics of RCS jets impose minimum limits on burn times, which degrade the accuracy of vehicle response to small rate change requests. Quantization and higher-order effects in CMG behavior become significant at a level several orders of magnitude lower (where phenomena such as gimbal stiction and hysteresis become important), thus CMGs provide a much wider dynamic range and are capable of attaining the small momentum transfers needed to "fine point" a spacecraft.

2.2) CMG Kinematics

The total momentum of a CMG system is the vector sum of the individual rotor momenta:

$\underline{h}_i$ = Angular momentum stored in CMG rotor #1 (assumed constant in magnitude)

1) $\underline{h}_{tot} = \sum\limits_{CMGs} \underline{h}_i$

$\underline{h}_{tot}$ = Total momentum stored in CMG system

The total momentum of the spacecraft/CMG system is constant in the absence of disturbance torques; any change in the momentum state of the CMG system is transferred to the spacecraft:

2) $\underline{H}_s + \underline{h}_{tot} = $ constant

3) $\dfrac{\partial \underline{H}_s}{\partial t} + \underline{\omega}_s \times \underline{H}_s = - \dfrac{\partial \underline{h}_{tot}}{\partial t} \equiv \underline{\tau}_{CMGs} = - \underline{\omega}_s \times \underline{h}_{tot} - \sum\limits_{CMGs} (\underline{\sigma}_i \times \underline{h}_i)$

$\underline{H}_s$ = Angular momentum of spacecraft

$\underline{\omega}_s$ = Spacecraft angular rate

$\underline{\sigma}_i$ = "Gimbal" axis of CMG #i (magnitude is gimbal rate). For single gimballed CMGs, $\underline{\sigma}$ is the actual gimbal axis and rate, however for dual gimballed devices, the $\underline{\sigma}$ defined above is a composite quantity representing the instantaneous rotation of the rotor angular momentum vector.

$\underline{\tau}_{CMGs}$ = Net CMG torque on spacecraft

$\underline{\tau}_{CMGs}$, as defined above, is the torque exerted on the space-craft by the CMG system. It is derived by taking the time derivative of Eq. 1 with respect to spacecraft-fixed coordinates. The "$\underline{\omega}_s \times \underline{H}_s$" term on the leftmost side of Eq. 3 is due to Euler coupling of spacecraft axes and does not arise from the presence or action of CMGs, thus is ignored in this analysis. Both terms in the rightmost side of Eq. 3 are caused by changes in the stored CMG momentum ($\underline{h}_{tot}$). The first term is due to changes in the orientation of the CMG rotors relative to inertial space caused by the spacecraft angular rate. This will always contribute unless the spacecraft is holding inertial attitude or the component of CMG stored momentum orthogonal to the spacecraft rotation axis is zero. Since this contribution depends on the spacecraft rotation rate (which is a commanded state), it can not be turned on and off at will, hence is not considered as an adjustable parameter in the CMG steering law and must be accounted for as a disturbance torque or exploited in higher-level momentum management schemes. The effect of this term can be directly compensated by adjusting the torque command input to the steering law, ie:

4) $\quad \underline{\tau}_{input} = \underline{\tau}_{command} + \underline{\omega}_s \times \underline{h}_{tot}$

Thus, in absence of any commanded torque $\underline{\tau}_{command}$, the steering law always drives the CMG system such that the total stored CMG momentum ($\underline{h}_{tot}$) points in a constant inertial direction.

The second term in Eq. 3 is due to internal rearrangement of the CMG rotors ($\underline{h}_i$) by gimbal rotation, which can cause changes in the

8

magnitude and direction of $\underline{h}_{tot}$. Its value can be controlled by adjusting the CMG gimbal rates, hence this term is used to establish a control torque $\underline{\tau}_{ctl}$:

$$5) \quad \underline{\tau}_{ctl} = - \sum_{CMGs} (\underline{\sigma}_i \times \underline{h}_i)$$
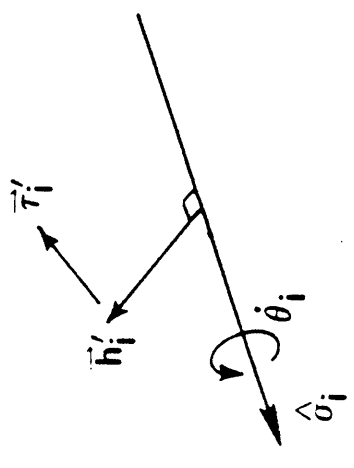
The purpose of the generic CMG "steering law" is to command a set of gimbal rates $\underline{\sigma}_i$ such that $\underline{\tau}_{ctl}$ above is equal to $\underline{\tau}_{input}$ as expressed in Eq. 4. Attitude control systems using CMGs are generally structured to be underdetermined, and include more available degrees of freedom (ie. more effective $\underline{\sigma}_i$) then the minimum required for control purposes. The redundancy in the system creates several sets of $\underline{\sigma}_i$ which may be commanded to attain $\underline{\tau}_{ctl} = \underline{\tau}_{input}$. "Optimal" CMG steering laws select a set of gimbal rates which attain the above equality constraint while exploiting the excess degrees of freedom available to the system in order to avoid moving the CMG rotors into undesirable configurations. The "optimality" of a CMG state is generally reflected in the value of an objective function such as described in detail in Chapter 3 of this report.

The CMG torque defined in Eq. 3 results from the kinematics of ideal devices, and does not contain contributions due to effects such as gimbal acceleration torques, stiction and hysteresis, servo behavior, etc., which exist with actual CMGs (see Refs. 3,4,5). These effects are of higher order and become significant in demanding applications such as fine pointing[5]. CMG steering laws generally do not account for these terms (the identity in Eq. 3 is assumed for CMG selection), but they may be incorporated by methods such as post-processing gimbal rates output from the steering law, adjusting input requests, or commanding vernier actuators (such as the small reaction wheels originally planned for the Large Space Telescope[5]) for compensation.

- LINEAR CMG SELECTION (BASIS OF MOST CMG STEERING LAWS) USES INSTANTANEOUS APPROXIMATIONS TO CMG OUTPUT TORQUES, $\quad \vec{\tau}_i = -(\hat{\sigma}_i \times \vec{h}_i)\dot{\theta}_i$
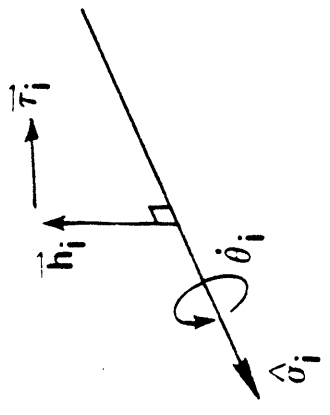
→ AS CMG ROTORS MOVE, OUTPUT TORQUE $\vec{\tau}_i$ CHANGES DIRECTION:

∴ CMG SELECTION MUST BE RECOMPUTED OFTEN AS CMGs MOVE

FIGURE 2: CMG SELECTION AND NONLINEAR EFFECTS

2.3) CMG Selection and Steering

As defined earlier, the purpose of a CMG steering law is to move the CMGs in response to an input torque or momentum transfer request, usually managing system redundancy with regard to an optimization function. Gimbal rates are assigned via the control torque expressed in Eq. 5. This is an instantaneous expression; as the CMGs move, the rotor vectors $\underline{h}_i$ (and inner gimbal axes of dual gimballed CMGs) change orientation, affecting the value of $\underline{\tau}_{ctl}$ (this is diagrammed in Fig 2; the effect is termed "cross coupling"). The $\underline{\sigma}_i$ assigned by the steering law to an input torque profile or vehicle rate-change request are thus certainly not constants, but must vary in order to continue to provide the requested output as the CMGs rotate and the system configuration mutates. The gimbal rates $\underline{\sigma}_i$ are in this case not simple step functions or constants (as with jet firing times), but can possess more complex time dependence.

The application of optimal control to a "classical" CMG steering law may be defined as determining the set of gimbal rate functions $\{\underline{\sigma}_i(t)\}$ which satisfy an input momentum transfer request while optimizing an objective function which depends upon both the absolute CMG gimbal angles and the relative angles between CMG rotors (see Ch. 3). The exact torque and momentum equations for a standard CMG as a function of gimbal angles and rates are summarized in Section 2.5 (Eqs. 15-22). These equations represent the rotation of a unit vector about a circle (single gimbal) or sphere (double gimbal), thus the gimbal angles appear in trigonometric form. The relations for standard Euler mounted double gimballed CMGs (Eqs. 18,21) involve products of sines and cosines of both gimbal angles (since the inner gimbal is rotated within the outer gimbal). The complexity of these relations makes the direct solution of such a system for a final CMG state (eg. set of end-state gimbal angles) or a set of gimbal rate functions $\{\underline{\sigma}_i(t)\}$ highly difficult, especially when incorporating an objective function or constraints such as gimbal stops. Related efforts[6] have suggested that this method of
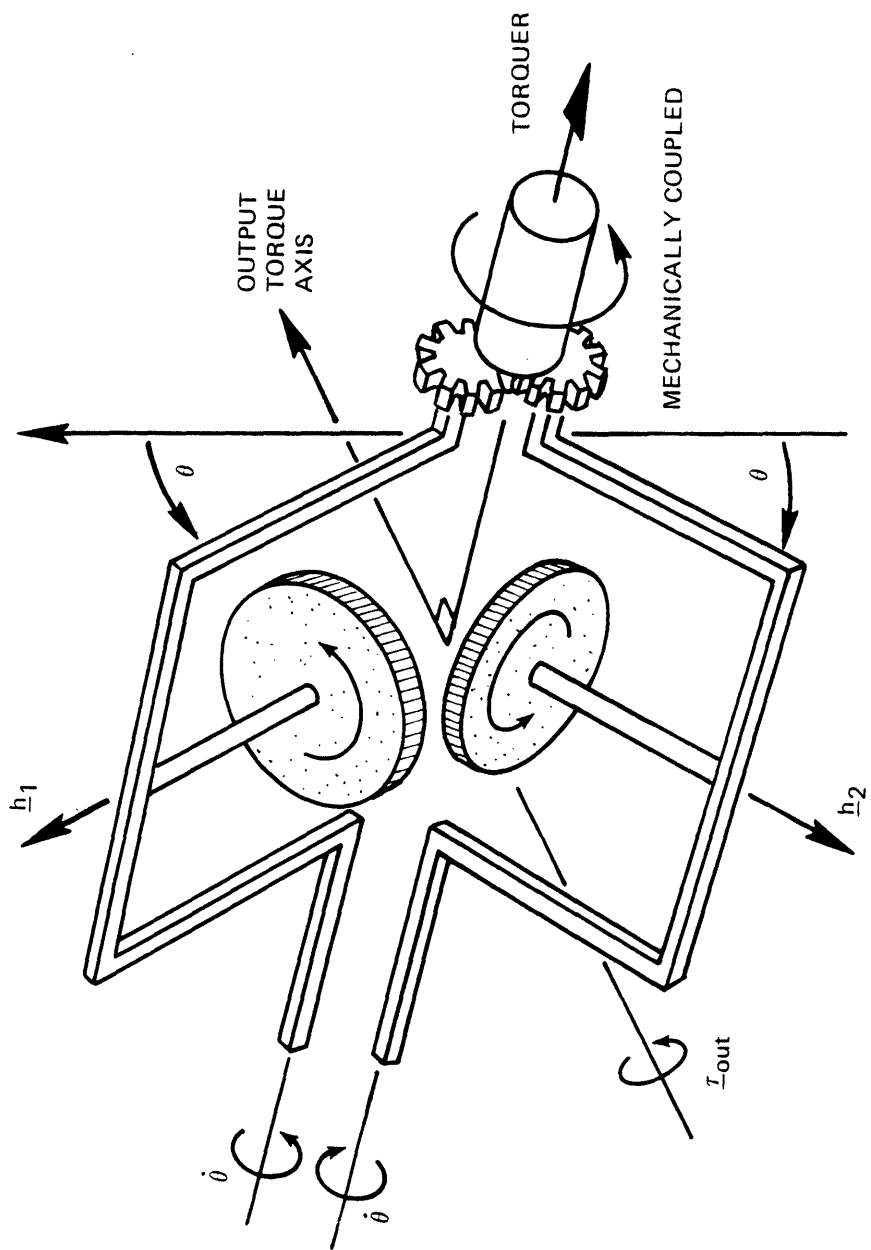
11

FIGURE 3: TWO SINGLE GIMBALLED CMGs CONFIGURED AS A SCISSORED PAIR

12

global optimal steering is not practical within the scope of available flight computation facilities. Other attempts[7] to apply techniques of optimal control to linearized CMG behavior have not realized feasible steering laws.

Another method, which groups the CMGs into "scissored pairs" (as depicted in Fig. 3), has been applied as a simple means of compensating for the cross coupling effect. In a scissored pair (also termed "V" configuration), two CMGs mounted with parallel gimbals and anti-aligned rotor axes are constrained to move with equal and opposite gimbal rates. This causes the CMG momentum component along the anti-aligned axes to cancel and results in a momentum storage and transfer only along the axis which bisects the angle between the CMG pair (see Fig. 3). The magnitude of the momentum transfer varies with the cosine of the half-angle between the CMGs, however it occurs about a single axis (ignoring contribution from the disturbance torque in Eq. 4, which depends on the axis of stored momentum relative to the spacecraft rate). Three single gimballed scissored pair units are required for complete 3-axis control; this creates a large amount of hardware overhead needed to be supported by the spacecraft (there are 2 rotors per scissored unit), and the scissoring constraint of 2 operational rotors per axis is not conducive to reconfiguration necessities due to hardware failures, etc.

Scissored pair configurations have found applications[8] in satellite attitude control systems. They were generally proposed where digital computation facilities were very restricted or specific attitude control requirements took advantage of their unique properties. Before highly capable onboard computers became available, "gyrostabilizer"[9] systems, employing both individual CMGs and scissored pairs with damped gimbals, had been considered for passive attitude stabilization of satellites. Three small single-gimballed scissored pairs (1 ft-lb-sec rotors) were incorporated into the Astronaut Maneuvering Unit[10] (predecessor to the MMU), which was sucessfully tested during Skylab missions.

The gimbal drive systems of scissored pairs may be mechanically or electrically coupled. Mechanically coupled double gimballed CMG pairs have been shown[11] to restore the effect of torque amplification, but can be difficult to construct. Analytical methods[12-14] have been developed to drive pairs and even triads of standard single-rotor CMGs in a "scissoring" fashion. The resulting steering laws can be extremely complex; the scissoring constraint makes this principle very rigid and generally does not manage the system resources in an efficent and fault-adaptable manner.

The methods used in most CMG steering laws (including the version discussed here) calculate a set of instantaneous gimbal rates which satisfy an input torque request via Eq. 4. As the CMGs rotate, the control torques are updated by re-evaluating Eq. 4, and a new selection is performed. In this fashion, the problem is reduced to a linear system at each iteration, and the CMG gimbal rates are adjusted in a stepwise fashion to approximate $\{\underline{\sigma}_i(t)\}$.

One of the simplest techniques used to obtain "instantaneous" gimbal rates via an approximation such as Eq. 5 is termed the "cross product" steering law.[14,15] This procedure drives each CMG independently with a gimbal rate proportional to the projection of its output torque onto $\underline{\tau}_{input}$ (Eq. 4). Since each CMG is considered independently, this strategy produces an output torque which only approximates $\underline{\tau}_{input}$, thus the steering law exhibits poor response and depends heavily upon a feedback loop closed through the vehicle dynamics. Cross product laws were developed in the period before advanced digitial flight computers were available, and their major advantage was ease in realization via analog circuitry.

From the early 1970's onward, the advance in spacecraft onboard computational power enabled more complex steering laws to be considered. Most procedures[12,16-19] in use today calculate gimbal rates via a pseudo-inverse (the pseudo-inverse is used to solve Eq. 7; see Sec. 2.4). This method takes no account of CMG "optimality" and gives the

"minimum norm" solution; ie. moves mainly those CMGs which project significantly onto the input request, and avoids using CMGs which have little authority (ie. approaching problematic and singular states). This requires additional gimbal rates to be calculated which exploit the system redundancy to distribute the CMGs into a more favorable orientation without changing the total stored angular momentum and torquing the spacecraft. These "Null Motion" rates can be derived from the null space[19] of the pseudo-inverse (projecting such null motion into a "direction" which avoids singular states can be an involved task) or via constraints imposed on system behavior[16]. Upper bounds are not considered in pseudoinverse calculations; peak limits on gimbal rate, gimbal excursion, etc. must be imposed after CMG selection. Computation of the pseudo-inverse (which must be perfomed during each selection cycle) is a non-trivial process; it requires several matrix operations, including an inversion. The size of the pseudoinverse is determined by the number of active actuators; changes due to hardware re-configuration often imply altering dimensions of vector/matrix quantities and related calculations.

One of the most straightforward strategies applied to solve an input request (re. Eq. 4) via a set of linear actuators is consulting a lookup table. This has been effectively applied in cases[20] involving static actuators such as RCS jets. CMG output torques, however, are always changing with rotation. The linearized actuator configuration is thus very dynamic, which forces any lookup tables to be continually re-defined. Recent work[21] has successfully applied lookup tables to singularity avoidance in single gimballed CMG systems (where singu-larities can occur only at specific gimbal states), however these algorithms still require pseudo-inverse calculation of gimbal rates to answer input torque requests.

The particular steering law discussed in this report also uses the instantaneous torque defined in Eq. 5, but selects effective gimbal rates via linear programming, which offers several advantages over the

pseudo-inverse technique. Actuators are represented by "activity vectors" derived from the instantaneous CMG torques of Eq. 5. A list of activity vectors is scanned for actuator selection, the dimension of which defines only the extent of the search, thus is not a critical calculation parameter and is easily altered. Activity vectors can model a diverse group of linearized actuators (eg. CMG gimbals or RCS thrusters) and are easily included into or deleted from consideration in the search list. Changes in vehicle mass properties, peak gimbal rates, etc. are incorporated by modifying constants used in the calculation of activity vectors. The version of simplex adapted to solve this linear programming problem allows upper bounds to be imposed on the decision variables, thus enables limits (eg. on gimbal angle freedom) to be considered in the selection process. The desirability of using a particular actuator in the solution is represented by the value of a corresponding objective coefficent which is considered in the process of linear selection. Linear programming thus incorporates an instantaneous optimization into the selection process.

The iterative application of linearized selection procedures (such as linear programming or pseudo-inverse calculation) to the non-linear problem of CMG dynamics and optimization falls under the general heading of "linear optimal" control, which has also been attempted in other situations[22] where a global optimization was not feasible. Under the scheme discussed in this text, objective coefficents and activity vectors calculated at the current system position are consulted by the linear selection procedure. The coefficents bias the selection to include CMGs in such a fashion that they move away from singular and problem states as determined in the instantaneous system. After a modest time interval passes, the CMGs have moved by a small amount, and the system characteristics have changed. New CMG activity vectors are calculated, and the new system configuration is examined to formulate updated objective coefficents. The selection process is then re-invoked. This "step-wise" procedure is continued until the original request is satisfied.

Each selection is a linear optimization based on a segment of what may be a nonlinear set of objectives and constraints. The objective functions are chosen such that they anticipate problems before they occur; ie. the cost of choosing a set of CMG activities moving toward a singular orientation increases before they become critical, thus informing the selection process to steer them away before control is degraded. This step-wise selection encourages the CMGs to follow a trajectory which approximates an "optimal" path. Since the solution of the nonlinear problem to find $\{\sigma_i(t)\}$ can be highly impractical (as discussed earlier in this section), the linear optimal technique is a logical compromise for steering CMG systems.

2.4) Linear Programming

Linear Programming has been employed[23] in performing real-time optimal jet selections onboard the Shuttle orbiter. The flexibility implicit in linear programming techniques creates a selection process which is extremely adaptable to changes in jet properties and configuration. The resulting software has performed successfully during on-orbit flight testing[24], and the linear selection scheme was seen to run on the shuttle AP-101 flight computers without introducing significant delay.

The work discussed in this document originated from the earlier effort made to adapt linear programming into performing optimal jet selections. The concept of hybrid actuator (eg. CMG/RCS) selection and the promise of achieving a highly adaptive steering law inspired an investigation into a method of considering CMGs in the selection process. The remainder of this chapter describes the means by which this has been accomplished.

The standard linear programming problem is posed as a linear equality constraint paired with a linear objective function. The linear program works to find the solution to the equality constraint which minimizes (or maximizes) the objective. The problem may be stated quantatively:

6) Minimize: $Z = \sum\limits_{j=1}^{N} c_j X_j$

7) Subject to: $\sum\limits_{j=1}^{N} \underline{A}_j X_j = \underline{R}$

Eq. 7 represents the equality constraint and Eq. 6 an objective function to be minimized (linear programming can find either extreme, however the selection problem has been posed here as a minimization). The summations run over the full set of "N" actuators considered.

The $\underline{A}_j$ are "activity vectors" derived from the vehicle response to the j'th actuator. Under the current approach, the $\underline{A}_j$ are 6-dimensional vectors containing the rotational (first three elements) and translational (last three elements) accelerations produced by each actuator, ie:

8) $\underline{A}_{j(jet)} = \begin{bmatrix} [I]^{-1} \underline{r}_j \times \underline{T}_j \\ \hline \underline{T}_j / M \end{bmatrix}$ $\underline{A}_{j(CMG)} = \begin{bmatrix} [I]^{-1} \underline{\tau}_{CMG} \\ \hline \underline{0} \end{bmatrix}_j$

where $[I]$ = Spacecraft inertia tensor

$\underline{r}_j$ = Position of jet #j relative to the vehicle center of mass.

$\underline{T}_j$ = Thrust of jet #j

M = Vehicle mass

$\underline{\tau}_{CMG}$ = Output torque of CMG gimbal #j (ie. $\underline{\tau}_{CMG} = -\underline{\sigma}_j \times \underline{h}_j$)

$\underline{0}$ = 3-vector of zeroes

The vector $\underline{R}$ represents the input request, here formulated to be a rotational ($\underline{\Delta\omega}$; first three elements) and translational ($\underline{\Delta V}$; last three elements) rate change:

$$9) \quad \underline{R} = \left[\frac{\Delta \omega}{\Delta V} \right]$$

The scalars X_j in Eqs. 6 & 7 are the "decision variables" which are determined as the solution to the linear programming problem. As the problem is currently construed, the X_j represent effective "on-times" of their respective actuators. This is interpreted literally for the jets, however we define the "on-time" of a CMG to represent the angular displacement of the selected gimbal, from which a gimbal rate may be extracted (this is discussed in Sec. 2.5 in greater detail). Linear programming techniques intrinsically enforce a "feasibility" constraint, with all X_j required to be non-negative. This rule has been re-defined for use with CMGs, as will be detailed later in this section.

The linear program works to find the solution of Eq. 7 which minimizes the value of Z evaluated by the objective function (Eq. 6). The c_j in Eq. 6 are "objective coefficents" of their respective activity vectors. They represent the relative "penalties" of including activity vectors $\underline{A}_j$ in the final solution. "Expensive" activity vectors with large c_j are discouraged from being used (ie. assigned low or zero X_j), in favor of the "cheaper" alternatives.

Linear programming always results in an optimal solution which includes activity vectors that form a basis spanning the dimension of the equality constraint (Eq. 7). The revised simplex algorithm[26] (which is used to solve the jet selection of Ref. 25) starts with a sub-optimal basis and converges to the optimal solution via a series of activity vector exchanges, maintaining the rank of the basis after each exchange. The solution is always linearly independent; for the standard linear programming problem (Eqs. 6,7), it can be proven[26] that any solution which includes more activity vectors than required by the basis has at best the same cost as the optimal basic solution. Simplex thus results in solutions containing three (rotational control only) or six (rotation and translation) activity vectors in the final basis.

19

The situation changes somewhat when upper bounds are imposed on the decision variables, ie:

10) $X < u_j$

where "u_j" are the upper bound values associated with activity vectors $\underline{A}_j$. The traditional means of solving this problem is to reformulate the inequalities in Eq. 10 to become equality constraints by adding "slack" variables, ie:

11) $X_j + X_{N+j} = u_j$

By adding the "slack variable" X_{N+j} to the problem (and remembering the feasibility constraint forcing all X to be non-negative), the inequality of Eq. 10 has been converted into an additional equality constraint which can be included with those of Eq. 7. This increases the order of the problem appreciably; in addition to the three (or six) kinematic dimensions present in the original formulation, the rank of Eq. 7 is augmented by the slack variable of each activity vector with an upper bound.

Upper bounds are needed in order to realistically choose CMGs via the simplex process. Most CMGs possess gimbal stops, which may be incorporated into the CMG selection logic by imposing an upper bound on the angular displacements X_j. In addition, upper bounds on X_j express a limit to the allowed CMG control authority, which is useful when CMGs approach saturation and necessary in hybrid RCS/CMG maneuvers (as will be elaborated in Chapter 4).

When applying simplex to the original problem (Eq. 7) without accounting for upper bounds, the basic solution will contain no more than three activity vectors (rotation only is considered). Since activity vectors represent CMG gimbals, the basic solution to the original problem will be capable of only using three gimbals at a time; generally a small

20

fraction of the total system resources. For a large rate-change request, simplex will persist in using only three gimbals in the solution, but assigns them very large angular displacements X_j. This does not reflect realistic properties of a CMG system, where each gimbal (in conjunction with the others) can provide only limited momentum before the system reaches saturation. In contrast to RCS jets, CMGs are non-linear devices (as detailed in Section 2.3), and a linearized solution which moves several CMGs by a smaller amount is much more realistic than one which spins only a few gimbals over large angles. It is thus imperative that the linear selection process incorporate upper bounds in order to achieve relevant solutions.

Each CMG gimbal is represented by an activity vector. Individual gimbals may be rotated in two directions (ie. increasing or decreasing gimbal angle). By allowing X_j for CMGs to go negative (as discussed below), a single activity vector may represent gimbal rotations in both directions, however the consequences of gimbal rotation in either direction may be entirely different (rotation in one direction may encounter a stop or singularity, while the opposite sense of rotation avoids the problem). Each activity vector thus has two associated objective coefficents (one c_j^+ for positive gimbal rotation, the other c_j^- for negative gimbal rotation) in order to favor gimbal motion in a direction to avoid difficulty. There are also two upper bounds (u_j^+, u_j^-) associated with each activity vector, which dictate the maximum gimbal displacement (ie. maximum X_j) allowed in either direction $(u_j^+ \neq u_j^-$ in the event of gimbal stops). The existance of two upper bounds per activity vector implies the addition of two more slack constraints (as in Eq. 11) with each CMG gimbal included in the system. If the standard simplex method is used to solve the resulting system, the problem rapidly becomes unmanageable.

Fortunately, a much simpler means exists to account for maximum bounds in simplex calculations. The additional equality constraints (Eq. 11) and associated slack variables not only serve to exclude

solutions which exceed upper bounds, but also create additional solutions which possess a set of decision variables at their upper bounds along with a basis of the same dimension as the original problem. Simplex may then keep a much smaller basis sized to the original equality constraint (Eq. 7), and externally keep track of decision variables reaching or exceeding their maximum limits. This "Upper Bound Algorithm"[27] adds only a few additional tests and calculations to the simplex process; it is much simpler than solving the augmented system with the slack constraints of Eq. 11, yet still enables a realizable solution to the full CMG problem.

The logic flow for the upper bound selection process is diagrammed in Figs. 4 through 8. These schematics are fairly close to the computational detail; the following text outlines the procedure more descriptively.

Simplex is a process which successively improves a solution to the equality constraint by replacing activity vectors in the solution basis. It must be started with an initial basis which solves Eq. 7. This may be any mathematical solution (not necessarily feasible or optimal) using activity vectors which represent "real" actuators present on the spacecraft. Simplex will proceed to introduce other activity vectors until it achieves the "final" optimal, feasibile solution. This starting strategy was applied in Ref. 25, where an initial solution was "guessed" and assembled via a table of existing RCS jets. Very few simplex iterations were then usually required to achieve the optimal solutions. A variant of this method has been applied to form an initial basis of CMGs by assembling a "best guess" solution from the "cheapest" CMG activity vectors. Although the number of simplex exchanges required for optimization were successfully reduced, the software and CMG definitions were evolving rapidly after this routine was written, hence it was replaced with a much simpler start sequence which is less "knowledge based" and shifts more computational burden to the simplex process.
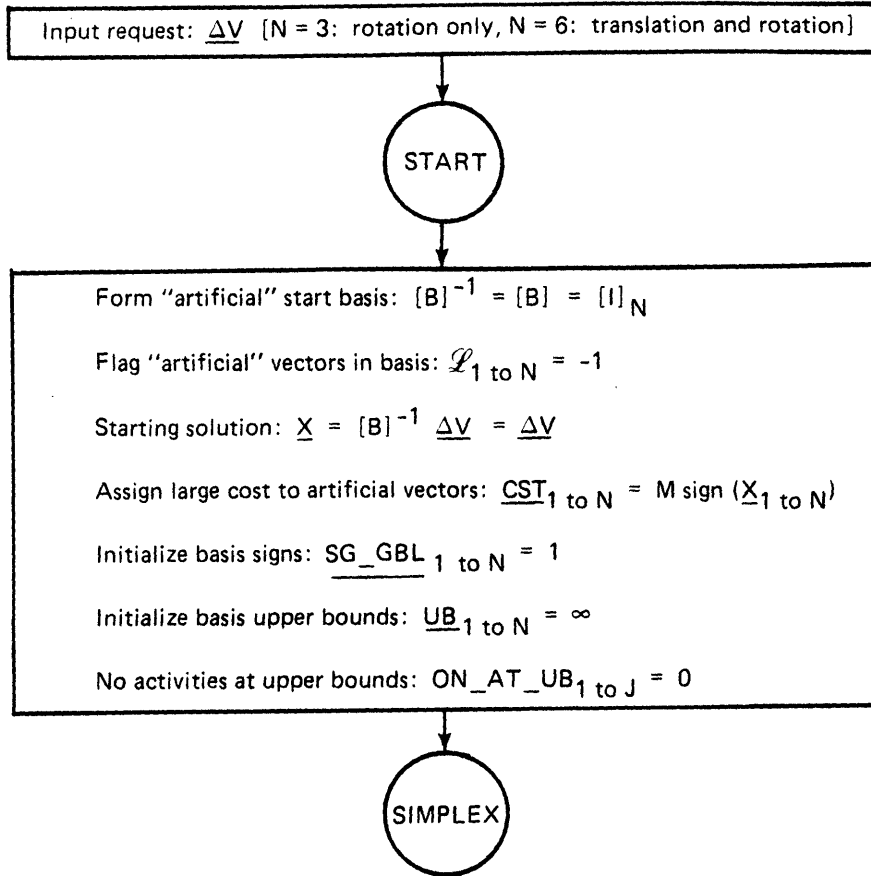
22

This procedure employs an "artificial" start basis, as proposed in Ref. 28. The details are diagrammed in Fig. 4. The equality constraint of Eq. 7 may be stated in terms of a basis "[B]" of activity vectors coupled with a vector $\underline{x}$ of corresponding decision variables:

12) $[B]\underline{x} = \underline{R}$

> Note: In the discussion below, the vector $\underline{x}$ contains decision values for basic variables only, while the array X contains "on-times" for all activity vectors (basic and non-basic).

The columns of the matrix [B] are composed of the $\underline{A}_I$ which are included in the initial basic solution. All other $\underline{A}_I$ are assumed to be non-basic at their lower bounds (which are zero through feasibility) and have $\underline{X}_I = 0$ (The A_I contained in the basis have X_I equal to their corresponding x_j). By constructing an initial [B] from "artificial" activity vectors (which make [B] an identity matrix, but do not represent physical actuators) and equating $\underline{x}$ with $\underline{R}$, a solution is created which can be used to start simplex. The "artificial" vectors are assigned very high costs, thus they are generally exchanged immediately for activity vectors representing real devices. If simplex converges to a solution which still contains artifical vectors, the constraints on the problem are determined to preclude an actual solution.

The upper-bound simplex process consists of three distinct sections; an "invite loop", which determines the most effective activity vector to consider for inclusion in the basis (or upper-bound substitution), an "exclude loop", which determines which element is best removed from the basis to allow the invited vector in, and a decison section which determines whether a simplex pivot, upper-bound substitution, or both are performed.

Input request: $\underline{\Delta V}$ [N = 3: rotation only, N = 6: translation and rotation]

START

Form "artificial" start basis: $[B]^{-1} = [B] = [I]_N$

Flag "artificial" vectors in basis: $\mathscr{L}_{1\ to\ N} = -1$

Starting solution: $\underline{X} = [B]^{-1}\ \underline{\Delta V} = \underline{\Delta V}$

Assign large cost to artificial vectors: $\underline{CST}_{1\ to\ N} = M\ \text{sign}\ (\underline{X}_{1\ to\ N})$

Initialize basis signs: $\underline{SG\_GBL}_{1\ to\ N} = 1$

Initialize basis upper bounds: $\underline{UB}_{1\ to\ N} = \infty$

No activities at upper bounds: $ON\_AT\_UB_{1\ to\ J} = 0$

SIMPLEX

Definitions: J = total number of activity vectors in system

[B] = solution basis (simplex requires only $[B]^{-1}$)

$\mathscr{L}$ = List of activity vectors in basis [i.e. $\mathscr{L}_L$ = j corresponds to a_j]

CST = objective values of vectors in basis

SG_GBL = sign of vectors in basis [decision variables X_j are kept positive)

UB = upper bounds on decision variables of cectors in basis

M = large number

∞ = larger number

Note: $\mathscr{L}$, CST, SG_GBL, and X are all parallel arrays.

FIGURE 4: UPPER BOUND SIMPLEX (INITIALIZATION)

The invite loop is diagrammed in Fig. 5. The vector "$\underline{U}$" is first formed by projecting the costs associated with the current basis vectors into the kinematic space spanned by the activity vectors:

13) $\underline{U} = \underline{CST} \; [B]^{-1}$

where $\underline{CST}$ = Row vector of costs associated with current
              basis elements.

        $[B]^{-1}$ = Inverse of current basis.

The quantity $\underline{U} \cdot \underline{A}_I$ ("F" in Fig. 5) represents the decrease in the cost of the current basis with respect to a unit increase in the decision variable X_I associated with the non-basic activity vector $\underline{A}_I$. By subtracting the objective value associated with $\underline{A}_I$, one forms a quantity which describes the decrease in the total objective function (Z; Eq. 6) with unit increase in X_I:

14) $CG = \dfrac{\Delta Z}{\Delta X_I} = \underline{U} \cdot \underline{A}_I - c_I$

The invite loop considers all non-basic activity vectors $\underline{A}_I$, and chooses the activity with the largest effect on objective minimization (ie. with the largest positive value of CG) for further consideration. If the CG values are non-positive for all $\underline{A}_I$, the objective value can not be further improved, and the current solution is optimal (this is the "normal exit" in Fig. 5).

The remainder of the logic in Fig. 5 is associated with upper bounds and the relaxation of the feasibility constraint ($x_j > 0$) for CMGs. As mentioned earlier, a CMG gimbal may be moved in two directions (increasing or decreasing gimbal angle). Reversing the rotation of a gimbal reverses the sign of its output torque, which effectively toggles the sign of its activity vector (Eq. 8). One may incorporate this by
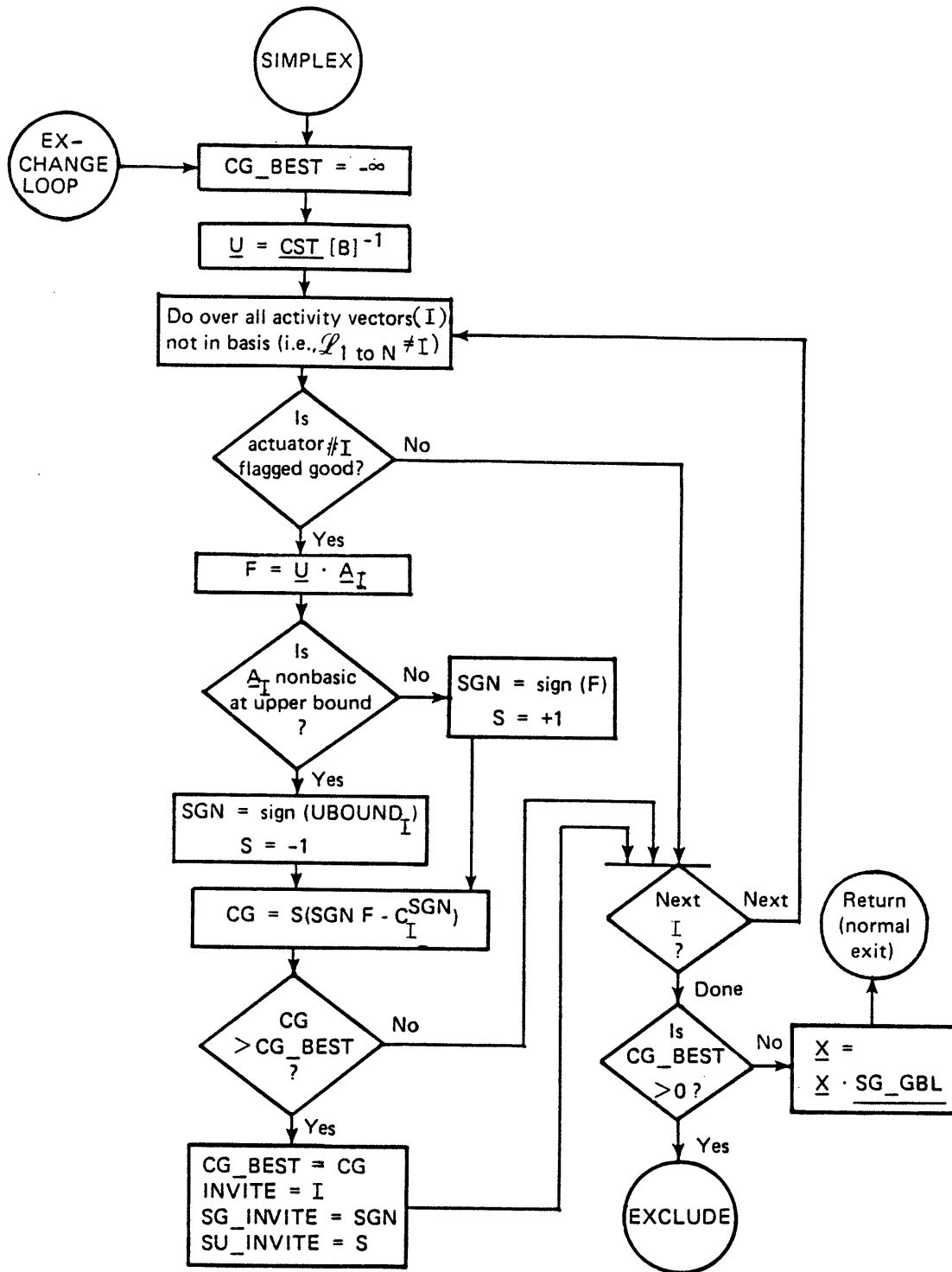
SIMPLEX

EX-CHANGE LOOP

$CG\_BEST = -\infty$

$\underline{U} = \underline{CST}\,[B]^{-1}$

Do over all activity vectors(I) not in basis (i.e., $\mathscr{L}_1$ to N $\neq I$)

Is actuator #I flagged good?

No

Yes

$F = \underline{U} \cdot \underline{A}_I$

Is $\underline{A}_I$ nonbasic at upper bound ?

No

$SGN = sign\,(F)$
$S = +1$

Yes

$SGN = sign\,(UBOUND_I)$
$S = -1$

$CG = S(SGN\;F - C_I^{SGN})$

CG $\geq$ CG_BEST ?

No

Yes

$CG\_BEST = CG$
$INVITE = I$
$SG\_INVITE = SGN$
$SU\_INVITE = S$

Next I ?

Next

Done

Is CG_BEST >0 ?

No

Yes

Return (normal exit)

$\underline{X} = \underline{X} \cdot \underline{SG\_GBL}$

EXCLUDE

FIGURE 5: UPPER BOUND SIMPLEX (INVITE LOOP)

26

including two feasible activity vectors per CMG; one for each sense of rotation. Because the simplex basis must be linearly independent, no benefit (via Eq. 14) will be seen in inviting a CMG activity vector and its opposing "anti-vector" into the basis simultaneously. The standard simplex structure can be used with intrinsic feasibility constraints; if an anti-vector is found in the solution, the sign of its decision variable is reversed.

This method was used in the original software, however the amount of bookkeeping and storage overhead required for the redundant anti-vectors was substantial. Another method was adopted which keeps only a single "pseudo-feasible" activity vector (with positive x_j) for each CMG gimbal, and adds a parallel array in which the "hidden" sign of the x_j is retained. The crux of the process is evident in Eq. 14, where it is seen that an activity vector can only improve the objective function in one sense; improvement in both positive and negative directions is not possible. To have any hope of attaining CG > 0, $\underline{U} \cdot \underline{A}_I$ must be positive, hence $\underline{A}_I$ must point into the hemisphere along the direction of $\underline{U}$. If $\underline{U} \cdot \underline{A}_I$ is negative, then $-\underline{A}_I$ is chosen for evaluation in Eq. 14 (this is flagged by "SGN" in Fig. 5).

If an activity vector is already at its upper bound, inclusion in the basis can only decrease the decision variable (relative to its bound), hence the sign of CG is inverted and $\underline{U} \cdot \underline{A}_I$ is considered only in the direction opposing the bound on $\underline{A}_I$ (this is accomplished in Fig. 5 via S = -1 and SGN = sign of present bound on $\underline{A}_I$).

Once the non-basic activity vector with the largest positive CG has been isolated, the basis must be examined for the element most beneficial to exclude. The logic for this process is shown in Fig. 6 (the "exclude loop"). The element which is chosen for exclusion is that whose decision variable x_L either first reaches its upper bound or goes to zero as the contribution of the invited activity vector x_{INVITE} is increased. The "exclude" logic first calculates a vector $\underline{T}$ of "linear combination coefficents" which are the coordinates of the invited
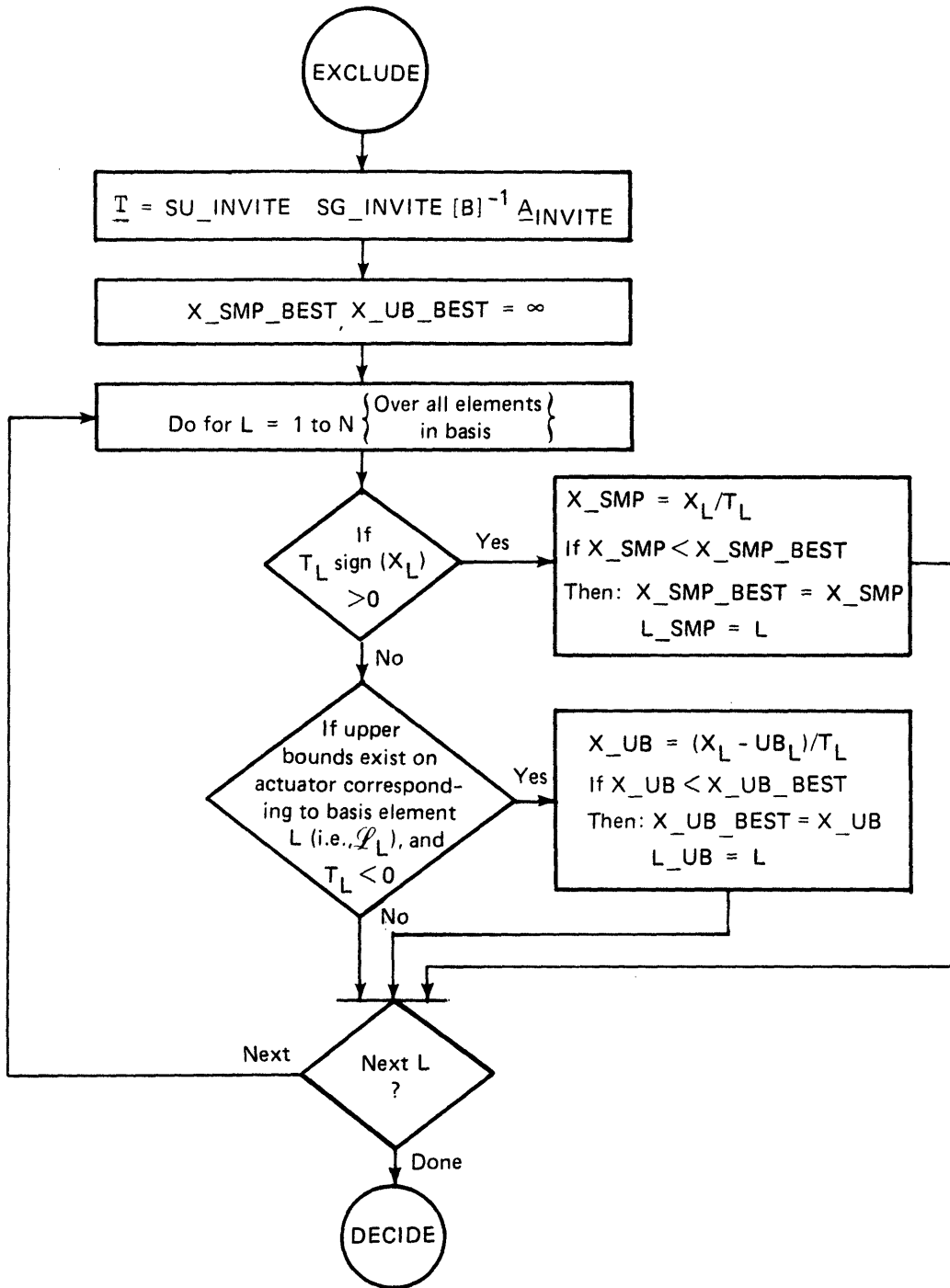
27

FIGURE 6; UPPER BOUND SIMPLEX (EXCLUDE LOOP)

activity $\underline{A}_{INVITE}$ relative to the basis vectors
(ie. $\underline{A}_{INVITE}$ = [B]T). The sign reversals resulting from $\underline{A}_{INVITE}$
at its upper bound or in reversed rotation (SU_INVITE and SG_INVITE) must
be factored into $\underline{T}$.

The basic decision variables (x_L) must change in order to
maintain the equality constraint as the amplitude of the invited activity
vector (X_{INVITE}) is increased. The change in x_L needed to
maintain the equality constraint with unit increase in X_{INVITE} is
T_L (ie. $T_L = \Delta X_L / \Delta X_{INVITE}$). Each basis element with a
decision variable which decreases as the contribution of the invited
activity increases (ie. $T_L > 0$) is examined; the element is isolated
which requires the minimum amount of the invited activity vector
(X_{INVITE}) to drive its x_L to zero and remove it from the basis.
This amount is the current decision value of the basis element to be
excluded (x_L) normalized by T_L. The quantity x_L / T_L is
termed the "pivot ratio". The "sign(x_L)" factor on T_L in the
conditional of Fig. 6 accounts for potentially infeasible solutions (w.
negative x_L) associated with the artificial variables in the initial
basis.

Each bounded basis element with a decision variable that increases
in proportion to the contribution of the invited activity vector (ie.
$T_L < 0$) is also examined; the element is isolated which reaches its
upper bound most quickly (thus also becoming non-basic). The amount of
invited activity needed to drive x_L to its bound is determined by the
"upper bound ratio" (x_L - UB_L)/T_L; the basis element which
reaches its bound most quickly has the minimum value of this quantity.
The numerator represents the "distance" to the bound with respect to the
activity vector to be excluded; the amount of the invited vector required
to achieve this is obtained by normalizing by the combination coefficent
T_L.

When increasing the amount of the invited activity vector included
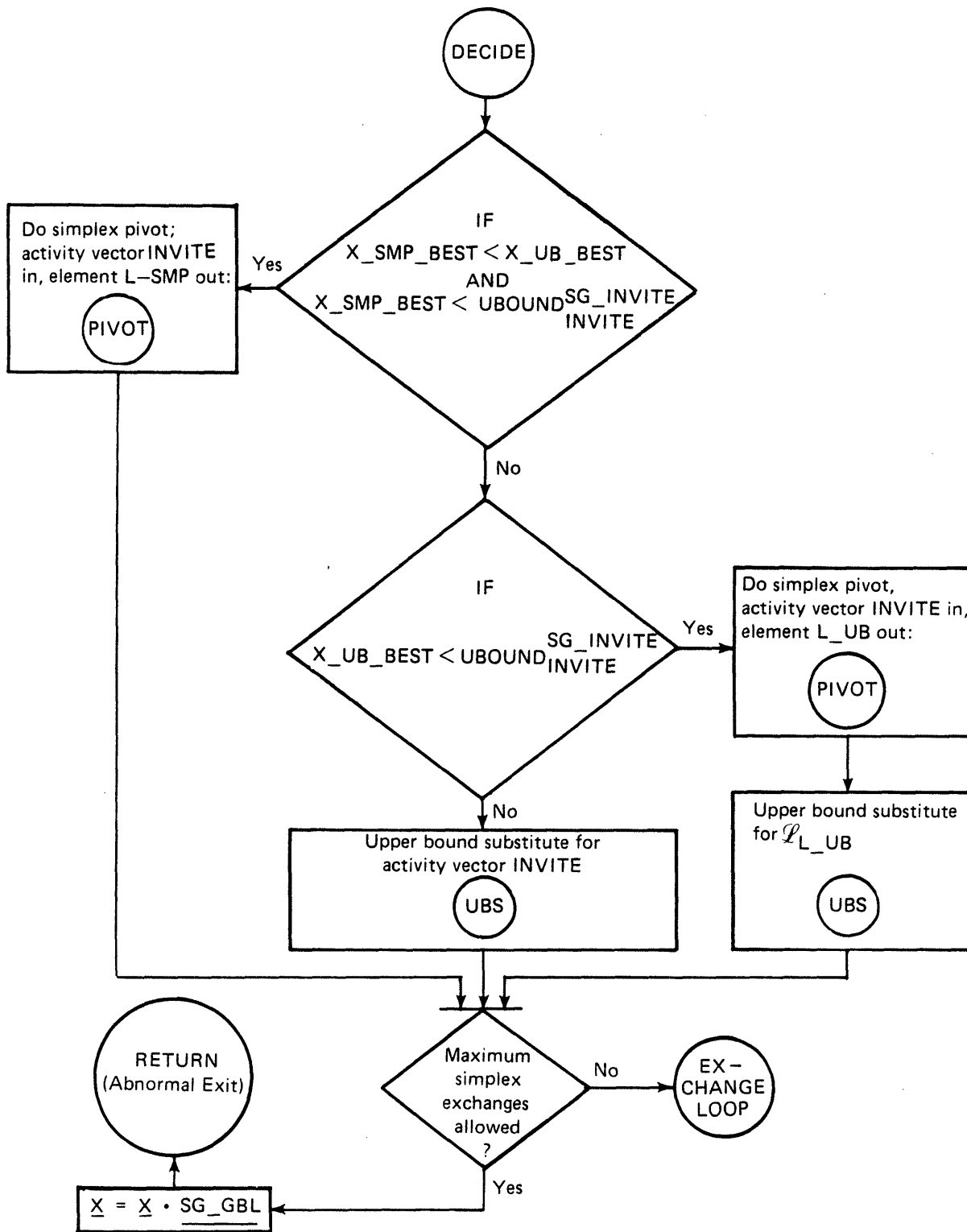in the solution, one of three things will happen:

DECIDE

IF
X_SMP_BEST < X_UB_BEST
AND
X_SMP_BEST < UBOUND$^{SG\_INVITE}_{INVITE}$

Yes → Do simplex pivot; activity vector INVITE in, element L–SMP out:
PIVOT

No

IF
X_UB_BEST < UBOUND$^{SG\_INVITE}_{INVITE}$

Yes → Do simplex pivot, activity vector INVITE in, element L_UB out:
PIVOT

Upper bound substitute for $\mathscr{L}_{L\_UB}$
UBS

No

Upper bound substitute for activity vector INVITE
UBS

Maximum simplex exchanges allowed ?

No → EX – CHANGE LOOP

Yes

$\underline{X} = \underline{X} \cdot SG\_GBL$

RETURN (Abnormal Exit)

FIGURE 7: UPPER BOUND SIMPLEX (DECISION STRUCTURE)

1) The decision variable x_L of a basic activity vector will go to zero.

2) The decision variable x_L of a basic activity vector will reach its upper bound.

3) The amplitude of the incoming activity vector will reach its upper bound.

The phenomenon which occurs first is determined via the minimum pivot and upper bound ratios defined in the preceeding paragraphs. The logic of the "decision structure" (Fig. 7) sketches the action taken for each possibility, as summarized below.

If the upper bound associated with the incoming activity vector is smaller than both the minimum pivot and upper bound ratios, Condition 3 will occur first. In this case, the invited activity vector is brought into the solution at its upper bound (ie. "upper bounding substitution"), and the basis remains untouched.

If the minimum upper bound ratio is smaller than both the minimum pivot ratio and the upper bound on the invited activity vector, Condition 2 will occur first. In this case, the basis element reaching its bound is removed (but kept in the solution at its upper bound), and the invited activity vector is pivoted into the basis in place of the excluded element.

If the minimum pivot ratio is the smallest of the three, Condition 1 applies, and the invited activity vector is pivoted into the basis in place of the excluded element.

The details of the pivoting operation and upper bounding substitution are given in Fig. 8. The simplex pivot updates the inverse basis $[B]^{-1}$ and basic decision variables ($\underline{x}$) to account for the swap of activity vectors. The pivoting calculations are based upon principles of the "revised simplex method"[26], which provides an efficent means of updating $[B]^{-1}$ without extensive matrix operations.

31

PIVOT
[Perform simplex pivot]

IN = Activity vector to pivot into basis

OUT = Basis element to pivot out

Update $[B]^{-1}$:

(1) Column $j \neq$ out:

$$B^{-1}_{*,j} = B^{-1}_{*,j} - T_j \frac{B^{-1}_{*,out}}{T_{out}}$$

(2) Column j = out:

$$B^{-1}_{*,out} = \frac{B^{-1}_{*,out}}{T_{out}}$$

Update $\underline{X}$:

(1) Element $j \neq$ out:

$$X_j = X_j - T_j \frac{X_{out}}{T_{out}}$$

(2) Element j = out:

$$\mathscr{L}_{out} = \frac{X_{out}}{T_{out}}$$

$\mathscr{L}_{out}$ = IN,
Update other lists, etc.

(RETURN)

UBS
[Perform upper bound substitution]

IUB = Activity vector to place @ upper bound

SUB = Sign of upper bound

Set upper bound array:

$$ON\_AT\_UB_{IUB} = UBOUND^{SUB}_{IUB}$$

$$- ON\_AT\_UB_{IUB}$$

$$\underline{X} = \underline{X} - UBOUND^{SUB}_{IUB} \underline{T}$$

Update lists, etc.

(RETURN)

NOTES: ON_AT_UB is an array which holds the upper bounds values of activity vectors which are nonbasic at their upper bound

$\underline{T}$ is a vector of linear combination coefficients calculated in "Exclude" (Fig. 6)

FIGURE 8: UPPER BOUND SIMPLEX (UTILITY ROUTINES)

The upper bounding substitution stores the relevant upper bound of the activity vector in a parallel "On At Upper Bound" array and adjusts the decision variables associated with the basic vectors to account for the new solution (the basic coordinates of activity #I at its upper bound are expressed by the product of $\underline{I}$ and U_BOUND ; this quantity must be subtracted from the basic decision variables $\underline{x}$ to maintain the equality constraint).

After performing the operations dictated by the decision structure of Fig. 7, the invitation process (Fig. 5) is repeated, and simplex starts another cycle. Simplex will repeat until either no objective benefit is seen by considering another activity vector in the solution (ie. all CG $<$ 0), or too many iterations have elapsed without convergance (to prevent real-time cycle wrap). Upon exiting, the decision variables are given the "intrinsic" signs stored in the parallel SGN_GBL array.

The final simplex solution consists of the activity vectors forming the basis (with decision values contained in $\underline{x}$) and non-basic vectors at their upper bounds (with contributions contained in array ON_AT_UB).

2.5) Determination of Activity Vectors, Gimbal Rates, and Upper Bounds

The previous section described the means by which the linear actuator selection was performed with regard to an objective function and a set of equality constraints describing the state of the instantaneous system. CMG representations and coordinate systems have not yet been precisely specified, since they were not needed to cover the topics discussed earlier. In order to apply the selection/steering concept outlined in this report to an array of real devices, the framework must be defined under which quantities such as activity vectors, gimbal rates, upper bounds, etc. can be calculated.

The coordinates and conventions given in Ref. 29 to describe double and single gimballed CMGs are also used in this analysis. Fig. 9 shows a schematic of a single gimballed CMG. We have defined $\hat{\sigma}$ and $\hat{h}_o$ to be unit vectors along the fixed gimbal axis and initial rotor axis (the $\underline{\sigma}$
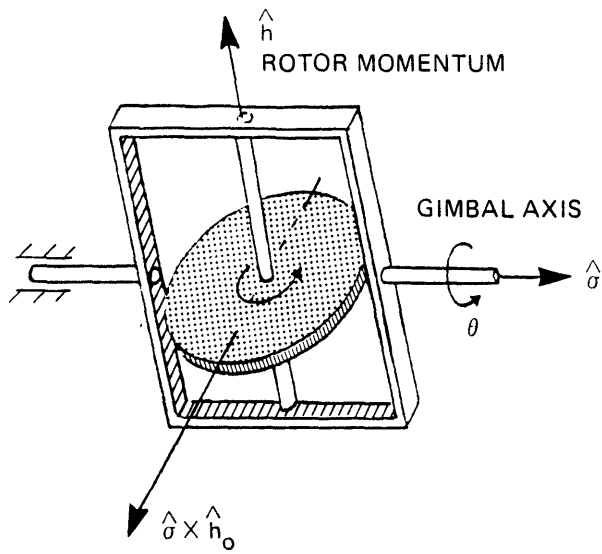
(a) DRAWING
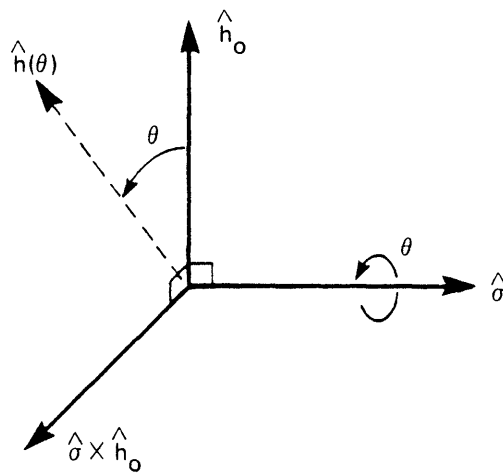
(b) SCHEMATIC

FIGURE 9: SINGLE GIMBALLED CMG

34

used in the previous CMG discussions is a vector pointing along $\hat{\sigma}$, but with a magnitude equal to the gimbal rate; vectors with "hats", ie. $\hat{\sigma}$, denote unit vectors). The rotor rotation angle along $\hat{\sigma}$ is denoted by θ; this is referenced to the initial rotor position $\hat{h}_o$ at $\theta = 0$, hence $\hat{h}(\theta=0)=\hat{h}_o$ and $\hat{h}(\theta=90°)= \hat{\sigma} \times \hat{h}_o$. This leads to a general expression for $\hat{h}(\theta)$ with a single gimballed CMG:

$$15) \quad \hat{h}(\theta) = \hat{h}_o \cos \theta + (\hat{\sigma} \times \hat{h}_o) \sin \theta$$

We use an extension of this same principle to update rotor positions for double gimballed CMGs. Figure 10 shows a diagram of an Euler mounted dual gimballed device; $\hat{\sigma}_\delta$ is defined as a unit vector along the outer gimbal axis (which is assumed fixed to the spacecraft), $\hat{\sigma}_{\gamma_0}$ is a unit vector along the initial inner gimbal axis, and $\hat{h}_o$ is a unit vector along the initial rotor position. $\hat{\sigma}_\gamma(\delta)$ is rotated about $\hat{\sigma}_\delta$ (with rotation angle δ), and $\hat{h}(\delta,\gamma)$ is rotated first about $\hat{\sigma}_\delta$ (with rotation angle δ) and then about $\hat{\sigma}_\gamma(\delta)$ (with rotation angle γ). γ and δ are respectively the inner and outer gimbal angles. The initialized parameters $\hat{h}_o$, $\hat{\sigma}_\delta$, and $\hat{\sigma}_{\gamma_0}$ are defined to form a right-handed set in order to simplify calculations (and to reflect physical realities of the dual gimballed CMG).

In order to calculate $\hat{h}(\delta,\gamma)$, we must first rotate about the outer gimbal axis, $\hat{\sigma}_\delta$. Using the principles of Eq. 15, and noting that $\hat{\sigma}_\delta \times \hat{h}_o = -\hat{\sigma}_{\gamma_0}$ as defined above, we have:

$$16) \quad \hat{h}(\delta)\big|_{\gamma=0} = \hat{h}_o \cos \delta - \hat{\sigma}_{\gamma_0} \sin \delta$$

Next, we must rotate about the "rotated" inner gimbal axis $\hat{\sigma}_\gamma(\delta)$. We again use relation 15, and take note that $\hat{\sigma}_\gamma(\delta) \times \hat{h}(\delta)\big|_{\gamma=0} = \hat{\sigma}_\delta$ for all δ:
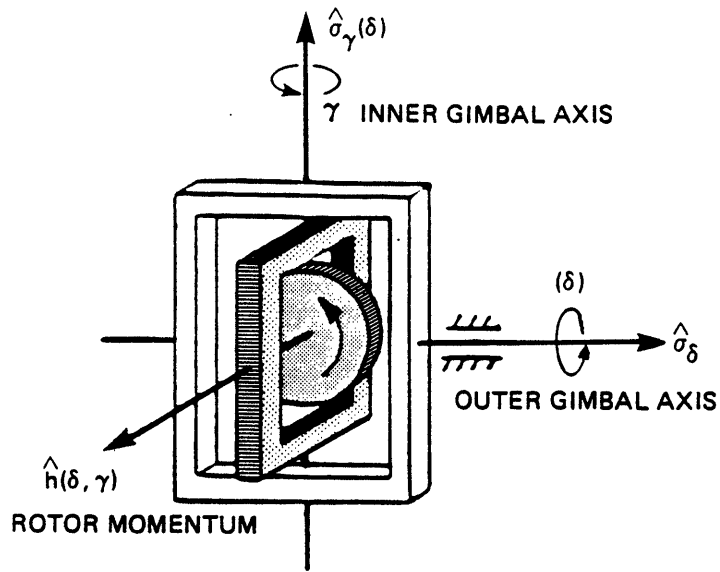
a) Drawing
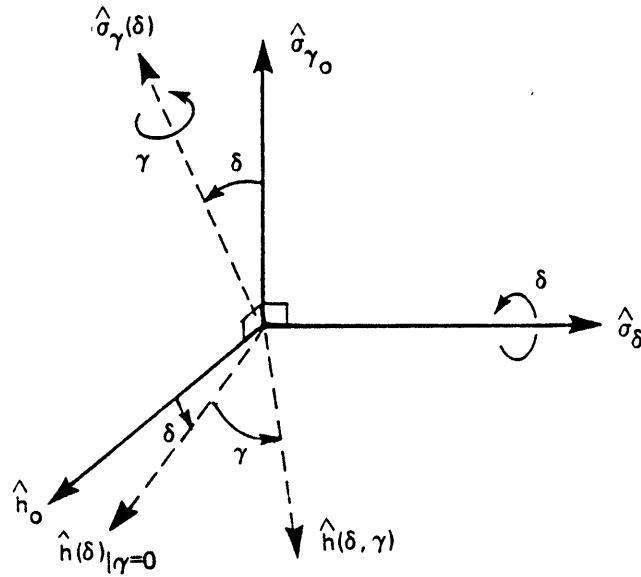
b) Schematic

FIGURE 10: DOUBLE-GIMBALLED CMG

36

17) $\hat{h}(\delta,\gamma) = \hat{h}(\delta)\big|_{\gamma=0} \cos\gamma + \hat{\sigma}_\delta \sin\gamma$

Substituting Eq. 16 into Eq. 17, we get our final expression

18) $\hat{h}(\delta,\gamma) = (\hat{h}_0 \cos\delta - \hat{\sigma}_{\gamma_0} \sin\delta) \cos\gamma + \hat{\sigma}_\delta \sin\gamma$

Eqs. 15 (single gimballed) and 18 (double gimballed) describe the unit vector pointing along the CMG rotor axis as a function of gimbal angle(s). An expression for the output torque is easily obtained by taking the time derivative of these relations. This is straightforward for single gimballed devices (Eq. 15):

19) $\underline{\tau}_{SG}(\theta) = -\dfrac{d\underline{h}(\theta)}{dt} = -\dot{\theta}\left[-\hat{h}_0 \sin\theta + (\hat{\sigma} \times \hat{h}_0)\cos\theta\right]h_{mag}$

The factor h_{mag} is the magnitude of the angular momentum stored in the CMG rotor (assumed constant), and $\dot{\theta}$ is the gimbal rate. Using the identity $\hat{\sigma} \times (\hat{\sigma} \times \hat{h}_0) = -\hat{h}_0$ (see Fig. 9) and borrowing Eq. 15, Eq. 19 becomes:

20) $\underline{\tau}_{SG}(\theta) = -\dot{\theta}\,(\hat{\sigma} \times \hat{h}(\theta))\,h_{mag}$

This agrees with our kinematic definition of CMG output torque (Eq. 5).

One may similarly take the time derivative of Eq. 18 to calculate the output torque of a double-gimballed CMG:

21) $\underline{\tau}_{DG}(\delta,\gamma) = -\dfrac{d\underline{h}(\delta,\gamma)}{dt}$

37

$$= -h_{mag}\left[-\dot{\gamma}(\hat{h}_o \cos \delta - \hat{\sigma}_{\gamma_o} \sin \delta) \sin \gamma - \dot{\delta}(\hat{h}_o \sin \delta + \hat{\sigma}_{\gamma_o} \cos \delta) \cos \gamma \right.$$

$$\left. + \dot{\gamma} \hat{\sigma}_\delta \cos \gamma \right]$$

$$= -h_{mag}\left[\dot{\gamma}((\hat{\sigma}_{\gamma_o} \sin \delta - \hat{h}_o \cos \delta) \sin \gamma + \hat{\sigma}_\delta \cos \gamma) \right.$$

$$\left. - \dot{\delta}(\hat{h}_o \sin \delta + \hat{\sigma}_{\gamma_o} \cos \delta) \cos \gamma \right]$$

If one uses Eqs. 18 and 21, it can be shown that:

22) $\quad \underline{\tau}_{DG}(\delta,\gamma) = -h_{mag}\left[\dot{\gamma}(\hat{\sigma}_\gamma(\delta) \times \hat{h}(\delta,\gamma)) + \dot{\delta}(\hat{\sigma}_\delta \times \hat{h}(\delta,\gamma))\right]$

Given that (see Fig. 10)

23) $\quad \hat{\sigma}_\gamma(\delta) = \hat{\sigma}_{\gamma_o} \cos \delta + \hat{h}_o \sin \delta$

$\qquad \hat{\sigma}_{\gamma_o} \times \hat{h}_o = \hat{\sigma}_\delta$

$\qquad \hat{h}_o \times \hat{\sigma}_\delta = \hat{\sigma}_{\gamma_o}$

$\qquad \hat{\sigma}_\delta \times \hat{\sigma}_{\gamma_o} = \hat{h}_o$

Eqs. 21 and 22 show that the output torque of a double gimballed CMG (at a given δ and γ) separates into two components which depend independently upon inner and outer gimbal rates. Each "linearized" CMG gimbal may thus be represented by an individual activity vector; $\dot{\gamma}$ and $\dot{\delta}$

are then independently selected via the linear programming scheme discussed in Sec. 2.4.

Referring to the format introduced in Eq. 8, the detailed CMG activity vectors can be specified:

$$
24) \quad \begin{aligned} \underline{A}_{Inner} &= -h_{mag}\ \dot{\gamma} \begin{bmatrix} [I]^{-1}[\hat{\sigma}_{\gamma}(\delta) \times \hat{h}(\delta,\gamma)] \\ \hline 0 \end{bmatrix} \\ \underline{A}_{Outer} &= -h_{mag}\ \dot{\delta} \begin{bmatrix} [I]^{-1}[\hat{\sigma}_{\delta} \times \hat{h}(\delta,\gamma)] \\ \hline 0 \end{bmatrix} \end{aligned} \quad \underline{0} \equiv \begin{bmatrix} 0 \\ 0 \\ 0 \end{bmatrix}
$$

(Referencing Eq. 22, and assuming 6-component vectors)

Eq. 24 is used to calculate activity vectors for dual gimballed CMGs in the current software scheme; if a single gimballed device is desired, one gimbal is "failed" (ie. frozen at constant angle and inhibited from selection). The expansion given in Eq. 21 is used to calculate the "$\hat{\sigma} \times \hat{h}$" terms in the non-zero upper halfs of the activity vectors.

As mentioned in the previous section, the linear selection problem has been posed as a rate-change request (Eq. 7). This is a natural framework for a jet selection, where each jet generates a fixed torque which is integrated over the on-times specified in the solution to yield a resultant change in the vehicle rates. Since the output torque of a CMG can be adjusted by varying the gimbal rates ($\dot{\gamma},\dot{\delta}$), most CMG steering laws are instead structured to solve directly for gimbal rates in response to an input torque request. The selection algorithm is iterated frequently, and the requested torque changes with the vehicle dynamic response.

If the activity vectors of Eq. 24 are constructed without scaling by the $\dot{\gamma}$, $\dot{\delta}$, $[I]^{-1}$ factors and the equality constraint of Eq. 7 is

re-formulated, the same linear program can be employed to provide "optimal" gimbal rates in answer to an input torque request:

$$25) \quad \sum_{j=1}^{N} A_j' X_j' = \underline{M} \quad \text{where:} \quad \begin{array}{l} A_j' = -h_{mag} \, (\hat{\sigma}_j \times \hat{h}_j) \\ \underline{M} = \text{input torque request} \\ N = \text{total CMG gimbals in system} \end{array}$$

In this case, the decision variables X_j' become the CMG gimbal rates $\dot{\gamma}$ and $\dot{\delta}$; these are picked by the selection procedure to attain the input torque request $\underline{M}$. The advantages of linear programming also apply here; ie. upper bounds may be enforced on the decision variable to prevent a "peak" gimbal rate from being exceeded, and the selection is intrinsically "optimal" with respect to a linear objective function.

It was mentioned earlier that the output torque of a conventional jet is considered constant over a jet firing and can not be varied, thus the corresponding jet selection is made in an "impulsive" fashion and specifies on-times in response to an input rate-change request. The "on-time" formalism, however, can also be applied to CMGs, since the angular displacement of a CMG gimbal creates a proportional (to leading order) rate change in the vehicle. Because of this, it is much simpler and more direct for CMGs to answer a rate-change input than it is to manipulate a system of jets to respond to a torque request. The rate-change formalism is thus highly advantagous in providing the capability of selecting both sets of actuators with the same procedure.

Solving for CMG angular displacement as opposed to instantaneous output torque possesses other potential advantages. The selection logic may not need to be executed at such a high periodic rate, as is conventional when solving for output torque. Since a CMG selection provides an effective CMG "on-time" under the rate-change context, selections involving small gimbal displacements may often be answered with only one selection (strategies to minimize effects of CMG nonlinearity and thereby reduce the number of required CMG selections are

discussed in Section 4.1). If one solves directly for gimbal rates, at least two selections (one to start the gimbals, one to stop them) are necessary. In either case, the resultant CMG/vehicle motion will appear "smoother" as the frequency of selection is increased, however solving for the angular displacement enhances the possibility of reducing the number of required selections and thereby cutting computer scheduling overhead.

Solving for gimbal displacements leaves the absolute normalization of the $\dot{\gamma}$'s and $\dot{\delta}$'s as a potentially free parameter. In the present software, the $\dot{\gamma}$ and $\dot{\delta}$ values used in calculating the activity vectors (Eq. 24) are set to the maximum gimbal rates attainable by the CMG hardware. The X_j resulting from the linear CMG selection thus indeed represent the "on-times" at the peak gimbal rates $\dot{\theta}_{P_j}$ required to attain the input rate change. The ensuing angular displacements are:

$$26) \qquad \Delta\theta_j = \dot{\theta}_{P_j} X_j$$

where θ_j is assumed to be a "generic" CMG gimbal angle (ie. inner (γ) or outer (δ), depending on the activity vector under consideration). Equation 26 is then re-formulated to drive all CMGs at different gimbal rates, such that the device with maximum $|X_j|$ is driven at the peak CMG gimbal rate, while those with smaller $|X_j|$ are driven at proportionally lower speeds. The resulting gimbal rates $\dot{\theta}_j$ and "on-time" Δt can be expressed:

$$27) \qquad \dot{\theta}_j = \left[\frac{\dot{\theta}_P}{X}\right]_m X_j \qquad\qquad \text{where } X_m = \max \{X_j\}$$
$$\Delta t = X_m$$

The formulation presented above will drive all CMGs at various gimbal rates (normalized with the fastest run at its peak rate) such that all CMGs achieve their targeted angular displacement $\Delta\theta_j$ simultaneously after a time interval Δt has elapsed. If $\dot{\theta}_{p_j}$ is different for various gimbals, the gimbal which dictates the minimum scale factor $\dot{\theta}_{p_j}/X_j$ (thus being driven closest to or furthest above its peak rate) is chosen for use in Eq. 27 (denoted by the "m" subscript).

Since the activity vectors of Eq. 24 are scaled by $\dot{\theta}_{p_j}$, any gimbal with excessively low $\dot{\theta}_p$ possesses correspondingly reduced control authority and has an activity vector of smaller magnitude. The selection will generally prefer other gimbals with higher peak rates, unless otherwise dictated by the objective function (see Ch. 3). As hinted in the previous section, the average "amount" by which a CMG gimbal is included in the solution ($|X_j|$) is also related to the value of its objective coefficent, thus one can optionally avoid excessive useage of particular CMGs (ie. those with hardware faults, etc.) by increasing their respective objective amplitudes.

Since it always normalizes gimbal rates to a peak value, Eq. 27 represents the "fastest" route to attaining the desired vehicle rate change. This is what we have actually used in our simulation examples (Ch. 5), where the main objective was to test the properties of the steering law, hence the CMGs were driven as hard as possible to conserve simulation time. This mode may not suit applications where a small rate change is requested (which is typical for quiescent on-orbit operations). In this case, a "linear" response may be preferred, where the CMGs are driven with rates proportional to the input request and not continually "hammered" on and off at their maxumum rate (which might wreak havoc into any flexible spacecraft structure). This can be incorporated by adapting Eq. 27:

a) $\quad \dot{\theta}_j = (\alpha \, \dot{\theta}_{P_j}) X_j \qquad\qquad$ If all $\dot{\theta}_j < \dot{\theta}_{P_j}$

$\quad\quad \Delta t = 1/\alpha \qquad\qquad\qquad$ ie: $X_j < 1/\alpha$

28)

b) $\quad \dot{\theta}_j = \left[\dfrac{\dot{\theta}_P}{X}\right]_m X_j \qquad\qquad$ [otherwise]

$\quad\quad \Delta t = X_m$

Eq. 28 incorporates both a "linear" set of gimbal rates, which form solutions to smaller rate-change requests (Eq. 28a, where all resulting gimbal rates are below their maxima) and the "saturated" set of gimbal rates for larger rate-change requests (Eq. 28b, where Eq. 28a would produce at least one $\dot{\theta}_j$ above its peak rate). Gimbal rates are thus normalized to be smaller only if they exceed their peak limits; a linear rise in gimbal rates with request magnitude is allowed until this occurs. The "linear" portion of the gimbal rate transfer function (ie. gimbal rate vs. request magnitude) has a slope which is determined by the constant α in Eq. 28a. When a peak gimbal rate is exceeded, the "saturation" function of Eq. 27 is used (Eq. 28b) to determine $\dot{\theta}_j$. Changes in the peak gimbal rates can be accomodated by altering the values of $\dot{\theta}_p$ used in the calculations of activity vectors (Eq. 24) and gimbal rates (Eq. 28).

The gimbal rates derived via Eq. 28 will show little difference from those which would arise from a direct torque request (Eq. 25), since in either case the request is generally derived from the same sources (ie. weighted sum of vehicle attitude and rate errors; see Sec. 7.1). The major difference between the two formulations is the choice of units for the decision variables; torque requests pick gimbal rates driven over a fixed cycle time, while the rate-change requests choose the time interval over which a fixed gimbal rate is applied.

Upper bounds specify the location of gimbal stops relative to the current gimbal positions and clamp a maximum limit onto the allowed CMG control authority. Using our current rate-change convention (ie. activity vectors of Eq. 24), upper bounds are calculated as follows:

$$29) \quad u_j^{+/-} = MIN \begin{bmatrix} L/\dot{\theta}_{P_j} \\ (\theta_{stop}^{+/-} - \theta_j)/\dot{\theta}_{P_j} \end{bmatrix}$$

Where:

$u_j^{+/-}$ = Upper bound on decision variable X_j in direction "+/-".

$\theta_{stop}^{+/-}$ = Location of stop on gimbal #j in the "+/-" direction.

L = Maximum allowed CMG displacement (externally imposed limit on CMG control authority).

$\dot{\theta}_{P_j}$ = Peak rate for gimbal #j.

If the CMG is far from its stop on the gimbal and in the direction concerned, the upper limit "L" (which is a "global" clamp set on the allowed CMG control authority) will be selected as the upper bound. As a CMG approaches a stop, the distance to the stop from the current gimbal position dominates in Eq. 29, hence is chosen as the upper bound in the rotation sense that brings the CMG further in that direction. It should be noted that gimbal stops may be dynamically re-defined by changing the constant θ_{stop} in the upper bound calculation of Eq. 29 and cost contribution of Eq. 32. This capability may prove useful in situations where gimbal motion must be limited in potentially failing hardware.

Eq. 29 allows one to directly incorporate gimbal stops into the selection process. It also introduces a means of dealing with torque and momentum saturation. If an input request is sufficiently large, several CMGs must be brought on at their upper bounds to provide the requested output. This indicates "torque saturation", where the CMGs are required

44

to be operated at their peak rates in order to answer an input request. As the CMGs near a detected "momentum saturation" state (where the maximum possible CMG momentum is projected in the desired direction; see Section 4.2), the limit "L" on allowed CMG displacement is correspondingly reduced, which allows the selection process to account for the decreasing amount of available momentum. If upper bounds restrict the CMG system from exclusively answering the input request, RCS jets are automatically introduced. This topic is elaborated at length in Section 4.3.

The peak gimbal rates could be imposed directly as upper bounds on the decision variables of the torque request problem (Eq. 25), thus explicitly accounting for torque saturation. In order to consider gimbal stops, one would have to adjust the bounds on gimbal rate, while assuming a fixed cycle time (Δt) between CMG selections. Again, we see the effect of assumptions made under the two formulations. With the rate-change structure, gimbal stops and momentum saturation can be explicitly incorporated, while torque saturation must be inferred. With the torque request formalism, torque saturation is explicitly imposed, while gimbal stops and momentum saturation must be indirectly taken into account.

Activity vectors for jets are constructed from their rotational and translational accelerations, as depicted in Eq. 8 and calculated in Ref. 25. If merely rotational control is desired, the software only considers the first three components of the activity vectors and propagates a 3x3 basis, which significantly expedites the process when compared to the computational requirements imposed by the 6x6 dimension of the full rotational/translational control problem.

In the software used to produce the results of Chapter 5, upper bounds were not considered on the decision variables corresponding to jets. If upper bounds were imposed, jets would only be allowed to fire up to a maximum duration, and more than three jets would be included in the simplex solutions to large requests. Only one bound need be specified per jet (they are not bi-directional devices such as CMGs). The corresponding u_j (as in Eq. 29) would thus be set to the maximum jet firing times.

CHAPTER 3

OBJECTIVE FUNCTION

3.1) Overview

The previous chapter described the process by which actuators were
selected to satisfy an equality constraint (Eq. 7) while minimizing an
objective function (Eq. 6) reflecting the "optimal" means of commanding
the CMGs relative to the instantaneous system configuration. The
objective function has thus far been presented in general terms; the
purpose of this chapter is to discuss its structure in detail. Some of
the concepts described in this chapter are primarily suited to double
gimballed CMGs; extensions of these ideas which adapt the logic to a
single gimballed system are described in Ch. 6.

Eq. 6 defines the objective function as a value "Z", which is
determined by summing the product of objective coefficients c_j and
decision variables X_j resulting from a solution to the equality
constraint. The c_j dictate the penalty of using a particular actuator
in the solution, and they are determined for each activity vector
according to the following relations:

a) $c_j = K_{jet}$ (Activity vector #j corresponds to RCS jet)

30)

b) $c_{j,s} = K_o + K_A F_{Angle}(j,s) + K_S G_{Stops}(j,s) + K_L Y_{Lineup}(j,s)$

(Activity vector #j corresponds to CMG gimbal)

s = Sense of rotation (+/-)

47

The objective coefficients corresponding to RCS jets are currently set to a uniform value "K_{jet}" (as in Eq. 30a). K_{jet} is defined to be much larger than the objective factors associated with CMGs in order to account for the smaller CMG control authority and to favor (wherever possible) selection of CMGs over jets. K_{jet} can be reduced to make CMG and jet costs roughly compatible, as is necessary in cases of hybrid CMG/RCS maneuvers and jet-assisted desaturation (discussed in Ch. 4). A selection bias for one class of jets over another can be indicated by specifying different values of K_{jet}; jets with lower cost will be preferred in the solution. All jets modeled in the simulations of Ch. 5 are assumed to be identical and are assigned a uniform K_{jet}. Simplex will then converge to solutions with minimum burn times (these are fuel-optimal).

The CMG objective coefficients are calculated via the formula in Eq. 30b. Since each CMG gimbal can be moved in two directions, two objective coefficients are calculated per gimbal (corresponding to rotations which increase or decrease gimbal angle). The first term in Eq. 30b (K_0) is a constant bias which keeps the objective factors non-zero. This bias is identical for every CMG gimbal; if K_0 is large, all CMGs will have nearly equal objective coefficients, thus selections will minimize the CMG angular displacements without regard to any other "optimality" criteria. If K_0 is relatively small (which is typically the case), the remaining terms dictate the best means of moving the CMGs in order to avoid configuration problems (possibly resulting in greater displacement). The value of these terms is a function of the CMG gimbal (j) and direction of gimbal rotation (s) under consideration. If a group of identical CMGs are oriented in a "best" configuration, all gimbals will have the same cost (since the consequences of moving each gimbal will be similar); as the CMGs drift into other orientations, the objective contributions will differ in order to favor rotating those CMGs which are approaching problematic states into a direction that avoids trouble.

The values of three objective contributions (F_{Angle}, G_{Stops}, Y_{Lineup}) are evaluated at the current CMG orientation and summed in Eq. 30b with relative weights K_A, K_S, and K_L. Adjusting the magnitude of a weighting factor affects the amount by which the corresponding objective component is considered in the net optimization. By tweaking the relative magnitudes of the weighting factors, one trims the balance in avoiding the various phenomena associated with the different objective components. The constants K_O, K_A, K_S, and K_L are thus adjusted empirically (see Ch. 5) such that the CMGs will be selected to avoid problem states before the configuration is allowed to become critical. The individual structure and purpose of each objective component (F_{Angle}, G_{Stops}, Y_{Lineup}) is discussed below.

3.2) Inner Gimbal Angle Minimization

As the inner gimbal of an Euler mounted double gimballed CMG is rotated such that the rotor axis approaches alignment with the outer gimbal axis (referencing Fig. 11, $\gamma \to 90°$ infers $\hat{h}(\delta, \gamma) \to \hat{\sigma}_\delta$), the component of rotor angular momentum perpendicular to the outer gimbal axis is decreased, thus the torque output potential of the outer gimbal is progressively degraded. This is quantitatively seen in Eq. 21, where the $\cos\gamma$ factor on the $\dot{\delta}$ term goes to zero (thus eliminating the outer gimbal contribution) at $\gamma = 90°$.

The function F_{Angle} adds an amplitude into the objective that penalizes simplex solutions which increase inner gimbal angles, as seen in Fig. 11 and quantitatively expressed below:

31) $\qquad F_{Angle}(j,s) = \begin{cases} |\gamma_j| & \text{If } j=\text{inner gimbal and rotation "s"} \\ & \text{increases } |\gamma_j|. \\ 0 & \text{Otherwise } \ldots. \end{cases}$

OUTER GIMBAL CONTROL OF 2-DOF CMG IS DEGRADED SEVERELY IF INNER GIMBAL ANGLE γ APPROACHES $\pm 90°$ AND CMG ROTOR $h(\delta, \gamma)$ ALIGNS WITH OUTER GIMBAL AXIS $\hat{\sigma}_\delta$:

$\delta \rightarrow$ OUTER GIMBAL
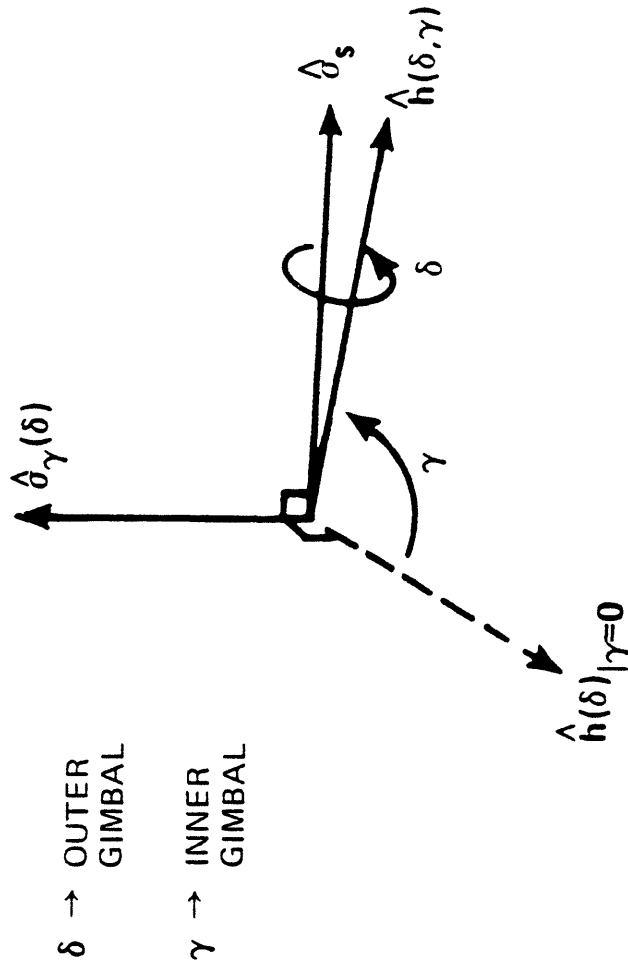
$\gamma \rightarrow$ INNER GIMBAL

$\rightarrow$ SELECT CMGs TO MINIMIZE INNER GIMBAL ANGLES

FIGURE 11

Inner gimbal rotations which increase the magnitude of the inner gimbal angle $\left|\gamma_j\right|$ are assigned a cost contribution in direct proportion to the current value of $\left|\gamma_j\right|$. Rotations which decrease $\left|\gamma_j\right|$ (or outer gimbal rotations which have no effect on γ_j) are given no cost contributions via F_{Angle}. Rotations that increase the inner gimbal angle become linearly more expensive as the angle grows. Solutions involving the activity vector and decision variables that bring $\left|\gamma_j\right|$ back to zero thus become increasingly favored as $\left|\gamma_j\right|$ rises.

3.3   Gimbal Stops Avoidance

Gimbal stops are hardware-imposed limits on CMG gimbal angle freedom. If a CMG gimbal has moved against a stop, it is only capable of rotating in one direction (away from the stop), thus half of its control potential is eliminated (as depicted in Fig. 12). This can restrict the directions into which the total CMG momentum can be projected (ie. in cases with at least one CMG pinned against a stop and the others aligned in saturation). Obviously, any state with one or more CMGs moved against their stops is undesirable and must be avoided.

The G_{Stops} cost contribution signals a "warning" to the selection procedure as a gimbal nears its limit. In contrast to the linear form of F_{Angle}, G_{Stops} contributes a nearly insignificant amount to the objective if the gimbal is removed from its stop (allowing the other terms in Eq. 30b to act unimpeded), but increases rapidly after the gimbal has approched to within a pre-set distance from the stop location. As depicted in Fig. 12, G_{Stops} can be expressed:

$$32)\quad G_{Stops}(j,s) = \begin{cases} \Lambda(\theta_j) & \text{If stops are present on gimbal \#j, and rotation "s" moves CMG toward stop.} \\ 0 & \text{Otherwise....} \end{cases}$$

$$\text{where:}\quad \Lambda(\theta_j) = \tan\left[\frac{\pi}{2}\left((1-\beta_o)\left[\frac{\theta_j}{\theta_{Stop}}\right]\right)+\beta_o\right] - \tan\left(\frac{\pi}{2}\beta_o\right)$$

51

AVOID CASES WHERE CMG IS PINNED AGAINST GIMBAL STOP
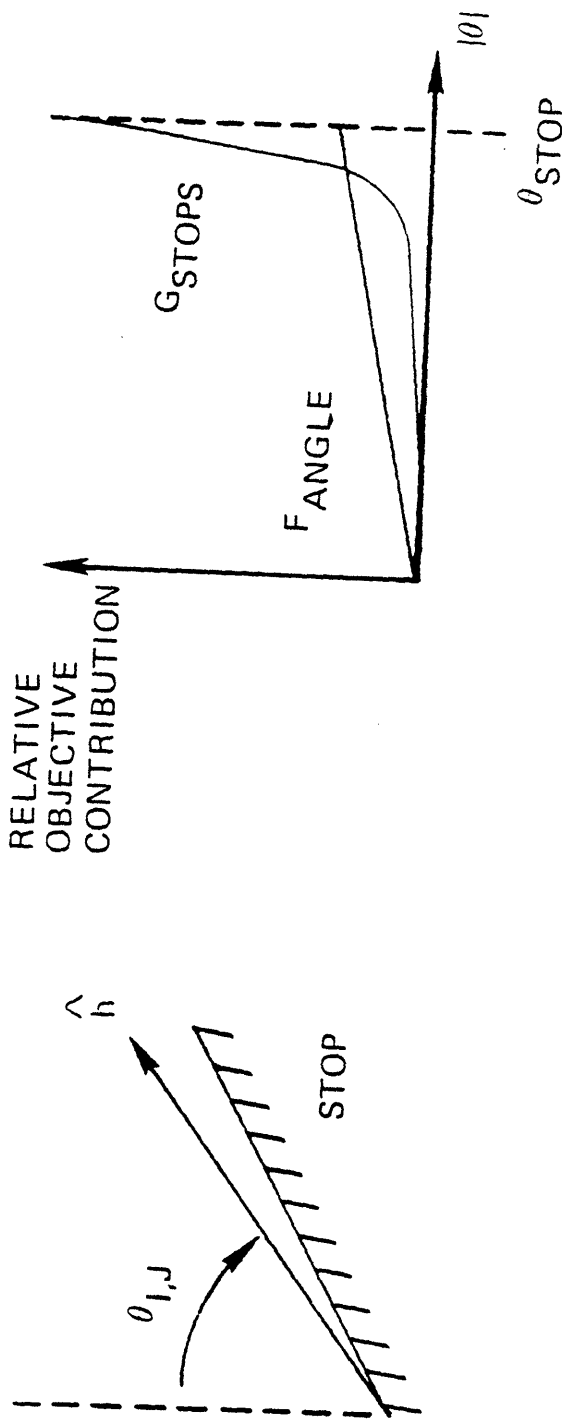
FIGURE 12: RELATIVE CONTRIBUTION OF F_{ANGLE} AND G_{STOPS} TO OBJECTIVE VS θ

52

β_O = "Steepness" parameter, $0 < \beta_O < 1$

θ_j = Gimbal angle (ie. γ or δ)

The function Λ has a small value for low θ_j, however as θ_j/θ_{Stop} approaches unity, Λ diverges asymptotically to infinity. One may control the "breakpoint" at which Λ diverges by adjusting the "β_O" parameter in Eq. 32. For small β_O, the function begins to contribute at lower θ and slowly diverges as θ increases. If β_O approaches unity, Λ begins to diverge more sharply at higher θ_j, until for $\beta_O \to 1$, $\Lambda(\theta_j)$ produces a delta function peaking when gimbal #j is against its stop.

If the rotation "s" brings a CMG toward an existing gimbal stop, the objective contribution will be proportional to Λ. No such contribution will be added to the objective coefficent if a gimbal either has unlimited freedom or rotation "s" will remove it from a stop. If a CMG gimbal has neared its stop, the function Λ will contribute appreciably, and solutions which rotate the CMG away from the stop are heavily favored in contrast to those which move it closer. The breakpoint on Λ set by β_O has been determined to yield best results around $\beta_O = 0.96$ (corresponding to $\theta_{Break} \simeq 0.8 \ \theta_{Stop}$). The form of Λ in Eq. 32 may be simplified (one can use several divergent functions); it was set up in its present realization to facilitate modifications during testing. Both functions F_{Angle} and G_{Stops} attempt to minimize gimbal angles, however the "steep" G_{Stops} contribution works primarily at large θ_j and only with those gimbals constrained by stops, whereas the function F_{Angle} is much milder and is applied solely to inner gimbals (both are plotted for comparison in Fig. 12).

3.4) Prevention of Rotor Lineup

Since the output torque of a CMG is always perpendicular to its rotor, a CMG is unable to produce a torque along the rotor axis (aside

from altering the rotor rate, but this is held constant and not considered a control variable). If two CMGs are aligned with their rotors parallel or antiparallel, control along the direction of the alignment must be performed exclusively with the remaining devices in the system, which can degrade the 3-axis control capability of the CMG configuration. Internal singular states (ie. CMG orientations removed from saturation which suffer a loss of control about at least one axis) of double-gimballed CMG systems are always related to CMG rotor alignments. In order to maintain a high level of three-axis controllability, the rotors of double-gimballed CMG systems are conventionally steered away from either parallel or antiparallel alignments. The situation is graphically presented in Fig. 13, where we see that the rotor orientation in Fig. 13b is preferred over that in Fig. 13a.

The terms discussed in the previous sections (F_{Angle} and G_{Stops}) assign cost contributions to the objective coefficents of an activity vector which depend only on the corresponding gimbal angle. They do not account for the orientation of a CMG rotor with respect to other CMGs. The term (Y_{Lineup}) that is discussed here differs considerably in that it expresses an amplitude which drives the CMG under consideration to avoid encountering parallel or antiparallel alignment with other CMGs in the system. Y_{Lineup} is quantified below:

33) $Y_{Lineup}(j,s) = Y_o(j,s) + B$

Where: $\qquad (I \neq J)$

$$Y_o(j,s) = \sum_{I=1}^{R} SG(I,j,s)\ m(I,J)$$

R = Number of CMG rotors in system

J = Rotor index associated with CMG gimbal #j.

Note: The sum runs over all CMG rotors except that associated with gimbal #j. Uppercase variables denote CMG rotors (ie. J), whereas lowercase variables denote CMG gimbals (ie. j).

54

(a)

h_4 h_3 h_2 h_1

$= h_{TOT}$ {UNDESIRED STATE

CONTROL TORQUE LIMITED ALONG LINEUP AXIS

(b)

h_4 h_3 h_2 h_1

$= h_{TOT}$ {EQUIVALENT PREFERRED STATE
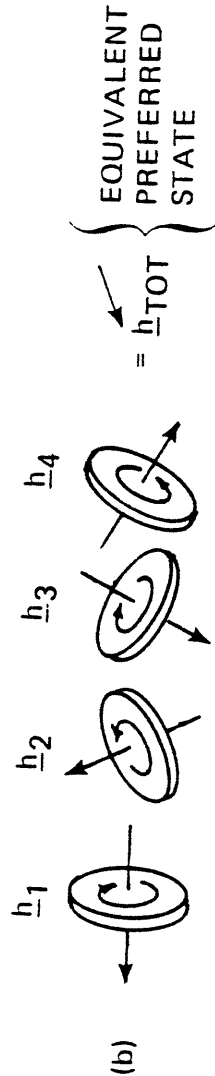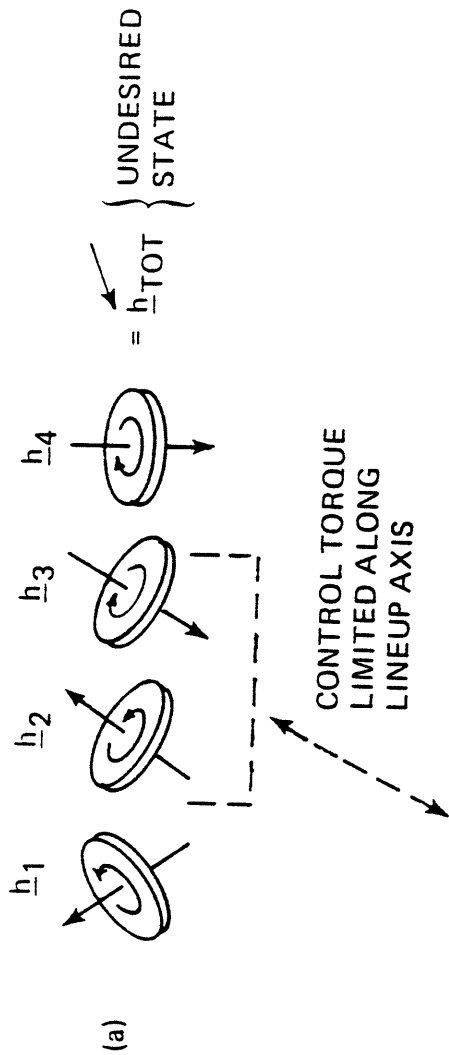
WHEN TWO OR MORE CMG ROTOR AXES BECOME PARALLEL OR ANTIPARALLEL, CONTROL IS DEGRADED ALONG ALIGNMENT DIRECTION

→ INTRODUCE "REPULSION" BETWEEN CMG ROTORS TO AVOID LINEUP

FIGURE 13

55

$m(I,J) = $ "Urgency" of lineup condition (increases as rotors I and J approach one another).

$$SG(I,j,s) = \begin{cases} +1 \text{ if rotation "s" moves rotor J toward rotor I} \\ -1 \text{ if rotation "s" moves rotor J away from rotor I} \end{cases}$$

$B = $ Bias to keep all $Y_{LINEUP}(j,s)$ non-negative
(ie. $B = -\min Y_o(j,s)$)

34) Details: $m(I,J) = \pi/2 - \cos^{-1}(\hat{h}_J' \cdot \hat{h}_I)$

$\hat{h}_J' = \hat{h}_J (\text{sign } (\hat{h}_I \cdot \hat{h}_J))$

$SG(I,j,s) = \text{sign}[(\hat{h}_I - h_J') \cdot \hat{R}(j,s)]$

$\hat{R}(j,s) = $ Direction of instantaneous rotor gimballing for CMG gimbal #j, sense "s".
[Unit vector in direction opposite gimbal #j's output torque (see Eq. 22).]

Eq. 33 defines the antilineup function Y_{Lineup}. The Y_0 term is a sum of amplitudes which reflect the lineup condition of the CMG rotor in question (#J) with respect to the other rotors in the system. If the rotation "s" of gimbal #j moves the associated CMG rotor toward parallel or antiparallel alignment with another rotor in the system (#I), the "SG(I,j,s)" flag will be positive; if the rotation moves the rotors mutually apart, "SG" will be negative. The "m" factor describes the "urgency" of the lineup condition; ie. $m(I,J)$ equals zero if the two CMGs in question are mutually perpendicular and linearly increases as the rotors approach one another, reaching a maximum of $m(I,J) = \pi/2$ at parallel or anti-parallel alignment. The products of "SG" and "m" are evaluated for the rotor and gimbal under consideration paired with all other rotors in the system; these are summed to form $Y_0(j,s)$.

The value of $Y_0(j,s)$ quantitatively represents the consequence of moving CMG gimbal #j in direction "s", with respect to lineup with other CMGs in the system. A positive $Y_0(j,s)$ indicates approaching lineup, and the magnitude of Y_0 indicates the degree of alignment. The opposite rotation will have the inverse consequence; ie. the $Y_0(j,-s)$ will be negative with equal magnitude, indicating the direction in which to move gimbal #j to escape alignment. Since negative objective values can yield unphysical solutions (see Sec. 4.4), a bias must be added onto Y_0 in order to keep all Y_{Lineup} non-negative. This bias (B) is the negative of the minimum $Y_0(j,s)$ over all j and s; the $Y_{Lineup}(j,s)$ will thus range from zero (ie. gimbal rotation with minimum $Y_0(j,s)$) on up.

Eq. 34 sketches the quantitative detail used in calculating the SG and m functions. The m(I,J) function is directly proportional to the angle between CMG rotors I and J. Amplitudes which drive the CMG rotors from both parallel and antiparallel alignment must be produced (ie. the minimum cost occurs when the rotors are orthogonal), thus the functions must be symmetric about a 90° separation between rotors. This is accomplished via the use of $\hat{h}'_J$, which equals $\hat{h}_J$ if the rotor separation is below 90° and $-\hat{h}_J$ otherwise. The "SG" function dictates the direction for gimbal #j to move in order to avoid lineup with rotor #I; it is formed by taking the sign of the dot product of the vector pointing from $\hat{h}'_J$ to $\hat{h}_I$ with a vector in the direction of gimbal #j's instantaneous rotation (ie. opposite the output torque). If SG is positive, gimbal rotation will cause rotor #J to approach rotor #I; if it is negative, the rotation will move the rotors apart.

The Y_{Lineup} function defined above uses an instantaneous approximation to the CMG rotation and does not consider the motion of one CMG with respect to another (these factors can not be directly accounted for under a linear selection, as discussed in Sec. 2.3). CMGs are encouraged via Y_{Lineup} to move independently away from one another; this strategy is found to be very effective in managing system redundancy to avoid lineups, as will be illustrated in the examples of Chapter 5.

Steering systems which include single gimballed CMGs away from rotor alignments is generally not adequate for avoiding singular orientations. This topic is assessed at length in Chapter 6.

CHAPTER 4

ADDITIONAL FEATURES

4.1)   Improving the Accuracy of Linear Solutions

Since the output torque direction changes while a CMG is
gimballing (see Fig. 2), the linear CMG selection must be repeated as the
CMGs are moving in order to maintain the desired torque or converge to
the requested rate change (as discussed in Sec. 2.3). A simplex solution
to the rate-change problem produces a set of gimbal angle displacements
$(\Delta\delta_j, \Delta\gamma_j)$ which may be added to the current gimbal positions in
order to yield a set of final angles δ_{F_j}, γ_{F_j}. These may be
substituted into Eq. 18 to calculate the final state CMG momentum vectors
$\underline{h}_j(\delta_{F_j}, \gamma_{F_j})$, which can be subtracted from the current CMG
momenta $\underline{h}_j(\delta_j, \gamma_j)$ to yield the exact momentum which would be
transferred from the CMG array to the spacecraft during implementation of
the simplex solution. By using the above process to compare the
requested momentum transfer against what would arise from applying the
simplex solution, one derives an estimation of the validity of the linear
solution with respect to the rotational cross coupling effects,
characterised by the ratio "Q" below:

$$35) \qquad Q = \frac{\left| \underline{\Delta H}_R - \underline{\Delta h}_s \right|}{\left| \underline{\Delta H}_R \right|}$$

Where: $\underline{\Delta H}_R$ = Requested momentum transfer into spacecraft,
              ie. $\underline{\Delta H}_R = [I]\underline{\Delta\omega}_s$

$\underline{\Delta h}_s$ = Calculated momentum change of CMG system due to
              simplex solution, ie:

$$\underline{\Delta h}_s = \sum_{j=1}^{\#CMGs} [\underline{h}_j(\delta_j, \gamma_j) - \underline{h}_j(\delta_{F_j}, \gamma_{F_j})]$$

The ratio Q represents the "quality" of the linear solution; ie. the linear approximation is valid for $Q \ll 1$, while rotational nonlinearities contribute significantly as Q approaches unity and can become problematic for $Q > 1$. Eq. 35 is easily computable; one needs only to calculate the final state rotor momenta via Eq. 18, which is a weighted sum of three fixed vectors. If a simplex solution produces very large angular displacements (ie. $\Delta\delta, \Delta\gamma > 30°$), the resulting value of Q will most probably be quite considerable (ie. $Q \gg 1$) because of the excessive gimbal swings involved. In these cases, only the initial portion of the gimbal trajectory is of interest in Eq. 35, since the linear selection will certainly have to be revised as the CMGs move. The angular displacements and momentum transfers used in Eq. 35 are then scaled back by a common factor which causes only the validity of the initial gimbal motion (ie. the first 10°) to be reflected in the value of Q.

As depicted in Figure 14, the value of Q produced by the linear selection is used to dictate which of three possible strategies is pursued. If $Q < Q_{Low}$, the linear solution is assumed adequately precise and is implemented unaltered. If $Q_{Low} < Q < Q_{High}$, rotational nonlinearities are deemed to play a significant role in undermining the precision of the linear solution. In this situation, the solution accuracy may be improved by performing an additional linear selection for the momentum transfer residual $(\underline{\Delta H}_R - \underline{\Delta h}_s)$ and summing the resulting angular displacements with those produced by the original selection. This yields a significant improvement; such composite solutions have been seen to drive the gimbals over 30% further than attained by the unaltered original solution before requiring an updated CMG selection. This often allows rate-change requests of modest magnitude to be solved via a single such second-order selection; the need
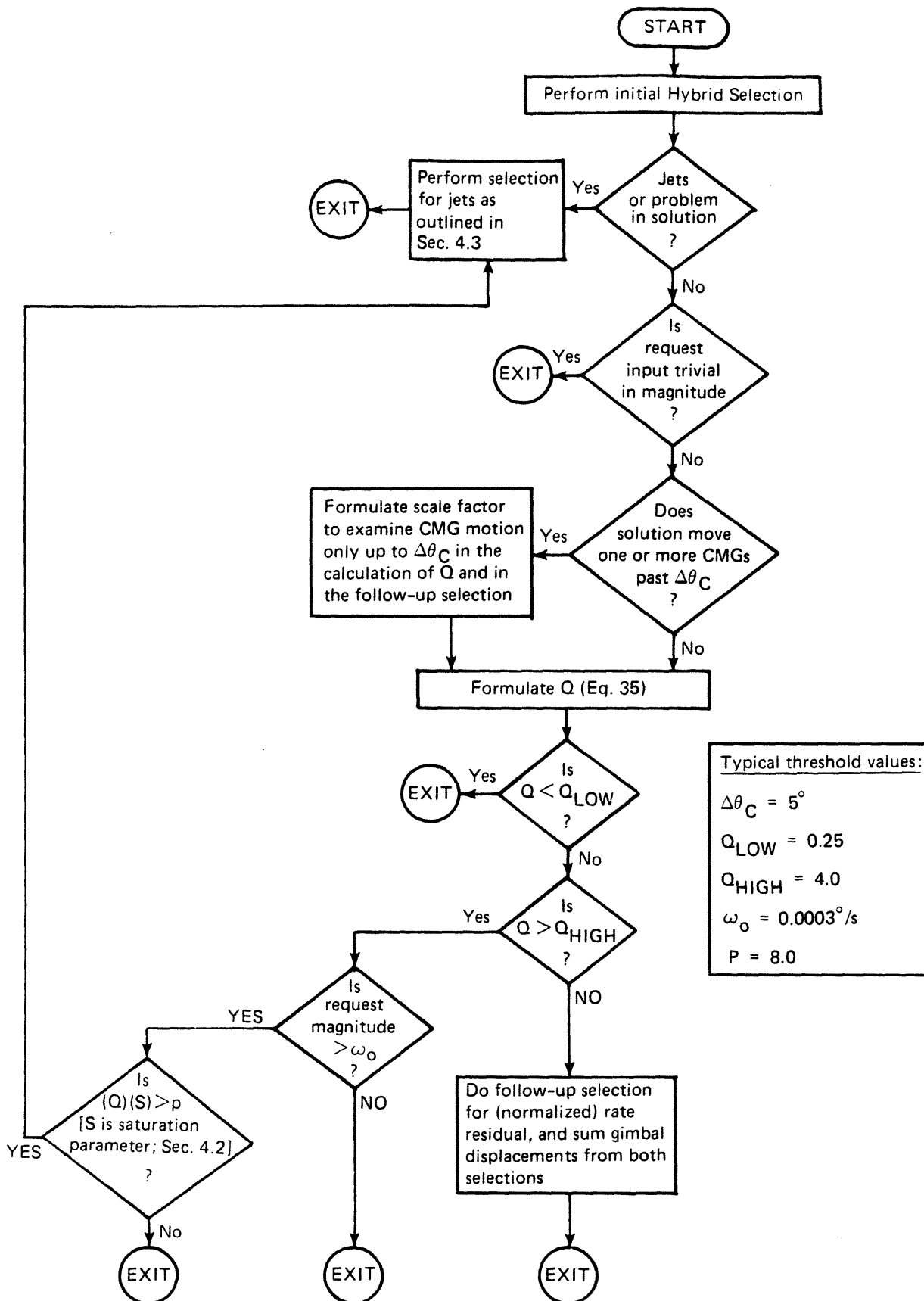
FIGURE 14: LOGIC FLOW FOR HYBRID SELECTION SUPERVISOR

for further "update" selections made during CMG rotation is generally eliminated. In cases where $Q > Q_{High}$, the non-linear effects contribute so heavily that a second-order solution will provide little (if any) improvement. In this case (provided that the request magnitude $\left|\frac{\Delta H_R}{}\right|$ is significant), an alternate strategy must be pursued (ie. encourage introduction of RCS jets, change upper bounds, etc.).

Rotational considerations have been seen to have greater effect as the CMGs approach saturation, hence the thresholds Q_{Low} and Q_{High} can be made functions of the saturation index (described below). It must be noted that the techniques proposed in this section are not limited to the simplex CMG selection proposed in this report; the accuracy of any linear selection process (such as pseudo-inverse) may benefit from application of these methods.

4.2) Calculation of the Saturation Index

Since double-gimballed CMGs can be pointed in any orientation (when given sufficient gimbal freedom), momentum saturation is easily detected in an array of such devices when all CMG rotors are seen to be aligned in a uniform direction. A configuration of this sort has delivered all of its momentum along an axis anti-parallel to the sense of alignment, and is unable to contribute further in that direction. The saturation condition is not so obviously recognized in a system including single-gimballed CMGs, since the rotors are constrained to gimbal in planes, thus are seldom able to align along any general direction.

A quantitative index has been developed in order to detect the approach of an arbitrary CMG system to momentum saturation:

36) $S = \left|\underline{h}_f\right| / \left|\underline{h}_m\right|$

Where: $\underline{h}_f$ = Desired final state CMG momentum.

$\underline{h}_m$ = Maximum momentum CMG system is able to project in that direction.

This "saturation index" is a ratio describing the relative distance of the desired final state CMG momentum (difference between present CMG momentum and requested transfer; ie. $\underline{h}_F = \underline{h}_{tot} - \underline{\Delta H}_R$) from the momentum envelope (surface defining the maximum momentum possible for CMGs to project). If $S < 1$, the desired final CMG state is within the envelope, and the system is able to deliver the requested momentum. As S approaches unity, the system nears momentum saturation; if $S > 1$, the requested CMG state lies outside the momentum envelope and can not be attained (indicating the necessity of RCS assistance).

The denominator of Eq. 36 describes the extent of the CMG momentum envelope in the final state direction. With sufficent gimbal freedom, double-gimballed CMGs may be oriented such that the rotors point precisely in the direction of the desired final state, thus are capable of delivering all of their momentum into the desired axis. Single gimballed CMGs, however, may not be able to align their rotors precisely along the desired final state, thus the closest possible alignment is used in calculating their contribution to the momentum envelope. When oriented in such a fashion, single gimballed CMGs can produce a finite momentum component perpendicular to the desired final state. This must also be absorbed by the CMG system, and is accounted for by being subtracted in quadrature from the projected momentum envelope. The calculation of
$\left| \underline{h}_m \right|$ may thus be detailed:

37) $\quad \left| \underline{h}_m \right| = \sqrt{(\underline{h}_p \cdot \hat{h}_F)^2 - \left| \underline{h}_p \times \hat{h}_F \right|^2}$

Where: $\quad \underline{h}_p = \sum_{j=1}^{R} \underline{h}_{p_j}$

R = total CMG rotors in system

$$\underline{h}_{p_j} = \begin{cases} h_{mag_j} \, \hat{h}_F & \text{Double gimballed CMG (both gimbals free)} \\ h_{mag_j} \; \text{unit}[\underline{h}_F - (\hat{\sigma}_j \cdot \underline{h}_F)\hat{\sigma}_j] & \text{Single gimballed CMG (or double gimballed CMG w. one gimbal failed or pinned against stop)} \end{cases}$$

The vector $\underline{h}_{p_j}$ represents the orientation of CMG rotor #j that has the maximum projection onto the desired final state $\underline{h}_F$. $\underline{h}_{p_j}$ lies precisely along $\underline{h}_F$ for double gimballed CMGs, while the projection formula detailed above is used to determine the closest alignment with $\underline{h}_F$ for single gimballed CMGs. The maximum projection vectors are calculated for all rotors and summed to yield the net momentum of the saturated CMG state $(\underline{h}_p)$. The first term in the radical of Eq. 37 represents the component of $\underline{h}_p$ in the direction of the desired final state $\underline{h}_F$. The component of $\underline{h}_p$ which is orthogonal to the final state must also be absorbed by the CMG array in order to point the total momentum along $\underline{h}_F$. This orthogonal component is expressed in the second term of the radical; it is subtracted in quadrature from the parallel component in order to yield the corrected maximum momentum $|\underline{h}_m|$ which can be used in Eq. 36 to calculate the saturation index (S).

The quadrature subtraction discussed above is an approximation; since the orthogonal component of $\underline{h}_p$ must be absorbed by the CMG system, it should also be projected onto the rotor planes in the fashion discussed above (thus we are led to a series of recursive operations). Since the component of $\underline{h}_p$ orthogonal to $\underline{h}_F$ is usually much smaller than its parallel projection, the correction is generally sufficently small that the orthogonal component is readily absorbed by the CMG system, and the quadrature approximation is warranted. Only single gimballed CMGs contribute to the orthogonal term; it is zero for double gimballed devices.

By allowing the upper bound "L" (placed on gimbal displacement in Eq. 29) to vary as a decreasing function of the saturation index, one may account for momentum saturation in the CMG selection process. If the input request will produce a final CMG state which approaches saturation, the ratio S nears unity and the bound L is dropped accordingly, allowing the CMGs less authority. S becomes smaller if the request will move the CMGs away from saturation, hence L increases, and more CMG activity is encouraged.

When the CMGs approach saturation, the upper bounds on angular displacement will be reduced (via the above logic), CMG costs will be high (via the anti-lineup contribution), and the CMG decision variables resulting from any solution must be exceedingly large (ie. the saturation state is singular). Reaction control jets will then become competitively priced and will automatically appear in simplex solutions.

4.3) RCS Interface

Because of their much higher objective values, jets are not selected by simplex unless translational control is desired, or a situation arises such as sketched above. Since the jets are so expensive and have much more control authority, the hybrid solutions to rotational requests often consist of very short RCS pulses coupled with extensive CMG activity. Such solutions are unphysical and problematic for several reasons, ie. nonlinearities introduced as CMGs gimbal over large angles, and the lower limit imposed on the duration of jet firings. These solutions also result in the transfer of all CMG momentum before resorting primarily to the reaction control system (which leaves the CMGs momentum saturated upon finishing the operation; certainly an undesired feature). Non-neglegible attitude errors can also occur under these realizations of hybrid maneuvers; RCS firings can deliver a momentum impulse very quickly (ie. on-time of the jets concerned), whereas extensive CMG motion requires a considerably larger interval as the CMGs gimbal over sizable angles to transfer the extra momentum needed to

complete the request. Attitude errors can accumulate during the period between completion of the jet firings and acquisition of the desired CMG state.

These difficulties are avoided by repeating the linear selection whenever jets and CMGs have been specified together in the original simplex solution. The second selection is performed with considerably reduced upper bounds on CMG gimbal displacement and lower RCS objective "costs". The maximum allowed gimbal displacement puts a ceiling on the amount of CMG involvement in answering the input request; by reducing this quantity, we restrict the CMGs from moving over large angles and thus limit the influence of nonlinear effects. CMGs are thus confined to a "trimming" role, and the primary maneuver is performed by "solid" jet firings (with non-trivial on-times).

In contrast to the much larger RCS cost, all CMGs appeared similarly priced in the original selection, and CMG useage did not discriminate between "favorable" and "unfavorable" rotations. In the second selection, the RCS cost is adjusted to the current mean CMG cost (after accounting for the reduced CMG control authority), thus the "cheaper" CMGs are encouraged to be used along with jet firings. This results in an effective "desaturation" tendency, where hybrid RCS/CMG operations often leave the CMGs in a lower cost (ie. more favorable) orientation.

When the CMG system is removed from saturation, finite upper bounds are still maintained on gimbal displacement. If a large rotational request is input to the selection procedure, those bounds can encourage the introduction of reaction control jets (even when the CMG system is unsaturated), which can instigate a re-selection (as discussed above) that prevents the CMGs from extensively responding to a request which would bring them into saturation. Such bounds may be expressed by a relation such as:

38) $L = L_o - S L_1$ (Referencing the "L" convention of Eq. 29)

If the system is removed from momentum saturation, S (as in Eq. 36) will be small, and the upper bound is determined by L_0. As the CMGs approach saturation, S increases, and the upper bound drops. The term L_0 represents an intrinsic limit to the control authority of each device (abstractly corresponding to torque saturation), and the L_1 factor reduces the bound to account for the increasingly limited transfer possible when momentum saturation is approached.

One may often avoid the requirement of a second simplex selection by consulting the saturation index discussed in the previous section to anticipate the need for RCS assists. If both the RCS costs and CMG upper bounds are appropriately adjusted in correspondance to the saturation index (in a form similar to Eq. 38), the primary solutions containing mixtures of CMGs and jets can be made realistic, and no re-selection will be necessary. In the software package used by the simulations presented in the following sections, the re-selection process is always performed wherever jets are detected in a solution; the single-selection logic illustrated in this paragraph is under development for implementation in future software generations.

4.4)   Null Motion

The process termed "Null Motion" re-distributes all CMG gimbals into a more favorable orientation (re. inner gimbal angles, stops, and lineups as discussed in Chapter 3) without transferring momentum to the host spacecraft. Gimbal rates derived through null motion are required to be superposed with those calculated via a pseudo-inverse in response to an input request, otherwise the system is ignorant of lineups, gimbal stops, etc. and will be drawn into singular states (see Sec. 2.3). Simplex selection is made with respect to an objective function which accounts for the effects incorporated by null motion; much of the preceeding material described how gimbals are commanded to attain input requests while avoiding configurational difficulties. Situations may arise, however, where a null capability might prove desirable under

67

simplex; ie. when the CMG system is initialized in a poor orientation. The present simplex selection process will only re-orient the CMGs in answer to finite input requests; one can not command it to bring the CMGs into an "optimal" configuration without torquing the spacecraft. As described below, a straightforward means of adapting simplex to accomodate null motion has been developed.

One would hypothesize that the simplex logic could be applied to attain null motion by invoking the selection procedure with a small or zeroed rate-change request. The simplex process, however, is structured to select CMGs such that the objective function is minimized; the optimal solutions to requests of trivial magnitude will create little (if any) CMG activity (since all objective coefficients are positive, the optimal solution to a zero input request is zero CMG displacement).

One may overcome this difficulty by re-formulating the objective function, which dictates the means of moving the CMGs to attain an improved configuration (as was detailed in Chapter 3). Each CMG gimbal possesses two objective coefficients corresponding to forward and backward rotation. Both coefficients are positive; if one is lower, gimbal rotation in the corresponding sense will bring the CMGs into a superior orientation. Under the null motion procedure, a bias is subtracted from each set of coefficients such that they form a bipolar pair centered about zero, ie.:

$$D_c \equiv (c_j^+ + c_j^-)/2$$

39)
$$c_j^+ = c_j^+ - D_c$$

$$c_j^- = c_j^- - D_c$$

The negative cost factors indicate that selection of their corresponding activity vectors is not only preferred, but encouraged. When simplex now solves the minimization problem, it will attempt to bring the activity vectors with negative objective coefficients into the solution with the combination of decision variables that maximizes favorable CMG motion while maintaining the equality constraint (zero rate change). With liberal upper bounds placed on angular displacement, such solutions can prescribe excesive gimbal swings, which degrade their accuracy. Upper bounds are thus tightened in calls to null motion in order to keep the resulting gimbal displacements within tolerable limits (bounds on the order of 10 degrees are used). There are usually many solutions within this constraint that satisfy the small rate change requests which are typical under null motion. Simplex will converge to the solution which creates the minimum objective evaluation (Z, Eq. 6).

The absolute "optimality" of a CMG configuration can be reflected in the sum of the resulting objective coefficients:

$$40) \quad \eta = \sum_{j=1}^{N} (c_j^+ + c_j^-)$$

The terms c_j^+ and c_j^- are positive coefficients (ie. not processed through Eq. 39). A large value of η indicates a problematic CMG configuration; a much lower η is evaluated for ideal CMG orientations. Application of a valid null solution should result in a smaller value of η after CMG displacement.

The amount of gimbal displacement permissable per null selection is dictated by the upper bounds. Null selections are iterated such that the net cost η is decreased and the system is moved into an improved orientation over a series of discrete steps. A global "Null Controller" keeps track of the change in η after each null iteration; when η ceases to exhibit an established decrease between null steps, the system is assumed to have attained a "best" orientation, and the null process is halted.

In order to avoid halting null motion in a local minimum, the change in η is integrated via a low-pass filter, ie.:

41) $\Delta\eta_F = (\alpha)\Delta\eta_{F-1} + (1-\alpha)\ \Delta\eta_o$

Where: $\Delta\eta_o$ = Change in η between current and previous steps, as calculated via Eq. 40.

$\Delta\eta_F$ = Current evaluation of low-pass filtered $\Delta\eta$.

$\Delta\eta_{F-1}$ = Filtered $\Delta\eta$ as evaluated at previous step.

α = Filter time constant (typically of order 0.9).

The null controller terminates the null motion process when $\Delta\eta_F$ rises above a pre-set negative threshold (ie. slope of $\eta_F(t)$ flattens out or increases). The filtering operation prevents early termination in a sub-optimal minimum; by continuing null operations, the CMGs are generally re-oriented such that the net objective continues to improve until a global optimum is reached and the slope of $\eta(t)$ persistantly levels out.

Logic has been integrated into the test controllers to request null motion when the net CMG cost has risen by a pre-set threshold over the cost evaluated at the conclusion of the last null motion attempt. Null motion may also be operator-invoked when desired (ie. to improve an initial CMG orientation, etc.).

The null motion procedure is monitored by software resident in the test controllers (as described in the following chapters). Small perturbations in the spacecraft rates (caused by the effect of cross coupling on the equality constraint) are subtracted from the succeeding null request; the null motion process thus always compensates for errors in the vehicle rate.

The rate-change requests under null motion are generally near (or exactly) zero. Simplex, however, can have difficulty starting with a trivial request vector (R; see Eq. 12). In order to start the exchange

process, simplex is initiated with the most favorable (ie. lowest cost) activity on at its upper bound. This creates a finite $\underline{R}$, causing simplex to bring on as many favorable activity vectors as possible while maintaining zero net momentum transfer.

One needs at least four independent CMG gimbals to perform null motion under three-axis control. As momentum saturation is approached, less freedom is available to the system, hence null motion capability is greatly reduced. If a null selection returns with jets or imaginary startup vectors in the solution (or produces the trivial solution of zero CMG motion), it is assumed that no null motion is possible, and the null procedure is terminated. The jet-assisted desaturation process (as described in the following section) can then be invoked to nudge the CMG array away from saturation and into a superior configuration.

Both null motion and normal maneuver requests work to "optimally" steer the CMG system. Conventional maneuver requests (solved with positive objective coefficents) re-distribute the CMGs in an "optimal" fashion while the request is being satisfied; the amount of re-distribution is related to the magnitude of the request. Null maneuvers try to orient the CMGs into a better orientation regardless of the request size; favorable CMGs are always moved as far as possible. By setting the objective coefficents negative (as in Eq. 39) during selections for normal maneuvers, all solutions would contain a considerable "null" CMG re-distribution component. The larger gimbal displacements allowed during normal maneuvering (to enable CMG resolution of nominal rate-change requests) imply the imposition of larger upper bounds than the restrictive ten degrees set during null motion. If one increases the upper bounds during a selection made with negative objective coefficents, simplex will still generally pick solutions with the CMGs responding "en masse" at their newly expanded limits. As mentioned before, nonlinearities degrade the accuracy of these types of solutions, and the "neater" results obtained by using positive objective coefficents are much more conducive to implementation. Both types of selections are thus performed independently; nominal maneuver requests are answered by optimal selections made under a positive set of objective

coefficents, while null motion is calculated when necessary for CMG re-distribution and is implemented by iterating selections using bipolar objective coefficents in a series of limited steps.

4.5)   Jet-Assisted Desaturation

The null motion scenario discussed in the previous section described how the objective factors indicate a means of moving the CMG ensemble into an orientation of lower net cost (η). By requesting a zero net rate change, the redistribution is accomplished without transferring momentum into the host spacecraft. The possibilities for null motion decrease as the CMGs approach saturation; momentum must then be dumped into the spacecraft via another system in order to move the CMG array into a less severe state. This may be accomplished over long time periods through techniques of momentum management[30], where the vehicle is commanded into a state acted upon by environmental torques which introduce angular momentum into the spacecraft appropriate for removing the CMGs from saturation. A more immediate means of desaturating the CMGs is provided by the Reaction Control System; jet firings change the momentum state of the spacecraft, which enable the CMGs to pull away from saturation.

This process can easily be accomodated by allowing RCS jets to be chosen in the null motion selection. Jet costs are reduced (but still kept positive) such that jets are priced competitively with CMGs (as discussed in Sec. 4.2). All other factors are as described in Sec. 4.4; ie. CMG costs are made bipolar as in Eq. 39, the rate-change request is set to zero, upper bounds are reduced, etc. The resulting solution maintains a zero net rate change, and consists of jets used in conjunction with CMGs (primarily negative-priced). This moves the CMG system into a lower-cost orientation at the expense of RCS fuel. The objective function (Eq. 30) contains several terms which participate in the desaturation process; in addition to moving the CMG rotors away from the total saturation lineup, CMGs are pulled off stops and inner gimbal angles are decreased. The process is halted when no further improvement is seen in η_F (as with Eq. 41 and associated discussion). The system is commanded to hold a constant rate throughout the operation.

72

Since simplex finds an optimal solution which burns a minimum amount of RCS fuel in order to lower CMG costs, the performance of this variety of RCS-assisted desaturation procedure can be influenced by the ratio of mean jet to CMG cost factors. Initial tests have been conducted, and are presented in Chapter 5.

CHAPTER 5

SIMULATION EXAMPLES: HYBRID SELECTION DRIVEN BY
RATE-FEEDBACK CONTROLLER

5.1)   The Rate-Feedback Controller

A simple vehicle rate-feedback controller has been developed in
order to test the behavior of the hybrid steering/selection procedure
described in the previous chapters. The controller drives the selection
package to achieve an input vehicle rate-change sequence; the resulting
gimbal rates are normalized to their peak values (as in Eq. 27) such that
the vehicle rate requests are achieved as quickly as possible. Each
request in the input stack is treated independently; as soon as a request
is resolved, the controller drives the selection package with the next
request in the sequence.

By loading the input stack with different request sequences, one
can quickly push the CMG ensemble into various difficult situations (ie.
saturations, gimbals against stops, lineups, etc.), and examine the
behavior of the selection principle under a variety of conditions. Since
the computational requirements of this control package are quite modest,
it provides a quick and economical means of exercising the operation of
the hybrid selection/steering procedure.

The structure of the rate-feedback controller is shown in Fig.
15. Upon initialization, either a vehicle rate-change vector is accepted
from the input stack (in the nominal case), or the desired rate change is
set to zero (in the case of null motion). A desired vehicle rate
$(\underline{\omega}_\delta)$ is then established by summing the current vehicle rate
$(\underline{\omega}_{now})$ with the request vector $(\underline{Rq})$ and the rate residual $(\underline{\Delta R})$ left

START

Rg = 0
Set parameters
for null selection

Flag
set for
null motion
?

Yes

No

Rg = Next vehicle rate-change
request in input sequence

ωDesired = ωNow + Rg + ΔR

R = ωDesired - ωNow

Call hybrid selection with
rotational rate-change
request "R"

If
null motion
is active, and null
abort is indicated by
either hybrid
selection or
cost filter

Then

Reset
Null
Flag

Else

Step vehicle environment by
ΔT = 80 ms
(Update ωNow and CMG
positions, fire jets)

ΔR = ωDesired - ωNow
D_p = D
D = ΔR

D < D_{min}
?

Yes

No

D - D_p > D_{max}
?

Yes

No

Δu_i > Δu_{max}
?

Yes

No

More
requests
left in
sequence
?

Yes

No

STOP

Calculate current CMG costs

Flag
set for
null motion
?

Yes

No

Accumulate
cost filter
(Eq 41)

Have
lineup or
stops cost risen
appreciably since last
null attempt
?

Yes

Set flag to request
null motion before
next input request
is processed

No

Have
lineup or
stop costs
risen appreciably
since last
selection
?

Yes

No

Have
jets stopped
firing and CMGs
stopped moving
?

Yes

No

FIGURE 15   LOGIC FLOW FOR THE RATE-FEEDBACK CONTROLLER

76

from the previous maneuver. Since $\underline{\omega}_\delta$ is not varied until the next maneuver cycle, the input request for the hybrid selection ($\underline{R}$) is always defined as the difference between desired and current vehicle rates.

A model of vehicle response is consulted to update $\underline{\omega}_{now}$ in time increments of 80 msec (this corresponds to the DAP cycle time onboard the Shuttle orbiter; much of the software was originally Shuttle-oriented). This model incorporates[29] a group of "ideal" CMGs; control torques due to gimbal rotation and "passive" torques arising from vehicle rates (ie. $\underline{\omega}_s \times \underline{h}_{tot}$) are included, while higher-order CMG dynamic effects (gimbal acceleration torques, friction, servo behavior, etc.) are ignored. Since the controller was designed not to produce a detailed vehicle simulation, but rather to economically push the CMG system to extremes, the present model takes no account of environmental effects (ie. gravity gradient or aerodynamic torques); only vehicle Euler coupling (ie. $\underline{\omega}_s \times [I] \underline{\omega}_s$) is incorporated.

The rate residual is calculated after every pass through the vehicle simulation. If its magnitude (D) is below a pre-set threshold (D_{min}), the desired rate is assumed to be attained, and the next sequential request is fetched. If the difference between the current magnitude of the residual and that attained over the previous step (ie. $D - D_p$) is greater than a maximum threshold (D_{max}), the vehicle rate is assumed to be diverging significantly from its desired value. In this case, the linear approximations used in the equality constraint (Eq. 6) are no longer deemed valid, and an update selection is forced.

The software that models the vehicle environment also propagates CMG rotor positions and gimbal angles over the 80 msec. simulation time step. A new hybrid selection is forced if a gimbal angle displacement ($\Delta\theta$) is found to have exceeded a pre-set maximum ($\Delta\theta_{max}$) since the previous selection was performed.

If the logic flow has passed these conditionals without meeting the criteria for re-selection, updated CMG objective contributions are calculated (as described in Chapter 3). A new CMG selection is forced if

the net CMG lineup, stops, or inner gimbal costs are seen to have risen appreciably since the last selection. A new CMG selection is also deemed necessary if the vehicle is seen to be sitting "idle" without jet firings or CMG motion (ie. actuators have completed their commands) and the vehicle rate has still not converged to its desired value.

If all cuts mentioned above have been passed without invoking an updated selection, the vehicle environment is stepped by another 80 msec., and the resulting situation is similarly scrutinized. In this fashion, CMGs are allowed to coast on their selected trajectories until the desired vehicle rate is attained, the rate residual grows appreciably worse, a maximum allowed angular displacement is reached, a stop or lineup is critically approached, or the actuators have completed their commands without having achieved convergence.

Since the CMG gimbal rates are normalized to a peak value (Eq. 27), the gimbals are driven to realize the rate-change solution as quickly as possible (ie. at the highest torque). This can produce a slightly discontinuous appearance in plots of the time-dependent CMG behavior, especially when coupled with the way in which the CMGs are allowed to coast with constant gimbal rates until a re-selection becomes necessary (vs. frequent iteration of CMG selections over a constant time step), and considering the fact that a new request (which may occur in an entirely different direction) is "instantly" fetched upon the completion of its predecessor. A smoother CMG response would be seen if the "linear" CMG gimbal rates of Eq. 28 were applied instead of the "saturated" gimbal rates calculated in Eq. 27, and if the CMG selection was forced to be iterated more frequently than under the "coast-until-problem" tactics described above. The hybrid selection process is easily amenable to all of these approaches. Again, it must be stressed that the rate-feedback controller was constructed for the express purpose of examining the behavior of the hybrid selection after forcing a simulated CMG configuration quickly into a variety of challenging situations. It is thereby structured only to exercise the

steering/selection law, and is not designed for application as an actual vehicle controller.

The rate-feedback controller takes no account of vehicle attitude; as noted in Fig. 15, it drives the CMGs and jets only to attain a desired rate. Coordinated attitude/rate control is accomplished via the phase space controller to be presented in Chapter 7. The software of Fig. 15 considers only rotational dynamics; translational control is not provided in these tests.

Fig. 15 also indicates portions of the logic flow which have been adapted to accomodate null motion (Sec. 4.4). When operational, the null process sets the input request R_q to zero, checks for an abort or cost plateau after each hybrid selection, and updates the cost filter (Eq. 41) after each 80 msec. time step. If, during normal maneuvering, the net cost is seen to have risen significantly over the cost calculated at the conclusion of the previous null attempt, a flag is set which requests null motion (when enabled) at the close of the current operation. Null motion (or jet-assisted desaturation; Sec. 4.5) may also be operator-requested at a pre-specified elapsed time.

5.2) Test Setup and Parameters

All tests use rigid-body simulations of the Power Tower Space Station[2] (mass properties given in Table 1), which is assumed to be controlled by an array of four double-gimballed CMGs. Except where explicitly noted, the CMG configuration used in the following tests appears as in Fig. 16b, which depicts the initial orientation of the CMG rotors. The mounting configuration was derived from the convention used in Skylab[31] (three CMGs initially perpendicular), with a fourth added skewed at equal angles to each of the others. Fig. 16 shows the CMG setup relative to the Power Tower coordinate axes. The configuration of Fig. 16 is not proposed as a "best" CMG mounting protocol, but has been used consistantly throughout development of the related algorithms and software, thus serves as a standard through which performance comparisons
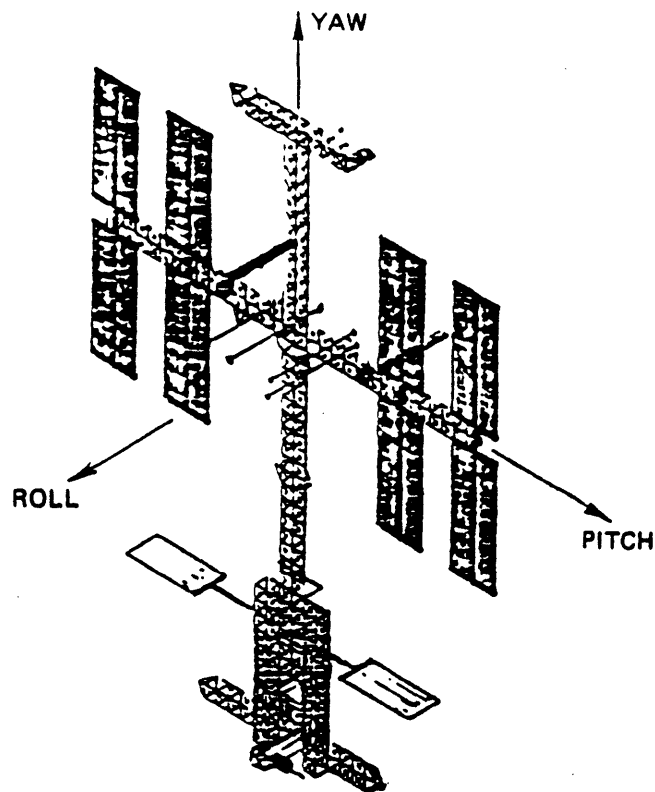
(a) POWER TOWER SPACE STATION
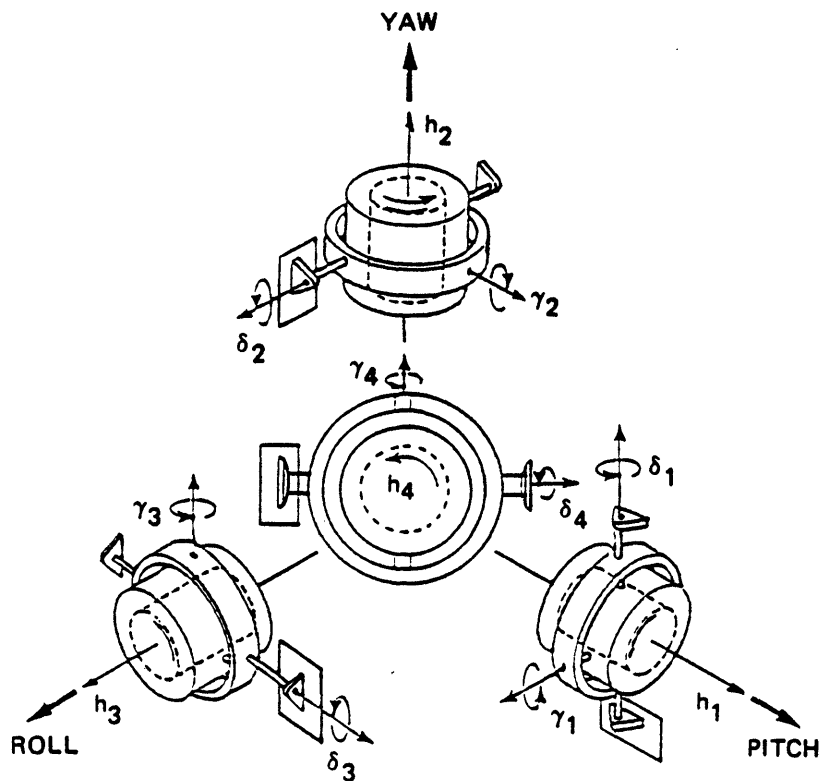
(b) INITIAL CMG ORIENTATION

FIGURE16: ORTHOGONAL MOUNTED CMG CONFIGURATION

can be established. A direct advantage of the steering principle proposed in this text lies in the ability to easily define any CMG mounting orientation (and change it dynamically if desired); the software is by no means tied to the Skylab-based mounting used in these tests (as will be demonstrated in Sec. 5.4). This contrasts with other steering laws (ie. Ref. 16), which exploit configurational symmetry to simplify calculations, thus are bound to particular mounting schemes.

The CMG hardware parameters are derived from specifications[32] of the devices proposed for use on the Power Tower, and are summarized in Table 1. The kinematic model described in Ref. 29 is used to simulate CMG behavior. "Ideal" CMGs are assumed, and higher-order dynamic effects (Sec. 2.3) are not currently included.

The Power Tower is assumed to possess 12 RCS jets, which operate at a nominal thrust of 75 lb each, and are clustered into mutually orthogonal triads located at four positions on the spacecraft (as depicted in Fig. 17 and described in Ref. 33). Due to the lack of detailed specifications on hardware intended for the Power Tower, RCS jet firings are not rounded or quantized into discrete values in the simulations presented throughout this chapter; jets are assumed to be constant-torque devices capable of achieving continuous firing intervals (nonetheless, the re-selection process presented in Sec. 4.3 generally results in "solid" jet firings with non-trivial on-times). Real jets are constrained by minimum burn times and substantial control granularity[25]; the tests presented in Chapter 7 (which use a more detailed vehicle environment) take these effects into account. No discrete "software switch" is employed to select RCS jets; they are prescribed and selected by simplex through the methods of Sec. 4.3.

The logic of Fig. 14 (and Sec. 4.1) was applied to manage nonlinear cross coupling effects. CMG selections were usually seen to be adequate without an additional follow-up, however convergence was often made more rapid in cases where the need for the second selection was indicated. Null motion and jet-assisted desaturation are not enabled unless explicitly noted.

YAW

ROLL

PITCH

REACTION
CONTROL
JET
CLUSTERS
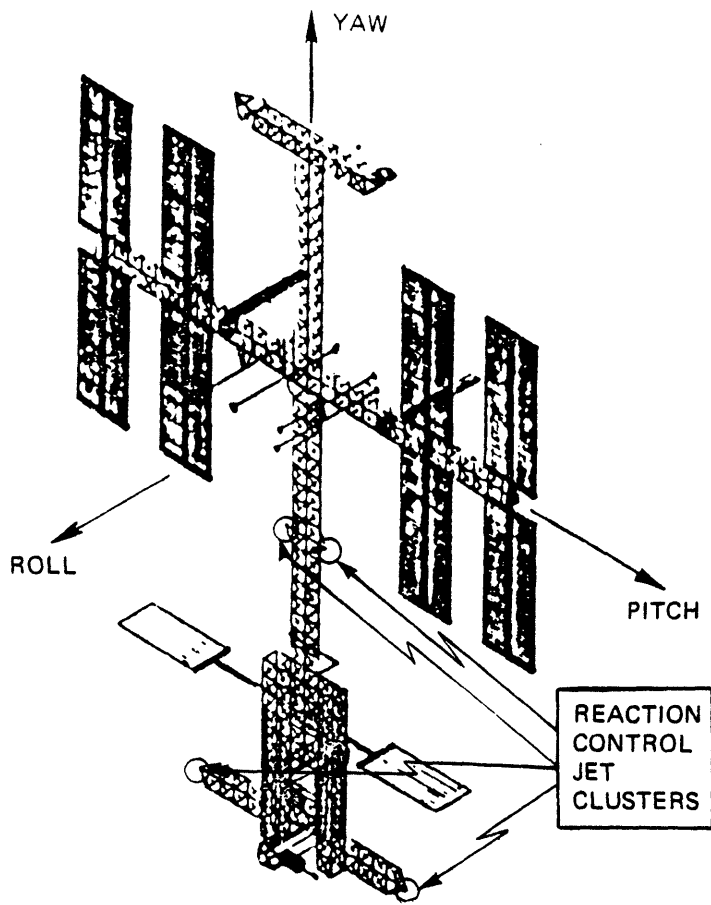
FIGURE 4: (a) POWER TOWER SPACE STATION

2

3

20'

5

1

6

100'

4

8

9

CM

70'

7

11

67.5'

12

10
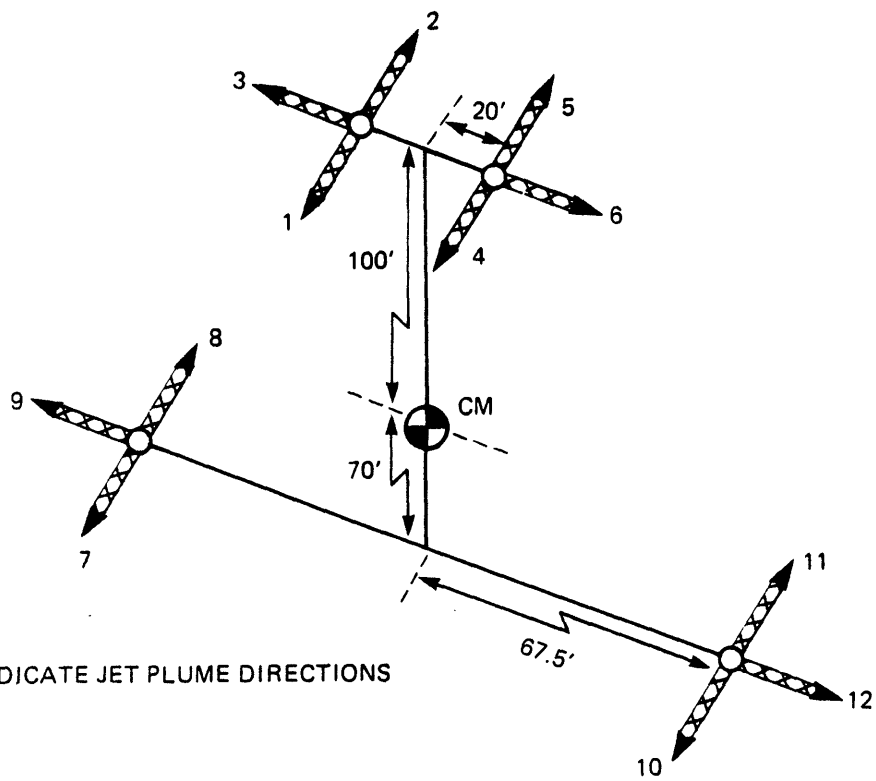
ARROWS INDICATE JET PLUME DIRECTIONS

(b) JET LOCATIONS

FIGURE 17: LOCATION OF RCS THRUSTERS

82

Hardware parameters used in the simulation and software constants required by the control and steering algorithms are summarized in Table 1. The controller pursues each request until it achieves the desired rate to within 10^{-4} deg/sec. All tests are initialized with zero inertial vehicle rates.

TABLE 1

CMG Control and Simulation Parameters

Definition	Value	Symbol

CMGs:

Definition	Value	Symbol
Angular momentum per rotor	3500 ft-lb-sec	h_{mag}
Peak gimbal rates	5 deg/sec	$\dot{\gamma}_p$, $\dot{\delta}_p$
Inner gimbal stop location	+/-90 deg	θ_s
Outer gimbal stop location	+/-∞ (ie. unlimited freedom)	

Linear Selection:
(the values listed below are typical)

Definition	Value	Symbol
Cost Factor; Singularity avoidance	850	K_L
Cost Factor; CMG stops	30	K_S
Cost Factor; Inner gimbal angle	10	K_A
Cost Factor; Minimum Δt (bias)	0.1	K_0
Cost Factor; Jets	10^8	K_{jet}

Feedback Control:

Accepted rate-change residual (convergence limit)	10^{-4} deg/sec	D_{min}
Rate-change divergence limit (for first three 80 msec. steps)	10^{-4} deg/sec	D_{max}
Rate-change divergence limit (thereafter...)	0	" "
Maximum allowed CMG displacement before forcing update selection	30 deg	θ_{max}

Power Tower Mass Properties:
(without payloads, no docked vehicles)

Vehicle Mass		8518.7 slugs	M_s
Vehicle Inertias (about center of mass)	Roll:	72.8174×10^6 slug-ft^2	I_{xx}
	Pitch:	69.8595×10^6 slug-ft^2	I_{yy}
	Yaw:	5.5683×10^6 slug-ft^2	I_{zz}
		-0.5217×10^6 slug-ft^2	I_{xz}
		0	I_{xy}
		0	I_{yz}

Each section below is dedicated to a series of tests (employing different run conditions) which drive the CMG array with an identical sequence of input rate-change requests. The particular input sequence used is summarized in the section title and detailed in the introductory text.

5.3) Demonstration of Lineup Avoidance and Inner Gimbal Minimization

This set of test runs directly demonstrates the performance of the lineup avoidance component of the objective function. The CMGs were initialized as depicted in Fig. 16. A series of small rate-changes were then input to the feedback controller. Each request was made proportional to the instantaneous activity vector associated with the outer gimbal of CMG #2, in order that the minimum-time solution to the linearized constraints would generally involve moving primarily this

gimbal (the magnitude of each request is set to encourage a 6 degree gimbal swing). The process is illustrated in Fig. 18.

Fig. 19 presents results obtained without including an anti-lineup contribution in the objective evaluation (ie. K_L in Eq. 30 is set to zero). The remaining contributions work to reduce inner gimbal swings, avoid gimbal stops (which exist only on the inner gimbal of our modelled CMGs), and otherwise minimize maneuver times. With an input request sequence dynamically encouraging advancement of CMG #2's outer gimbal (as sketched above), we would expect the most favored strategy to involve moving primarily that gimbal and leaving the remainder of the system generally untouched; this agrees with an objective that avoids useage of inner gimbals and prefers the "direct" outer gimbal solution which minimizes maneuver time.

Three plots are shown in Fig. 19; all depict quantites plotted against a common elapsed time coordinate (horizontal axis). Small vertical tick-marks are drawn across the horizontal axis whenever a sequential request is completed.

The upper plot shows the time history of inner gimbal angles for each CMG. Since inner gimbal swings are still penalized in the objective function, inner gimbal angles stay near zero (as predicted above), and very little inner gimbal activity is seen.

The middle plot is an analogous graph showing the time profile of the outer gimbal angles. The scale here is widened by a factor of two; inner gimbals are plotted up to $\gamma = +/-90°$ (gimbal stops are placed at these extremes), while outer gimbals are plotted between $-180° < \delta < 180°$ (there are no stops on the outer gimbals; the curve wraps around to the opposite sign when the plotted limits are exceeded).

Outer gimbals are seen to be more active in Fig. 19 (these aren't explicitly penalized in the objective function used with this test; they are selected only to minimize maneuver time). In particular, the outer gimbal of CMG #2 is seen to answer requests virtually exclusive of other CMGs, as was predicted earlier. This produces the consequence suggested

DYNAMICALLY ADJUST INPUT RATE-CHANGE REQUEST ($\underline{R}$) SUCH THAT IT ALWAYS
IS ORIENTED ALONG THE OUTPUT TORQUE OF CMG #2.

→ CMG #2 ENCOURAGED TO PASS THROUGH ANTIPARALLEL ROTOR
   ALIGNMENT WITH CMG #1
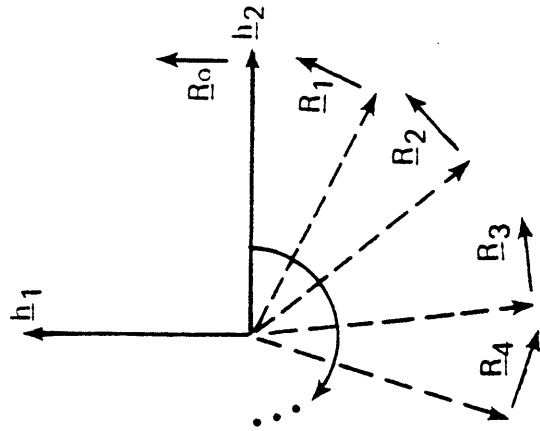
TWO CASES INVESTIGATED:

(1) NO ANTI-LINEUP CONTRIBUTION INCLUDED IN CMG COST CALCULATION

(2) BOTH ANTI-LINEUP AND INNER GIMBAL CONTRIBUTIONS INCLUDED

FIGURE 18: COMMAND SEQUENCE FOR TEST OF LINEUP AVOIDANCE AND INNER
GIMBAL ANGLE MINIMIZATION

INNER GIMBAL ANGLES

OUTER GIMBAL ANGLES
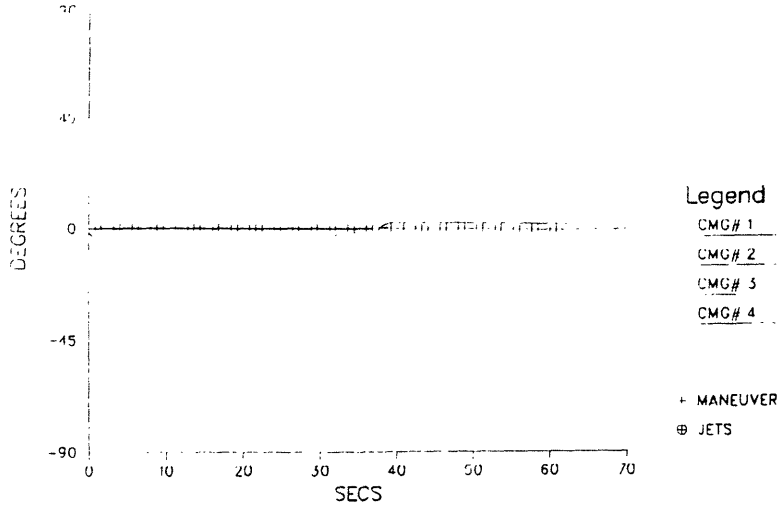
PARALLEL
LINEUP

RELATIVE ANGLES BETWEEN CMG PAIRS PLT#1
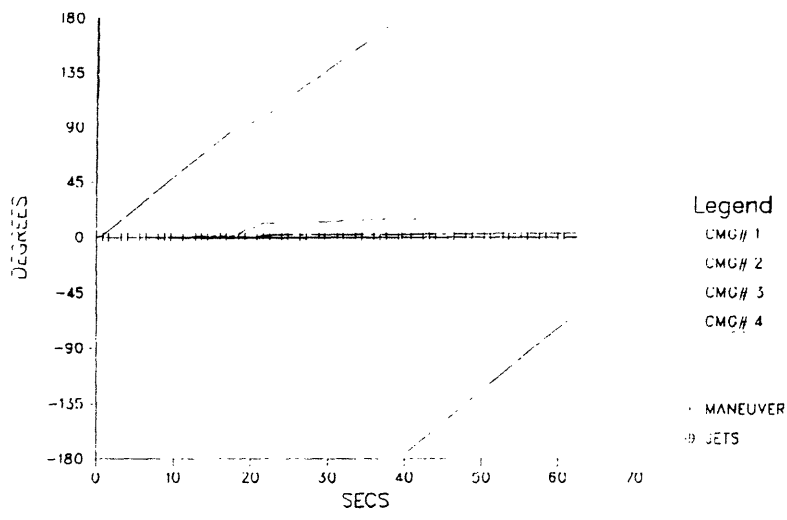
ANTIPARALLEL
LINEUP
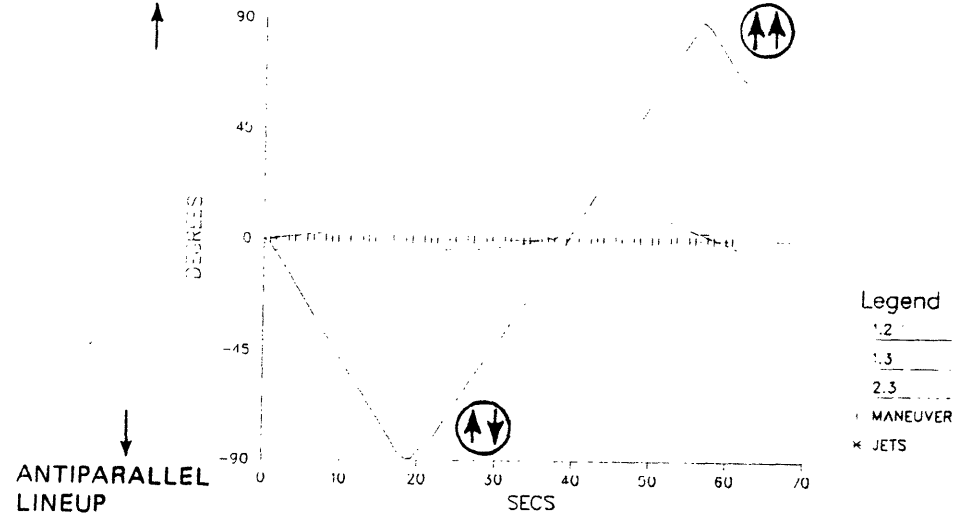
FIGURE 19: Encourage CMG#2 to Move Antiparallel to CMG#1,
No Antilineup in Objective

87

INNER GIMBAL ANGLES

Legend
CMG# 1
CMG# 2
CMG# 3
CMG# 4

+ MANEUVER
⊕ JETS

OUTER GIMBAL ANGLES

Legend
CMG# 1
CMG# 2
CMG# 3
CMG# 4

+ MANEUVER
⊕ JETS

PARALLEL
LINEUP
↑

RELATIVE ANGLES BETWEEN CMG PAIRS PLT#1

Legend
1.2
1.3
2.3
+ MANEUVER
✕ JETS

↓
ANTIPARALLEL
LINEUP
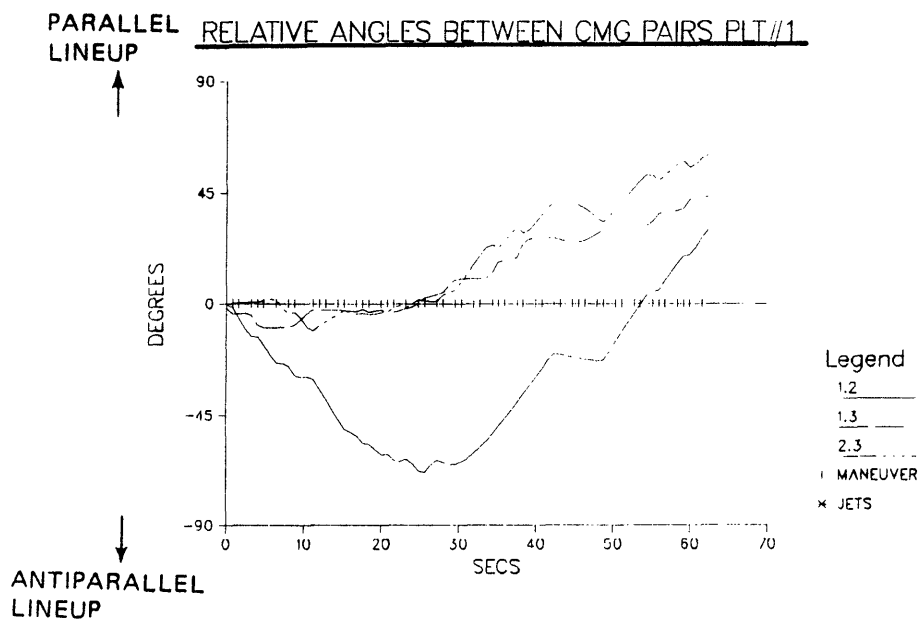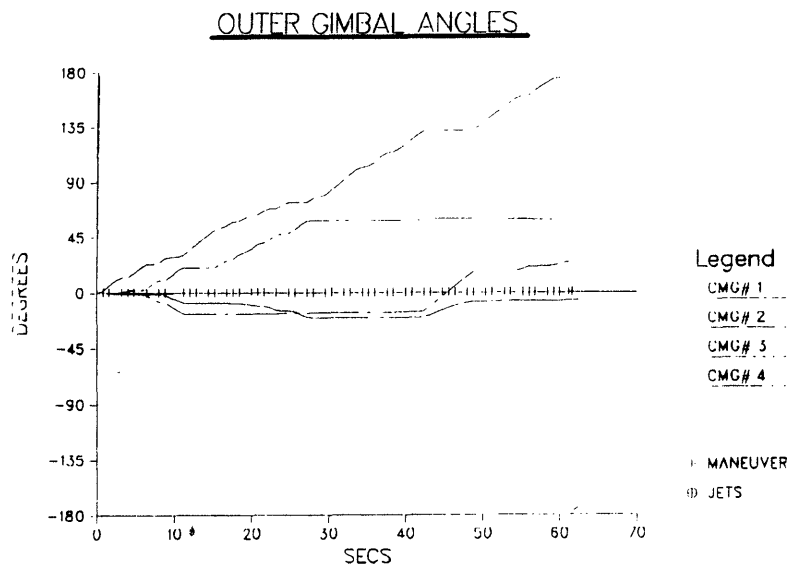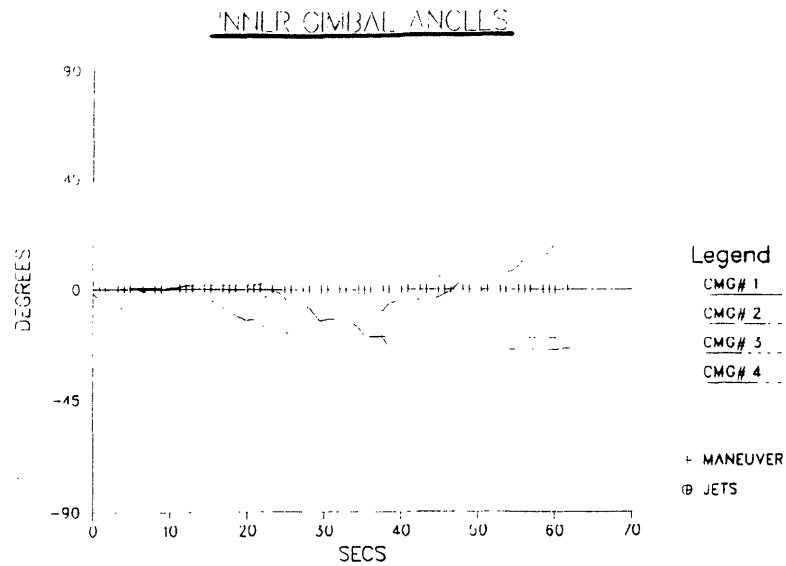
FIGURE 20: Encourage CMG#2 to Move Antiparallel to CMG#1,
Nominal Conditions

by Fig. 18; if CMG #2's outer gimbal is sufficently advanced, the configuration is structured such that the rotor of CMG #2 will enter anti-parallel alignment with that of CMG #1 when the outer gimbal angle (δ) of CMG #2 approaches $90°$. Since the objective function used in this test takes no account of rotor lineups, this scenerio is exactly what takes place.

The lower plot in Fig. 19 shows the relative angles between selected pairs of CMG rotors. The ordinate is specified in terms of the complement of the inter-rotor angles as calculated in degrees (ie. $90° - \cos^{-1}(\underline{h}_I \cdot \underline{h}_J)$). A parallel lineup is indicated when a curve approaches $+90°$ on this plot, an anti-parallel lineup is indicated when a curve nears $-90°$, and the respective CMG rotors are orthogonal (the "ideal" case) when the curve is in proximity to zero.

The particular curve in Fig. 19 that departs significantly from the horizontal axis reflects the time history of alignment between rotors of CMGs #1 and #2. Since they are not moved to avoid the encounter, a near perfect anti-parallel alignment is seen when the δ of CMG #2 reaches $90°$. After CMG #2 is moved by another $180°$, it is seen to reach again an alignment (this time parallel) with CMG #1. As mentioned in Sec. 3.4, control potential can be degraded along the lineup direction in these cases, hence the periods where rotors of CMGs #1 and #2 were aligned represented undesired configurations.

Fig. 20 shows an analogous set of plots from another run made under the same type of request sequence. The full anti-lineup component, however, was included in the objective evaluation (the objective factors of Table 1 were used). Much more inner gimbal activity has occured (top plot), but still no excessive swings are seen, and several other outer gimbals are now being used extensively (middle plot). The reason for this increased activity is evident in the lower plot; all lineups have now been avoided. Even though the input sequence still encourages the outer gimbal of CMG #2 to exclusively answer requests (since they are continually derived from its output torque), other CMGs were selected

89

during the course of maneuvers in order to avoid the lineups encountered in the previous test. The anti-lineup contribution to the objective function has managed the excess degrees of freedom available to the system such that rotor alignments were avoided.

5.4) CMGs Driven With Cyclic Request

In the following tests, the CMGs were driven by a sequence of 27 rate-change requests that were made to cycle through all possible combinations of negative-zero-positive components in all three coordinates. A permutation order was instituted which changed the yaw request component between each consecutive request, altered the pitch component after every three requests, and toggled the roll component after every nine requests. This can be summarized quantitatively:

$$42) \quad \begin{bmatrix} R_{Roll} \\ R_{Pitch} \\ R_{Yaw} \end{bmatrix} = R_o \begin{bmatrix} P(n/9) \\ P(n/3) \\ P(n) \end{bmatrix} = R_o \begin{bmatrix} 1, & 1, & 1, & 1, & 1, & 1, & 1, & \cdots \\ 1, & 1, & 1, & 0, & 0, & 0, & -1, & \cdots \\ 1, & 0, & -1, & 1, & 0, & -1, & 1, & \cdots \end{bmatrix}$$

$$n = \quad 0 \quad 1 \quad 2 \quad 3 \quad 4 \quad 5 \quad 6 \quad \cdots$$

Where:

$$P(x) = \text{"Permutation factor"} = 1 - \mathscr{R}_3(\text{int}(x))$$

$\mathscr{R}_3(m) = $ Remainder of integer division $m/3$

$\text{int} \rightarrow$ Truncation to integer

n = Request index (0 to 27)

R_o = Component magnitude (0.0008 deg/sec. is used here)

The permutation is actually realized via a simple programmed loop; the function $P(x)$ listed above repeats the sequence $\{1,0,-1\}$, and is given only for convenient quantitative description. The first seven steps are expanded on the rightmost side of Eq. 42. R_o is the

magnitude of the non-zero rate-changes requested about each axis (here we set R_0 to 0.0008 deg/sec; this is not a trivial magnitude in contrast to the Power Tower's large inertias). The cyclic request sequence starts and concludes with zero absolute vehicle rates.

Over the span of its orbit, the space station will be subject to environmental torques (gravity gradient and aerodynamic contributions; see Ref. 2). The Power Tower is intended to fly at an average "Torque Equilibrium Attitude", which is offset slightly from the local vertical such that momentum transfers due to the net gravity gradient and aerodynamic torques are made to cancel over an orbit. This produces little growth in secular momentum (thereby warranting the use of momentum exchange devices); residual momentum eventually accumulated due to finite torque mismatch is removed by techniques of momentum management[30] or desaturation (ie. see Sec. 4.5). In order to maintain attitude over an orbit, the CMGs are continuously commanded to counter environmental torques relative to inertial space. While holding attitude at the "Torque Equilibrium Angle", the CMG torque commands indeed produce a primary cyclic series of requests (relative to the orbital period), although the form of the resulting on-orbit request function differs considerably from that of Eq. 42. Future efforts will investigate performance of the selection/steering law under a detailed orbital environment. Until then, a simplified model (ie. Eq. 42) is used to demonstrate the response of the CMG steering process to a cyclic request sequence.

Fig. 21 shows the CMG gimbal angles resulting from this request sequence. This run was made under "nominal" conditions (ie. all CMGs completely operational and all cost contributions included in the objective function). Both inner and outer gimbals are used in answering the requests. No excessive inner gimbal angles were created (again, the inner gimbal scale is magnified by a factor of two over that of the outer gimbal).

INNER GIMBAL ANGLES

Legend

CMG# 1

CMG# 2

CMG# 3

CMG# 4

+ MANEUVER

× JETS

OUTER GIMBAL ANGLES

Legend

CMG# 1

CMG# 2

CMG# 3

CMG# 4
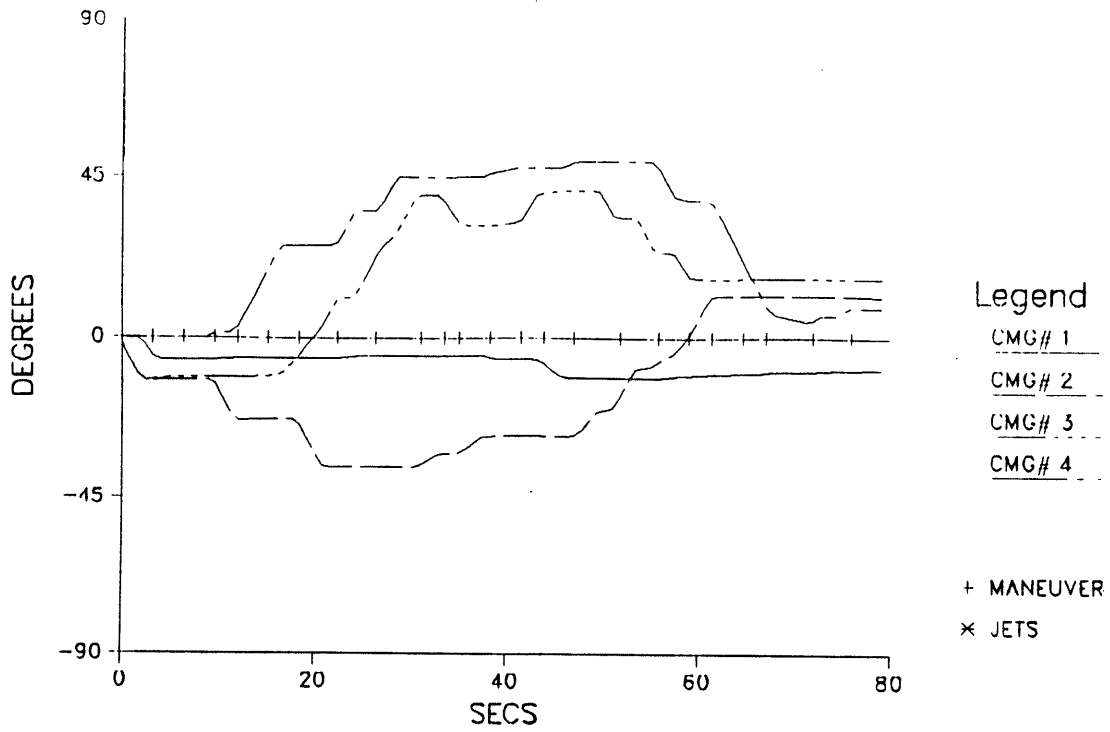
+ MANEUVER

× JETS
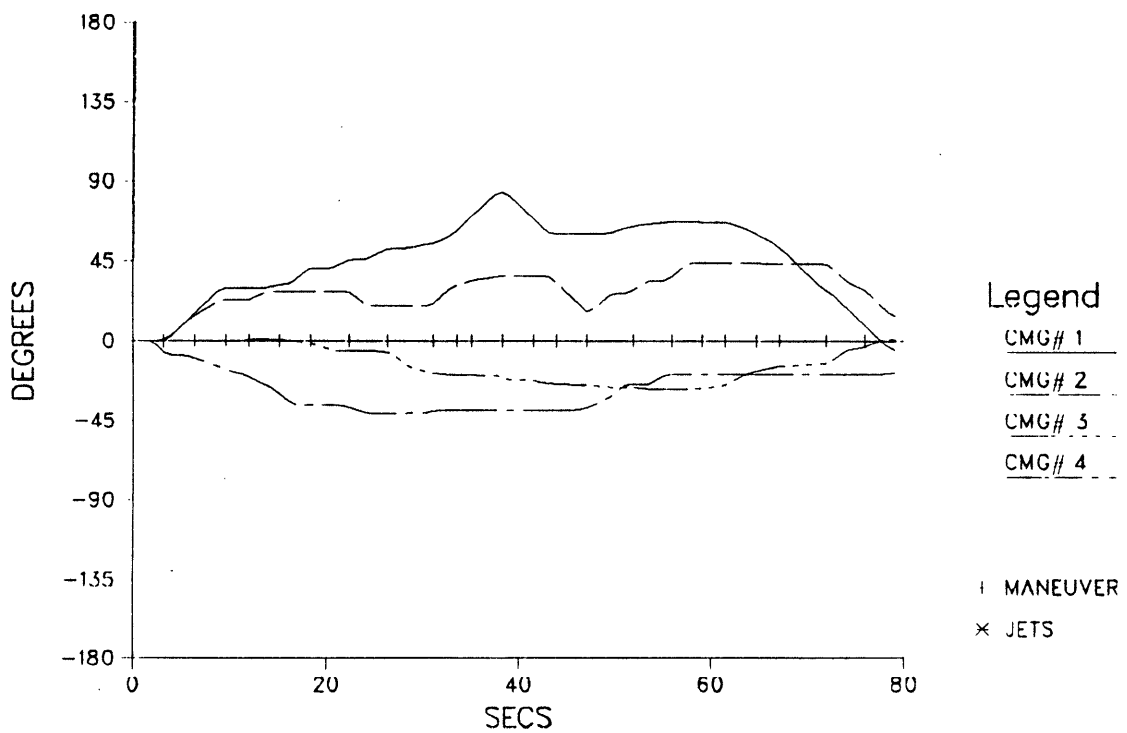
FIGURE 21: Cyclic Maneuver Sequence, Nominal Conditions

RELATIVE ANGLES BETWEEN CMG PAIRS PLT#1

Legend
1.2 _____
1.3 ___ ___
2.3 ... ...
| MANEUVER
× JETS

RELATIVE ANGLES BETWEEN CMG PAIRS PLT#2

Legend
1.4 _____
2.4 ___ ___
3.4 ....
+ MANEUVER
× JETS
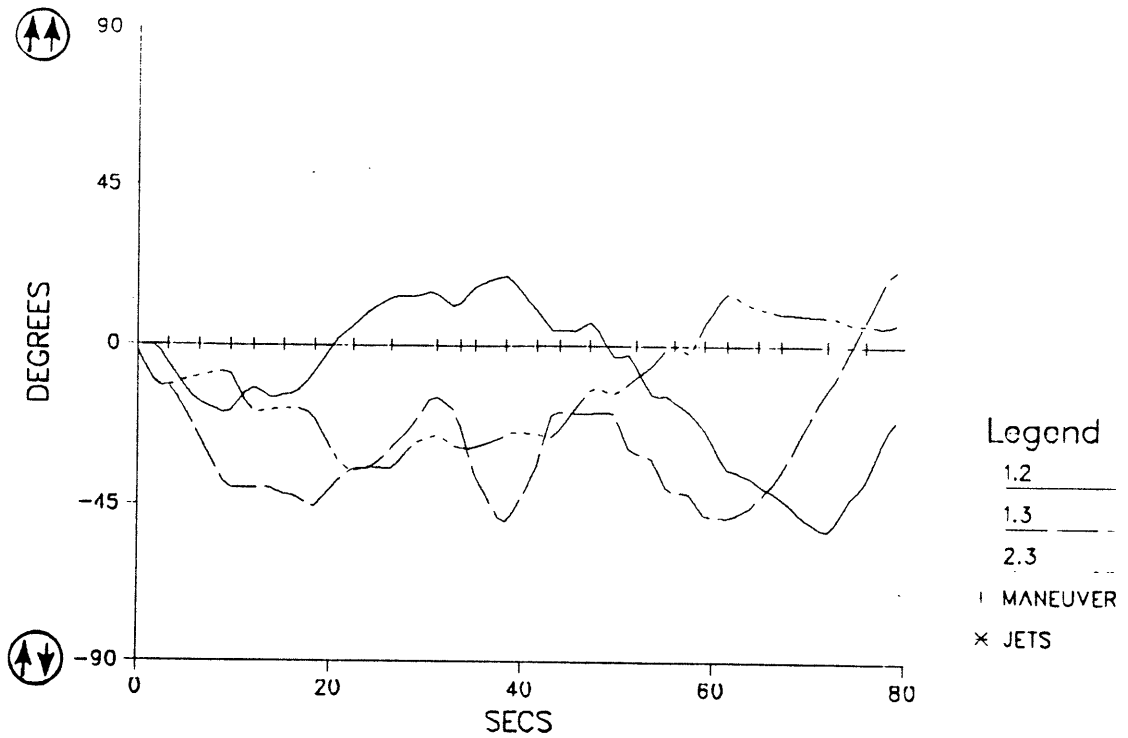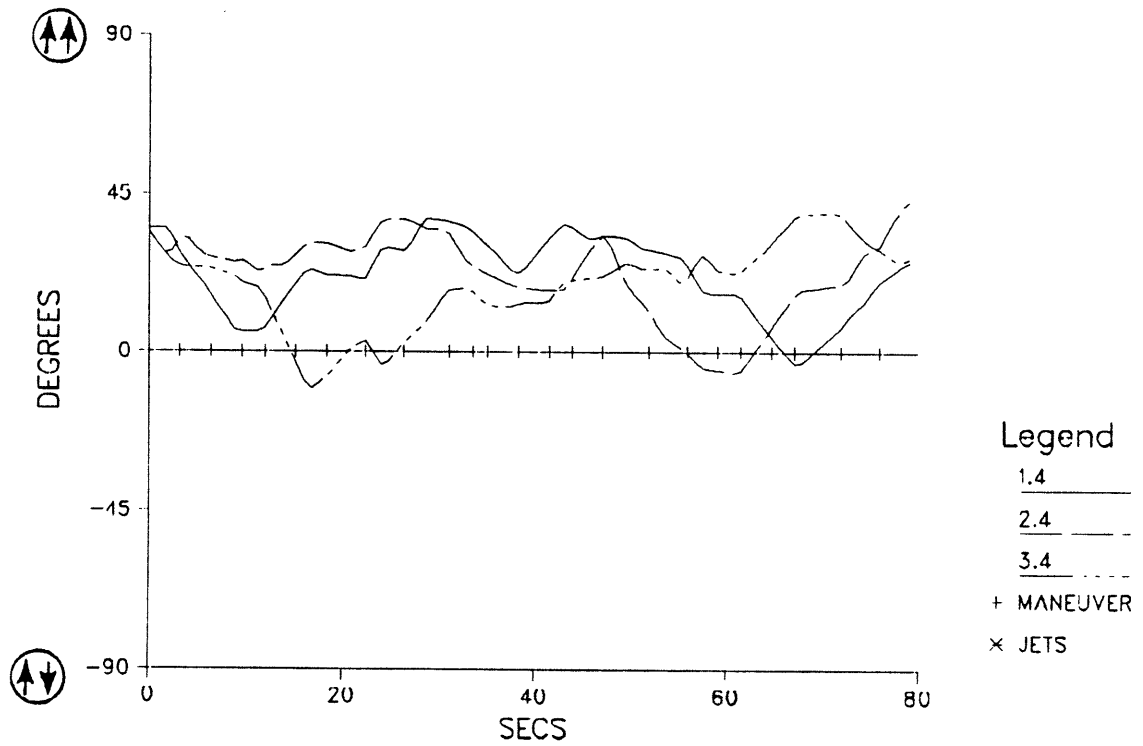
FIGURE 22: Cyclic Maneuver Sequence, Nominal Conditions

93

VEHICLE RATES

Peak Rates:

0.0072°/sec. in Roll
0.0024°/sec. in Pitch
0.0008°/sec. in Yaw

Legend

RATE: ROLL
RATE: PITCH
RATE: YAW

DEG/SEC. X 100

SECS.
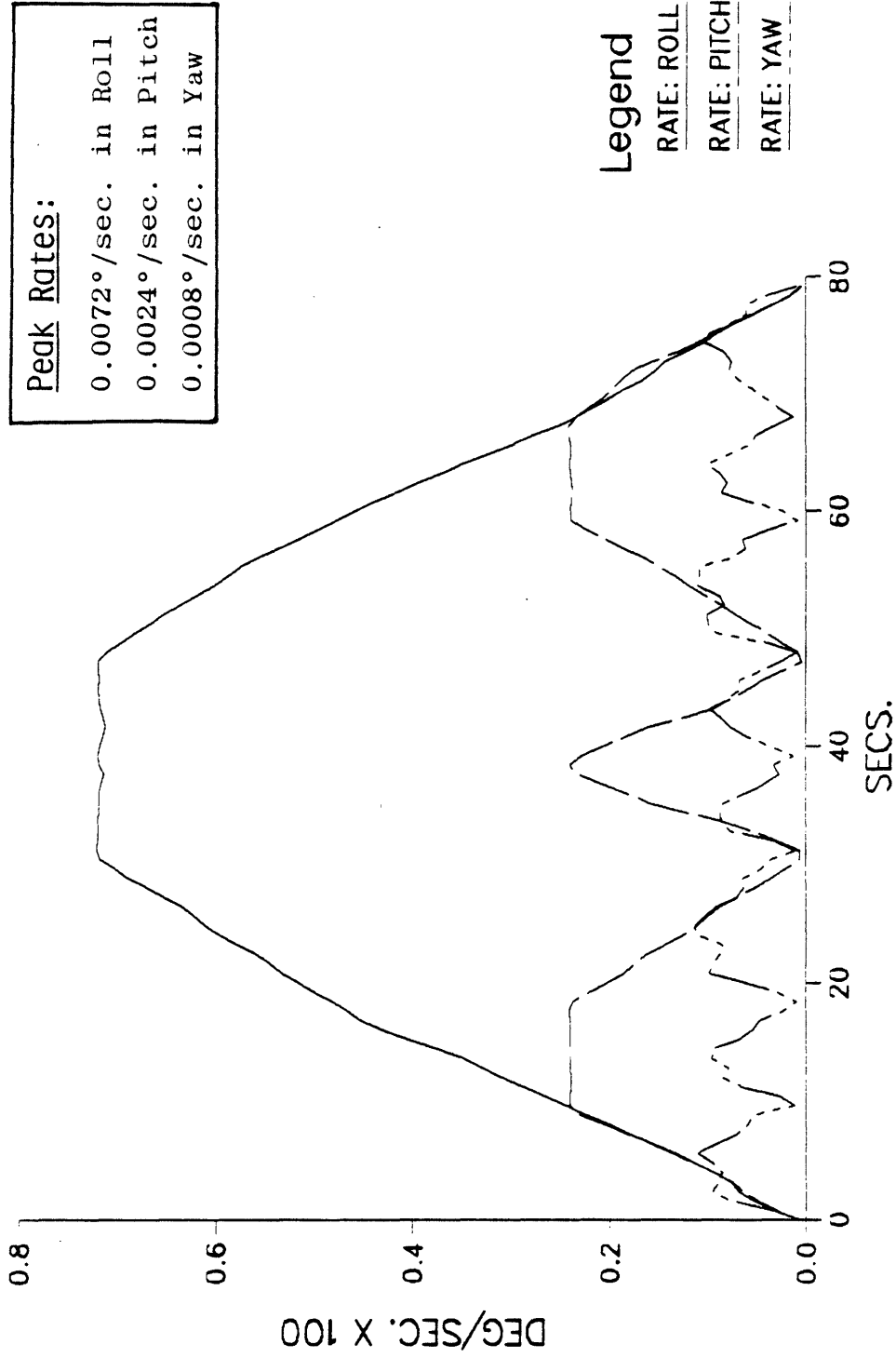
FIGURE 23: Cyclic Maneuver Sequence, Nominal Conditions

94

The number of two-rotor pairings possible in a CMG system is equal to N(N-1)/2, where N is the total number of CMGs. Since there are 4 CMGs in this simulation, we can form six possible rotor pairs, thus the lineup curves are split into two sets of three (the upper set is relative to the skewed CMG). Such a set of lineup curves is plotted in Fig. 22 for this test run. No parallel or anti-parallel alignments are seen throughout the test sequence (the closest approach between rotors is approx. 45°).

Fig. 23 shows the resulting vehicle rates. The periodic structure is due to the request sequence of Eq. 42 (as mentioned in Sec. 5.1, the controller fetches the next request in the sequence immediately after the vehicle converges to a desired rate). The request permutes most quickly in yaw, 1/3 as quickly in pitch, and 1/9 as quickly in roll, thus we build up the peak rates as listed in Fig. 23.

Since the moment of inertia about the vehicle yaw axis is nearly an order of magnitude smaller than the pitch and roll values (see Table I), the spacecraft is more susceptible to yaw disturbances. This contributes to the relatively uneven yaw response when contrasted to that achieved about pitch and roll. Because of computational constraints, several (ie. 3-10) simulation steps are averaged together per plotted point; this quantization can also affect the appearance of the yaw response as seen in these plots.

In the gimbal angle plots of Fig. 21, all gimbals start at the reference positions (ie. $\gamma, \delta = 0$). Since the vehicle rates return to zero at the close of the test sequence, one would expect the gimbals to return to their zero-displacement initial positions. This is not always the case; ie. as seen in Fig. 21, finite gimbal offsets are present at the conclusion of the test sequence.

The CMG motion is not entirely commutative. The steering principle always tries to instantaneously direct the CMGs into a better orientation; a superior response to a reversed request is preferred over that directly opposite to the previous gimbal trajectory. There are myriads of CMG configurations which can produce the zero-rate state

95

INNER GIMBAL ANGLES

Legend
CMG# 1
CMG# 2
CMG# 3
CMG# 4

+ MANEUVER
× JETS

OUTER GIMBAL ANGLES

Legend
CMG# 1
CMG# 2
CMG# 3
CMG# 4
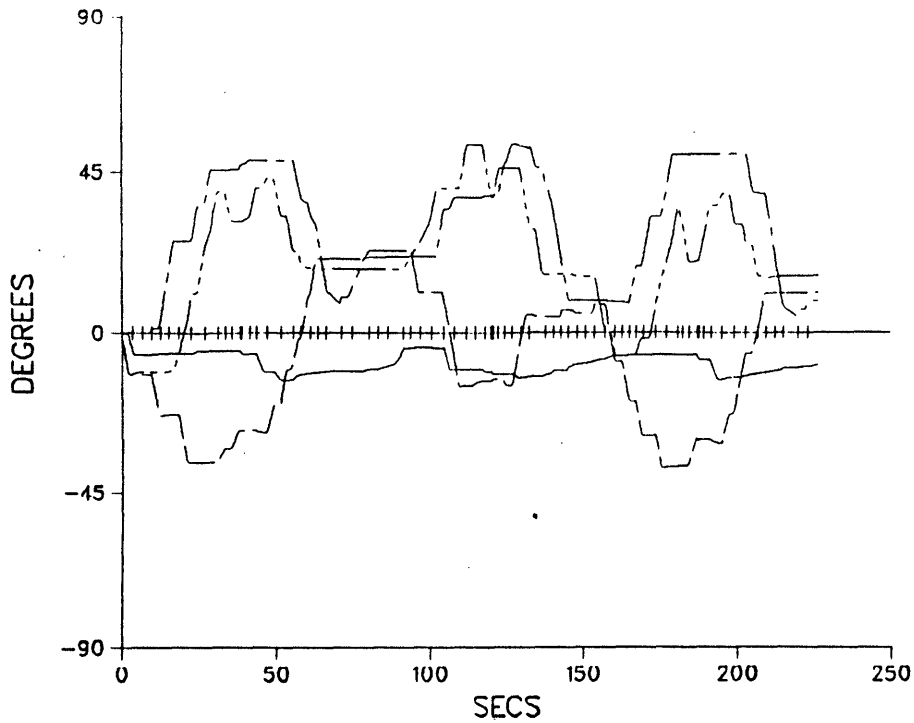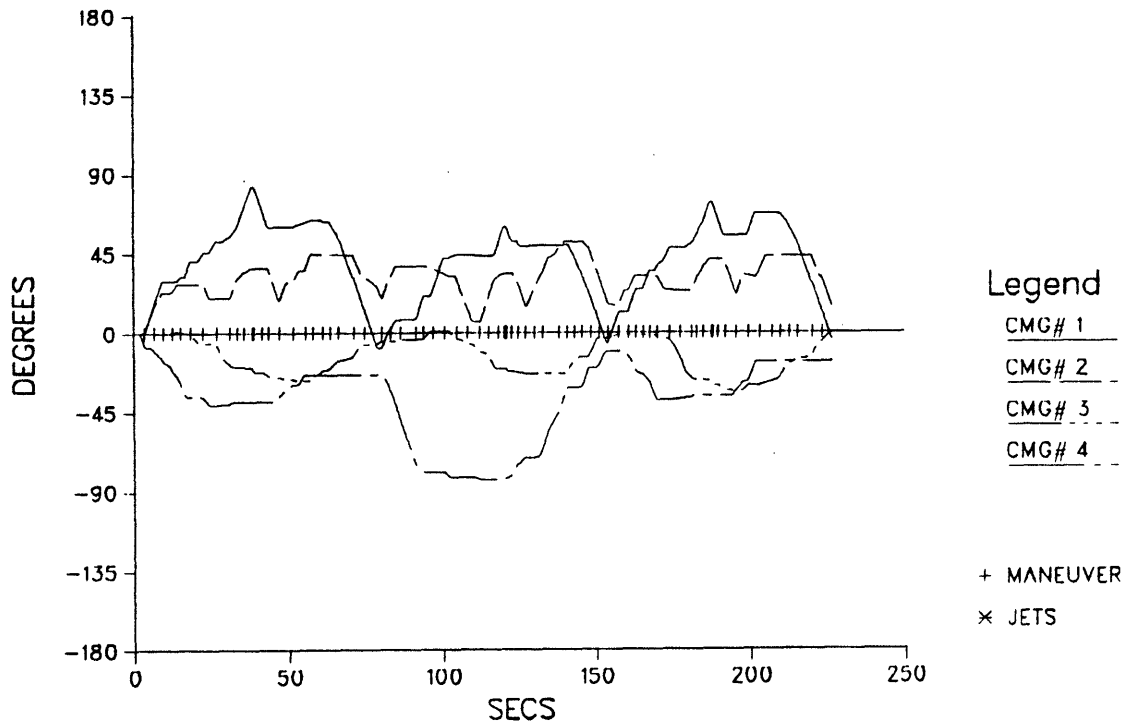
+ MANEUVER
× JETS

FIGURE 24: Cyclic Maneuver Sequence, 3 Iterations

TOTAL CMG COST

Legend
NRM. MANEUVER
X NULL MOTION

VEHICLE RATES

Legend
RATE: ROLL
RATE: PITCH
RATE: YAW
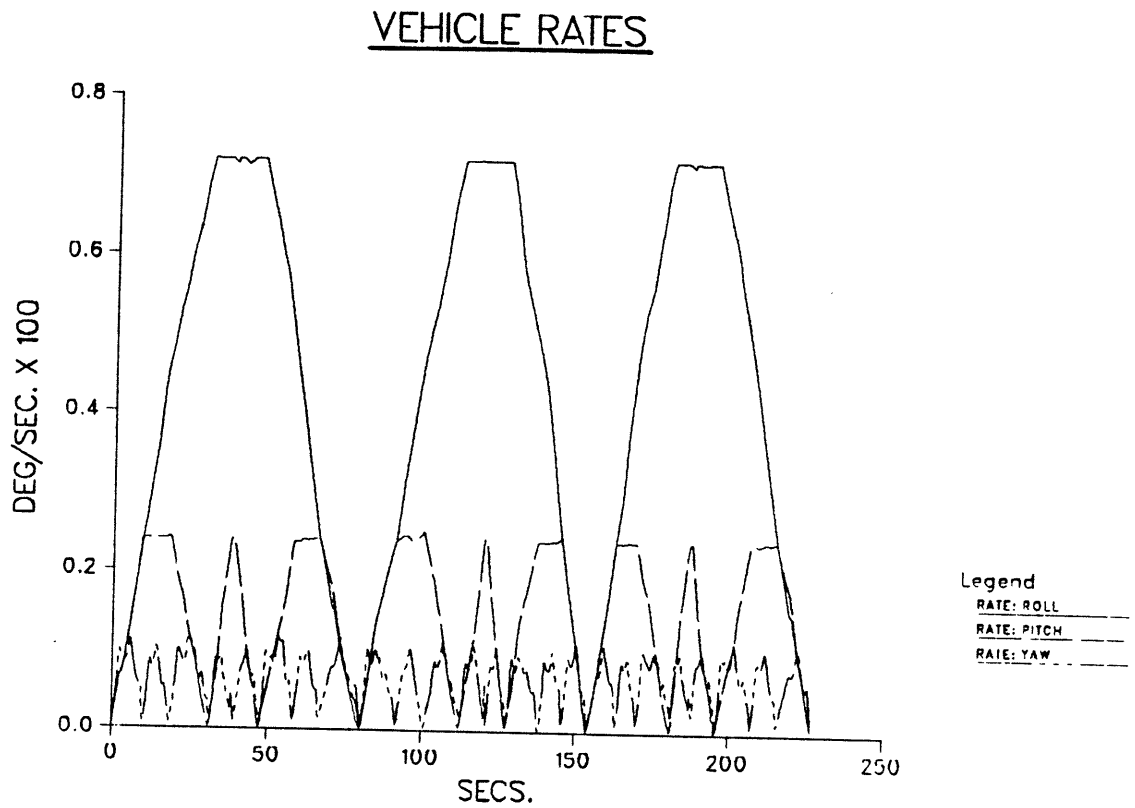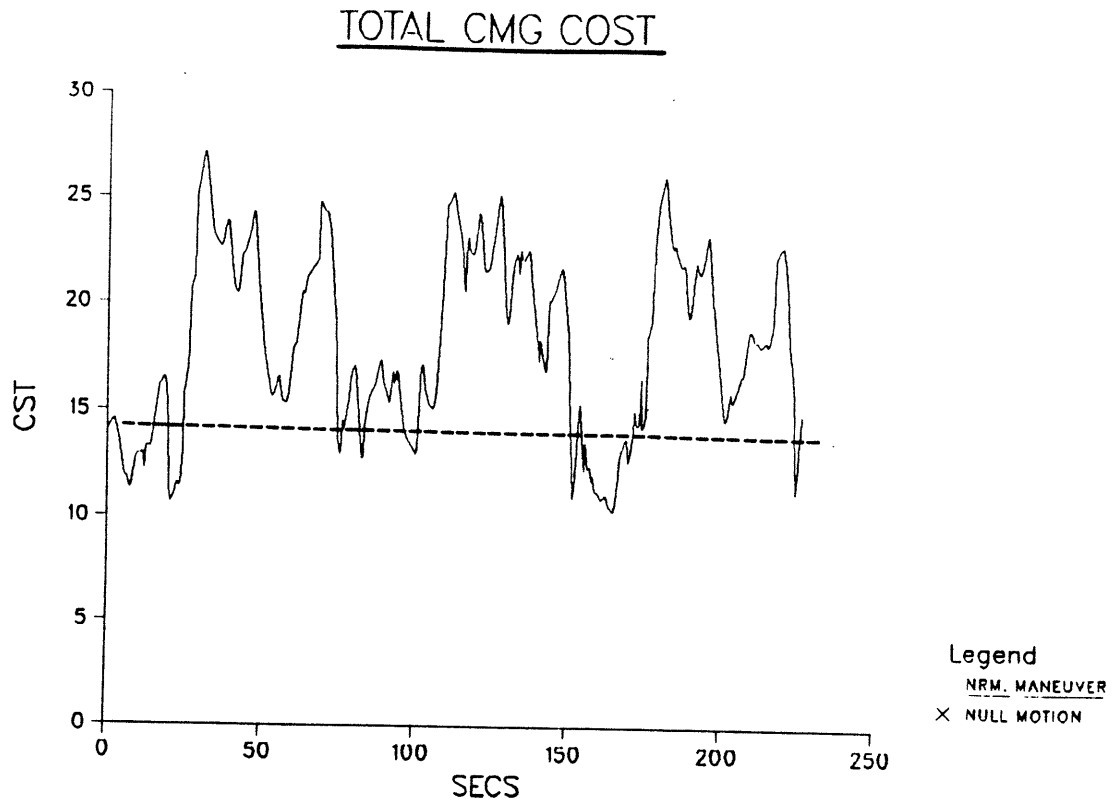
FIGURE 25: Cyclic Maneuver Sequence, 3 Iterations

97

existing at the beginning and end of the test run. The controller moves
the CMGs along stepwise-optimal trajectories during the course of the
test, and concludes the run in a CMG orientation which is generally of
similar net cost (η, Eq. 40).

Fig. 24 shows the gimbal angles resulting from a test run in which
the same set of 27 cyclic requests was repeated three times in
succession. Although gimbal trajectories are not identical, and all
angles are not returned precisely to the origin after each sequence, no
divergence effects are seen; the system has no difficulty in achieving
the desired rates, as presented in the lower plot of Fig. 25. The upper
plot in Fig. 25 shows the net cost (η) of the CMG configuration; the CMGs
were always returned to an orientation of similar cost when the vehicle
rates came back to zero throughout this test run. As seen in Figs. 24 &
25, the gimbal trajectories are quite similar over each cycle. The
pseudo-random differences between successive cycles are due to the
non-commutativity as discussed above; given sufficent degrees of freedom
in the CMG system (as seen here), the steering law has no difficulty in
repeatedly achieving the desired vehicle rates.

Fig. 26 shows the gimbal trajectories resulting from the same
cyclic request sequence (ie. Eq. 42; only one pass) with the anti-lineup
contribution omitted in the objective evaluation. The only component
remaining in the objective seeks to minimize inner gimbal angles, and we
indeed see a dramatic effect in the upper plot of Fig. 26 (when compared
to its analogue in Fig. 21). Inner gimbals are kept very close to zero
displacement; the majority of requests are now handled nearly exclusively
by the outer gimbal system. The lineup plots (Fig. 27) also look
substantially different from the nominal case of Fig. 22. The disregard
for rotor alignment is evident; CMG rotor pairs approach one another
often, and at least one total alignment is encountered. By comparing the
previous "nominal" results with those obtained here, the impact of the
objective function upon the mode of CMG steering is apparent.

INNER GIMBAL ANGLES

Legend
CMG# 1
CMG# 2
CMG# 3
CMG# 4

+ MANEUVER
× JETS

OUTER GIMBAL ANGLES

Legend
CMG# 1
CMG# 2
CMG# 3
CMG# 4
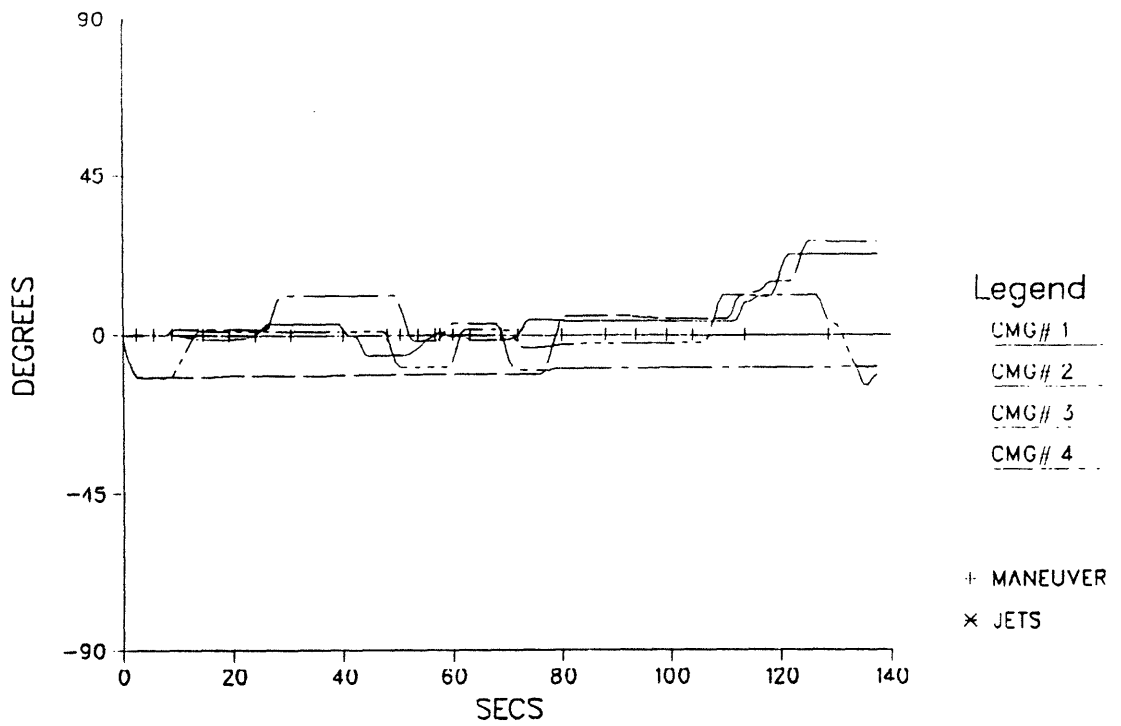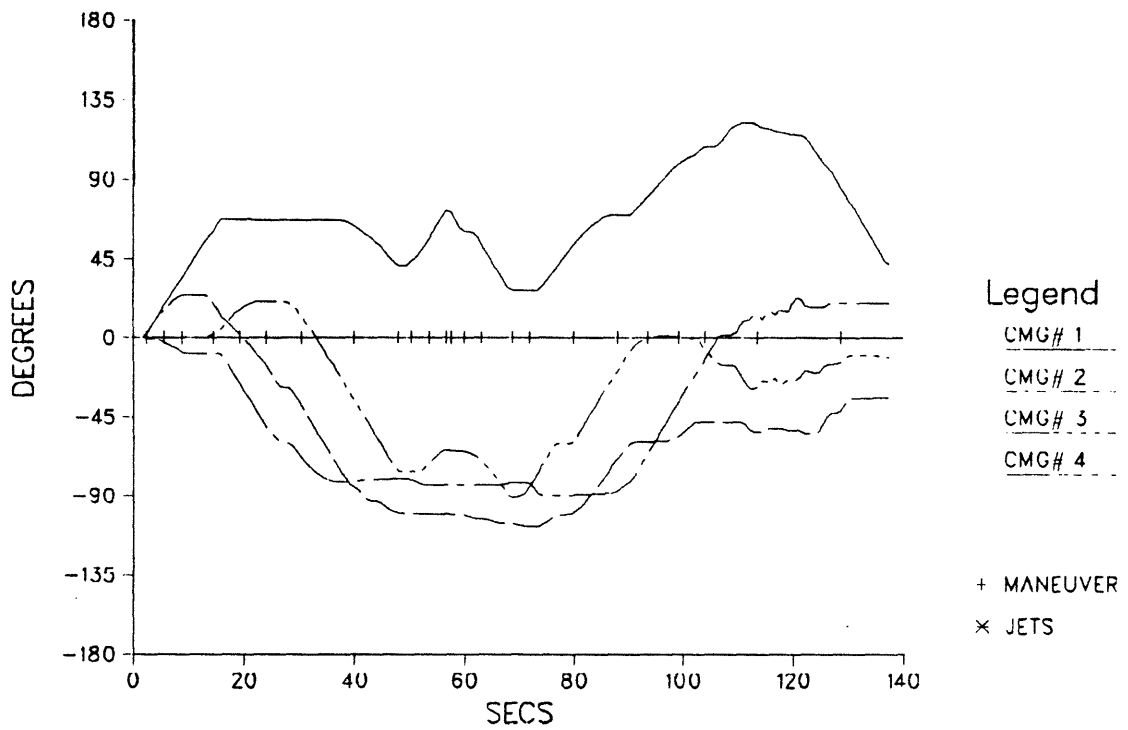
+ MANEUVER
× JETS

FIGURE 26: Cyclic Maneuver, No Antilineup in Objective

99

RELATIVE ANGLES BETWEEN CMG PAIRS PLT#1

Legend
1.2 ————
1.3 — — —
2.3 · · · ·
+ MANEUVER
× JETS

RELATIVE ANGLES BETWEEN CMG PAIRS PLT#2

Legend
1.4 ————
2.4 — — —
3.4 · · · ·
+ MANEUVER
× JETS
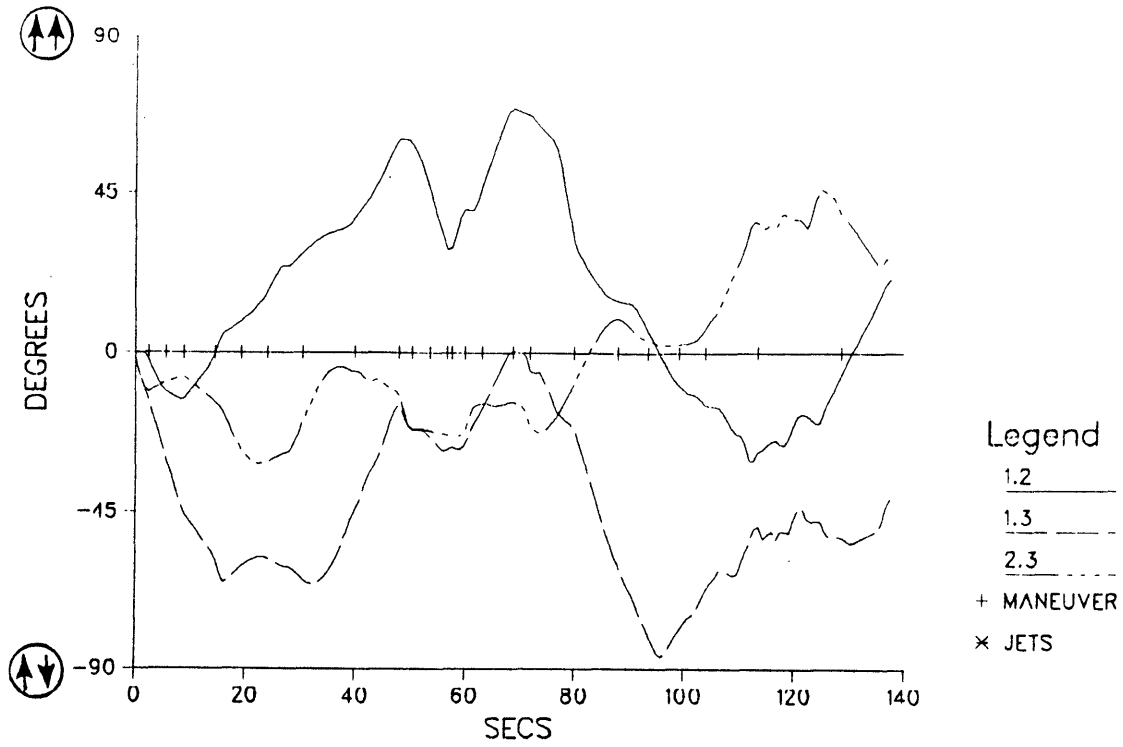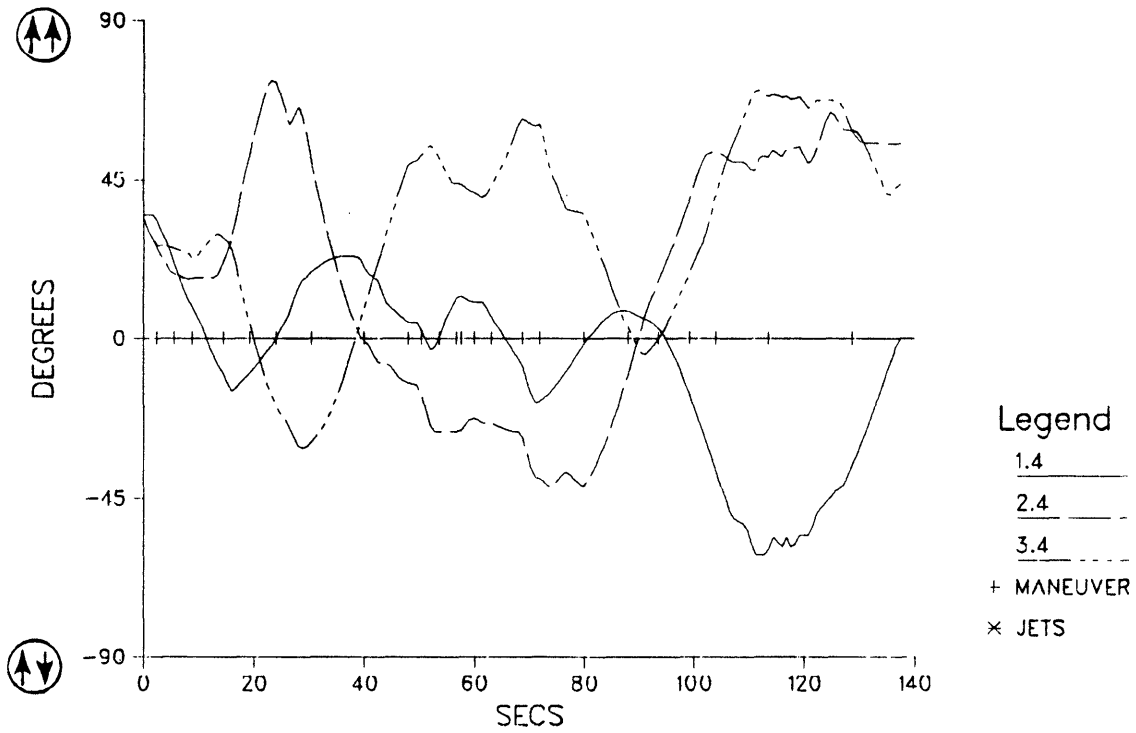
FIGURE 27: Cyclic Maneuver, No Antilineup in Objective

The next applications of the cyclic maneuver sequence account for all components in the objective function at nominal amplitudes (re. Figs. 21-23), but include CMG failures midway through the test run. A "CMG failure" is created by inhibiting a CMG (or appropriate gimbal) from selection and "freezing" the gimbal(s) concerned at their current positions.

Fig. 28 presents results where both gimbals of CMG #3 were failed halfway through the test. The initial gimbal trajectory is identical to that of Fig. 21 (as expected). A substantial difference is seen in the remainder of the test run; both gimbals of CMG #3 are held at constant positions (ie. "failed"), and the requests are answered exclusively by the surviving CMGs (and "optimally", since the objective is still evaluated amoung the functional devices). Since the stored momentum of the frozen CMG is held constant, the remaining CMGs are seen to finish in an orientation differing considerably from the initial configuration. As seen in the plot of resulting vehicle rates, all requests are still successfully achieved by the truncated system; little difference is seen between these rates and those resulting from the nominal run of Fig. 23.

Fig. 29 summarizes results of a similar test in which only the outer gimbals of CMGs #3 and #4 were failed halfway through the request sequence. The six surviving gimbals (including the inner gimbals of the degraded devices) were used extensively in order to continue to meet the desired vehicle rates; little difference is again seen between the vehicle rates plotted in Fig. 29 and those of the nominal run (Fig. 23).

These tests illustrate the flexibility inherent in the simplex process. Since each CMG gimbal is modeled and selected as an independent activity vector, a single gimbal may be inhibited from selection while its companion continues to be available. Because activity vectors are still selected in correspondance with the objective function, all CMGs are steered to avoid rotor lineups throughout this test.

Since the term "inner" gimbal no longer has any physical meaning, K_A for the affected CMGs is set to zero in Eq. 30 after single gimbal
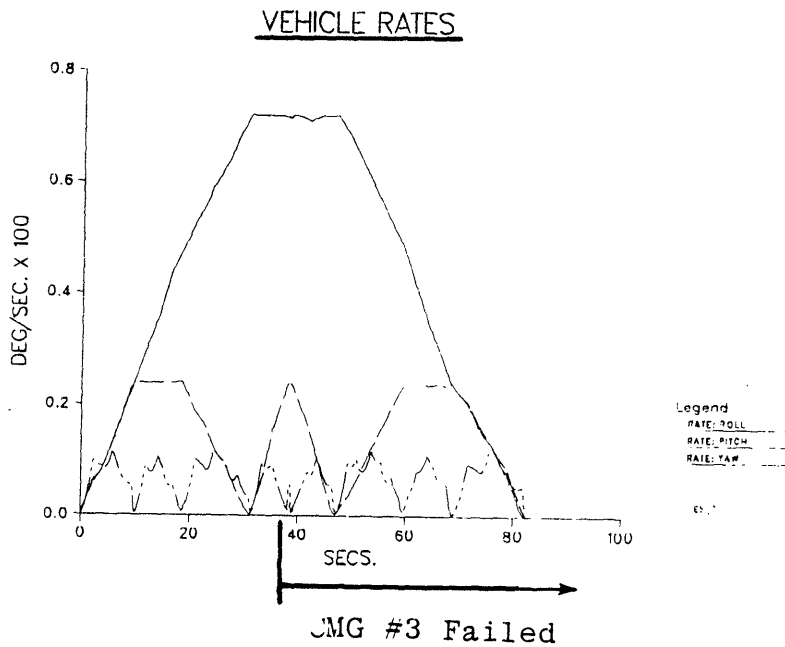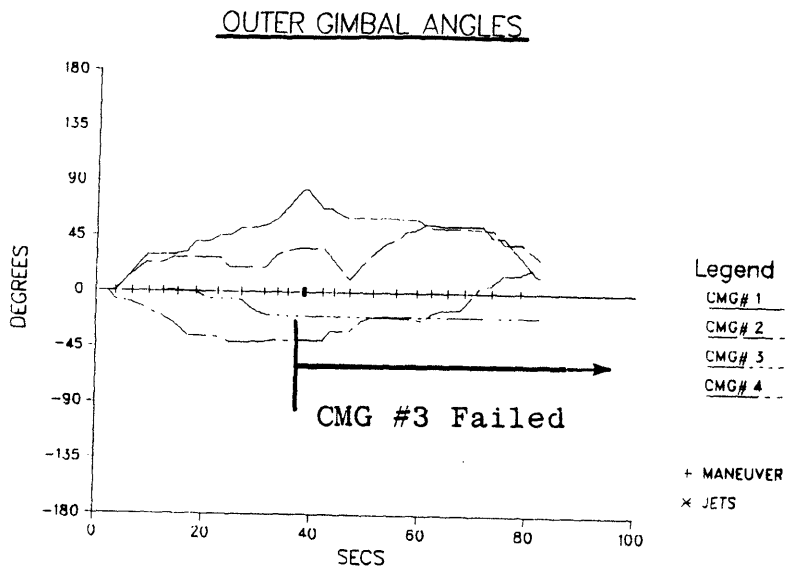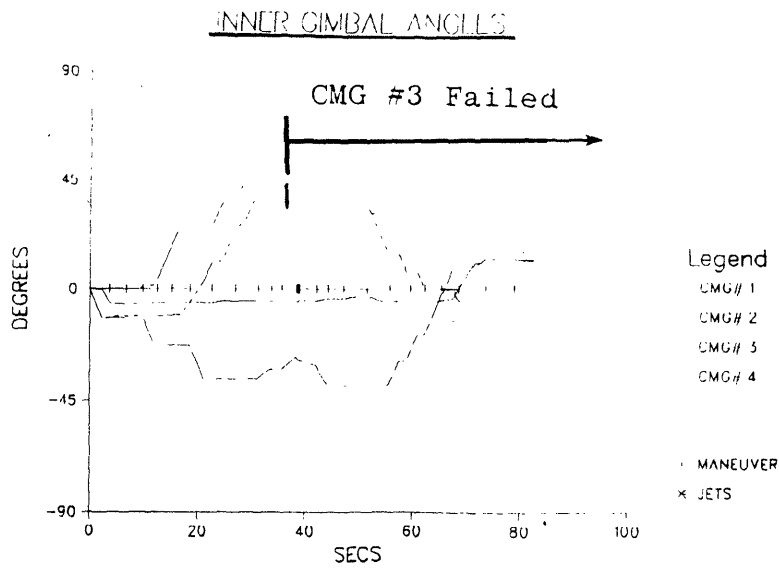
FIGURE 28: Cyclic Maneuver, Fail CMG #3

OG's of CMGs #3 & #4
Failed

Legend
CMG# 1
CMG# 2
CMG# 3
CMG# 4

⊢ MANEUVER
✕ JETS

OUTER GIMBAL ANGLES

OG's of CMGs #3 & #4
Failed

Legend
CMG# 1
CMG# 2
CMG# 3
CMG# 4

⊢ MANEUVER
✕ JETS

VEHICLE RATES

OG's of CMGs #3 & #4 Failed

Legend
RATE: ROLL
RATE: PITCH
RATE: YAW
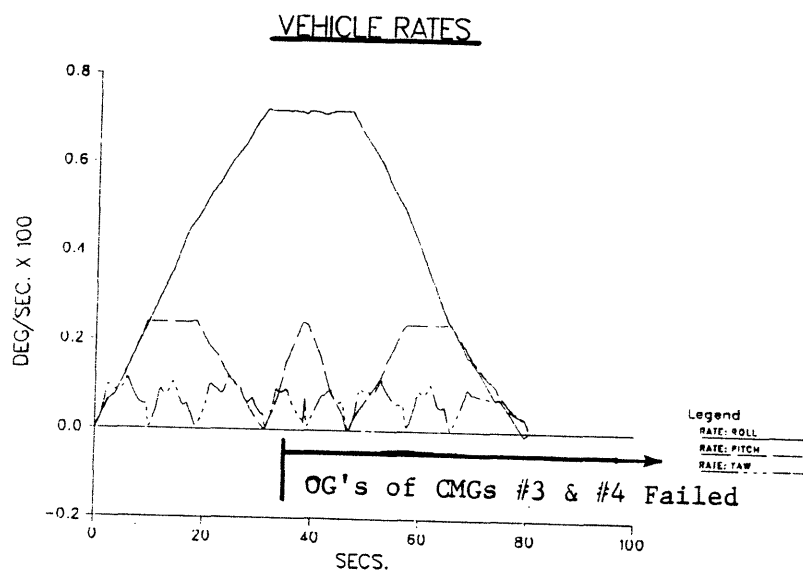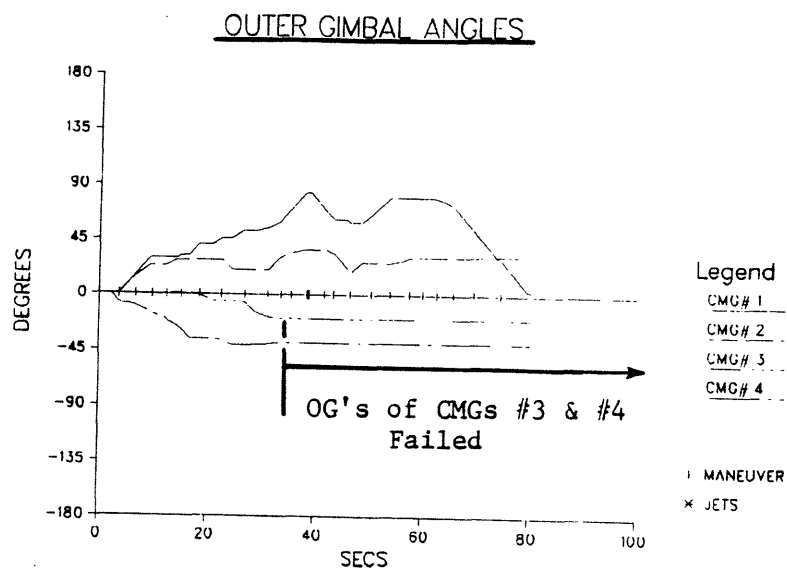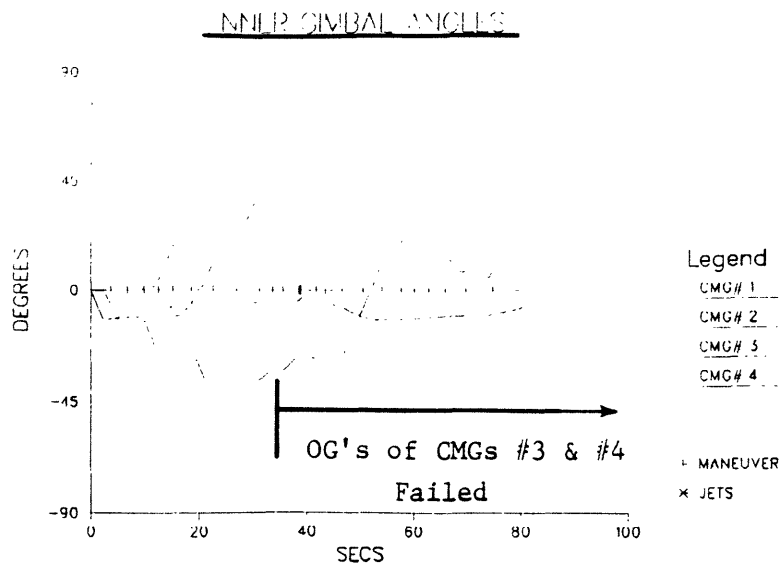
FIGURE 29: Cyclic Maneuver, Fail Outer Gimbals of CMGs #3 & #4

103

failure, thus the semi-failed CMGs contain no inner gimbal angle minimization component in the objective evaluation. Stops avoidance contributions are still maintained on all relevant gimbals.

Double gimballed CMGs having a single gimbal failure of this type become effectively single gimballed CMGs. A method of altering the objective function to steer a single-gimballed CMG system is described in Chapter 6. Although satisfactory results are obtained in the example of Fig. 29, steering a system containing single-gimballed CMGs away from lineups may not be sufficent to retain maximum controllability. If one modifies the objective coefficents to account for "internal" singular configurations (re. Ch. 6), the degraded single/double gimballed CMG system may be directly steered to maximize control potential.

Unlike many other CMG steering laws, the linear programming formulation presented here will accept CMGs mounted in any orientation. Gimbal coordinates are not "hardwired" into the algorithm, and any CMG configuration can be considered by specifying an appropriate $\hat{\sigma}_\delta$ and $\hat{\sigma}_{\gamma_o}$ in the equations of Sec. 2.5.

The final example using the cyclic request sequence assumes the CMGs to be mounted in a parallel configuration (Fig. 30), while maintaining nominal cost contributions and keeping all CMGs operational throughout the test run. This parallel configuration has been proposed for space station application[16] The CMGs are oriented with parallel outer gimbals rotating about the pitch axis, and parallel inner gimbals rotating about the roll or yaw axes (Fig. 30b). In order to avoid starting the simulation with the CMGs in saturation, the CMG rotors are initially displaced such that two have inner gimbal angles of +/-30° with zero outer gimbal angles, and two have outer gimbal angles of 180°+/- 30° with zero inner gimbal angles, as indicated in Fig. 30c. This yields two opposing sets of rotors scissored by 60° and oriented back-to-back in perpendicular planes, thus is a zero net momentum state lacking any total rotor alignments. Two full cyclic iterations are requested.
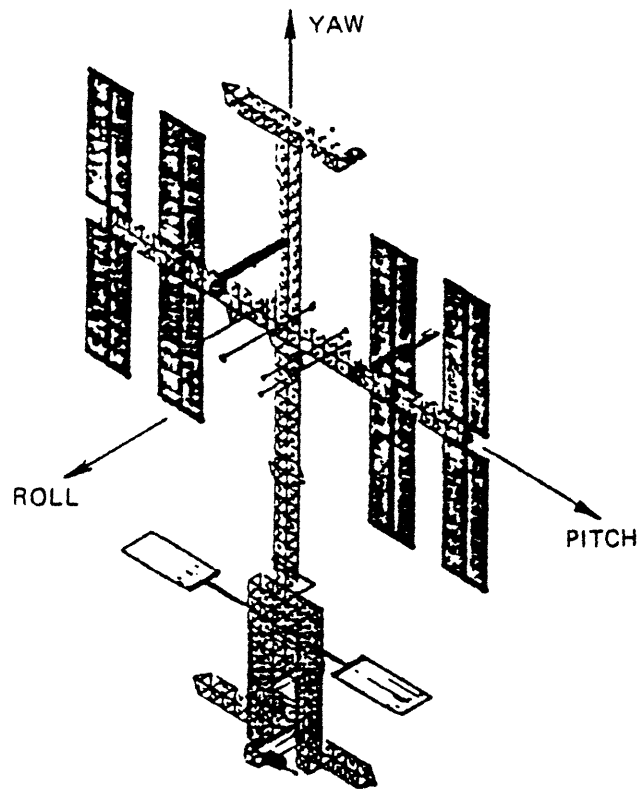
(a) POWER TOWER SPACE STATION
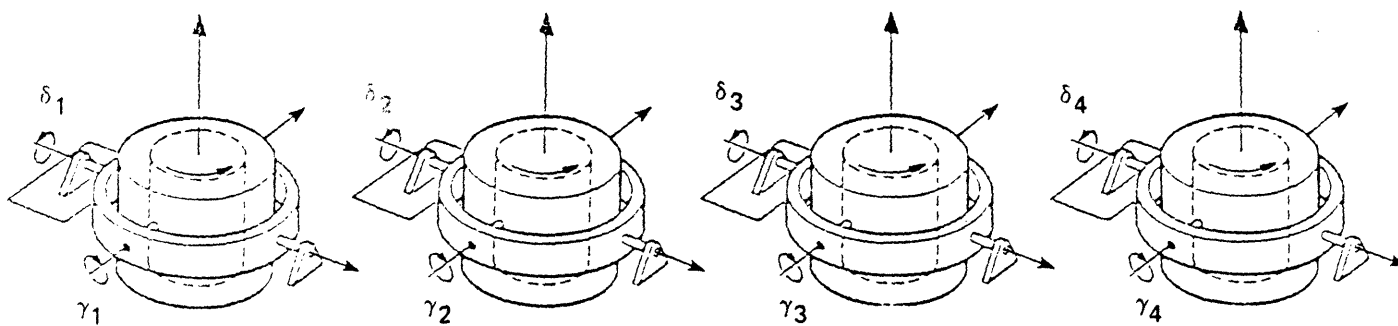
(b) PARALLEL MOUNTED CMG REFERENCE CONFIGURATION (ZERO GIMBAL ANGLES)
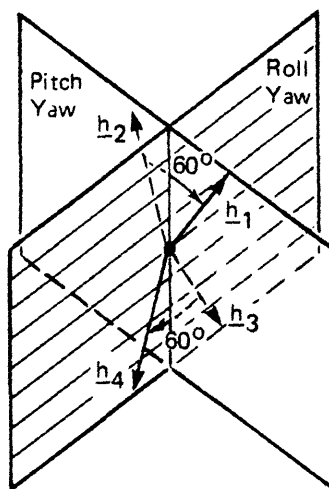
(c) INITIAL LINEUP-FREE ORIENTATION OF CMG ROTORS

FIGURE 30: PARALLEL MOUNTED CMG CONFIGURATION

105

INNER GIMBAL ANGLES

Legend
CMG# 1
CMG# 2
CMG# 3
CMG# 4

+ MANEUVER
✕ JETS

OUTER GIMBAL ANGLES

Legend
CMG# 1
CMG# 2
CMG# 3
CMG# 4
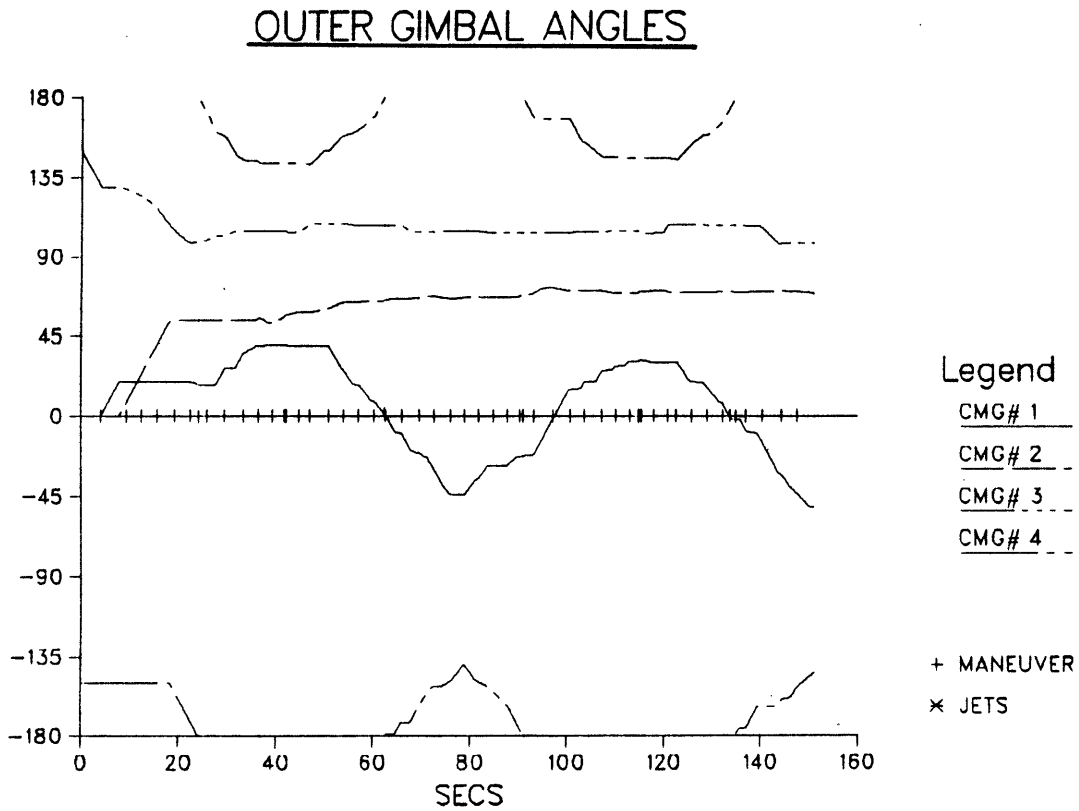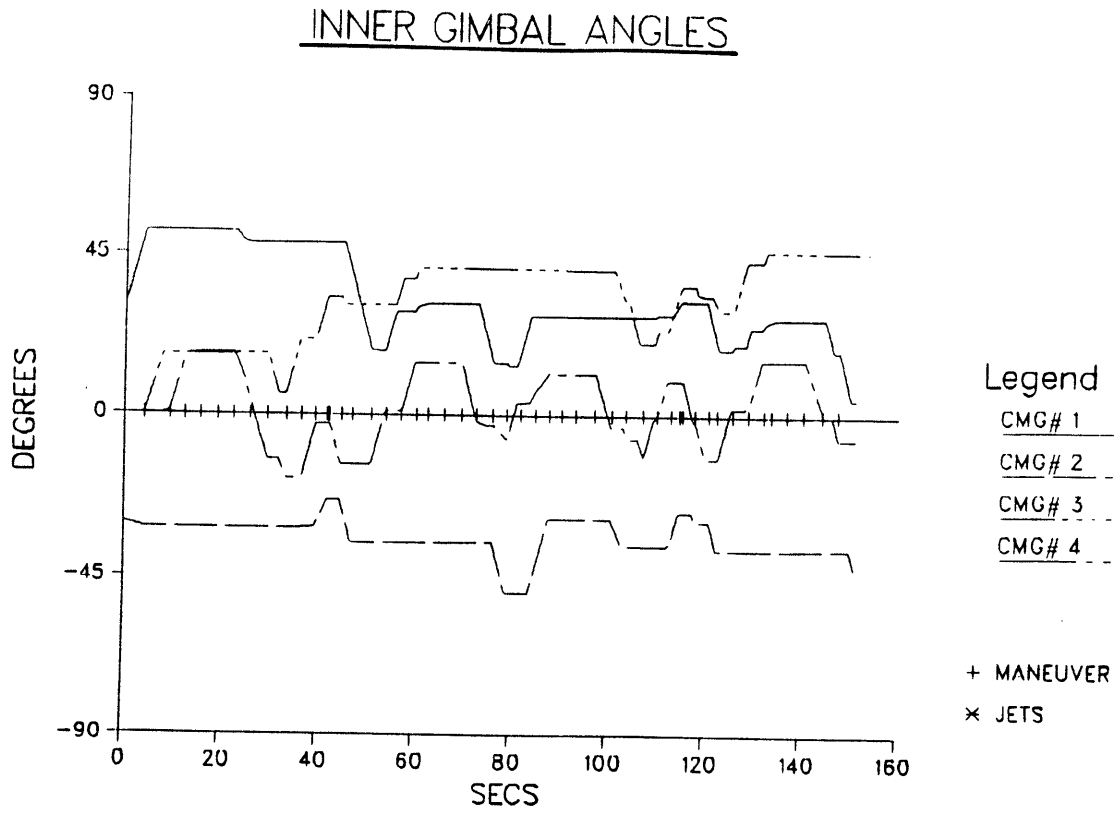
+ MANEUVER
✕ JETS

FIGURE 31: Cyclic Maneuver, Parallel Mounted CMGs

106

RELATIVE ANGLES BETWEEN CMG PAIRS PLT#1

Legend
1.2 ————
1.3 — · —
2.3 · · · ·
+ MANEUVER
✕ JETS

RELATIVE ANGLES BETWEEN CMG PAIRS PLT#2

Legend
1.4 ————
2.4 — · —
3.4 · · · ·
+ MANEUVER
✕ JETS
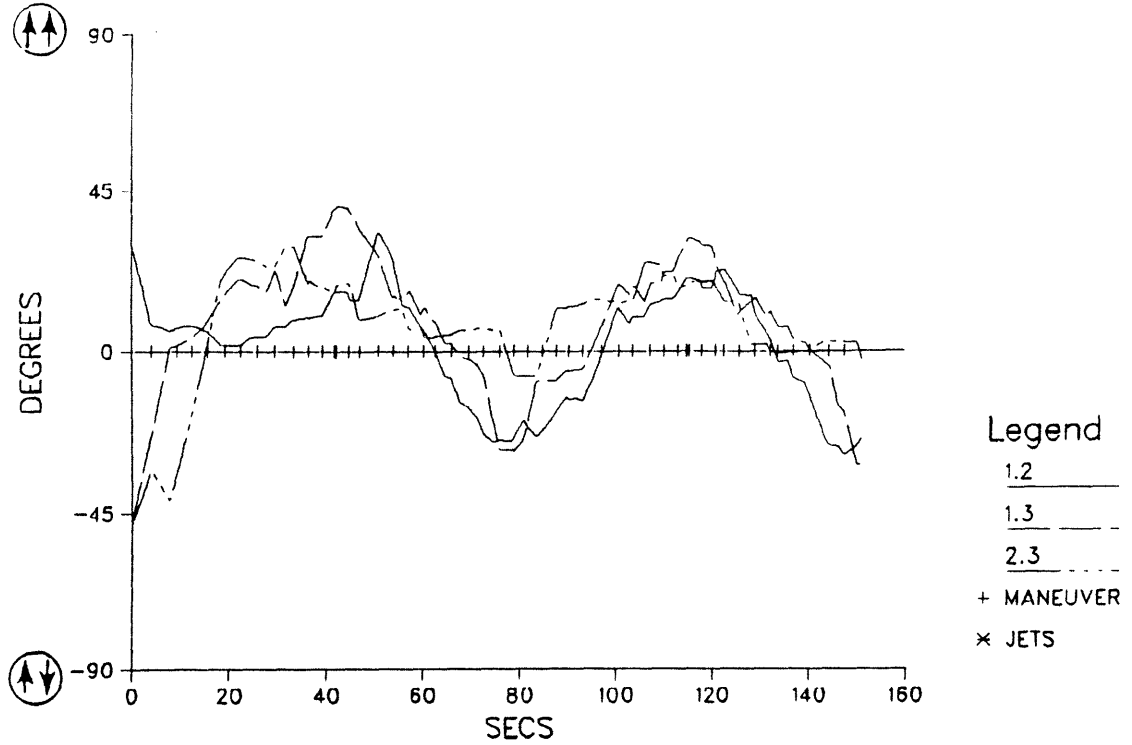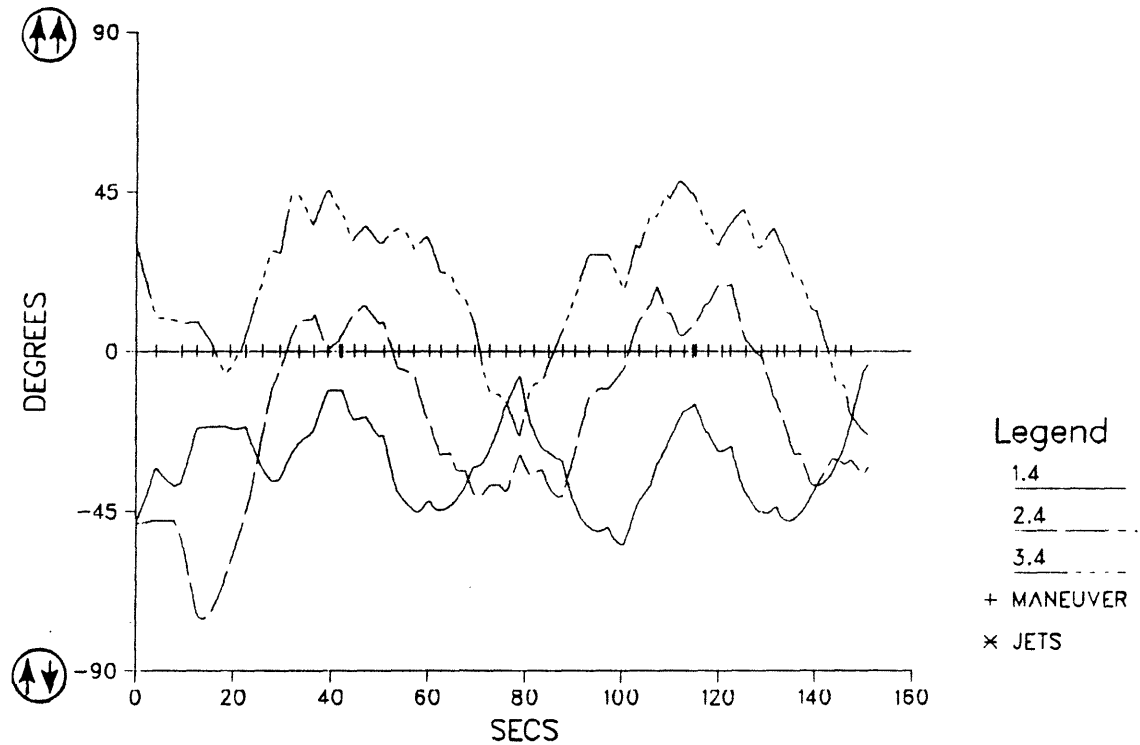
FIGURE 32: Cyclic Maneuver, Parallel Mounted CMGs

107

VEHICLE RATES

DEG/SEC. X 100

SECS.

Legend
RATE: ROLL
RATE: PITCH
RATE: YAW
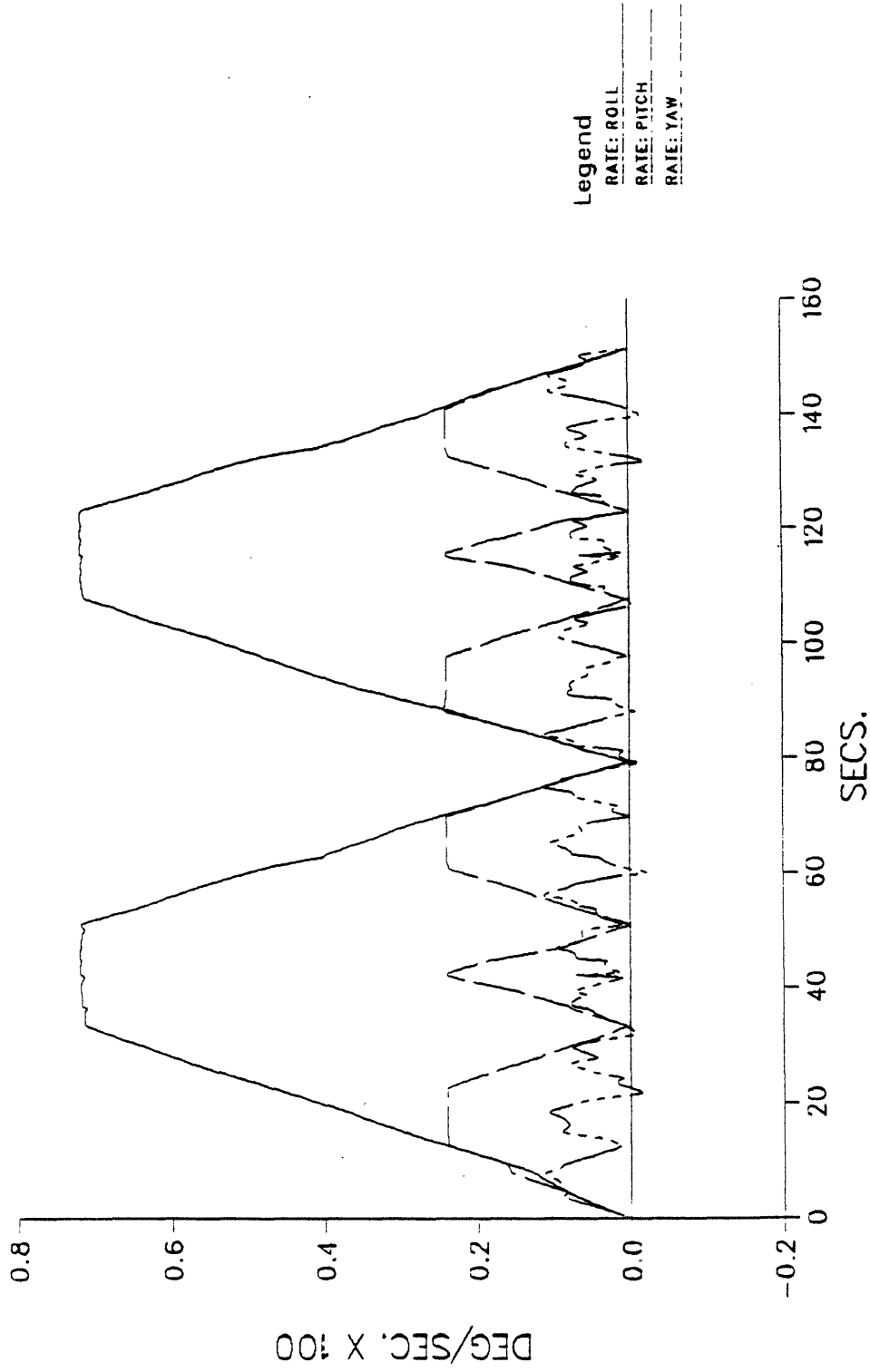
FIGURE 33: Cyclic Maneuver, Parallel Mounted CMGs

Gimbal angles are shown in Fig. 31 and lineup plots are given in Fig. 32. The initial CMG orientation is not entirely optimal; finite rotor alignments and inner gimbal angles are present at startup. Once maneuvers begin, excessive inner gimbal swings are avoided, and the system is generally steered away from significant rotor lineups.

The resulting vehicle rates are given in Fig. 33. The desired rate profile is repeatedly achieved without difficulty; the vehicle response under the parallel mounting configuration appears little different from that obtained using the standard configuration of Fig. 16 (Fig. 25). By changing only a set of initial vectors, the steering/selection process was able to "optimally" manage an entirely different CMG configuration.

5.5) Momentum Saturation of CMG System Along Pitch/Roll Axis

The following series of tests are performed using an input sequence of identical rate-change requests (each of 0.0008 deg/sec. in pitch and roll, zero in yaw), which eventually drive the CMG system into momentum saturation. The standard mounting configuration of Fig. 16 is used in all runs; RCS jets are defined via Fig. 17 and the associated discussion.

The first case is attempted under nominal conditions; ie. all CMGs operational and all components included in the objective function. Resulting gimbal angles are shown in Fig. 34. Inner gimbal angular swings are seen to be kept minimal through the entire trajectory. The asterisks plotted over the curves at the latter portion of the run correspond to RCS firings, which were required to complete the related requests.

Lineup plots for this run are given in Fig. 35. Rotor alignments are seen to be avoided until the latter portion of the test, at which time all rotors are moved such that they point into a uniform direction (and RCS assistance is required). This represents momentum saturation, where the CMG system has given all of its momentum into the vehicle axis

INNER GIMBAL ANGLES
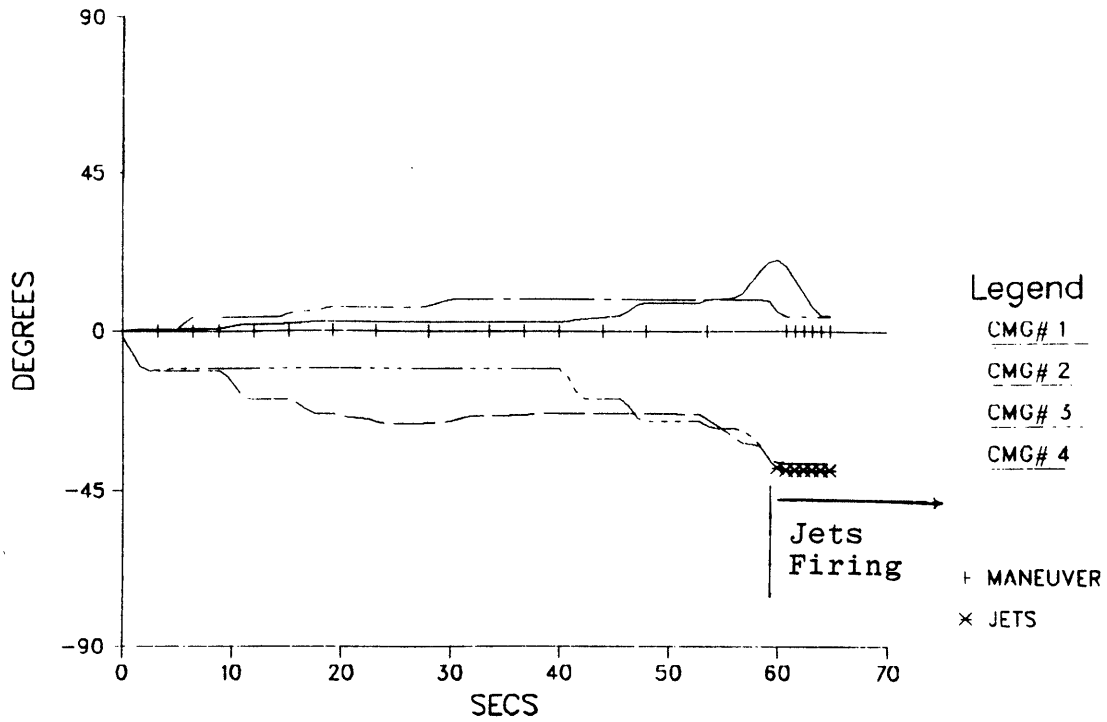
OUTER GIMBAL ANGLES
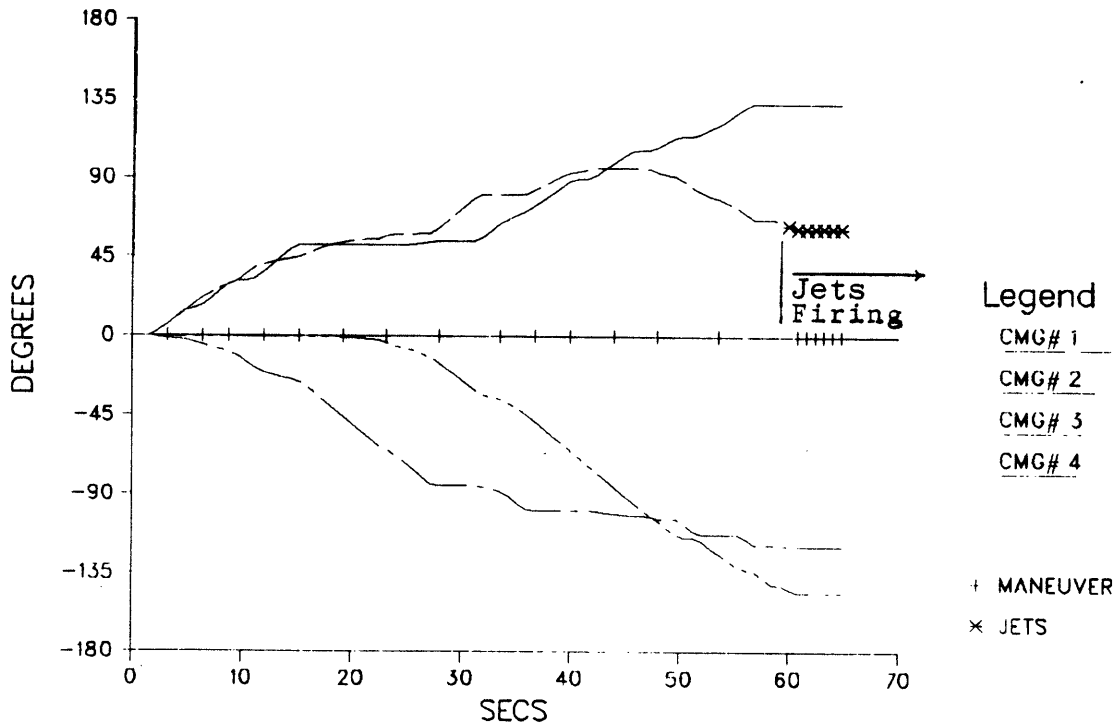
FIGURE 34: Saturate CMGs in Pitch/Roll, Nominal Conditions

RELATIVE ANGLES BETWEEN CMG PAIRS PLT#1

CMGs Momentum Saturated
Jets Required

Legend
1.2 ----
1.3 ----
2.3 ----
⊢ MANEUVER
✕ JETS

RELATIVE ANGLES BETWEEN CMG PAIRS PLT#2

CMGs Momentum Saturated
Jets Required

Legend
1.4 ----
2.4 ----
3.4 ----
⊢ MANEUVER
✕ JETS
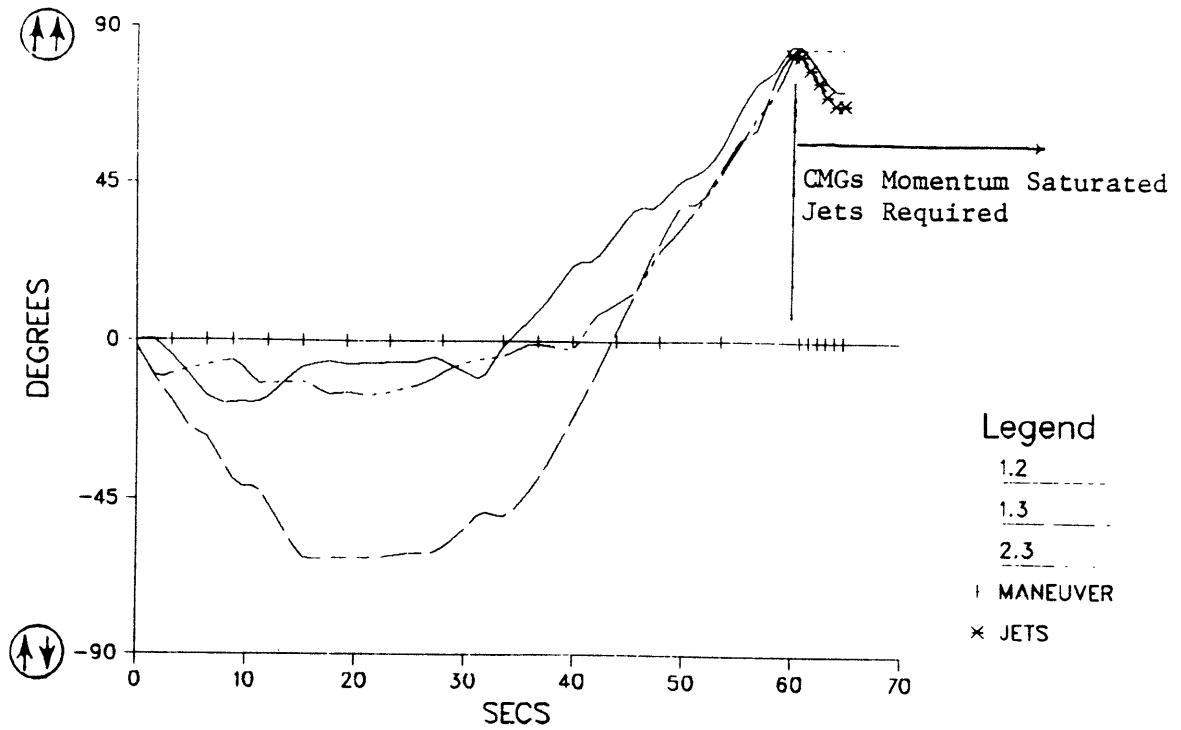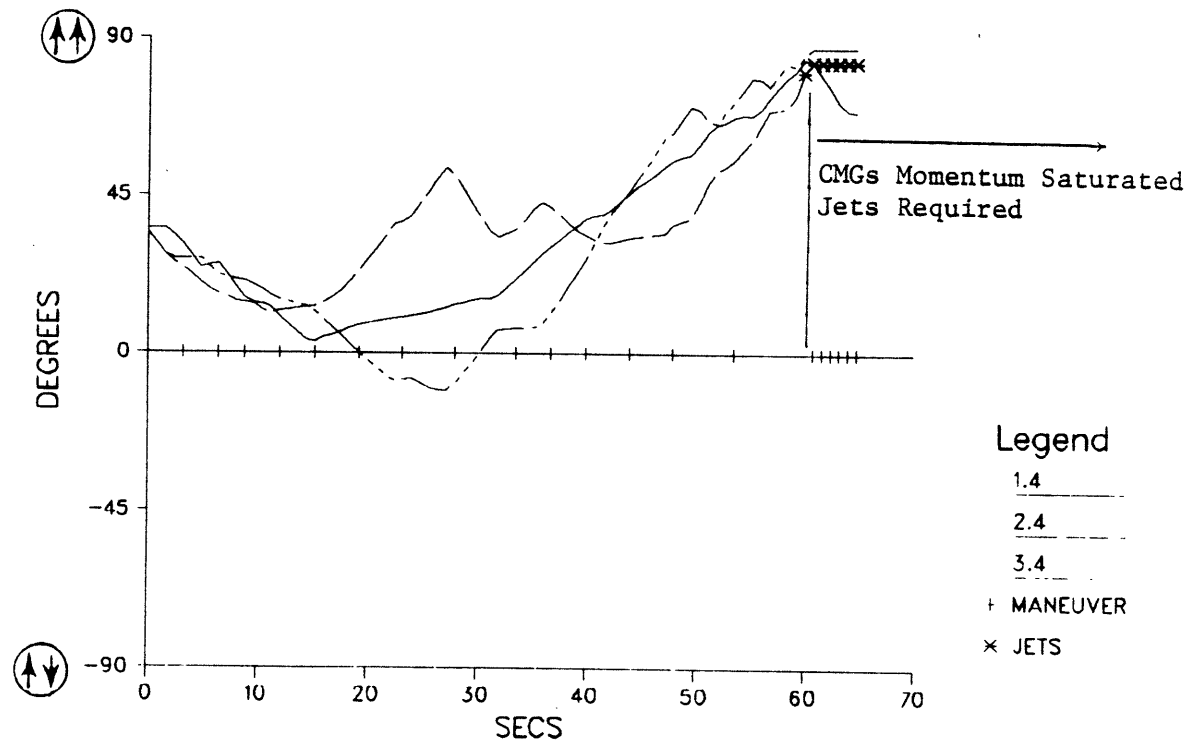
FIGURE 35: Saturate CMGs in Pitch/Roll, Nominal Conditions

111

a) SATURATION DETECT
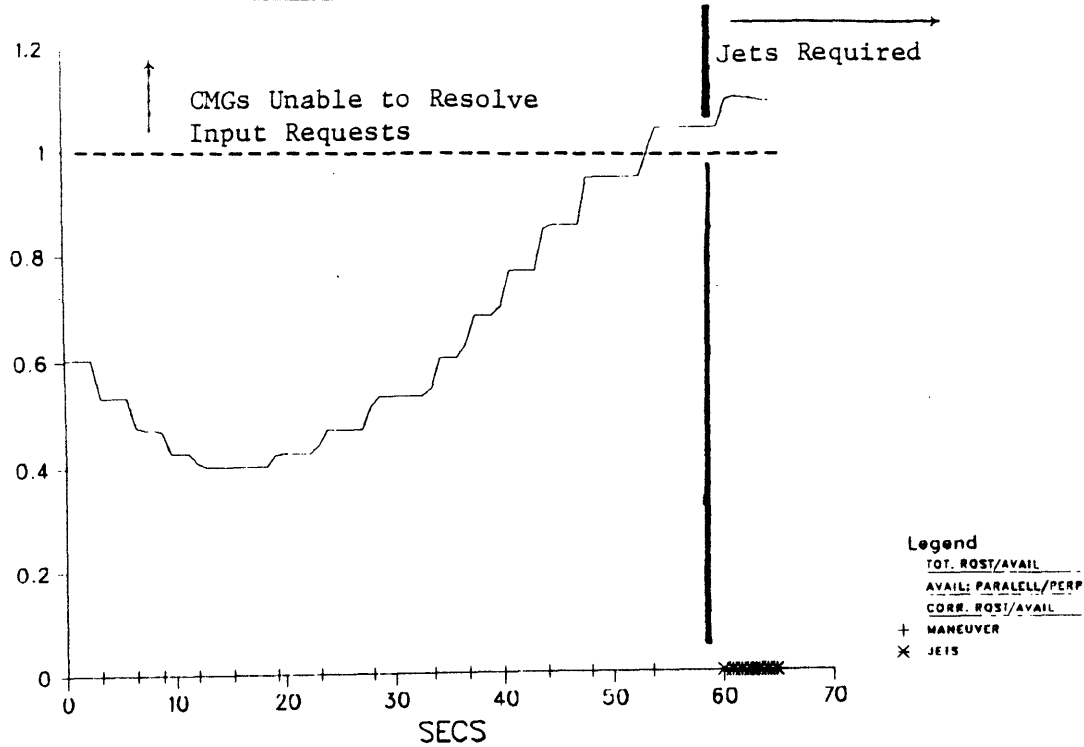
b) VEHICLE RATES
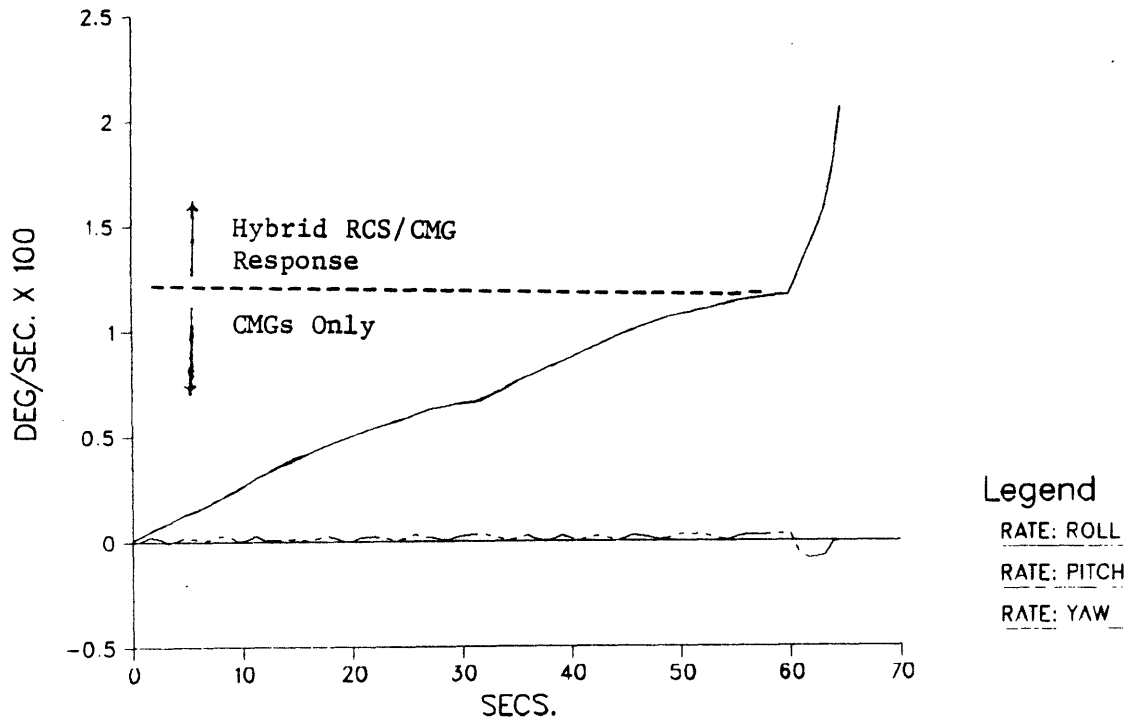
FIGURE 36: Saturate CMGs in Pitch/Roll, Nominal Conditions

anti-parallel to the sense of alignment. RCS jets are introduced through the simplex process only when required at saturation; jets were not included in solutions evaluated at prior stages.

The upper graph in Fig. 36 shows the saturation index ("S" defined in Sec. 4.2) resulting from this test run. Indeed, we see that jets (asterisks) are introduced shortly after S exceeds unity (indicating momentum saturation).

The saturation index is calculated for each input request relative to a "desired final state", which is defined as the difference between the current total CMG momentum and the amount of momentum necessary to transfer into the vehicle such that the request is achieved. The saturation index thus reflects the transition from present to final state; as the CMGs move, the total stored momentum changes in both direction and magnitude, thus the desired final state alters correspondingly (even though all input requests are equal). Since the CMGs were initially skewed such that they projected positively along the direction of CMG #4 (see Fig. 16), they were significantly close to saturation in the corresponding direction. The input requests are much smaller than the stored CMG momentum; when both are added to form the "desired final state", the stored momentum initially dominates, thus the saturation parameters reflect primarily the initial CMG orientation at the start of the test. As the CMGs respond to the input requests, they begin to move their stored momentum (initially along roll/pitch/yaw) toward the opposite direction, to eventually align with negative pitch/roll. This moves the CMG system gradually away from the initial semi-saturated state (as seen in the decreasing value of S; Fig. 36). As the CMGs become aligned along negative pitch/roll, the system again approaches momentum saturation, and the saturation curve rises to unity, as seen in Fig. 36.

The lower plot in Fig. 36 shows the resulting vehicle rates. The rate-feedback controller is structured to drive the CMGs to attain input requests as quickly as possible (gimbal rates are normalized to their

113

peak value via Eq. 27), and new requests are fetched immediately upon completion of their predecessors. Inputting a steady stream of identical rate-change requests to such a controller essentially yields a response of constant (nearly maximum) acceleration. This is what is seen in Fig. 36b, where the vehicle rate builds nearly linearly. The sudden increase in slope occuring at the end of the test is due to the introduction of jets; since their control authority is so much higher, jets produce a larger acceleration. The requests are still of the same magnitude, but they are answered much more quickly when jets are included, hence many more are accepted per unit time interval (as seen in the greater density of cross-hatches on the horizontal axes of Figs. 34 & 35 when the RCS is firing).

The input request sequence commands equal vehicle rates about pitch and roll axes. The rising curve in Fig. 36b is actually two curves; the controller had little difficulty generating equal pitch and roll rates, thus one curve is generally superposed over the other. The curve bouncing about the horizontal axis is the vehicle yaw rate, which is commanded to be zero (again, the vehicle inertia is an order of magnitude smaller about this axis, thus it is easier prey to disturbance and cross coupling).

Fig. 37 shows the gimbal angles resulting from the same "saturation" request sequence without adding the anti-lineup contribution to the objective function. Inner gimbal angles are highly minimized (compare to Fig. 34; the objective function now works solely to bring all inner gimbal angles to zero). Fig. 38 gives the plots of rotor alignment; CMG rotors approached lineup on several occasions (as marked) before entering saturation, at which point RCS firings were required to complete maneuvers. If one compares the plots of Fig. 38 with those derived using full cost contributions (Fig. 35), the effect of the anti-lineup function is immediately evident; the system redundancy was exploited in the "nominal" run of Figs. 35 & 36 in order to avoid the rotor alignments encountered with the incomplete objective function used in the test of Figs. 37 & 38.

114

INNER GIMBAL ANGLES

Legend
CMG# 1
CMG# 2
CMG# 3
CMG# 4

⊢ MANEUVER
✕ JETS

OUTER GIMBAL ANGLES

Legend
CMG# 1
CMG# 2
CMG# 3
CMG# 4
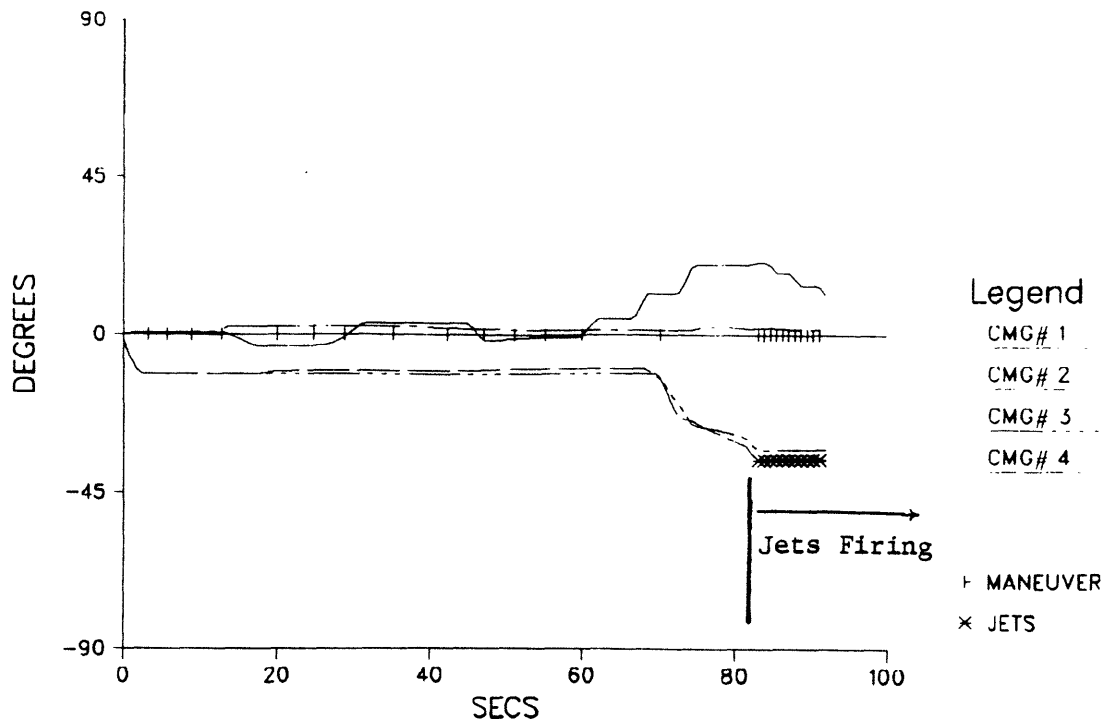
⊢ MANEUVER
✕ JETS
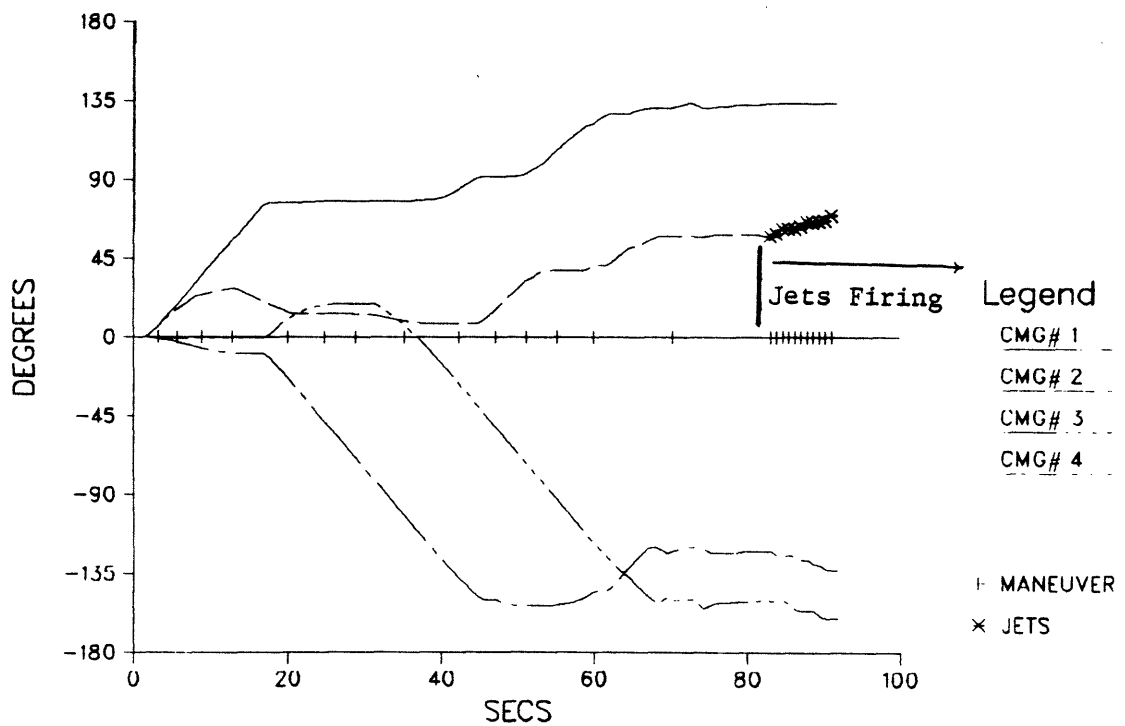
FIGURE 37: Saturate CMGs in Pitch/Roll, No Antilineup in Objective

RELATIVE ANGLES BETWEEN CMG PAIRS PLT#1

CMGs Momentum Saturated
Jets Required

Legend
1.2
1.3
2.3
+ MANEUVER
× JETS

RELATIVE ANGLES BETWEEN CMG PAIRS PLT#2

CMGs Momentum Saturated
Jets Required

Legend
1.4
2.4
3.4
+ MANEUVER
× JETS
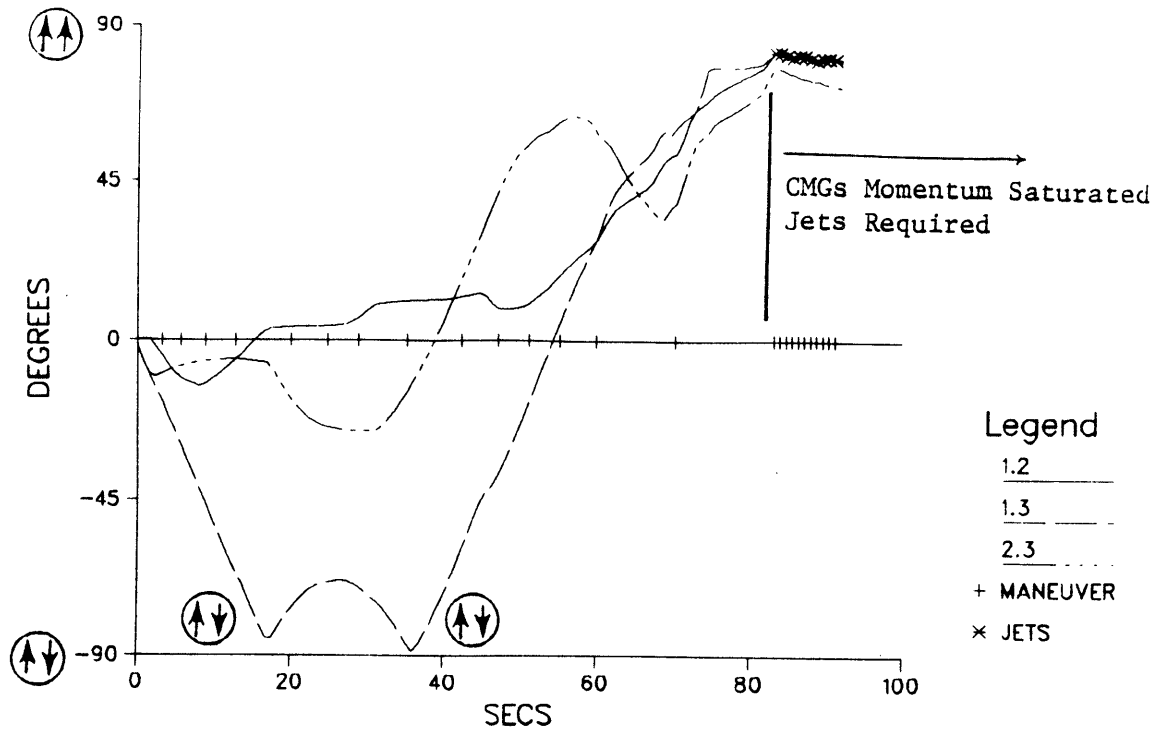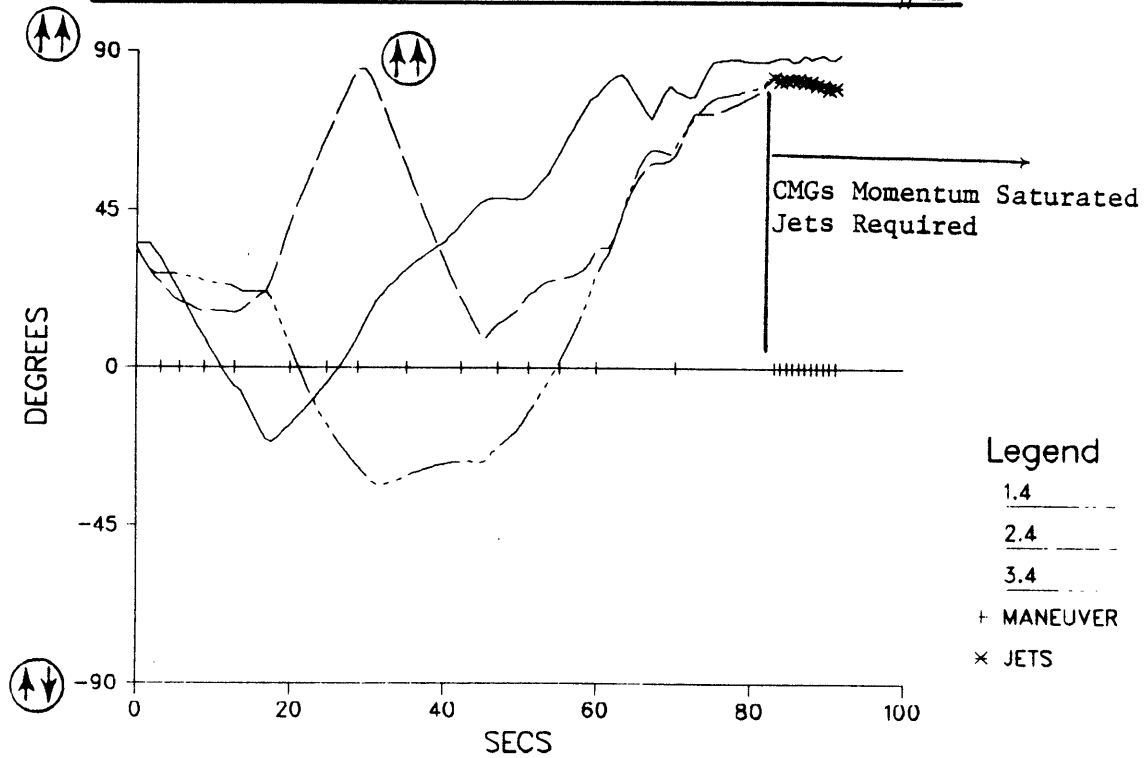
FIGURE 38: Saturate CMGs in Pitch/Roll, No Antilineup in Objective

As mentioned in the previous chapters, the balance between jet firings and CMG useage in hybrid maneuvers is governed by both the upper bounds placed on CMG angular displacement and the ratio of mean jet-to-CMG costs. Although upper bounds become more restrictive as the CMGs approach saturation (re. Sec. 4.2 & 4.3), the software used in these tests is structured to allow up to approx. 20 to 30 degrees of displacement per gimbal when the CMGs are in saturation. This gives sufficent latitude to specify the amount of CMG activity preferred over RCS firings by varying the mean jet-to-CMG cost ratio used in solving hybrid maneuvers.

The mean RCS/CMG costs were adjusted during all previous test runs such that CMGs and jets were essentially evenly priced in hybrid maneuvers (after accounting for the greater RCS control authority). The test run presented in Figs. 39 & 40 was made under "nominal" conditions (as in Fig. 34 & 35), but the effective RCS objective value was made to be over 1000 times higher than the cost of a typical CMG during hybrid maneuvers. The effect of this change is evident in the resulting plots.

Because RCS firings weren't needed, the initial pre-saturation behavior (before t = 60 sec.) is identical to what is seen in Figs. 34 & 35. After saturation, the higher RCS costs in the latter test discouraged the use of jets in hybrid maneuvers. An extended post-saturation interval is seen in Fig. 39, consisting of brief RCS firings coupled with extensive CMG useage. The process is best understood via the rotor alignment plots shown in Fig. 40. One sees a cyclic pattern, where jet firings occuring at saturation (all rotors are aligned at the top of the plot) momentarily allow the CMG system to desaturate slightly (rotors move away from total lineup). Since the input request sequence is a series of rate changes in a constant direction, the CMGs are quickly pushed back into saturation, thus another jet firing is required to complete the maneuver (or answer the next), and the process begins again. This is in stark contrast to the results of Figs. 34 & 35, where jet firings dominated in hybrid maneuvers, and CMG motion was much more restricted.

INNER GIMBAL ANGLES
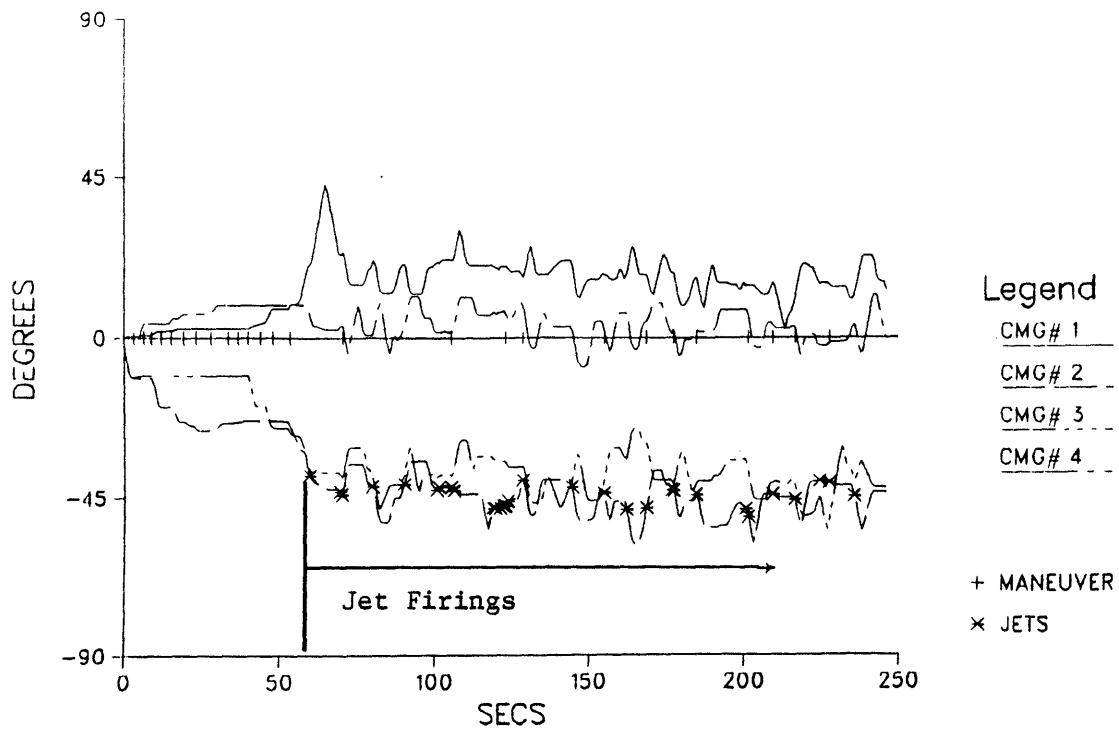
OUTER GIMBAL ANGLES
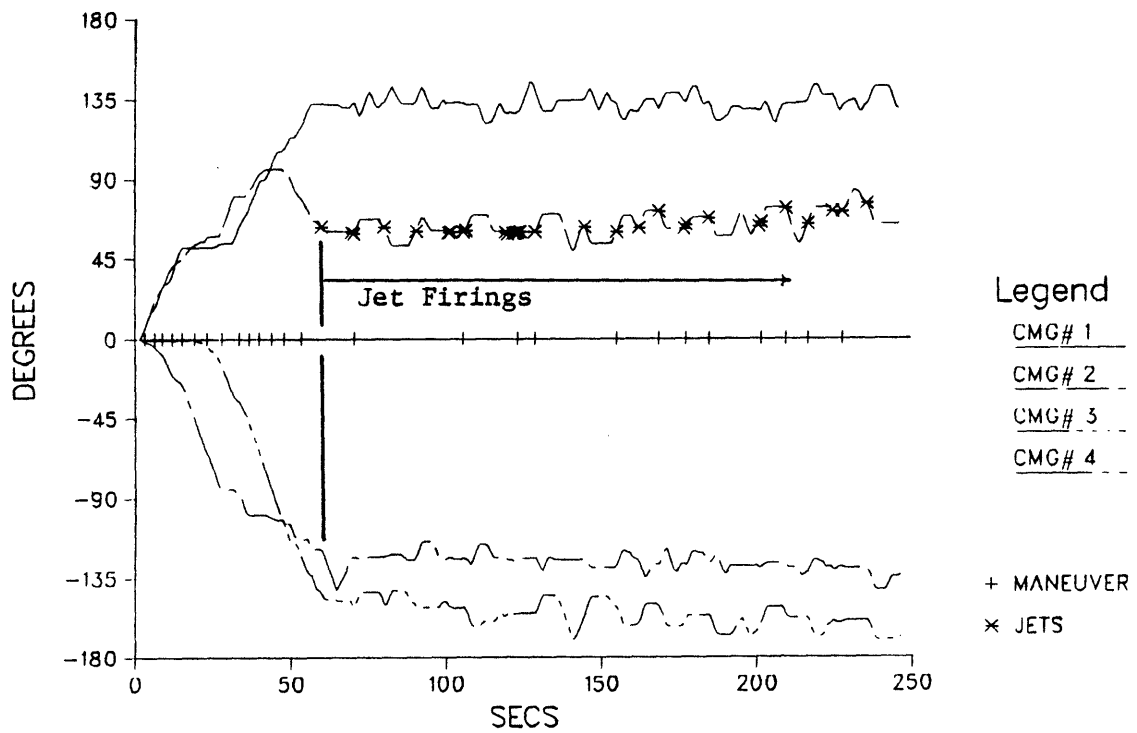
FIGURE 39: Saturate CMGs in Pitch/Roll, Increased Jet Costs
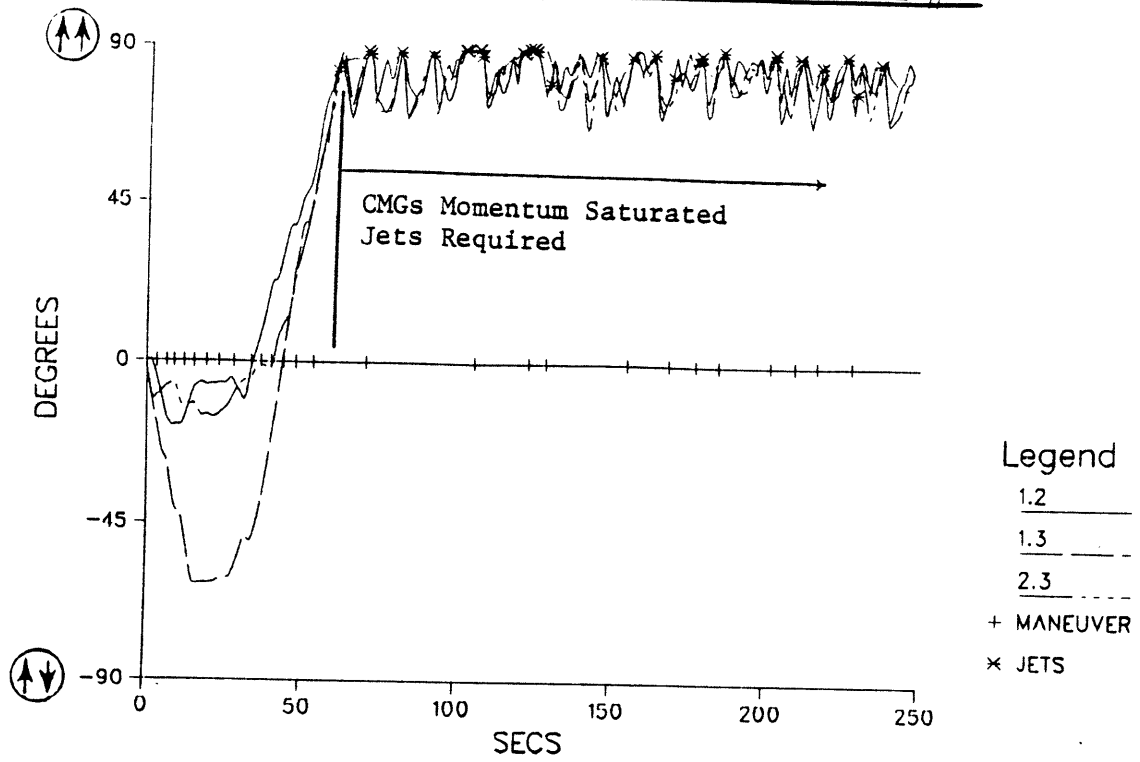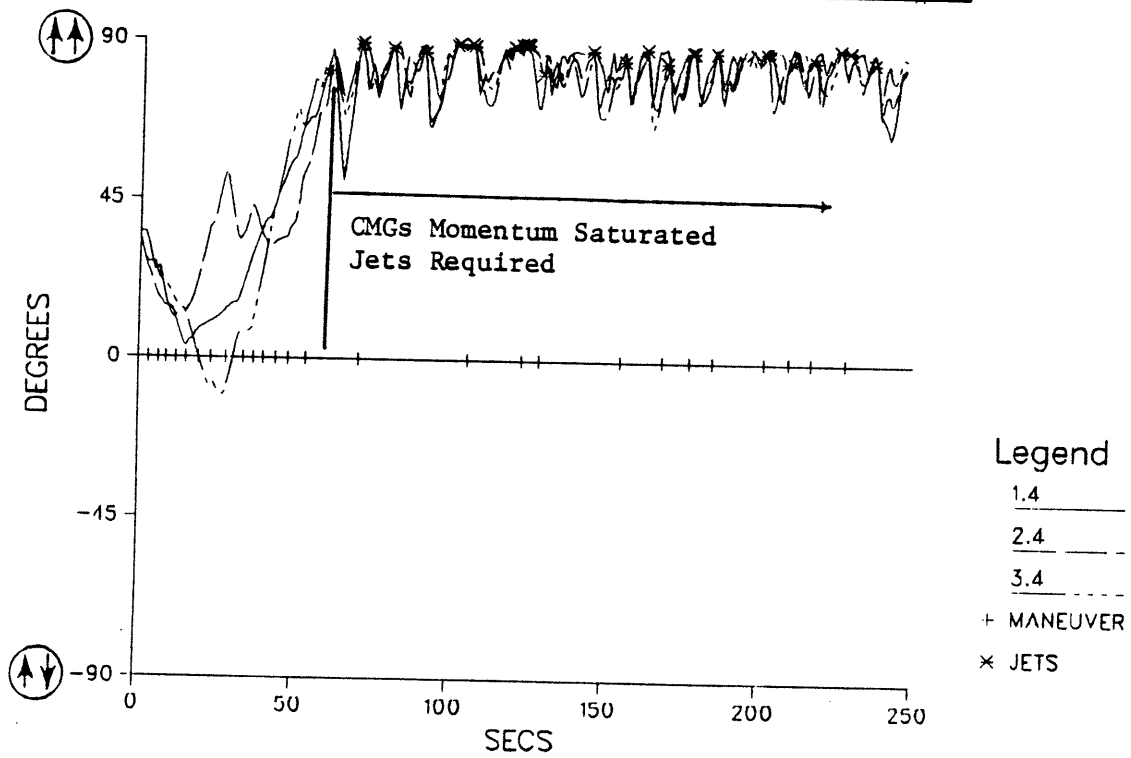
FIGURE 40: Saturate CMGs in Pitch/Roll, Increased Jet Costs

119

These two test runs represent extreme cases. In the first example (Figs. 34 & 35), the CMGs were limited to a strictly "trimming" role in hybrid solutions, thus the bulk of maneuvering was supported by the RCS system, which completed the requests very quickly (via the greater control authority of the jets). The second example (Figs. 39 & 40) used jet firings primarily to desaturate the CMG array, and performed considerable maneuvering exclusively with CMGs (which takes much longer due to the slower CMG response). The RCS/CMG cost ratio thus provides a means of choosing which strategy to pursue in hybrid maneuvering; rapid response achieved primarily with jets, or extensive CMG useage tending toward desaturation. Hybrid maneuvers of the latter type can also be performed in response to a small input request; a means of adapting null motion to allow jet-assisted desaturation is demonstrated later in this section.

The next application of this request sequence uses entirely nominal run conditions (as per the "baseline" results of Figs. 34, 35 & 36), however the CMGs are started in a "sub-optimal" initial orientation (with excessive lineups and inner gimbal angles), and null motion (Sec. 4.4) is attempted after completion of each request. Resulting gimbal angles are presented in Fig. 41. Although CMG #2 is started with an inner gimbal initialized at $\gamma = -75°$, all inner gimbal angles are returned to the origin at t $\simeq$ 40 sec. (as marked on the plot). The rotor alignment plots are presented in Fig. 42, where the finite lineup conditions at initialization are also seen to be brought to a minimum at t $\simeq$ 40 sec. (as marked). Rotors generally avoid alignment until momentum saturation is reached at t $\simeq$ 120 sec., at which point a hybrid RCS/CMG response is necessary.

The upper portion of Fig. 43 shows the net CMG cost (η, Eq. 40) plotted logarithmically across the test run. "X's" are drawn over the curve (and emphasis is added) during sequences where null motion was performed. Null motion is seen to generally produce reductions in total system cost (as noted by the "X's" plotted consistantly on the downward

INNER GIMBAL ANGLES
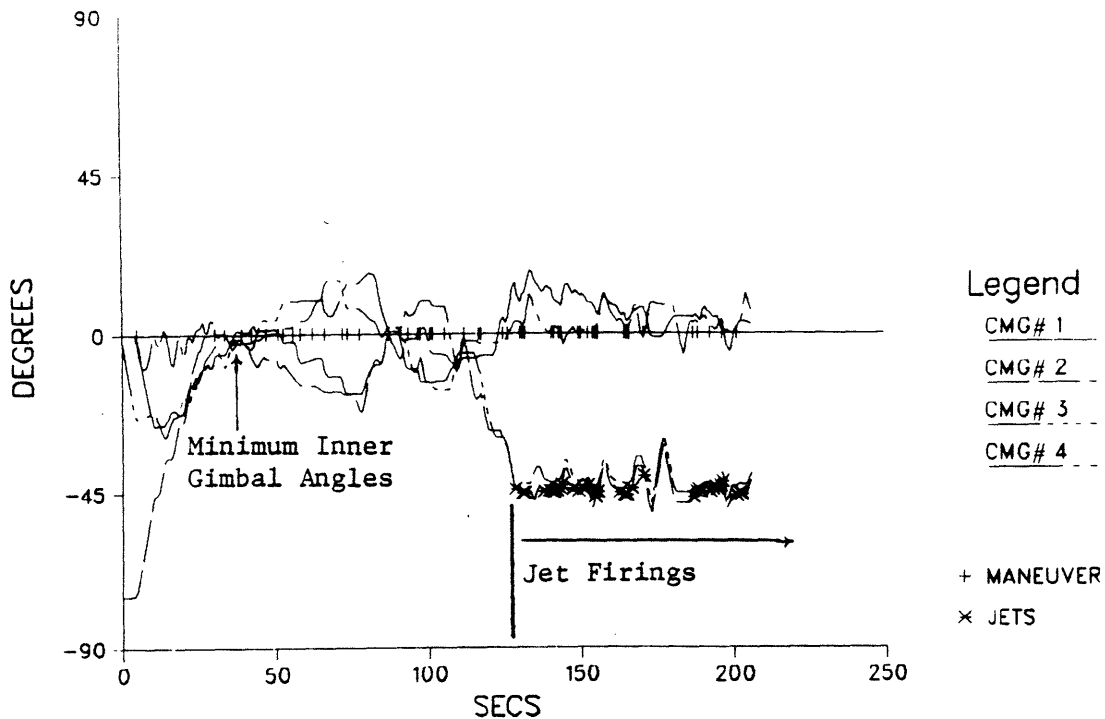
OUTER GIMBAL ANGLES
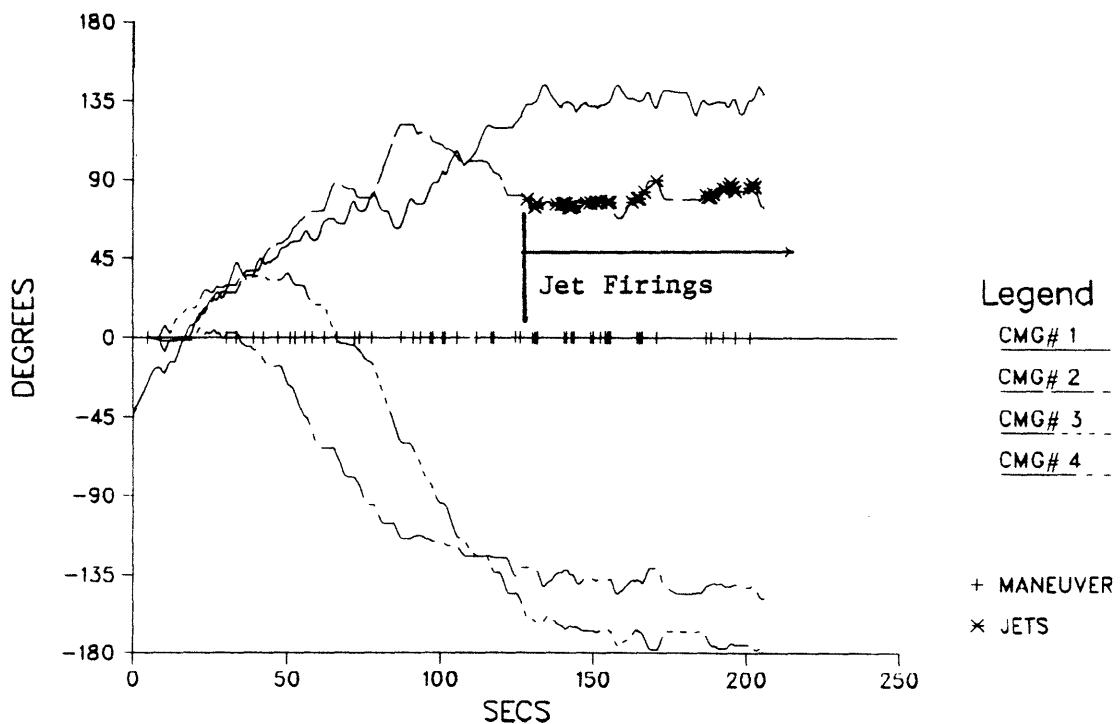
FIGURE 41: Saturate CMGs in Pitch/Roll,
Suboptimal Initialization & Null Motion

121

RELATIVE ANGLES BETWEEN CMG PAIRS PLT#1

Jet Firings

Minimum
Rotor
Lineup

Legend
1.2
1.3
2.3
+ MANEUVER
× JETS

RELATIVE ANGLES BETWEEN CMG PAIRS PLT#2

Minimum
Rotor
Lineup

Jet Firings

Legend
1.4
2.4
3.4
+ MANEUVER
× JETS
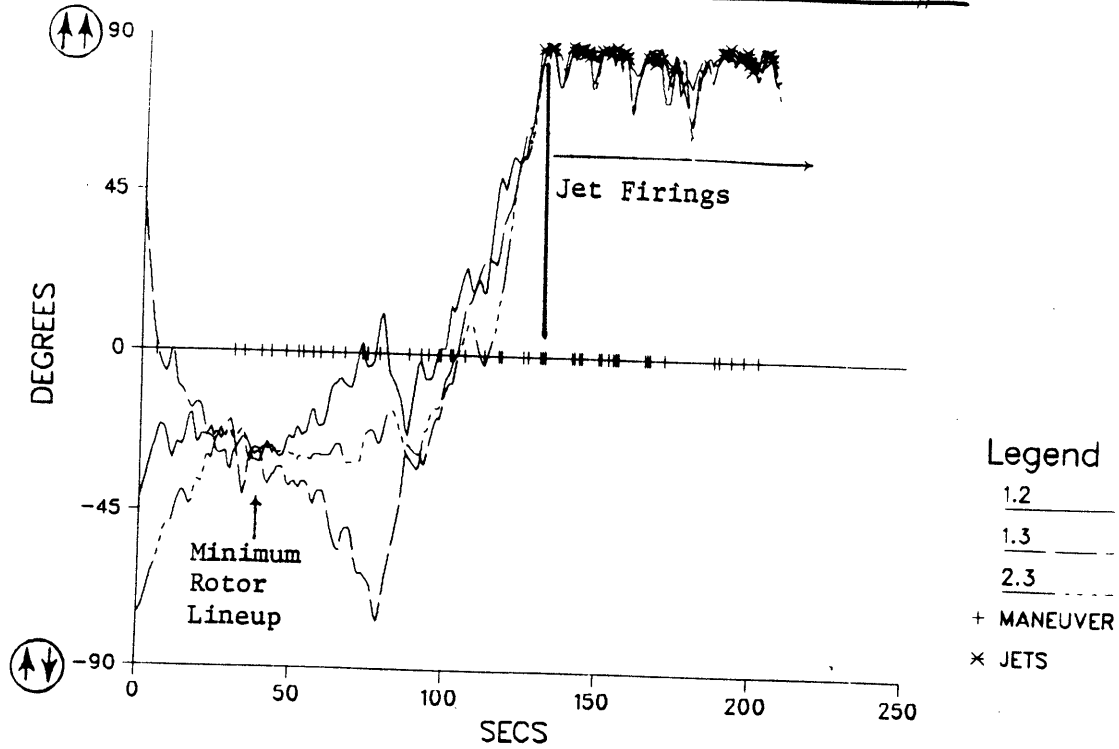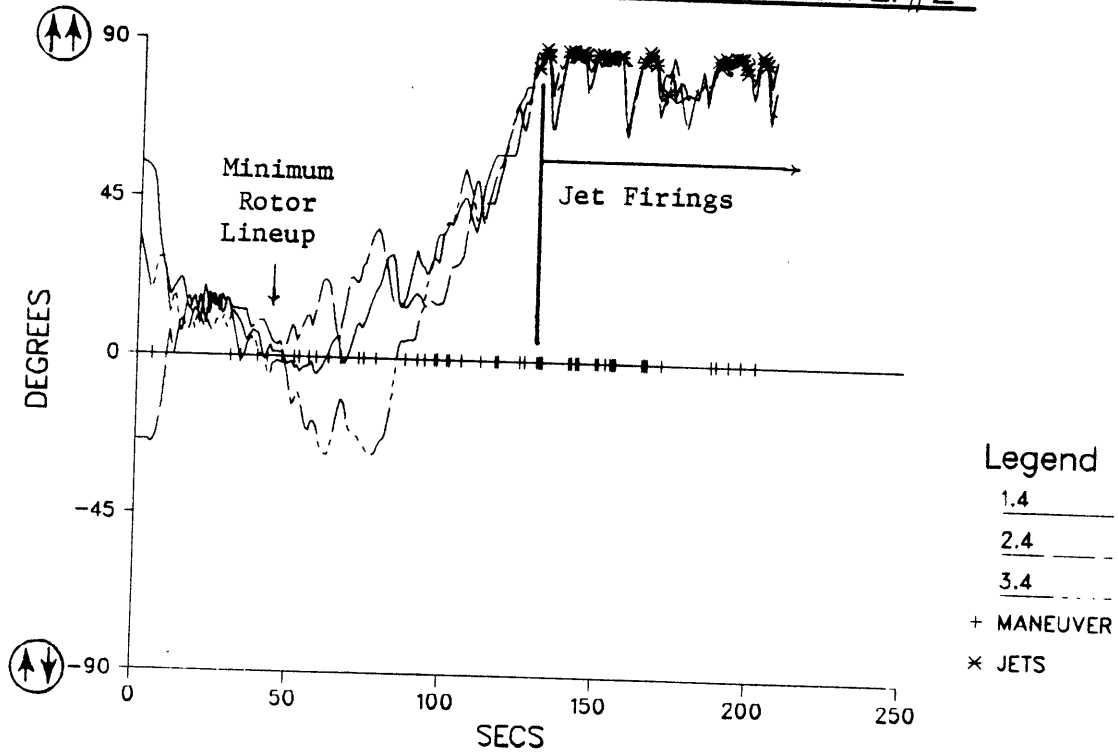
FIGURE 42: Saturate CMGs in Pitch/Roll,
            Suboptimal Initialization & Null Motion

122

TOTAL CMG COST

Legend
NRM. MANEUVER
X NULL MOTION

VEHICLE RATES

Legend
RATE: ROLL
RATE: PITCH
RATE: YAW
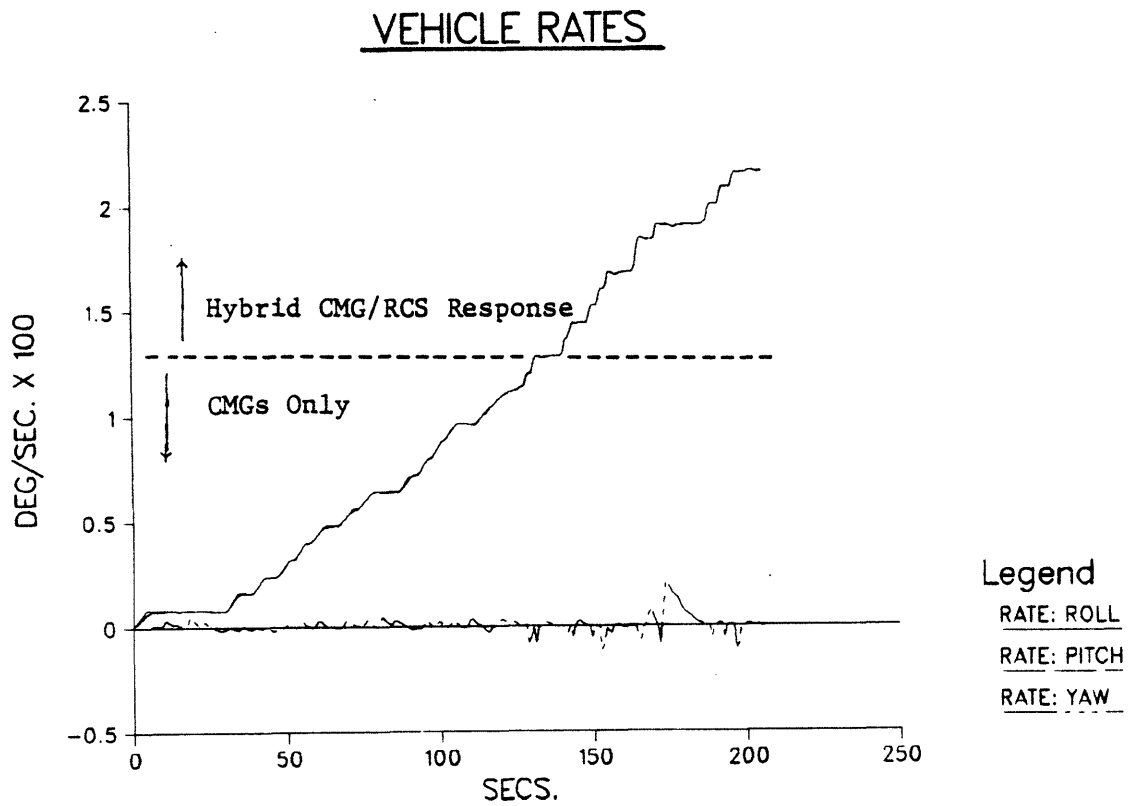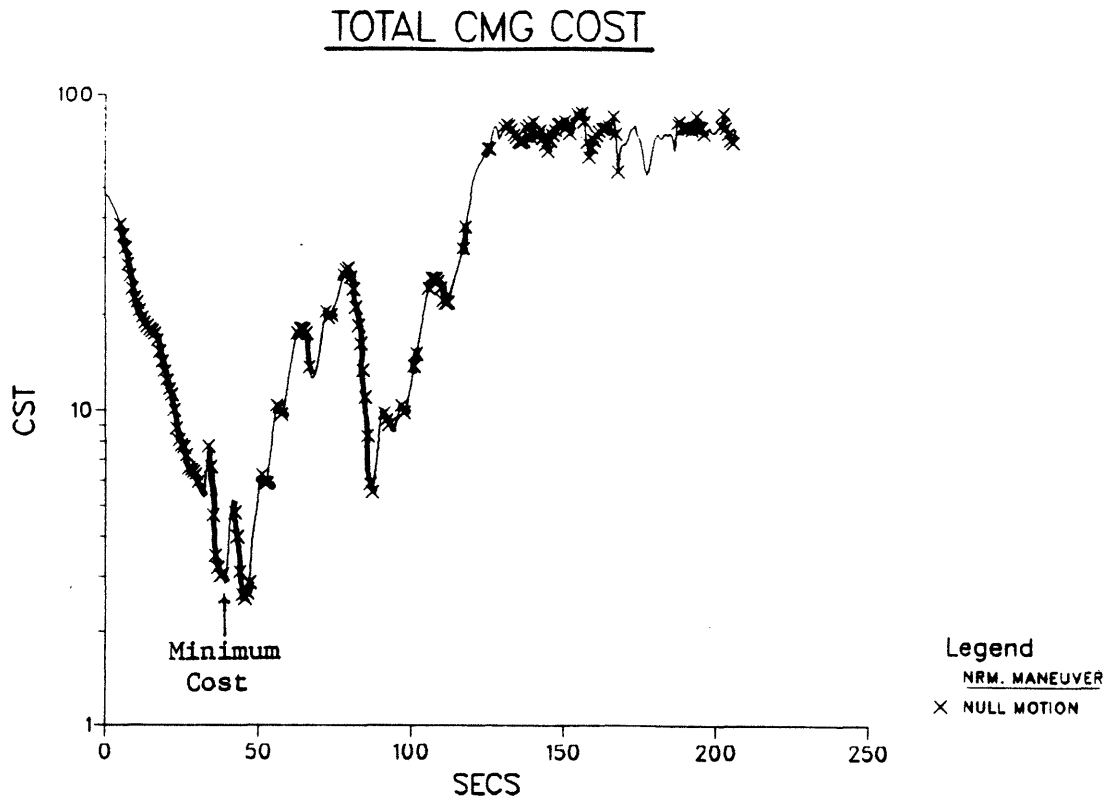
FIGURE 43: Saturate CMGs in Pitch/Roll,
Suboptimal Initialization & Null Motion

123

slopes of the curve). Most significant was the performance of the null procedure in reducing the cost of the expensive "sub-optimal" initial orientation by an order of magnitude. The arrow at $t \approx 40$ sec. (shown to mark a best case on previous plots) is also drawn here; one sees that this point is indeed reflected as a minimum in total CMG cost as achieved primarily via null motion. The null process continually tries to improve the instantaneous CMG configuration after every maneuver is completed. Less success is achieved after the optimum is reached and the CMGs proceed toward momentum saturation (and correspondingly higher cost); fewer possibilities are open for improving the CMG orientation via null motion as saturation is approached.

Resulting vehicle rates are given in the lower plot of Fig. 43. The linear rate increase is evident here (characteristic of the constant request sequence), however the slope possesses several flat areas of constant rate, yielding a "staircase" structure. These flat regions correspond to periods where null motion was performed; the null process is invoked with essentially a zero rate-change command, thus the vehicle is seen to hold constant rates while the CMGs are being re-arranged.

The next test run again uses nominal conditions (as in the baseline case of Figs. 34→36) and starts the CMGs in the standard orientation (all gimbals at zero angle) without using null motion. In this example, the "jet-assisted desaturation" procedure (allowing jets to participate in the null motion process re. Sec. 4.5) is activated after the CMGs become saturated. The resulting gimbal angles are shown in Fig. 44; the interval is noted during which jet-assisted desaturation was in operation. The inner gimbal angles are seen to be drastically reduced (the desaturation process works to drive the CMG costs to a lower value, thus alleviating problem configurations as well as achieving desaturation).

Fig. 45 presents the corresponding rotor alignment plots. Before desaturation begins, these plots depict a history identical to that of Fig. 35. The desaturation maneuver is then seen to pull the CMGs well

INNER GIMBAL ANGLES

Jet Desaturation

Jets
Firing

Jets Firing

Legend
CMG# 1
CMG# 2
CMG# 3
CMG# 4

+ MANEUVER
× JETS

OUTER GIMBAL ANGLES

Jet
Desaturation

Jets Firing

Jets
Firing

Legend
CMG# 1
CMG# 2
CMG# 3
CMG# 4
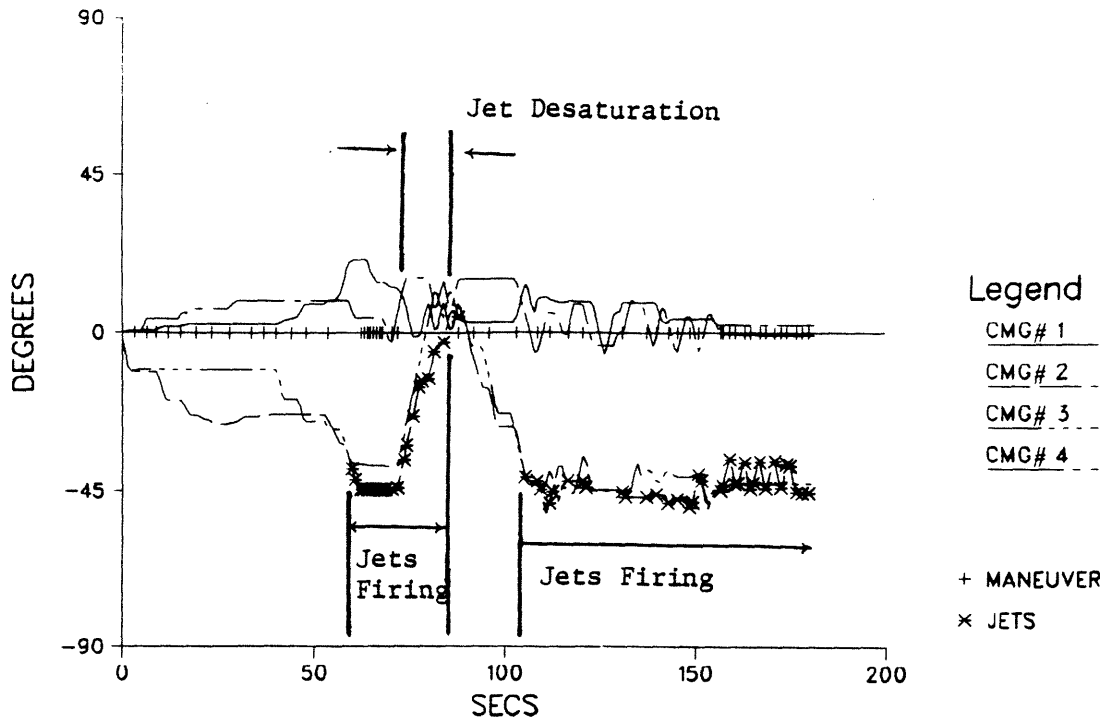
+ MANEUVER
× JETS
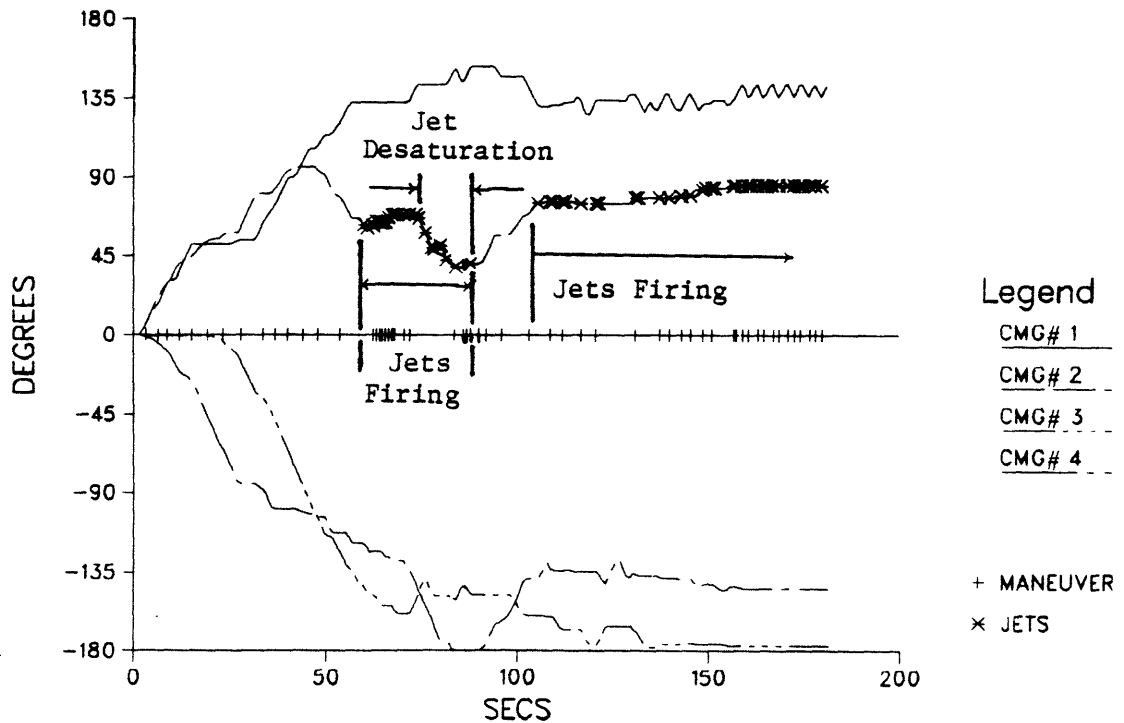
FIGURE 44: Saturate CMGs in Pitch/Roll,
Jet—Assisted Desaturation Commanded

125

RELATIVE ANGLES BETWEEN CMG PAIRS PLT#1
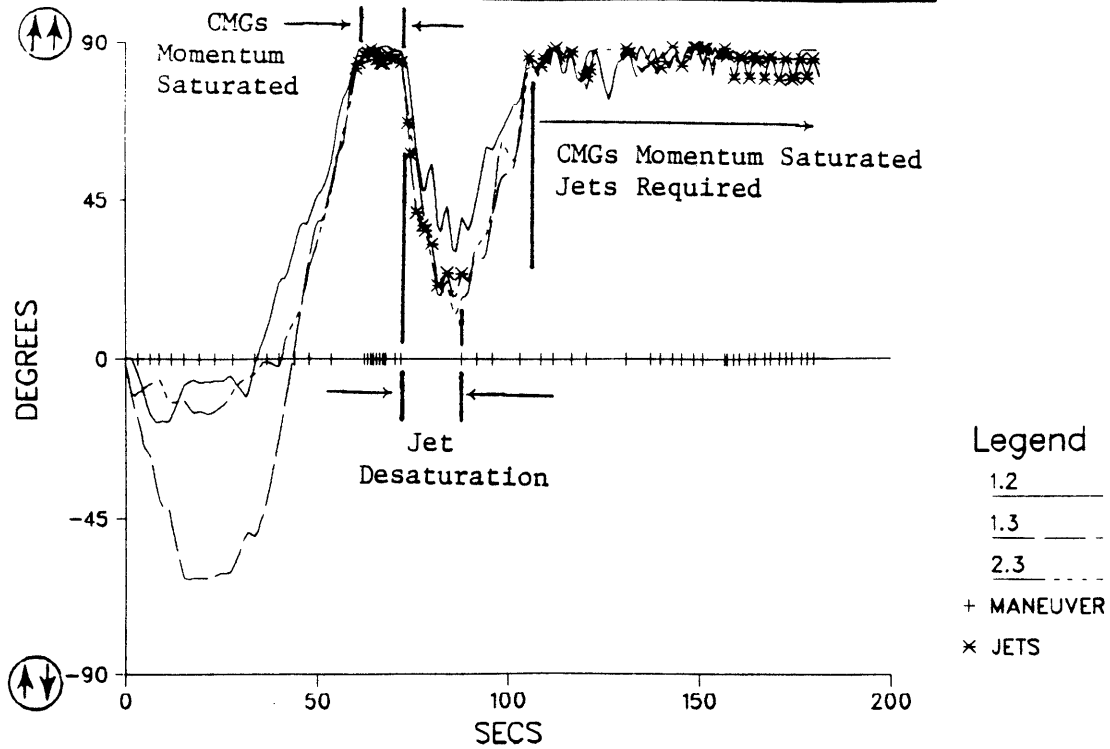
RELATIVE ANGLES BETWEEN CMG PAIRS PLT#2
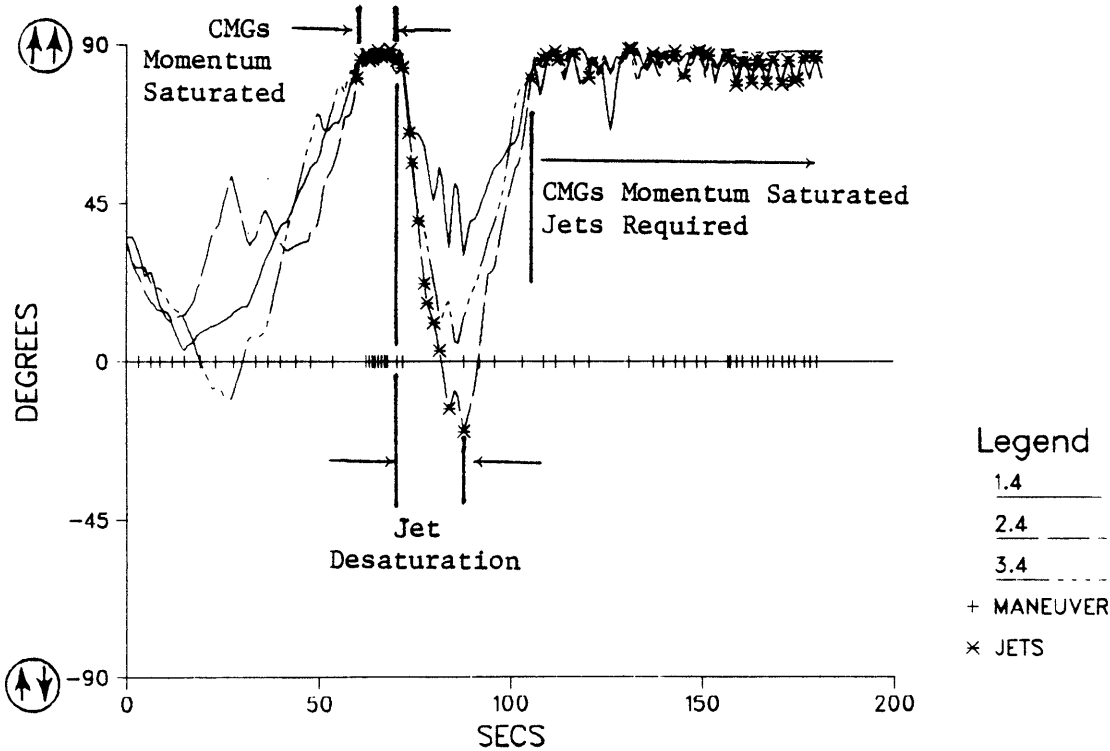
FIGURE 45: Saturate CMGs in Pitch/Roll,
Jet-Assisted Desaturation Commanded

126

TOTAL CMG COST

Legend
NRM. MANEUVER
X NULL MOTION

VEHICLE RATES

Legend
RATE: ROLL
RATE: PITCH
RATE: YAW
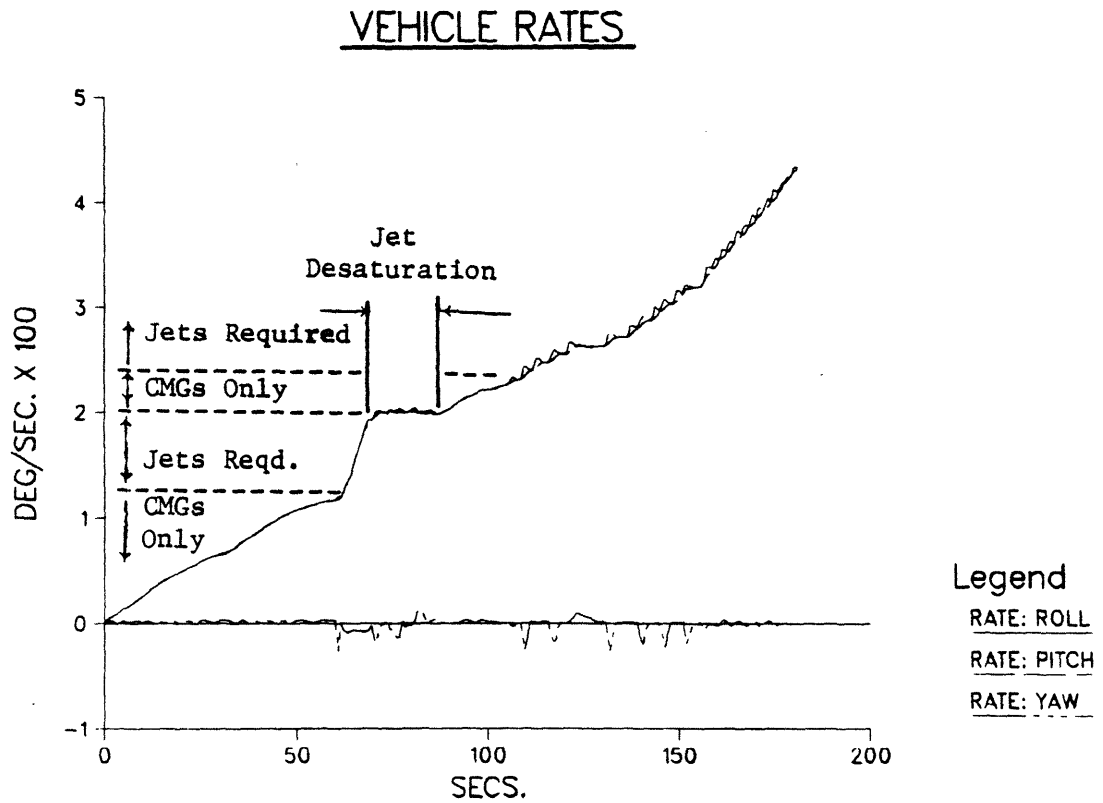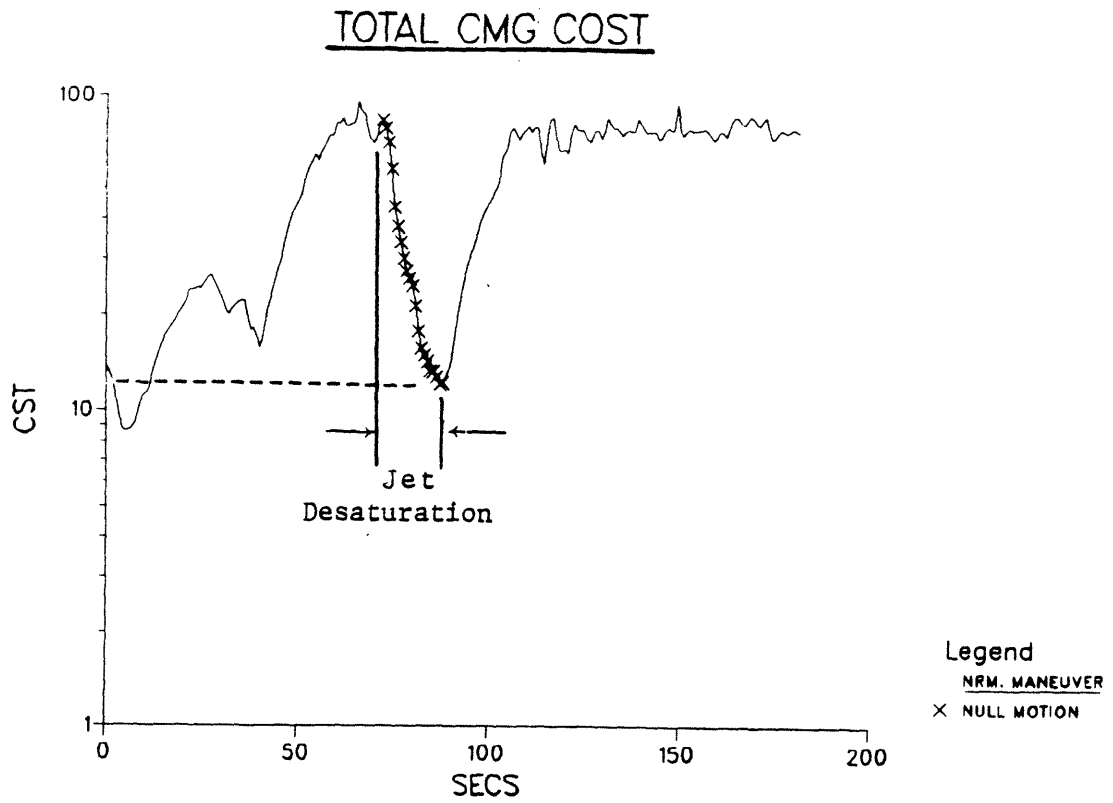
FIGURE 46: Saturate CMGs in Pitch/Roll,
Jet—Assisted Desaturation Commanded

127

II

away from the ultimate saturation alignment, after which an exclusive CMG response is again given to the input requests. The CMG system is eventually pushed once more into saturation (it must be remembered that the CMGs were initially pre-biased with momentum opposite to the input requests, as discussed earlier in this section; because of this, they saturated much more slowly from initialization than they do after the desaturation process).

The net CMG cost is given in Fig. 46; "X's" are drawn during the desaturation operation. One sees that the system is moved after desaturation into an orientation having a cost similar to that at initialization. Resulting vehicle rates are also plotted in Fig. 46; zero vehicle rate change is seen to have occured during the desaturation process. The efficency of such a step-wise desaturation operation depends upon the RCS/CMG cost ratio during hybrid selections, and the amount of momentum desaturation attained is determined by the formulation of the CMG objective coefficients. Detailed investigations into the performance of this process are a topic for future efforts.

5.6) Momentum Saturation of CMG System Along Roll/Yaw Axis

The following set of examples employ a sequence of identical rate-change requests (as in Sec. 5.5), however in these tests, the requests have each a magnitude of 0.0008 deg/sec. about the vehicle roll and yaw axes, and zero about pitch (vs. the cases of Sec. 5.5, which used 0.0008 deg/sec. about pitch and roll, with zero about yaw).

The first test is made including contributions from all cost functions (inner gimbal, stops, and lineup). Gimbal angle profiles are given in Fig. 47; the inner gimbal of CMG #3 is seen to advance to a maximum swing of about 70°, and then hold constant while other gimbals are used to answer requests; it participates again by decreasing its angle toward the conclusion of the test. Rotor alignment plots are given in Fig. 48. The system was steered to avoid rotor lineups; two rotor pairs are seen to approach one another to within approx. 20° during the last requests before saturation, but total alignment has been avoided.

INNER GIMBAL ANGLES

Legend
CMG# 1
CMG# 2
CMG# 3
CMG# 4

+ MANEUVER
× JETS

Jet Firings

OUTER GIMBAL ANGLES

Legend
CMG# 1
CMG# 2
CMG# 3
CMG# 4

+ MANEUVER
× JETS
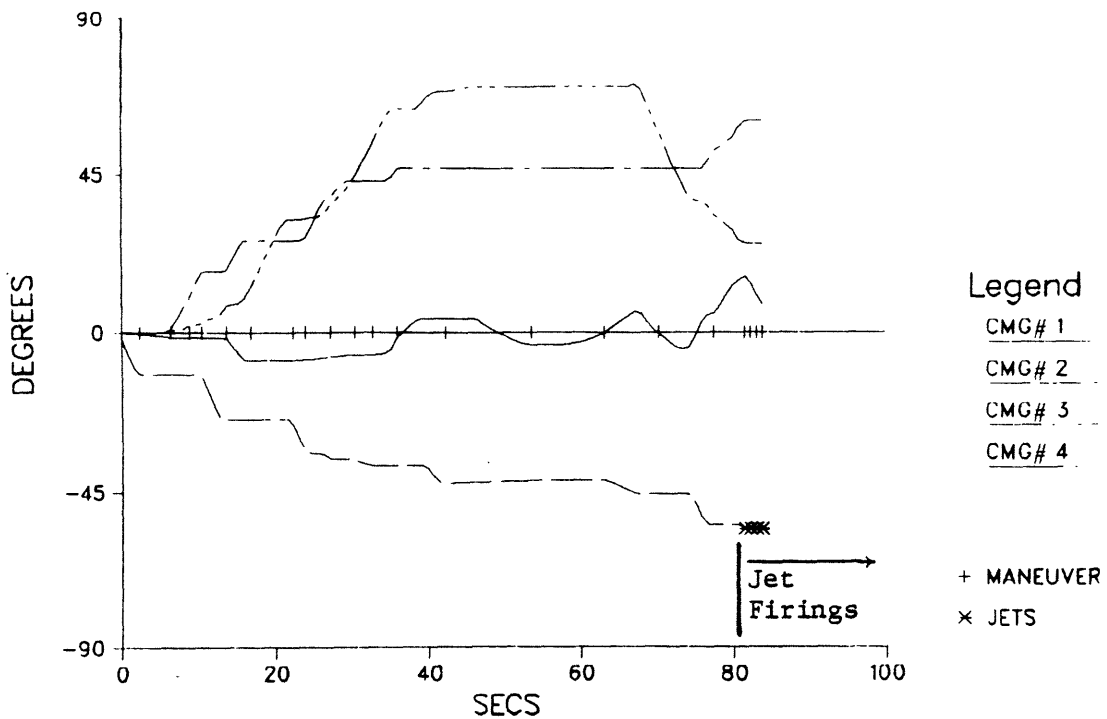
Jet Firings
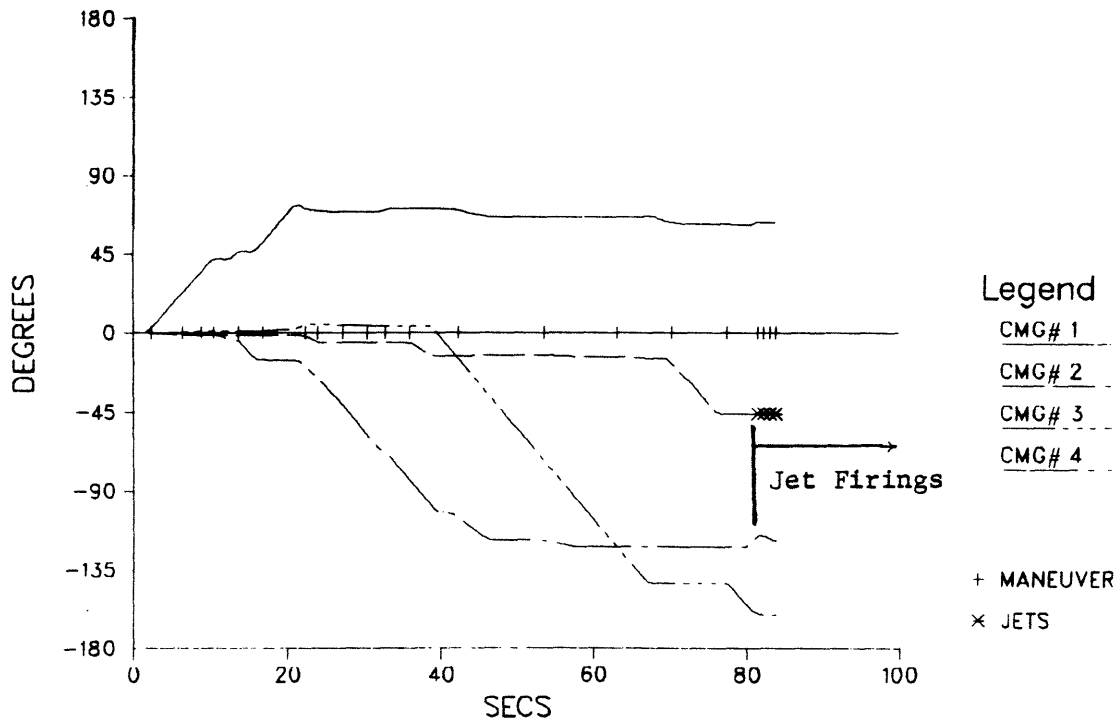
FIGURE 47: Saturate CMGs in Roll/Yaw, Nominal Conditions

129

RELATIVE ANGLES BETWEEN CMG PAIRS PLT#1

CMGs Momentum Saturated
Jets Required

Legend
1.2
1.3
2.3
+ MANEUVER
× JETS

RELATIVE ANGLES BETWEEN CMG PAIRS PLT#2

CMGs Momentum Saturated
Jets Required

Legend
1.4
2.4
3.4
+ MANEUVER
× JETS
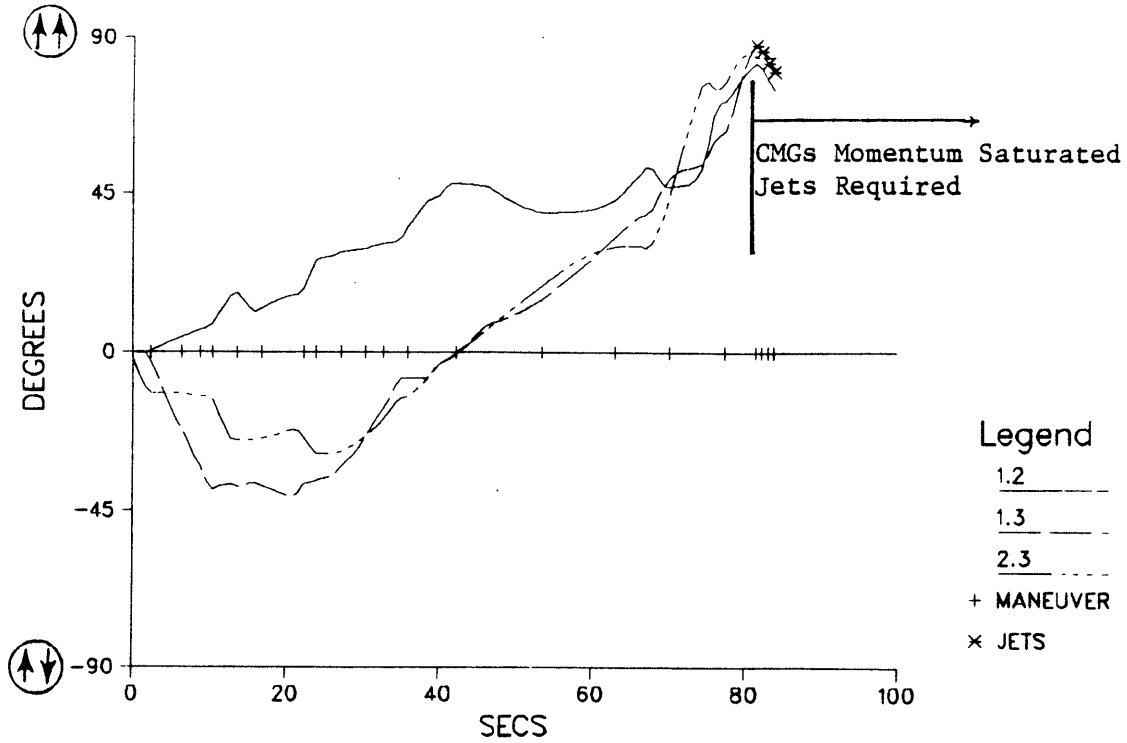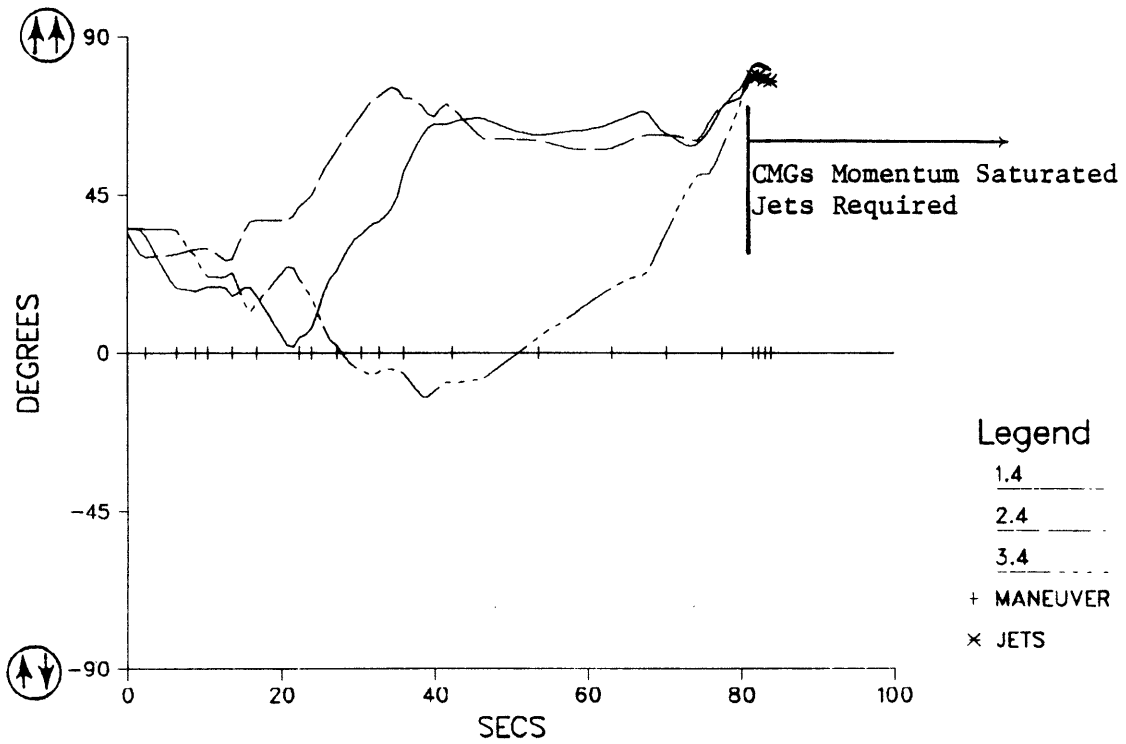
FIGURE 48: Saturate CMGs in Roll/Yaw, Nominal Conditions

SATURATION DETECT
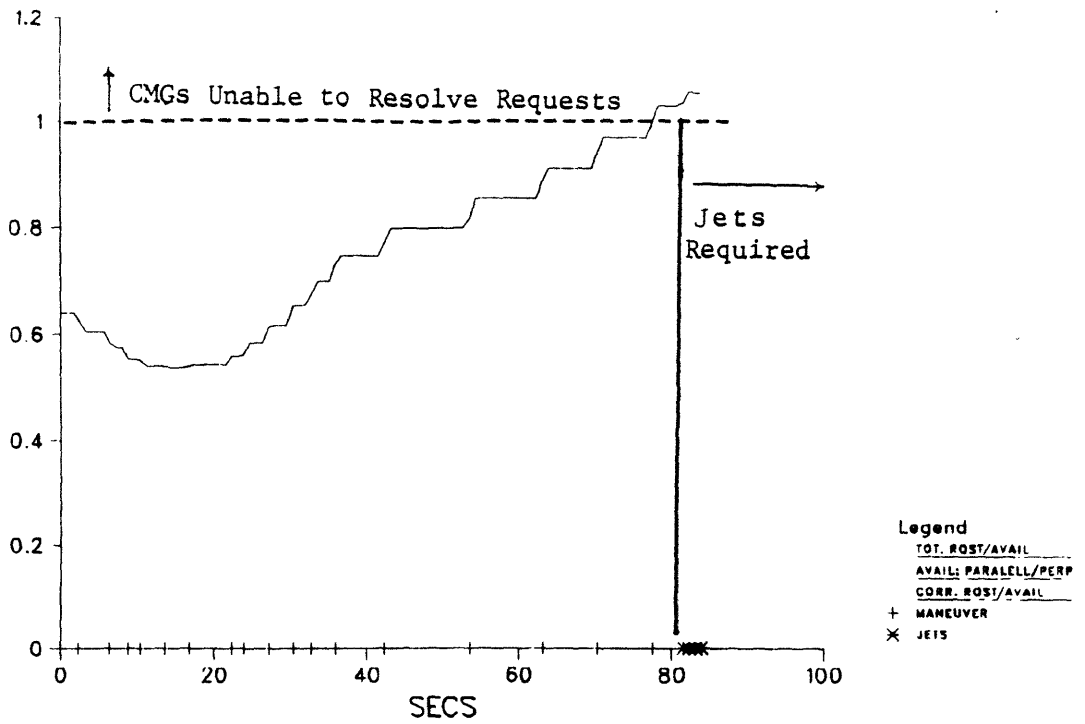
VEHICLE RATES
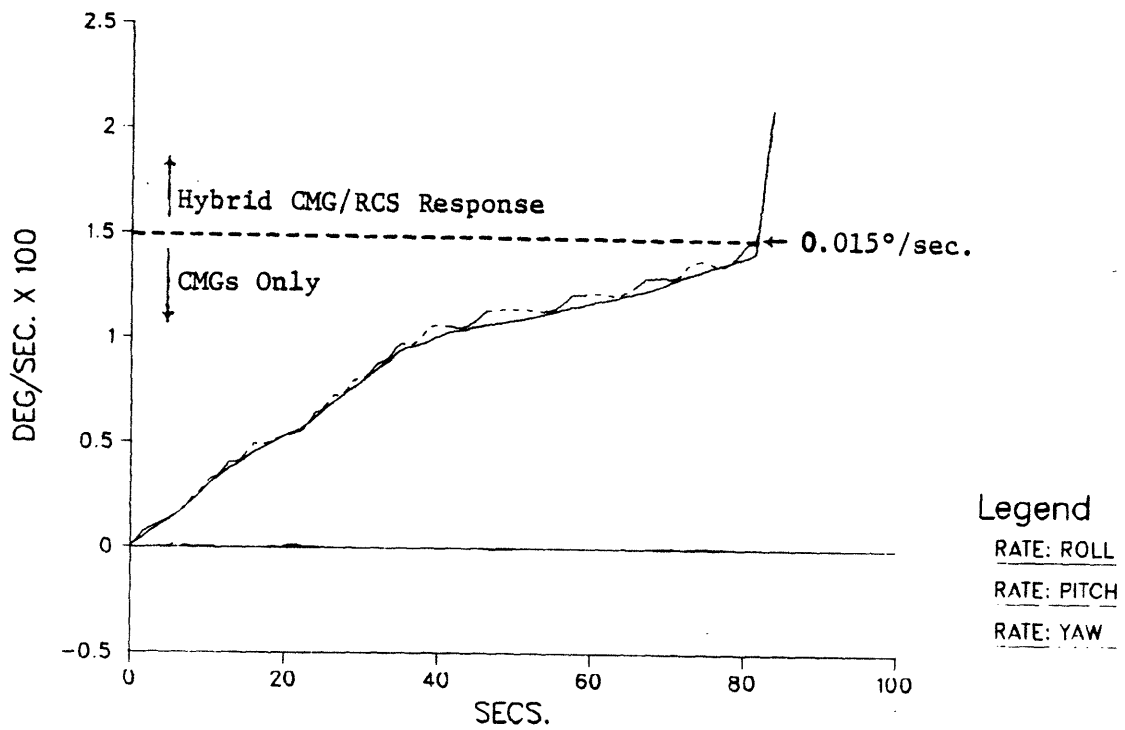
FIGURE 49: Saturate CMGs in Roll/Yaw, Nominal Conditions

131

When all rotors become parallel at saturation, jets are automatically introduced, as seen previously in the results of Sec. 5.5. The upper plot in Fig. 49 shows the saturation index (S) resulting from this run. Jets are not introduced until momentum saturation is indicated (S > 1). The lower plot portrays resultant vehicle response, where we see the nearly linear increase in roll and yaw rates caused by CMG-derived acceleration (the yaw axis does not respond as smoothly, due to its lower inertia), while the pitch rate remains solidly at zero. The increased control authority of the jets is evident at the point where they are introduced.

Fig. 50 shows the gimbal angles arising from a test run performed with the same request sequence, but with zero stops-avoidance objective contribution (ie. K_S = 0; Eq. 30). The inner gimbal angle of CMG #3 is again seen to increase, however it no longer halts at γ = 70°, but continues to advance until it runs against its stop, where it remains throughout the remainder of the test. Corresponding rotor alignments are given in Fig. 51. Lineups are completely avoided (the CMGs are being steered away from potential lineup at the expense of moving the inner gimbal of CMG #3 against its stop). The system is in an effective saturation state when jets are introduced; the three "free" CMG rotors align together in saturation, while the rotor that is pushed against its stop is unable to complete the alignment (thus yielding the curves in Fig. 51 which finish away from lineup). The saturation index (S) is plotted in the upper portion of Fig. 52. We see that jets are introduced at S $\approx$ 0.9; the CMG rotor which is held against its stop has prevented the system from reaching saturation at S > 1 and delivering all available CMG momentum into the vehicle. The additional curves which appear on the plot are corrections which reflect the fact that CMG #3 effectively becomes a single-gimballed device once a request pins its inner gimbal against a stop (see Sec. 4.2).

The resulting vehicle rates are presented in the lower plot of Fig. 52; a marked similarity to the analogous plot of the "nominal" Fig.

INNER GIMBAL ANGLES
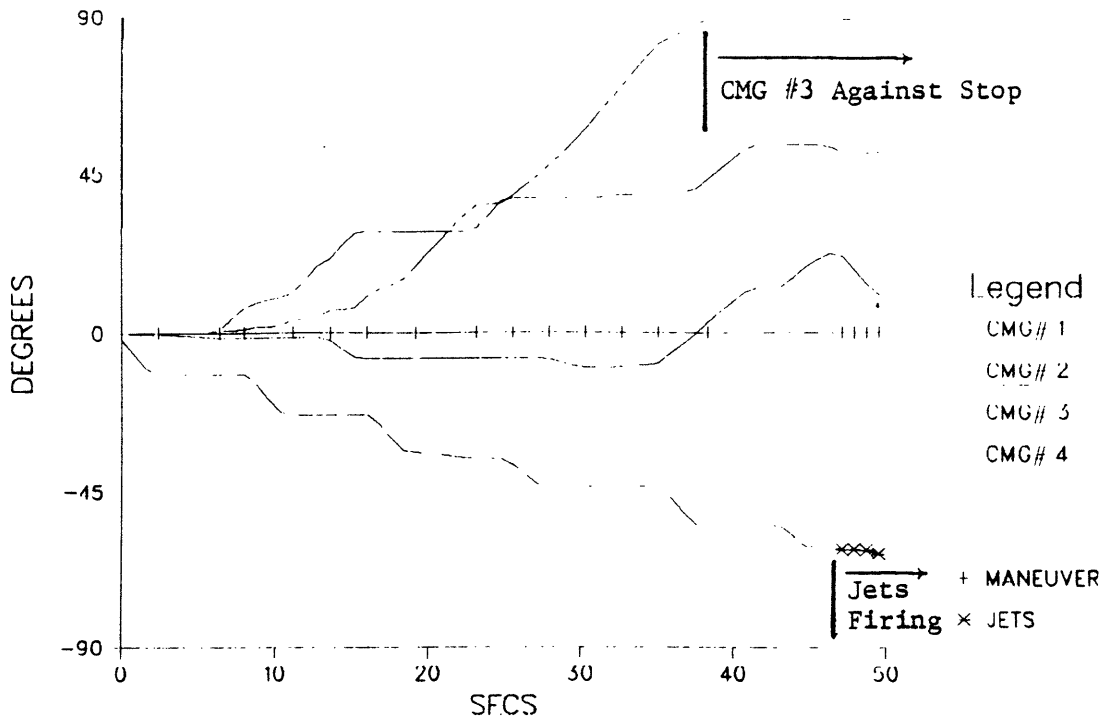
OUTER GIMBAL ANGLES
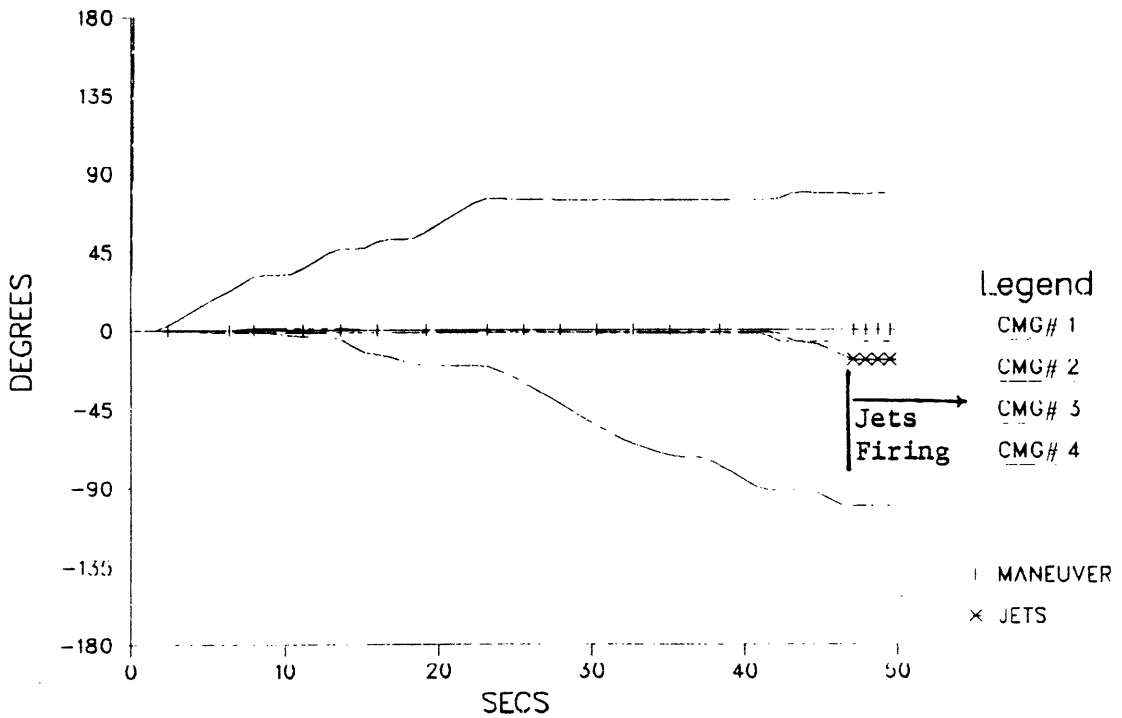
FIGURE 50: Saturate CMGs in Roll/Yaw,
No Stops Avoidance in Objective

133

RELATIVE ANGLES BETWEEN CMG PAIRS PLT#1

Jets
Required

Relative to
CMG #3

Legend
1.2
1.3
2.3
| MANEUVER
× JETS

DEGREES

90
45
0
-45
-90

SECS
0   10   20   30   40   50

RELATIVE ANGLES BETWEEN CMG PAIRS PLT#2

Jets
Required

Relative to
CMG #3

Legend
1.4
2.4
3.4
| MANEUVER
× JETS

DEGREES

90
45
0
-45
-90

SECS
0   10   20   30   40   50
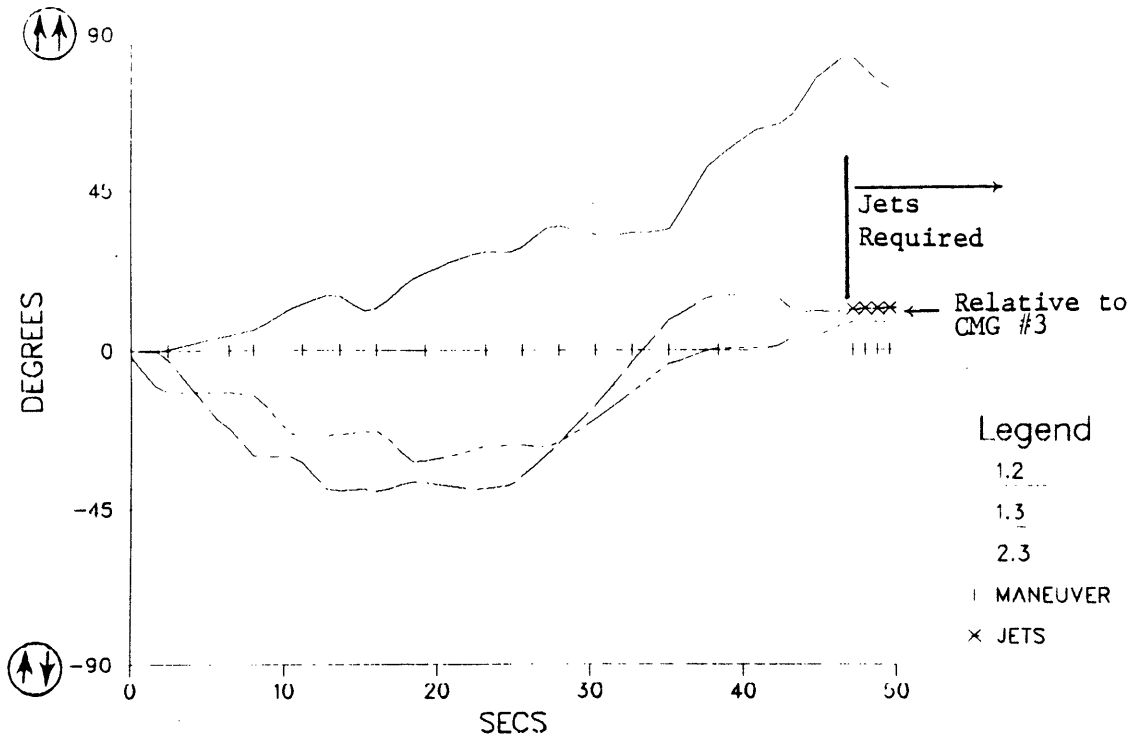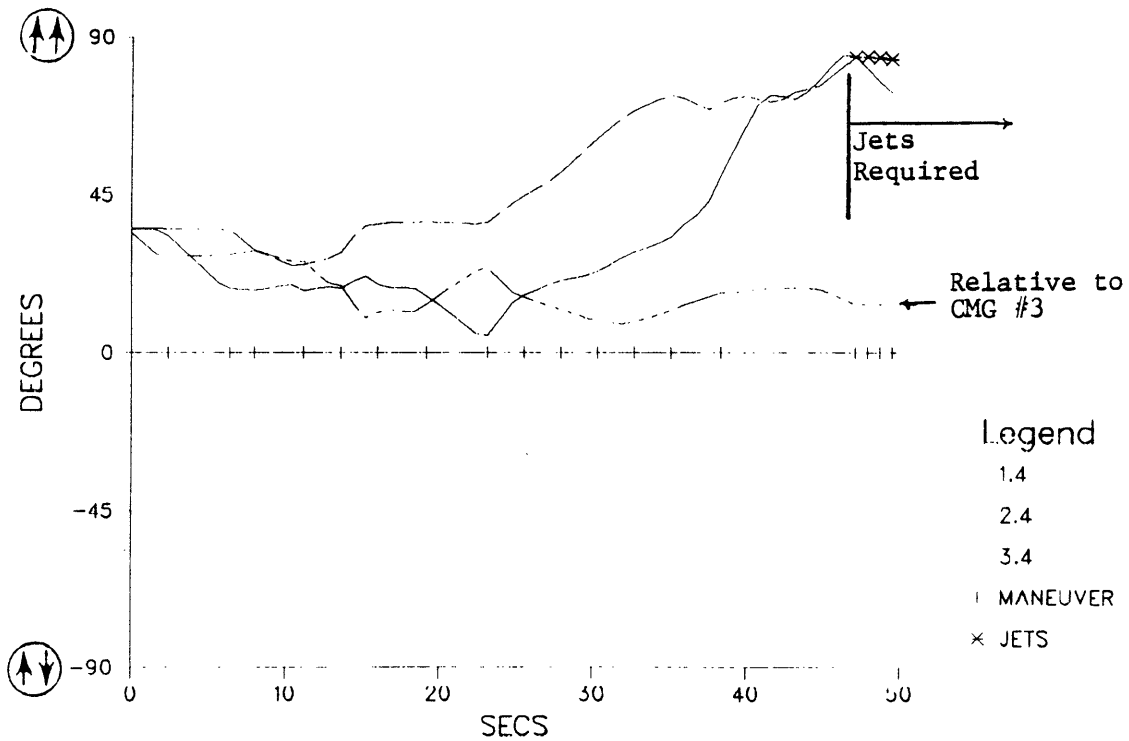
FIGURE 51: Saturate CMGs in Roll/Yaw,
No Stops Avoidance in Objective

134

SATURATION DETECT
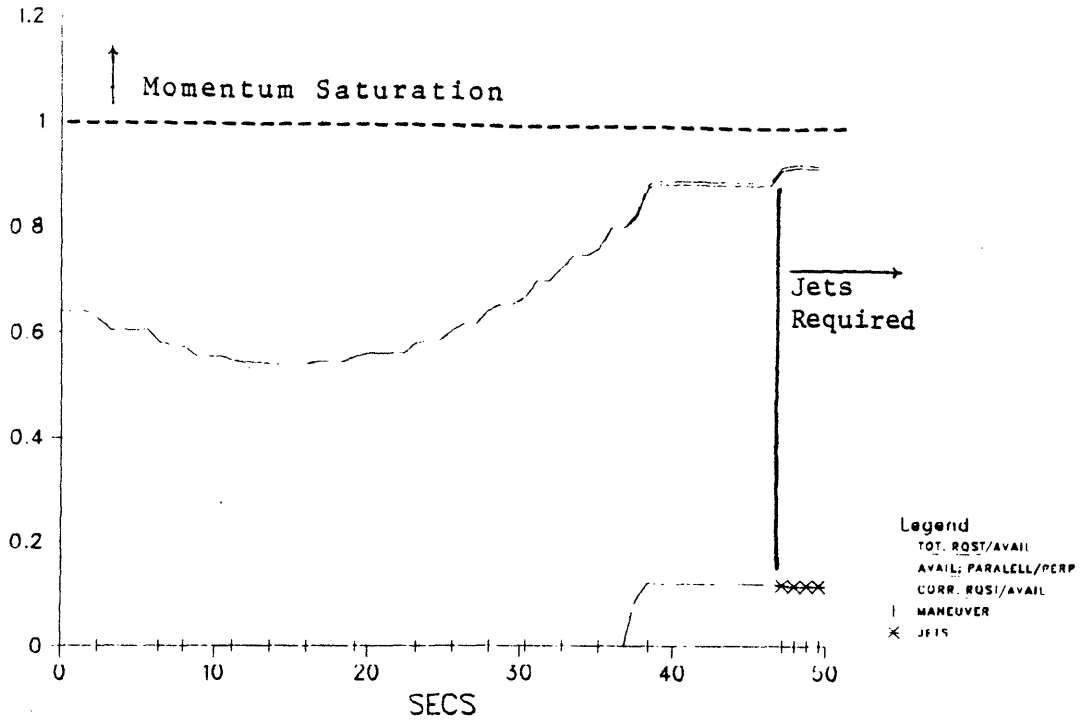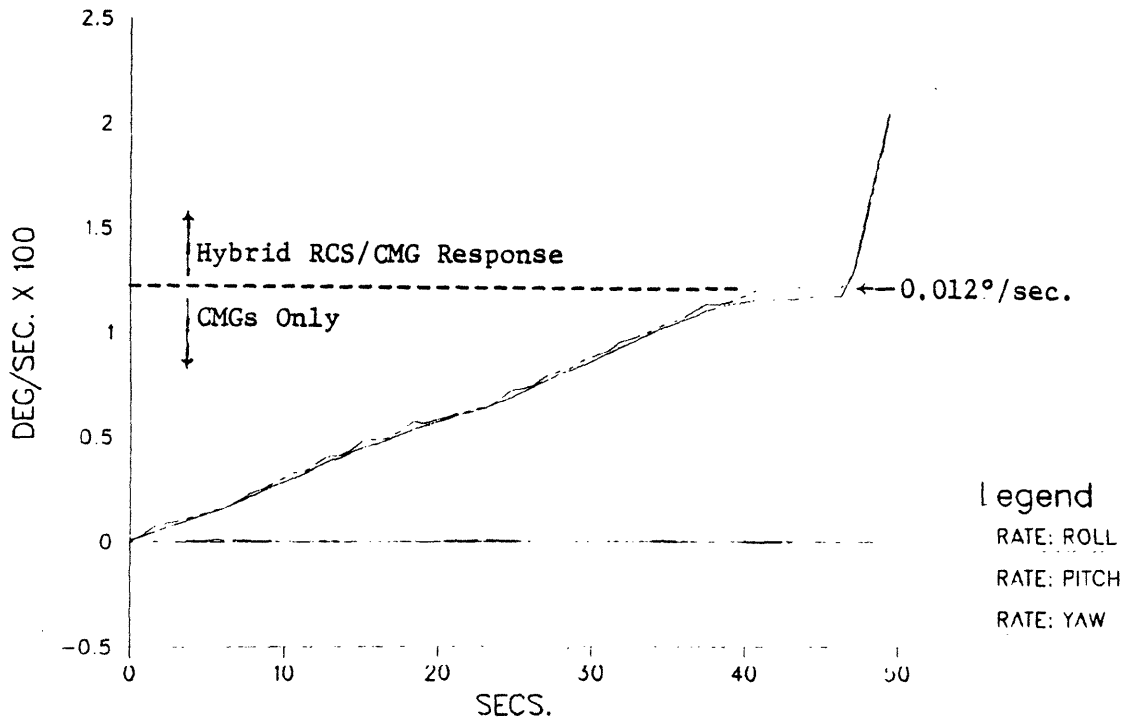
VEHICLE RATES

FIGURE 52: Saturate CMGs in Roll/Yaw,
No Stops Avoidance in Objective

135

49 can be noticed, with the exception that jets are required at a lower vehicle rate due to the lack of complete momentum transfer at saturation.

The preceeding examples have demonstrated the utility of the stops-avoidance function, whereby a quanitative "warning" is issued to the selection procedure that encourages an alternative strategy to be pursued before a CMG is forced against its stop (the configuration with a CMG hung against a stop and the others aligned in saturation is generally stable; desaturation efforts may be required to dislodge the affected CMG gimbal).

CHAPTER 6

INCORPORATION OF SINGLE GIMBALLED CMGS

6.1)   Overview

Single gimballed CMGs were introduced in Sec. 2.1, and a sample
device is diagrammed in Fig. 9. Relations needed to construct activity
vectors were specified in Sec. 2.5. Since the concepts presented and
demonstrated in the preceeding chapters can easily be applied to steer an
array of single gimballed CMGs, one might inductively assume that the
steering and objective criteria developed earlier for double gimballed
CMGs may be also adequate for a single gimballed system. This is not
generally true.

Each double gimballed CMG can exercise two degrees of freedom in
orienting the rotor angular momentum vector. This yields a significant
control advantage over single gimballed CMGs, which possess only one
degree of freedom per device, hence are constrained to gimbal in fixed
planes. Because of this limitation, single gimballed systems are
particularly prone to lockup in internal singular states (as discussed
below), hence present a significantly greater challenge[34] to candidate
steering procedures.

A CMG system is defined to be in an internal singular state when
it enters a configuration which loses three-axis controllability before
transferring all CMG momentum into the spacecraft (ie. total control is
lost before saturation is reached). All singular configurations in
double-gimballed systems are associated with rotor lineups, as was
outlined in Sec. 3.4. A pair of double gimballed CMGs with angular

137
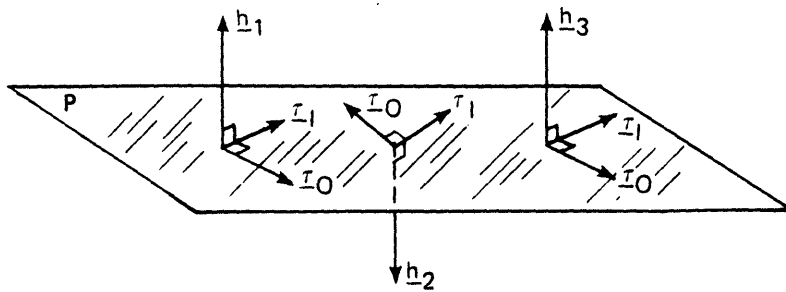
(a) SINGULAR STATE OF 3 DOUBLE GIMBALLED CMGs;
CONTROL RESTRICTED TO PLANE P.
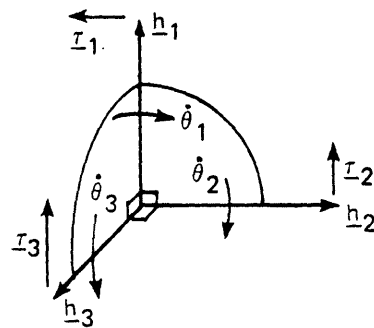
(b) SINGULAR STATE OF 3 SINGLE GIMBALLED CMGs
WITH ORTHOGONAL ROTORS. ROTORS $\underline{h}_1$ AND $\underline{h}_2$
GIMBAL IN THE PLANE $(\underline{h}_1, \underline{h}_2)$, AND ROTOR $\underline{h}_3$
GIMBALS IN PLANE $(\underline{h}_1, \underline{h}_3)$
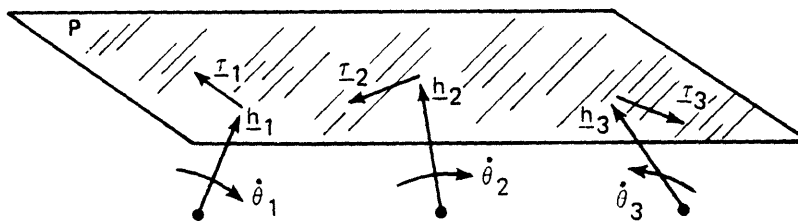
(c) SINGULAR STATE OF 3 SINGLE GIMBALLED CMGs
LACKING DIRECT TORQUE OR ROTOR ALIGNMENTS.
CONTROL RESTRICTED TO PLANE P. THE VECTORS
$\underline{\tau}_1, \underline{\tau}_2$, AND $\underline{\tau}_3$ ARE COPLANAR.

FIGURE 53: INTERNAL SINGULAR STATES OF CMG SYSTEMS

momentum vectors aligned can exert torques only in the plane perpendicular to their rotor axes; control is lost along the direction of alignment. The three-CMG system sketched in Fig. 53a is an example of an internal singular state of a double gimballed CMG ensemble. Because of the three aligned CMGs, control is lost along the lineup axis (all output torques lie in the plane **P**), yet the system has not reached saturation due to the anti-parallel alignment. The Y_{Lineup} objective contribution works to avoid these situations, as described in Sec. 3.4 and demonstrated in Sec. 5. The configuration of Fig. 53a also represents an internal singular state of a single gimballed CMG system, and may likewise be avoided by steering away from rotor lineups.

Because of the reduced freedom available to single gimballed systems, other types of configurations can also become singular. An example is shown in Fig. 53b, where the output torque vectors of two orthogonal CMG rotors have become aligned ($\underline{\tau}_2$, $\underline{\tau}_3$), causing the system to lose a degree of freedom, and limiting available control to the plane defined by the remaining two independent CMG torques. This singular state is not avoided by discouraging rotor lineup; it is in fact "favored" for this configuration, since all CMGs become orthogonal.

Singular states in single-gimballed systems are not always related to direct torque lineups. Fig. 53c illustrates a case where three CMGs form a singular configuration with all output torques coplanar, yet lack any direct torque or rotor alignments.

Recognition and avoidance of singular states is thus a considerably more complicated process for single gimballed CMG systems. It is generally not sufficent to only steer the CMG rotors away from alignments; the objective function must be re-formulated to identify and account for these other singular configurations in order to manage excess degrees of freedom such that 3-axis vehicle control is retained.

6.2) Adaptation of the Objective Function

Eq. 30b specifies the calculation of objective coefficents for double gimballed CMGs. Since the term "inner gimbal" has no relevance to a single gimballed CMG, the inner gimbal minimization component (F_{Angle}) is not calculated, and K_A is set to zero. Gimbal stops are unaffected, and the $K_S G_{Stops}$ term is retained. The Y_{Lineup} term acts to avoid internal singularities by steering the system away from rotor alignments. This function must be altered to account for the other types of internal singular orientations possible in single gimballed CMG systems.

One of the simplest methods which might be attempted involves steering the CMGs to avoid alignments between CMG output torques (as opposed to CMG rotors). The logic of Eq. 33 may easily be modified to attain this by exchanging the negative rotor directions $(-\hat{h})$ with the corresponding instantaneous rotation vectors $(\hat{R})$, and vice-versa (the CMG output torques lie along $-\hat{R}$, and the direction of instantaneous torque rotation is along $-\hat{h}$). Eq. 33 must be modified such that the summation runs over all CMG gimbals (i), as opposed to CMG rotors (I). The exchange outlined above must be performed to Eqs. 34, as detailed below:

43)
$$m(i,j) = \frac{\pi}{2} - \cos^{-1}(\hat{R}_j' \cdot \hat{R}_i)$$

$$\hat{R}_j' = \hat{R}_j \ \text{sign}(\hat{R}_i \cdot \hat{R}_j)$$

$$SG(i,j,s) = s \ \text{sign}\{(\hat{R}_i - \hat{R}_j) \cdot (-\hat{h}_j)\}$$

$\hat{R}_j$ = unit vector in direction of instantaneous rotor gimballing for CMG gimbal #j, positive sense assumed.

Eqs. 43, when inserted into the modified Eq. 33, produces a Y_{Lineup} function that acts to avoid alignments of CMG output

140

torques. This introduces an amplitude into the objective which directly attempts to steer CMGs away from singular orientations as portrayed in Figs. 53 a & b, which are characterized by torque vector alignments. The planar alignment of Fig. 53c is a more subtle càse; the torque antilineup function does not steer the system directly away from co-planar singularities. Since the mutual angles between output torques can be larger when all torque vectors are not co-planar, the torque anti-lineup function should generally encourage non-planar orientations.

The controllability provided by a general CMG system in any particular orientation may be specified by the determinant defined below:[12,17,19,21,34-36]

44) $\quad g = |M| \qquad$ Where: $\quad [M] = [T][T]^t$

$$[T] = [\underline{\tau}_1, \underline{\tau}_2, \cdots, \underline{\tau}_N]$$

$$\underline{\tau}_i = \text{Output torque of CMG gimbal \#i}$$

The matrix [T] defined above is of dimension 3 x N, with column vectors constructed from the CMG output torques. [T] represents the Jacobian matrix of the total CMG momentum (Eq. 1) with respect to CMG gimbal angles. [M] is a symmetric 3 x 3 matrix formed by taking the product of [T] with its transpose. The rank of [M] defines the span of control available from the CMG configuration; ie. if rank(M) = 2, control is restricted to a plane, and if rank(M) = 1, control can be established only along a line. Since an "optimal" CMG steering process attempts to direct CMGs to always retain full 3-axis control, it is desired to maintain rank(M) = 3.

A measure of the 3-axis controllability of the CMG system is defined by the determinant of the matrix [M] (called the "CMG gain"[21], or "index of regularity"[35], here denoted by g). When a dimension of control is lost, rank(M) drops below 3, and g becomes zero. An "optimal" degree of 3-axis control is attained if one steers the CMG system to maximize g. By replacing the $Y_{Lineup}(j,s)$ component of the objective

function with a term proportional to the derivative of g with respect to the gimbal angles (θ_j), one can directly incorporate "maximum gain" steering into the CMG selection process, as illustrated below.

The 3 x 3 symmetric matrix [M] may be expressed:

$$45) \qquad a) \qquad [M] = \begin{bmatrix} L_1 & A & B \\ A & L_2 & C \\ B & C & L_3 \end{bmatrix}$$

$$b) \quad \text{Where:} \quad L_i = T_{i,1}^2 + T_{i,2}^2 + \cdots + T_{i,N}^2$$

$$A = T_{1,1} T_{2,1} + T_{1,2} T_{2,2} + \cdots + T_{1,N} T_{2,N}$$

$$B = T_{1,1} T_{3,1} + T_{1,2} T_{3,2} + \cdots + T_{1,N} T_{3,N}$$

$$C = T_{3,1} T_{2,1} + T_{3,2} T_{2,2} + \cdots + T_{3,N} T_{2,N}$$

The variables $T_{m,n}$ are elements of matrix [T] (ie. CMG torque components). The determinant of [M] becomes:

$$46) \qquad g = \left| M \right| = L_1 L_2 L_3 + 2(ABC) - A^2 L_3 - B^2 L_2 - C^2 L_1$$

Using Eq. 46, the derivative of g can be taken with respect to any CMG gimbal angle:

$$47) \qquad \frac{\partial g}{\partial \theta_n} = \frac{\partial L_1}{\partial \theta_n} (L_2 L_3 - C^2) + \frac{\partial L_2}{\partial \theta_n}(L_1 L_3 - B^2) + \frac{\partial L_3}{\partial \theta_n} (L_1 L_2 - A^2)$$

$$+ \frac{\partial A}{\partial \theta_n} (BC - 2A L_3) + \frac{\partial B}{\partial \theta_n} (AC - 2B L_2) + \frac{\partial C}{\partial \theta_n} (AB - 2C L_1)$$

Each element of matrix [M] is a scalar product between two row-vectors of the Jacobian matrix [T] (see Eq. 45b). Since the columns of [T] are composed of CMG torques $\underline{\tau}_n$ (which depend only on θ_n for single gimballed CMGs), the derivative of any element of [M] with respect to θ_n will contain only a contribution from the term corresponding to the $\underline{\tau}_n$ column. Referencing 45b, we can specify the derivatives of each matrix element:

48)
$$\frac{\partial L_i}{\partial \theta_n} = 2\, T_{i,n}\, \frac{\partial T_{i,n}}{\partial \theta_n}$$

$$\frac{\partial A}{\partial \theta_n} = \frac{\partial T_{1,n}}{\partial \theta_n}\, T_{2,n} + \frac{\partial T_{2,n}}{\partial \theta_n}\, T_{1,n}$$

$$\frac{\partial B}{\partial \theta_n} = \frac{\partial T_{1,n}}{\partial \theta_n}\, T_{3,n} + \frac{\partial T_{3,n}}{\partial \theta_n}\, T_{1,n}$$

$$\frac{\partial C}{\partial \theta_n} = \frac{\partial T_{2,n}}{\partial \theta_n}\, T_{3,n} + \frac{\partial T_{3,n}}{\partial \theta_n}\, T_{2,n}$$

The elements $T_{i,n}$ represent the i'th component of CMG output torque $\underline{\tau}_n$. As discussed in the "torque steering" scenerio sketched at the beginning of this section, the derivative of a CMG output torque lies in the direction opposite the corresponding rotor momentum vector, ie.:

49)
$$\frac{\partial \underline{\tau}_n}{\partial \theta_n} = -\dot{\theta}_n \underline{h}_n$$

Eq. 49 can be inserted into Eqs. 48:

50)
$$\frac{\partial L_i}{\partial \theta_n} = -\dot{\theta}_n (2\, T_{i,n}\, h_{i,n})$$

143

50) (cont.)

$$\frac{\partial A}{\partial \theta_n} = -\dot{\theta}_n (h_{1,n} T_{2,n} + h_{2,n} T_{1,n})$$

$$\frac{\partial B}{\partial \theta_n} = -\dot{\theta}_n (h_{1,n} T_{3,n} + h_{3,n} T_{1,n})$$

$$\frac{\partial C}{\partial \theta_n} = -\dot{\theta}_n (h_{2,n} T_{3,n} + h_{3,n} T_{2,n})$$

Where $h_{i,n}$ denotes the i'th component of the rotor momentum of CMG #n.

The terms of Eq. 50 are expressed as products between components of rotor angular momenta and CMG output torques. Both of these quantities are continuously maintained and updated in the CMG selection/steering package in order to construct objective coefficents and activity vectors. Calculation of Eqs. 50 then becomes quite straightforward.

Matrix [M] is calculated from the CMG torque vectors via Eq. 44. One of the advantages of the linear programming selection process is its non-dependence on the number of active actuators; matrices and related arrays need not be re-dimensioned after actuators are failed. The introduction of the [T] matrix in Eq. 44 at first seems to undermine this principle; here we have a matrix dimensioned to the number of active CMGs in the system. Since [T] is used only in calculating M (which is always 3 x 3), this is not a problem; if a CMG gimbal is "failed", its corresponding column vector in [T] can be replaced with zeroes, and the other terms used to compute [M] are unaffected (see Eq. 45b); rank(M) still reflects the controllability of the now truncated system. [T] is thus dimensioned to the maximum number of active CMG gimbals, and columns are zeroed as devices are removed.

If one inserts matrix elements of Eq. 45 and their derivatives (Eq. 50) into Eq. 47, the derivative of CMG gain at the current gimbal positions $(dg/d\theta_n)$ can be calculated for each active CMG. This allows a new objective component to be specified:

51) $Y_{Gain}(j,s) = - \dfrac{\partial g}{\partial \theta_n} (s/\sqrt{g}) + B$

The sense of rotation ($s = +/-1$) is factored into Y_{Gain} to penalize gimbal rotations which decrease g (the bias B keeps Y_{Gain} positive, as illustrated in Eq. 33). The gain derivative is scaled by $1/\sqrt{g}$, such that further decrease of CMG gain becomes progressively more costly as g drops.

The net objective calculation for single-gimballed CMGs may be summarized in a form similar to Eq. 30:

52) $c_{j,s} = K_o + K_S G_{Stops}(j,s) + K_G Y_{Gain}(j,s)$

Y_{Gain} may be replaced with the torque antilineup function (as discussed at the beginning of this section), or other type of singularity avoidance amplitude. Because of the restricted freedom available in a single gimballed CMG system, the Y_{Gain} (or Y_{Torque_Lineup}) function is modified as stated below in order to further emphasize CMG motion in a favorable sense:

53) $Y_{mod} = \begin{cases} 10\ Y_{orig.} & (\text{if } Y_{orig.} > 0) \\[2mm] Y_{orig.} & (\text{if } Y_{orig.} < 0) \end{cases}$

This change makes selection of unfavorable CMG activities an order of magnitude more expensive than their preferred counterparts.

Since Y_{Gain} attempts to steer a CMG system away from singular orientations, it may also be adapted to a double-gimballed CMG system[17] and used in place of Y_{Lineup}. Additional terms will appear in Eqs. 48 due to the coupling between inner and outer gimbals. Satisfactory performance may be obtained, however, by keeping only the leading-order approximation (ie. only the terms depicted in Eqs. 48), and discouraging excessive inner gimbal angles with the F_{Angle} amplitude. Steering with Y_{Gain} is better suited to hybrid single/double gimballed CMG systems

(where all singular states might not be related to rotor alignments), as can be caused by one-gimbal failures (see Sec. 5.4).

As discussed in Sec. 2.3 and Chapter 3, the CMG selection is repeatedly performed in an "instantaneously optimal" fashion. If Eq. 52 is used as the objective, the selection process will tend to drive the CMG gimbals to follow contours of maximum system gain (g). This will work to avoid many singular orientations, but due again to the limited freedom of a single gimballed CMG system, contours of maximum gain can themselves lead into internal singularities. Steering via the instantaneous maximum-gain method is thus not considered to be adequate for complete singularity-avoidance control of a single gimballed CMG ensemble.

Various methods have been proposed to surmount this problem.[19,21,35] All require extensive calculation, which must be performed off-line and loaded into flight computers prior to execution. Most of these methods are based upon locating and ranking all possible singular orientations of a CMG system; this produces a table (which can be somewhat sizable) that is consulted by the real-time steering process in order to determine how to "optimally" move the CMGs. Other strategies[12] enforce constraints on CMG useage (ie. operation in pairs) to avoid singular orientations. These efforts have several drawbacks; ie. difficulty in reconfiguring in the event of failures, dependence upon particular CMG configurations, excessive computation or storage requirements, etc.

Steering with instantaneously maximal gain is a flexible method which does not require excessive computation; it is, however, a compromise which doesn't always guarantee complete singularity avoidance with single gimballed CMGs. Other types of objective contributions can be used in place of Y_{Gain}; further efforts may determine a superior method of commanding single gimballed CMGs with the hybrid selection/steering package.

6.3)   Simulation Examples

This section presents examples of the hybrid controller driving a simulated array of single gimballed CMGs. The modifications outlined in Sec. 6.2 are incorporated into the objective function, and the

146

steering/selection routines are driven by the rate-feedback controller described in Sec. 5.1. All simulations (except where noted) assume a 5-CMG configuration based around a "pyramid" mounting scheme,[21] which is one of the standard setups for single-gimballed CMG systems. The mounting arrangement is sketched in Fig. 54. The CMG rotors gimbal in planes inclined at 45° to the vertical. The rotor planes are displaced by equal angles such that adjacent gimbal axes (which are normal to the rotor planes) are separated by 64°, and a cross-section through the mounting arrangement forms a regular pentagon. The CMG mounting convention can influence the susceptibility of a single-gimballed system to singular states; other mounting schemes have been proposed, but the "pyramid-type" setup is generally retained as a standard for comparison throughout these tests.

The parameters of Table I (Sec. 5.2) are retained wherever possible. The mass properties of the Power Tower Space Station are assumed. CMG rotors of 3500 ft-lb-sec. are allowed to gimbal at a peak rate of 5 deg/sec., with stops now imposed at gimbal angles of θ = +/-180°. When steering via CMG gain (ie. Eq. 52), the parameter K_G is normalized to the number of active CMGs, and the RCS costs are increased by several orders of magnitude.

In the first example, the CMGs are driven with the cyclic request sequence (Eq. 42), again with a 0.0008 deg/sec. magnitude per vehicle coordinate. To establish a worst-case reference, the first test is run with no anti-singularity amplitudes in the objective function (ie. no Y functions are included).

Gimbal angles for this test are shown in the upper plot of Fig. 55. All CMGs are used in answering requests, and gimbal stops are avoided. Some difficulty was encountered in responding to requests between t = 50 and t = 75 sec., as is seen by the small oscillations superimposed onto the gimbal motion of CMGs #3 and #4 during this interval.
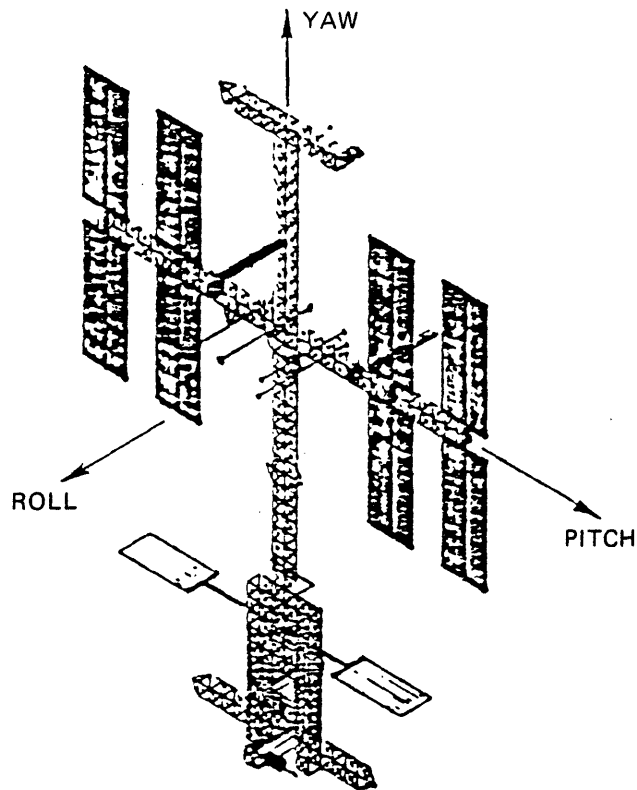
(a) POWER TOWER SPACE STATION
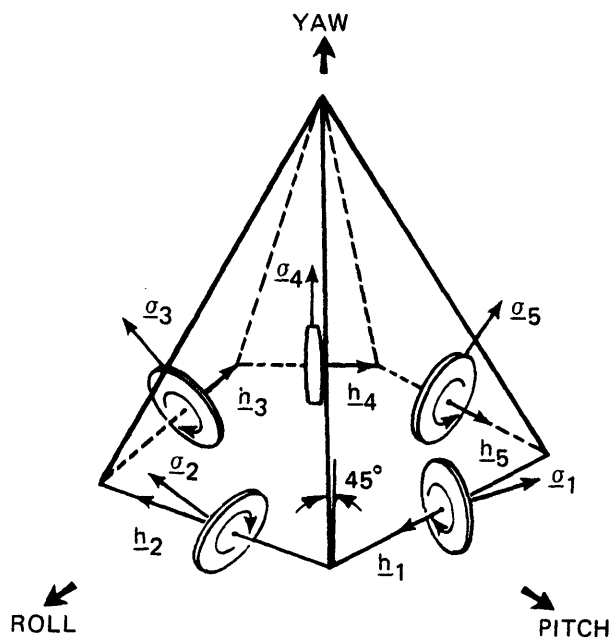
(b) INITIAL CMG ORIENTATION

FIGURE 54: "PYRAMID MOUNTED SINGLE GIMBALLED CMG CONFIGURATION

GIMBAL ANGLES

Legend
CMG# 1
CMG# 2
CMG# 3
CMG# 4
CMG# 5

+ MANEUVER
✕ JETS

CMG CONTROLLABILITY

Legend
CMG GAIN
EIGENVALUE 1
EIGENVALUE 2
EIGENVALUE 3
+ MANEUVER
✕ JETS
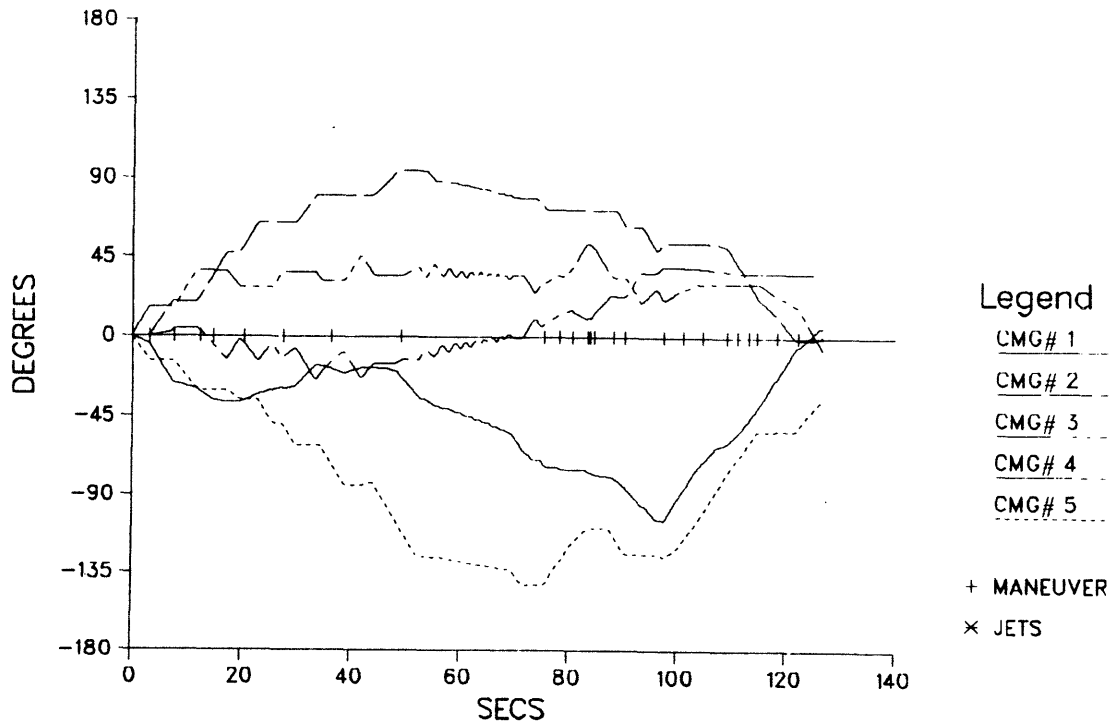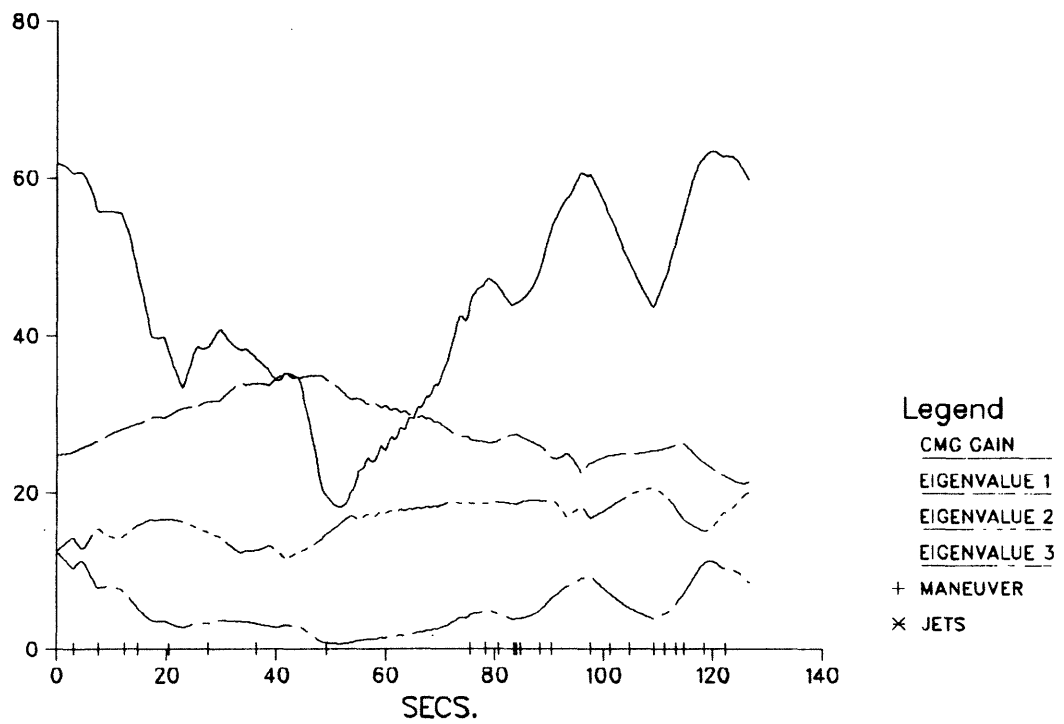
FIGURE 55: Cyclic Maneuver, No Singularity Avoidance in Objective

149

VEHICLE RATES
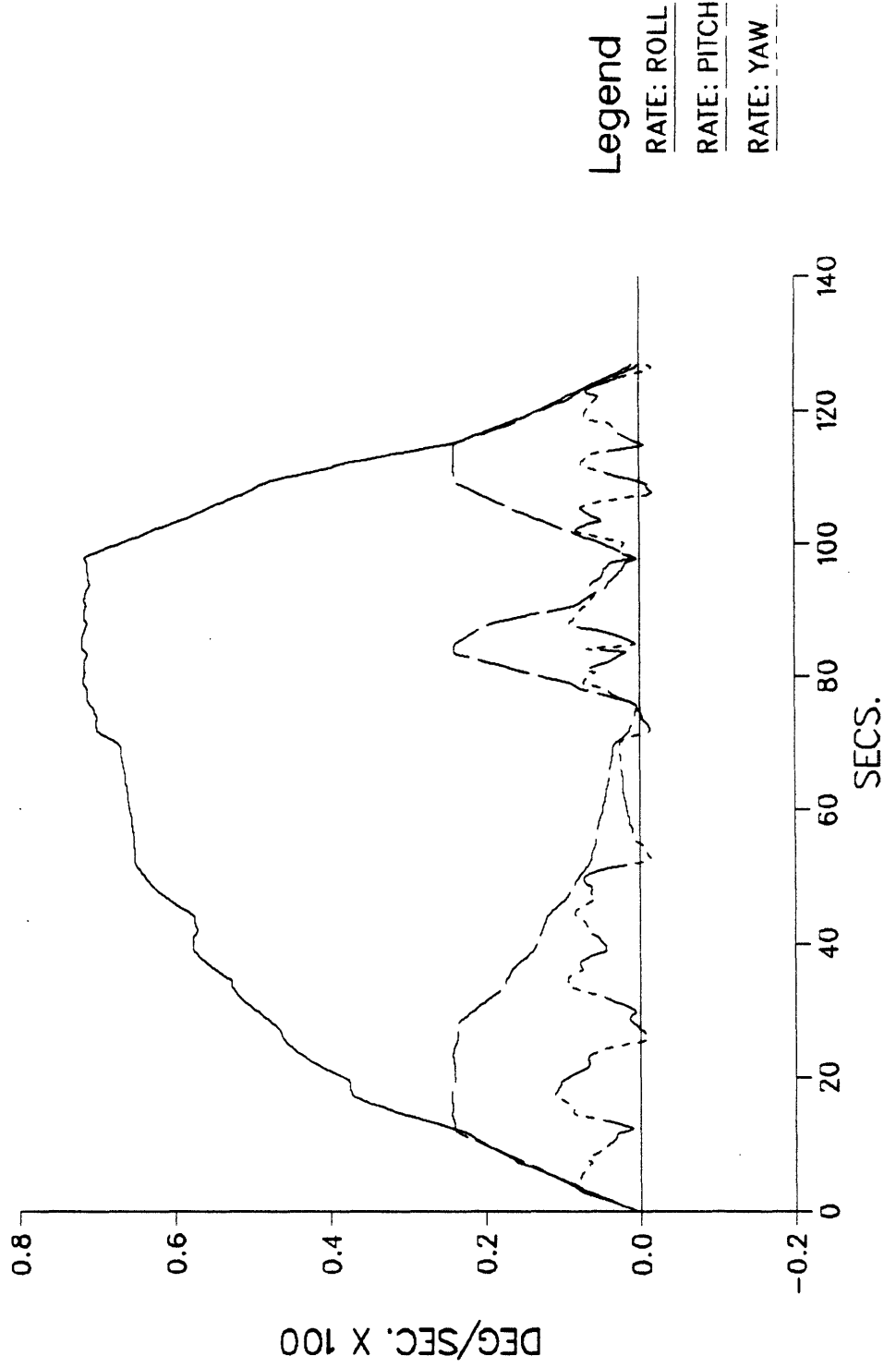
FIGURE 56: Cyclic Maneuver, No Singularity Avoidance in Objective

150

The lower plot of Fig. 55 shows curves which depict the time-history of CMG controllability. The upper curve is proportional to the square root of CMG gain (Eq. 44), and the remaining curves represent the eigenvalues of matrix M (ie. solutions to M's characteristic equation). We indeed see that the point at which control is marginal (t = 50 to 70 sec.) coincides with the lowest drop in CMG gain. An eigenvalue is correspondingly seen to approach zero, indicating proximity to a singular state and resulting in control being restricted to a plane; the respective eigenvector denotes the direction of least controllability (see Ref. 37).

Resulting vehicle rates are given in Fig. 56. A marked resemblance is seen when compared to the ideal double gimballed results (ie. Fig. 23), but a distortion in shape is seen between t = 50 to 70 sec., again corresponding to the drop in control as evidenced by the low value of CMG gain.

The next test uses an identical cyclic request sequence, but an anti-torque-lineup amplitude (ie. Eq. 43 and related discussion) is included to steer CMG torques away from encountering parallel or anti-parallel lineup. The upper plot of Fig. 57 shows the gimbal angles. Gimbal stops are avoided, and the CMG response seems considerably neater. The lower plot shows CMG controllability parameters; one sees a much less pronnounced dip in CMG gain and eigenvalues (indicating a more controllable situation) at t = 25 sec. Resulting vehicle rates are shown in Fig. 58; an improvement in vehicle response is seen over the worst-case run of Fig. 56.

When the CMG gain is low, the output torque of the CMG system is limited about at least one axis. As seen in the above tests, this can appreciably degrade control and lower the CMG response time. The rate-feedback controller is structured to drive the CMG/RCS system until each request is satisfied before picking up the next in the sequence. Any delays experienced in low-gain CMG orientations will thus sum to create an increased test duration. Because of the slower CMG response time, the

GIMBAL ANGLES

Legend
CMG# 1
CMG# 2
CMG# 3
CMG# 4
CMG# 5

+ MANEUVER
✕ JETS

CMG CONTROLLABILITY

Legend
CMG GAIN
EIGENVALUE 1
EIGENVALUE 2
EIGENVALUE 3
+ MANEUVER
✕ JETS
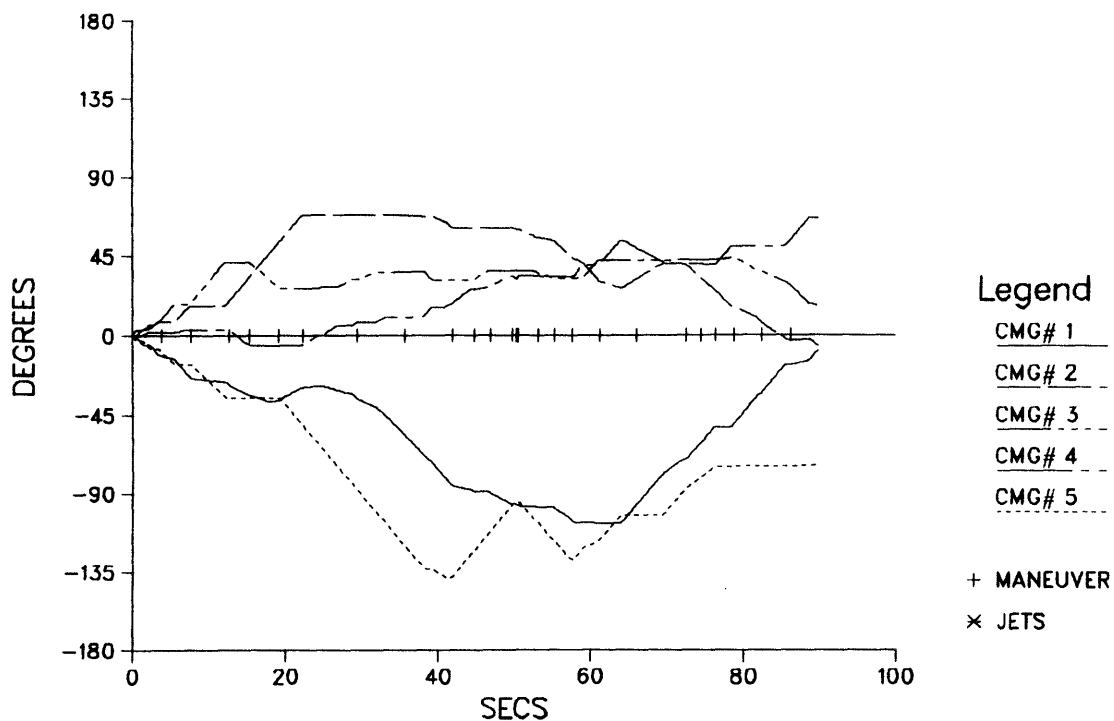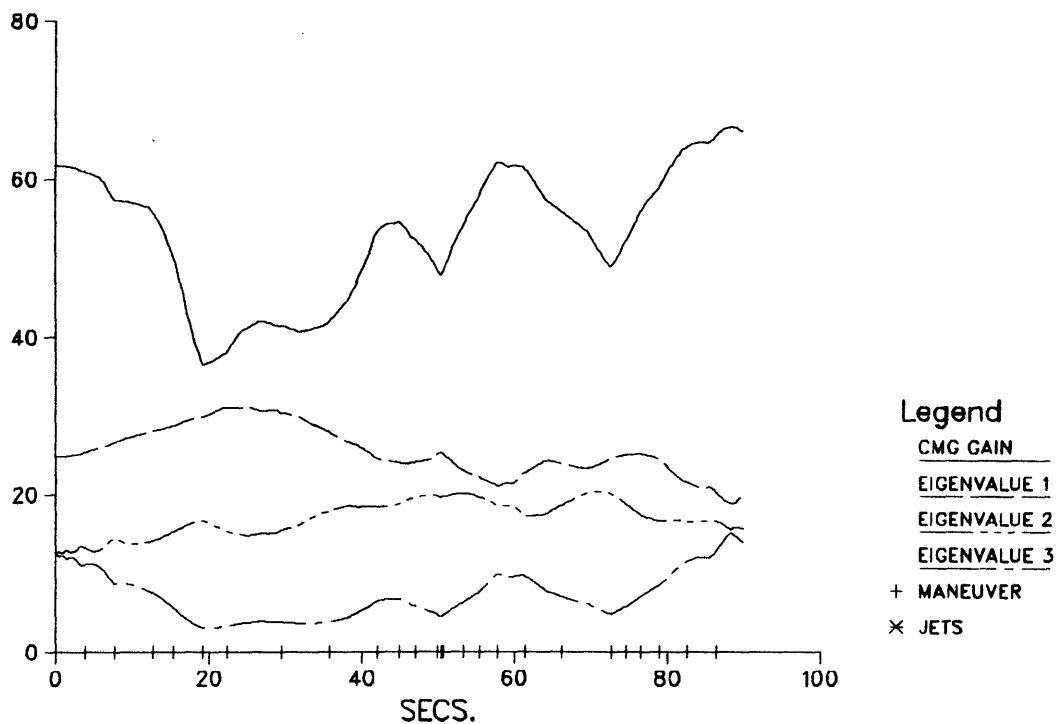
FIGURE 57: Cyclic Maneuver, Torque Steering
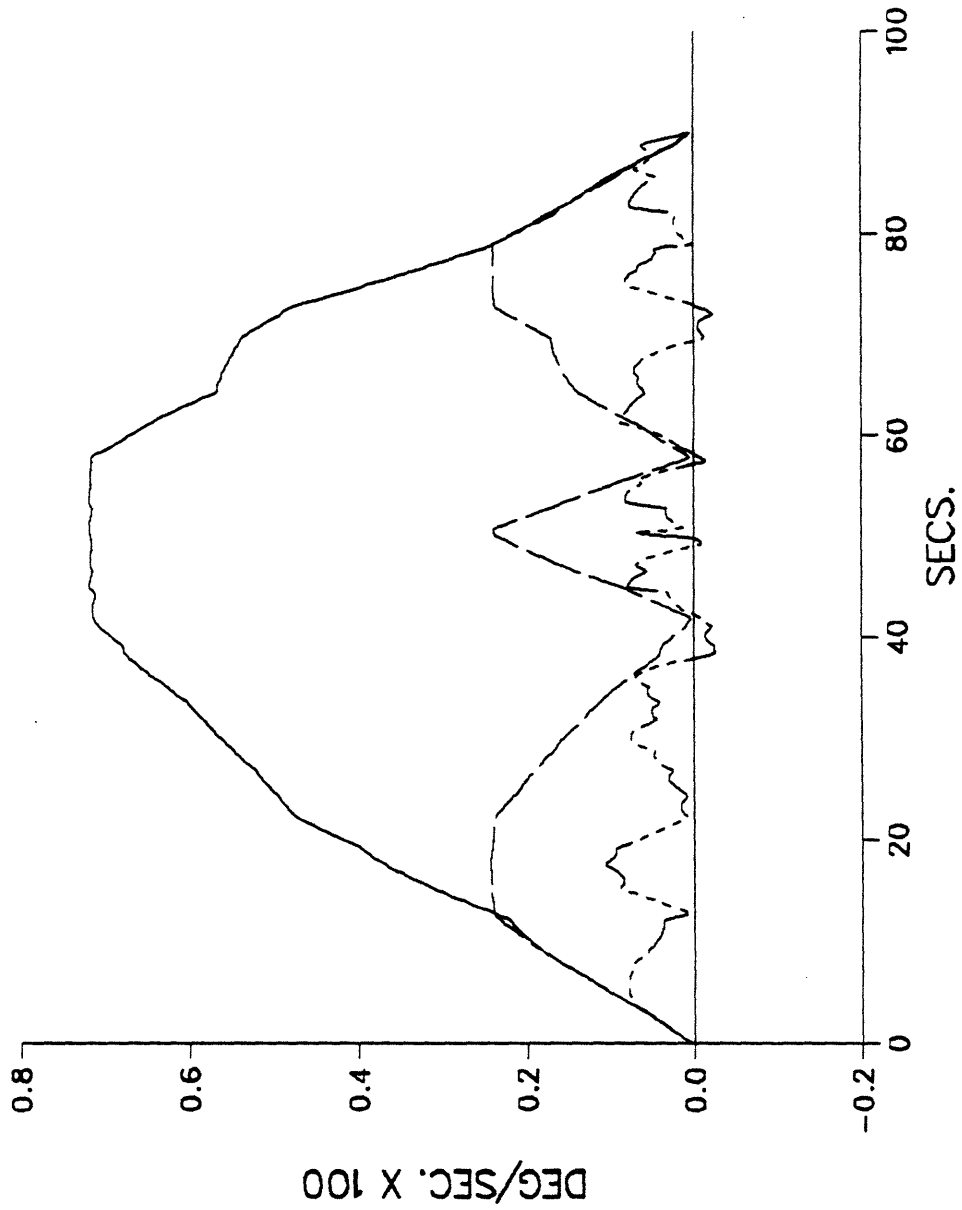
FIGURE 58: Cyclic Maneuver, Torque Steering

test run of Figs. 55 & 56 (with no singularity avoidance in the objective) required nearly twice the amount of time needed by the run of Figs. 57 & 58 (with anti-torque-lineup steering). The greater CMG control authority experienced in the latter test allowed the input requests to be answered much more rapidly, causing it to finish much earlier.

The next test uses the same cyclic request sequence, but the CMG gain derivatives (Eqs. 51, 52, and discussion) are used to steer the CMG system (instead of the torque-anti-lineup function). The upper plot of Fig. 59 shows the gimbal angle history; again a neat response is seen, and gimbal stops are avoided. The lower plot shows the corresponding CMG controllability curves; the CMG gain is seen to maintain a consistantly high value, and no appreciable drops in gain or eigenvalues are encountered. Fig. 60 gives the resulting vehicle rates; the desired profile is attained with little difficulty. Since best performance was seen to be realized under direct gain steering, this method is adopted as the default for single gimballed ensembles and is used in the remaining tests of this section, unless otherwise noted.

The gimbal angles plotted in Fig. 59 do not return to the origin after the request cycle is completed. Since the steering law is continuously attempting to drive the CMGs in order to maximize gain, CMG motion is not entirely commutative; this phenomenon was also noted in the double-gimballed results of Sec. 5.4. Fig. 61 shows the CMG gimbal angles and controllability in response to five full request cycles (again, gain steering is used). After the CMGs are re-distributed from their initial orientations, the CMG motion is seen to be primarily periodic, with some pseudorandom component. The CMG gain generally remains high (as seen in the lower plot), and the desired rates are achieved with little difficulty (Fig. 62).

The flexibility of the linear programming approach allows the CMG configuration to be defined in an arbitrary fashion. This was demonstrated in Sec. 5.4 for an array of double gimballed CMGs. The test

GIMBAL ANGLES

Legend
CMG# 1
CMG# 2
CMG# 3
CMG# 4
CMG# 5

+ MANEUVER
✕ JETS

CMG CONTROLLABILITY

Legend
CMG GAIN
EIGENVALUE 1
EIGENVALUE 2
EIGENVALUE 3
+ MANEUVER
✕ JETS
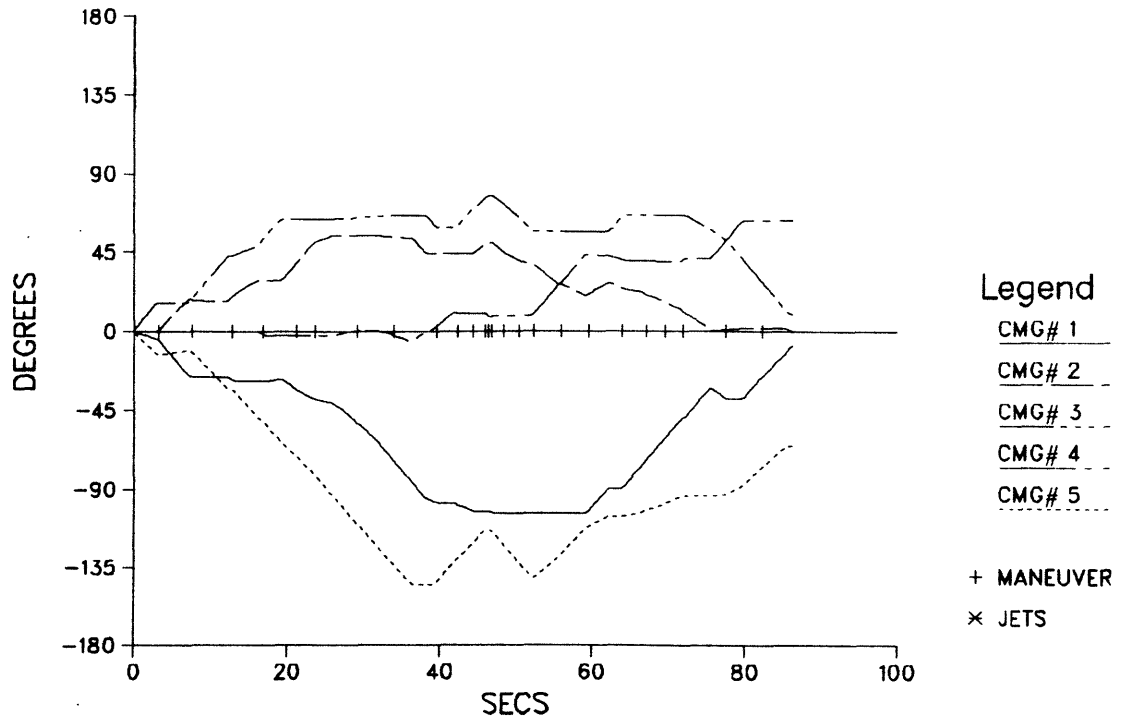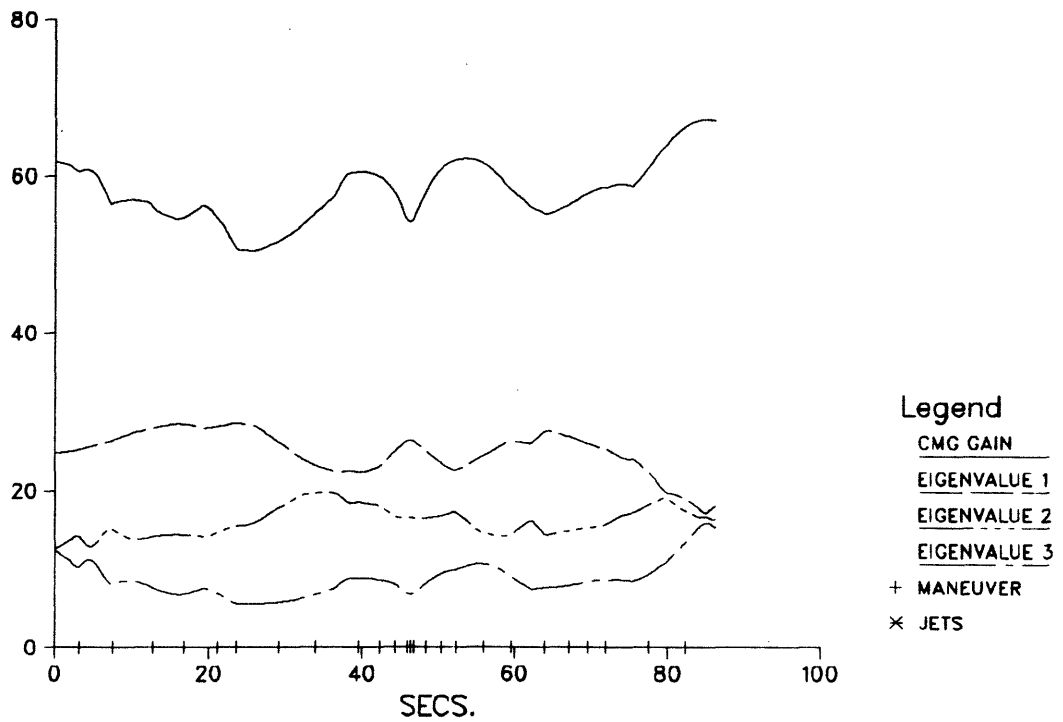
FIGURE 59: Cyclic Maneuver, Gain Steering

155

VEHICLE RATES

Legend
RATE: ROLL
RATE: PITCH
RATE: YAW

DEG/SEC. X 100

SECS.
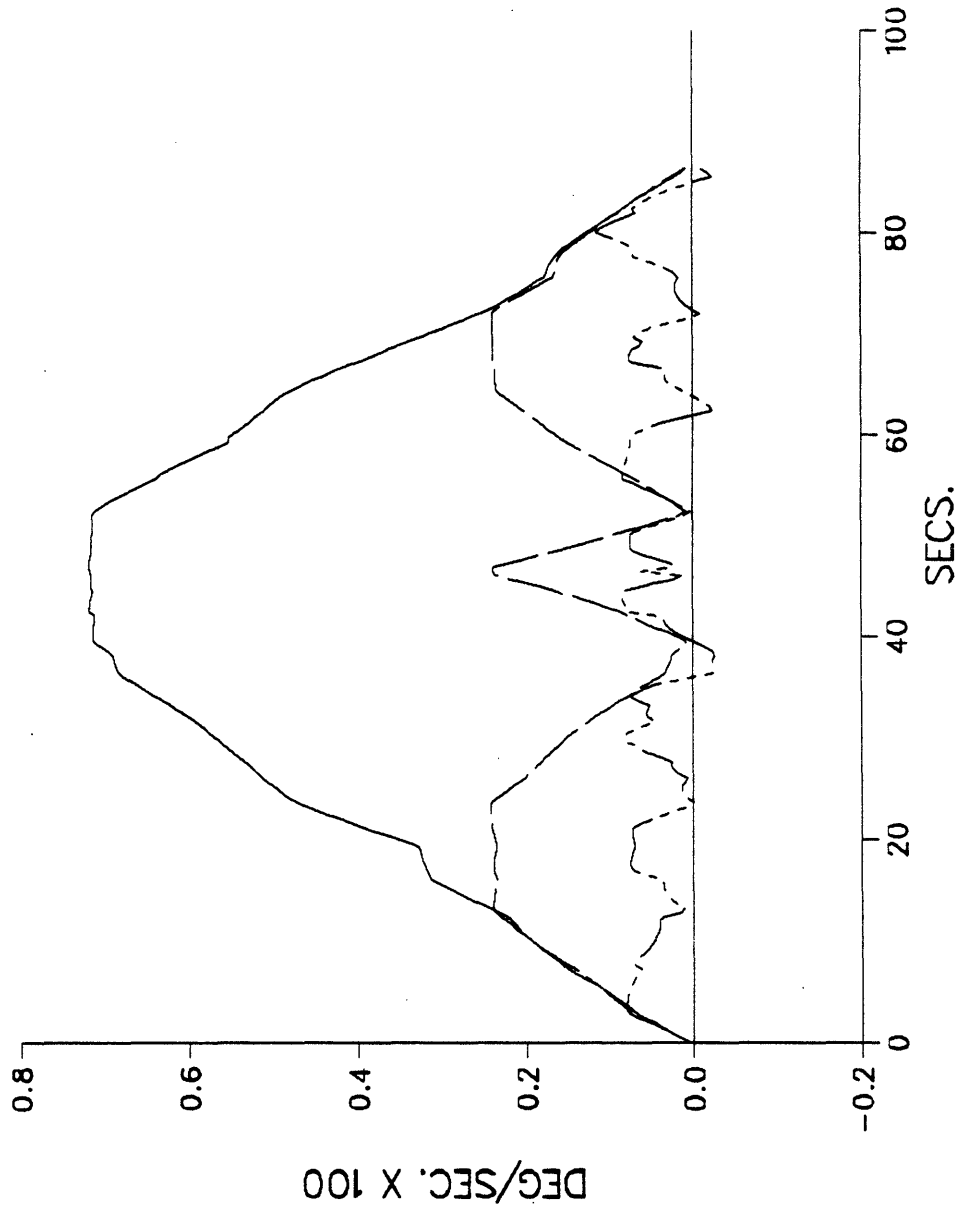
FIGURE 60: Cyclic Maneuver, Gain Steering

GIMBAL ANGLES

Legend
CMG# 1
CMG# 2
CMG# 3
CMG# 4
CMG# 5

+ MANEUVER
× JETS

CMG CONTROLLABILITY

Legend
CMG GAIN
EIGENVALUE 1
EIGENVALUE 2
EIGENVALUE 3
+ MANEUVER
× JETS
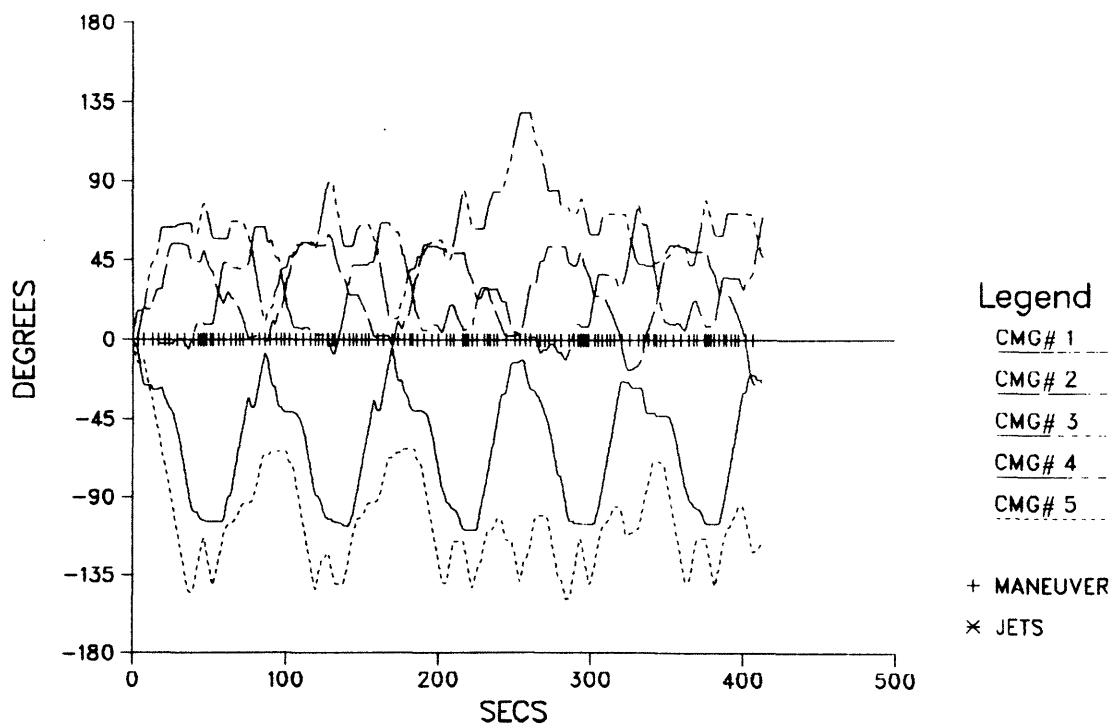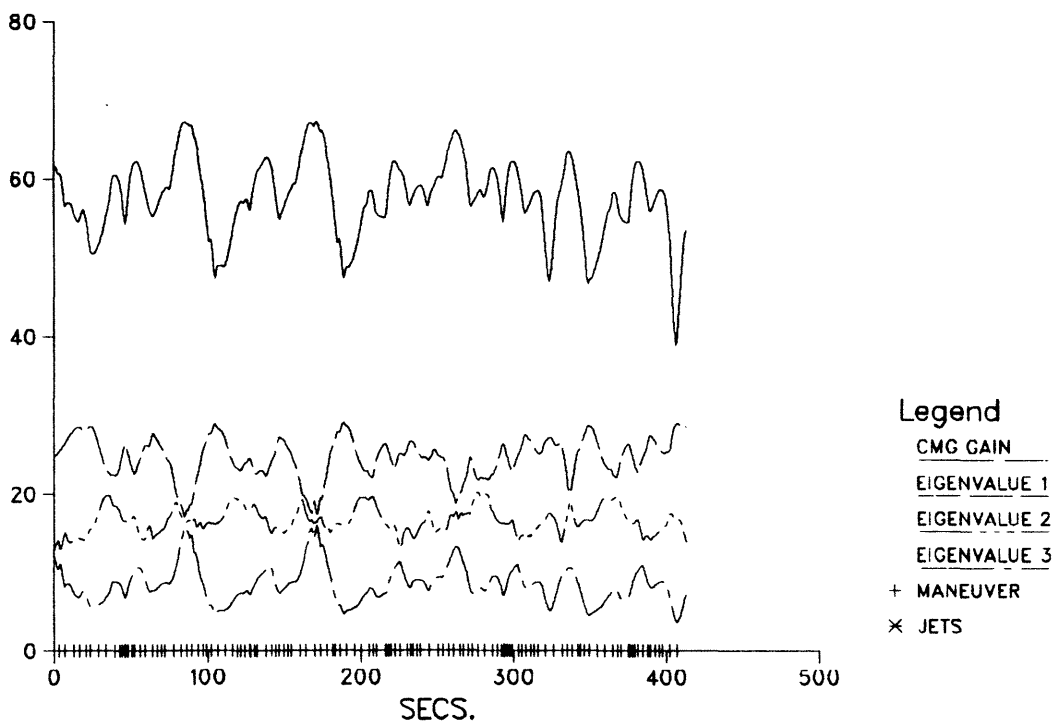
FIGURE 61: Cyclic Maneuver, 5 Iterations

157
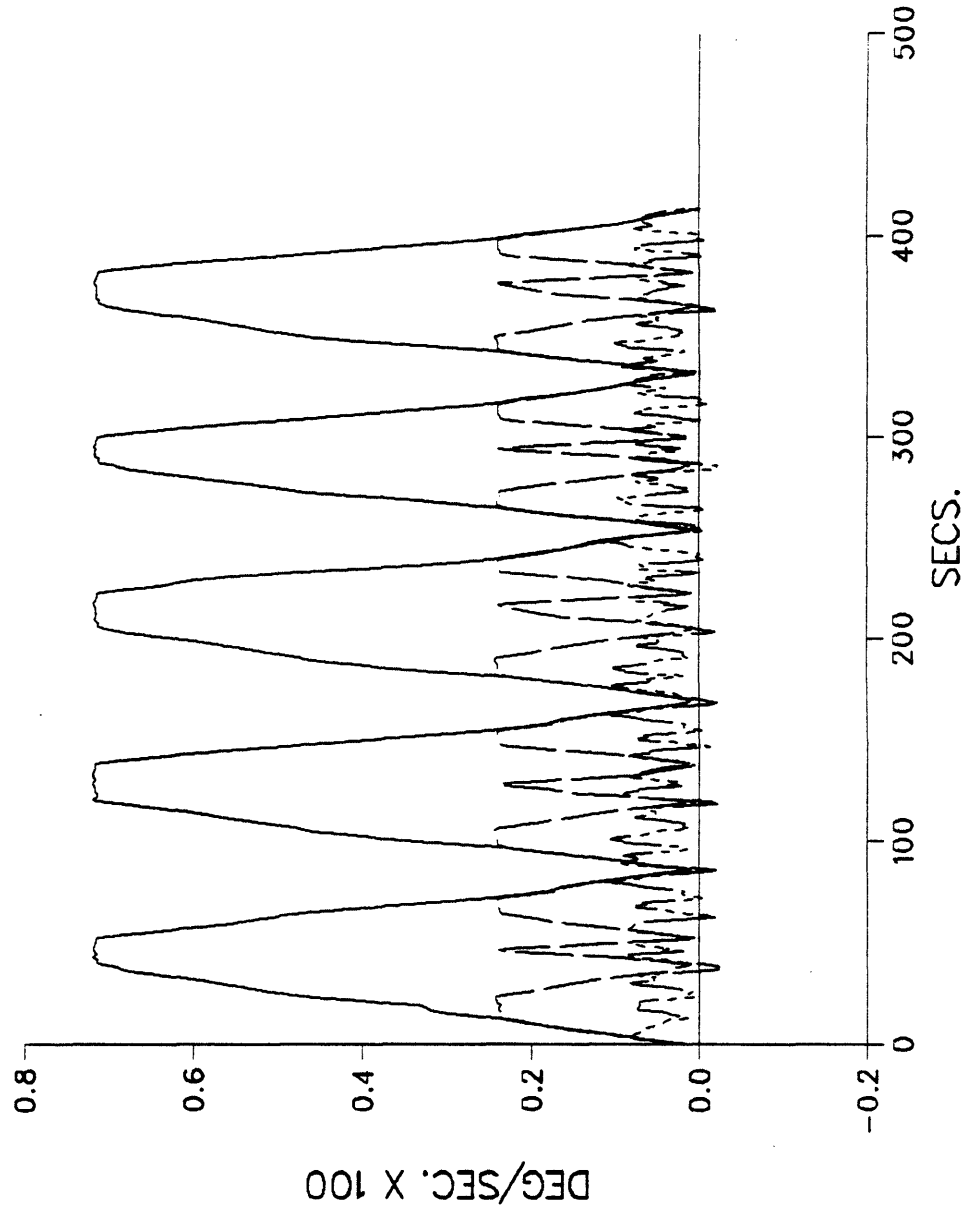
VEHICLE RATES

FIGURE 62: Cyclic Maneuver, 5 Iterations

Legend
RATE: ROLL
RATE: PITCH
RATE: YAW

DEG/SEC. X 100

SECS.

158

GIMBAL ANGLES

Legend

CMG# 1
CMG# 2
CMG# 3
CMG# 4
CMG# 5

+ MANEUVER
× JETS

CMG CONTROLLABILITY

Legend

CMG GAIN
EIGENVALUE 1
EIGENVALUE 2
EIGENVALUE 3
+ MANEUVER
× JETS
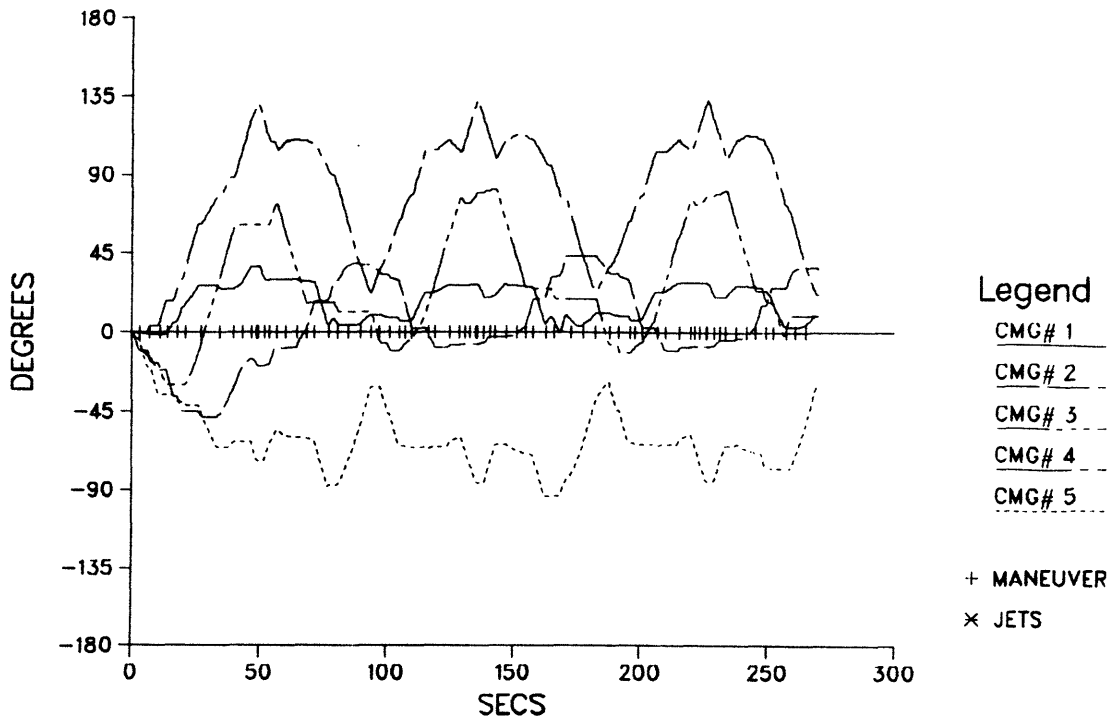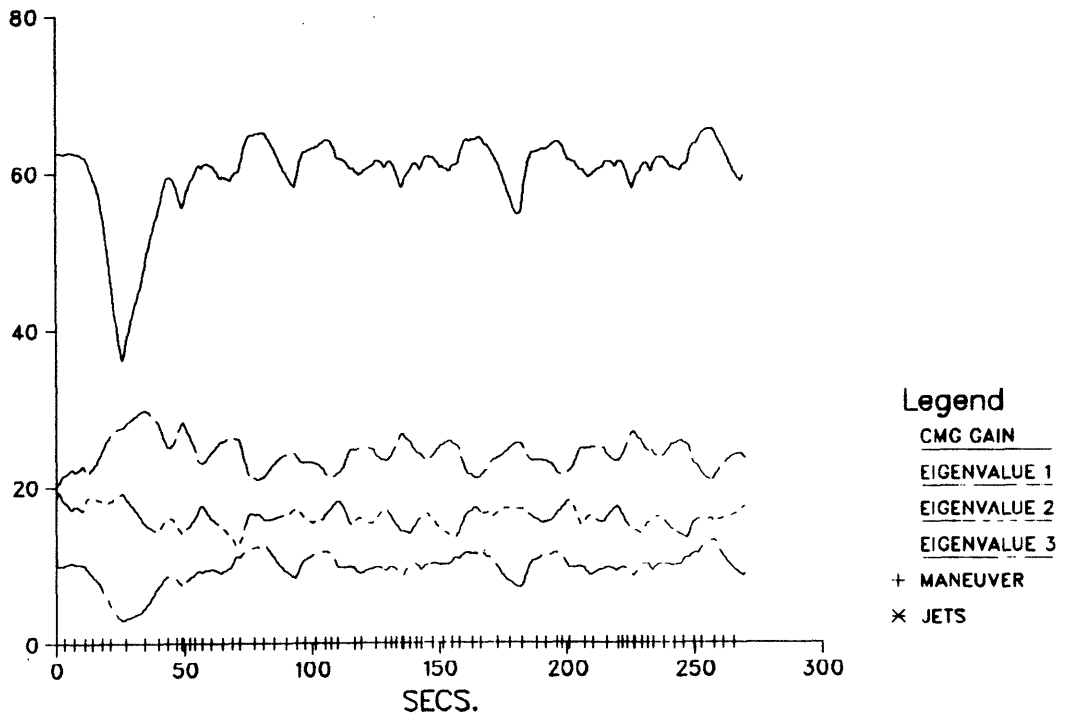
FIGURE 63: Cyclic Maneuver, Ortho—Mounted CMGs

159

VEHICLE RATES

Legend
RATE: ROLL
RATE: PITCH
RATE: YAW

DEG/SEC. X 100

SECS.
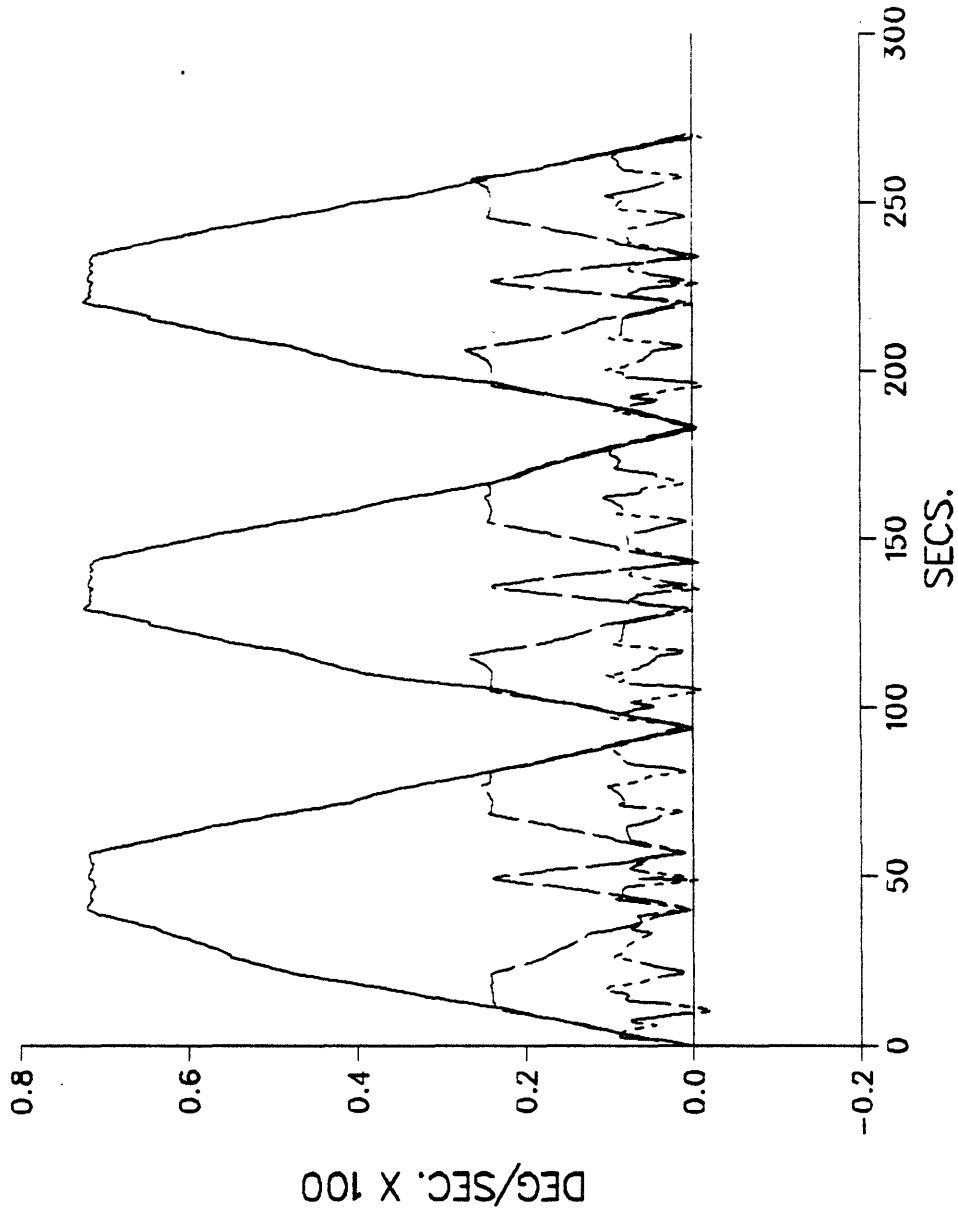
FIGURE 64: Cyclic Maneuver, Ortho-Mounted CMGs

160

run of Figs. 63 & 64 uses a 3-cycle request sequence (also with gain steering), however the 5 CMGs are now mounted after the fashion of Fig. 16 (three CMGs gimbal in mutually orthogonal planes, and two are skewed). Fig. 63 shows gimbal angles and controllability curves; again, the motion is somewhat periodic, and the CMG gain is generally kept at a high level throughout the test (a small drop exists at the beginning of the run when CMGs were re-distributed from their initial orientation). Fig. 64 shows the resulting rates; no difficulty was encountered in driving this alternate CMG configuration.

The next series of tests employ a sequence of constant rate-change requests about the vehicle roll and yaw axes. This request sequence is identical to that applied in Sec. 5.6; each request attains a rate increase of 0.0008 deg/sec. in both roll and yaw axes; the pitch axis is commanded to remain stationary.

In the first test run, a pyramid-mounted CMG array is driven with this request sequence using a complete objective function employing gain steering. Gimbal angles are shown in the upper plot of Fig. 65. Requests are answered entirely via the CMGs until t = 60 sec., at which time assistance from reaction control jets was required. The lower plot shows the resulting vehicle rates. A linear rate increase is seen, which is characteristic of this type of request sequence (ie. Fig. 49 and discussion). The sharp increase in slope occuring at the end of the run is due to RCS firings; jets have much higher control authority than CMGs, hence can answer requests more quickly. The roll and yaw rates are seen to build together throughout this test; the vehicle pitch rate is held at zero.

The saturation index (Sec. 4.2) is plotted in the upper graph of Fig. 66. Since momentum saturation in a single gimballed CMG system can not be measured by detecting total rotor alignment, this becomes the major means of monitoring the system approach to saturation. In Fig. 66, the RCS firings are indeed seen to have occured after the index had passed unity, indicating that the CMG system was unable to deliver the
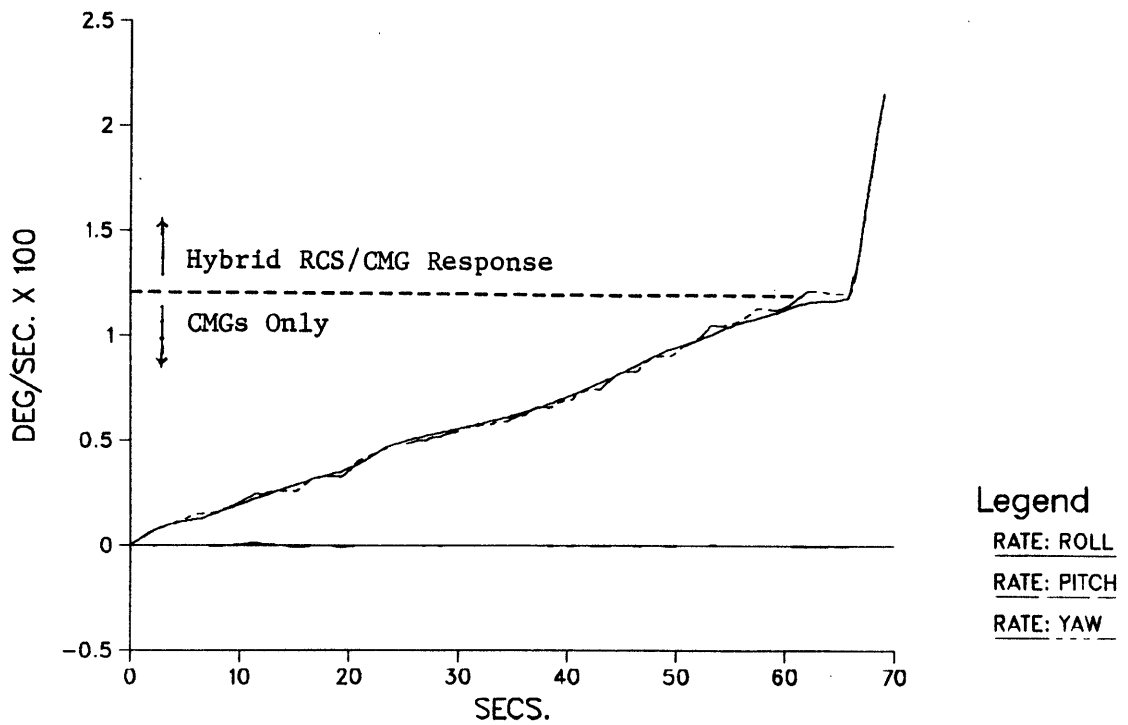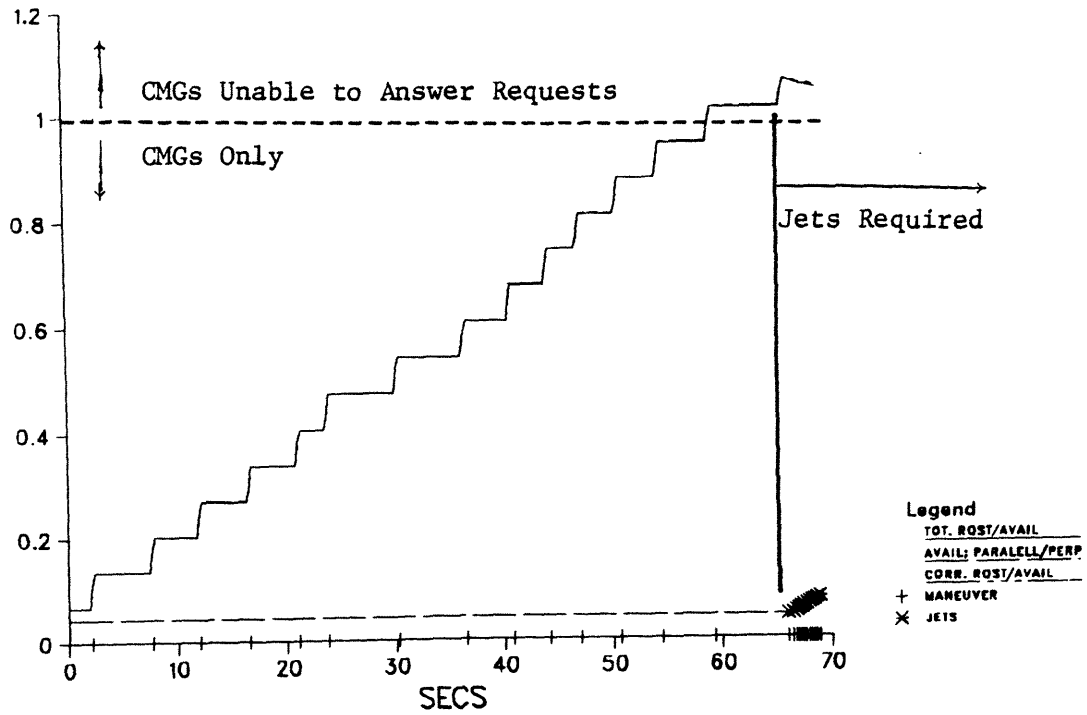
GIMBAL ANGLES

Legend
CMG# 1
CMG# 2
CMG# 3
CMG# 4
CMG# 5

+ MANEUVER
✕ JETS

Jet Firings

VEHICLE RATES

Hybrid RCS/CMG Response

CMGs Only

Legend
RATE: ROLL
RATE: PITCH
RATE: YAW
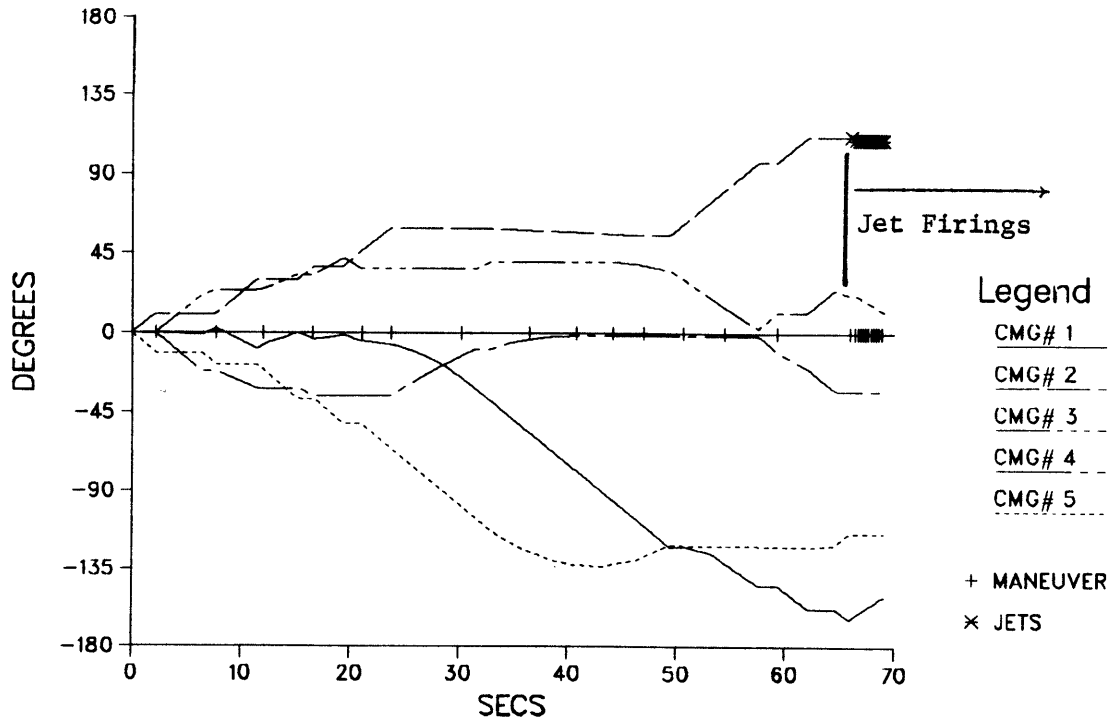
FIGURE 65: Saturate CMGs in Roll/Yaw, Nominal Conditions

162

SATURATION DETECT

Legend
TOT. RQST/AVAIL
AVAIL: PARALELL/PERP
CORR. RQST/AVAIL
+ MANEUVER
× JETS

CMG CONTROLLABILITY

Legend
CMG GAIN
EIGENVALUE 1
EIGENVALUE 2
EIGENVALUE 3
+ MANEUVER
× JETS
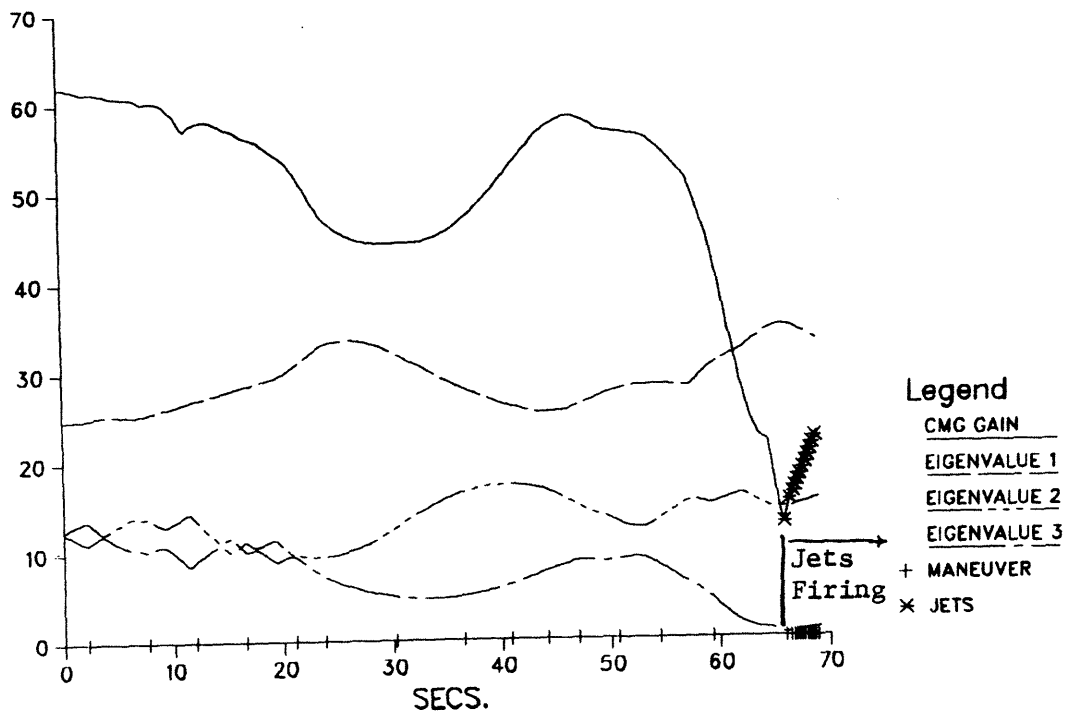
FIGURE 66: Saturate CMGs in Roll/Yaw, Nominal Conditions

163

momentum required to attain the desired final state, and thus was in saturation.

The lower graph in Fig. 66 shows the CMG controllability parameters plotted throughout the run. The CMG gain (aside from a shallow dip at t = 35 sec.) stays high until saturation, at which point the gain plummets and an eigenvalue approaches zero. This correlates with the loss of control about the request axis (created by momentum saturation), hence jets are introduced.

The next test run uses the same input request sequence, however no singularity-avoiding component is included in the objective calculation. Gimbal angles are given in the upper plot of Fig. 67. This run took nearly twice as long to complete as its predecessor; the "meandering" nature of the gimbal trajectories also indicates that difficulty was encountered in achieving the input requests. Resulting vehicle rates are plotted in the lower graph; the "flattened" region in the middle of the run indicates a reduced CMG control authority.

The saturation index is shown in the upper plot of Fig. 68. Jets were again not introduced into the solutions until the value of S exceeded unity, indicating momentum saturation. The controllability parameters are plotted in the lower graph of Fig. 68. A drop in CMG gain at the close of the run correlates with momentum saturation and the resulting RCS firings. Another sizable gain decrease was encountered before saturation (at t = 30 sec.), which indicates system approach to an internal singular state, causing the degradation in vehicle control noted in the analysis of Fig. 67. This singularity was successfully avoided in the previous test run (which included the gain-steering component in the objective function), yielding a higher global level of CMG gain and considerably improved vehicle control.

The request sequence used in the next example employs again a series of constant vehicle rate-change requests, now placed about the pitch and roll axes (as in Sec. 5.5). The run is performed using the conventional 5-CMG pyramid configuration with a full objective function
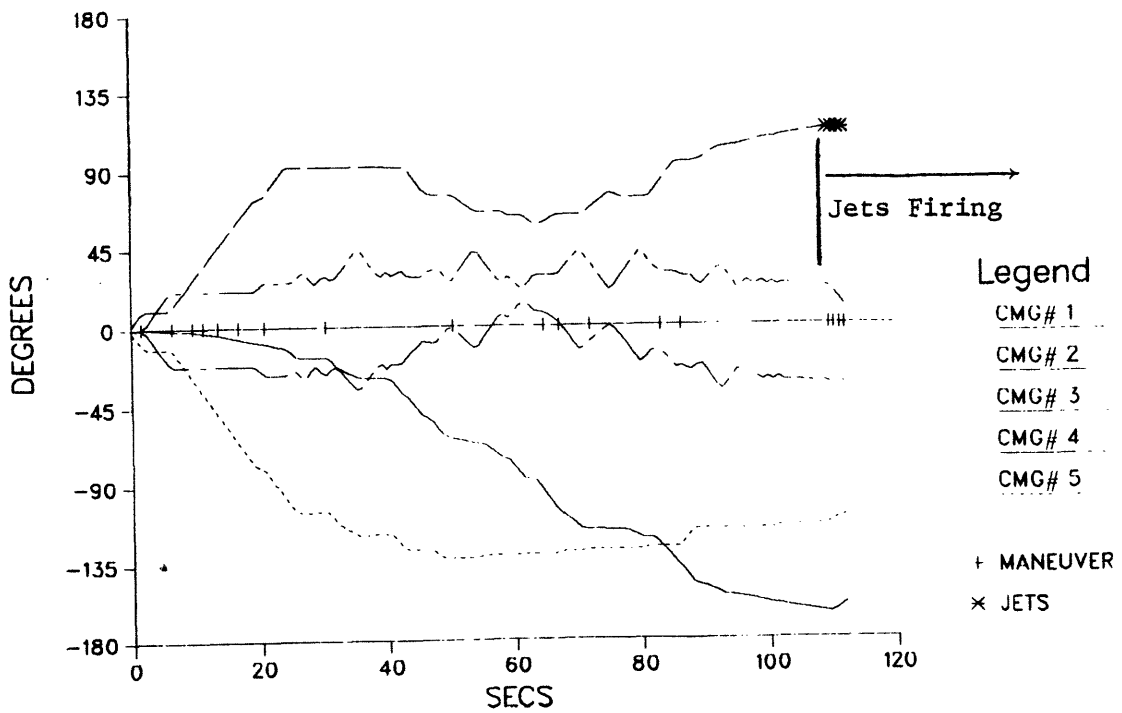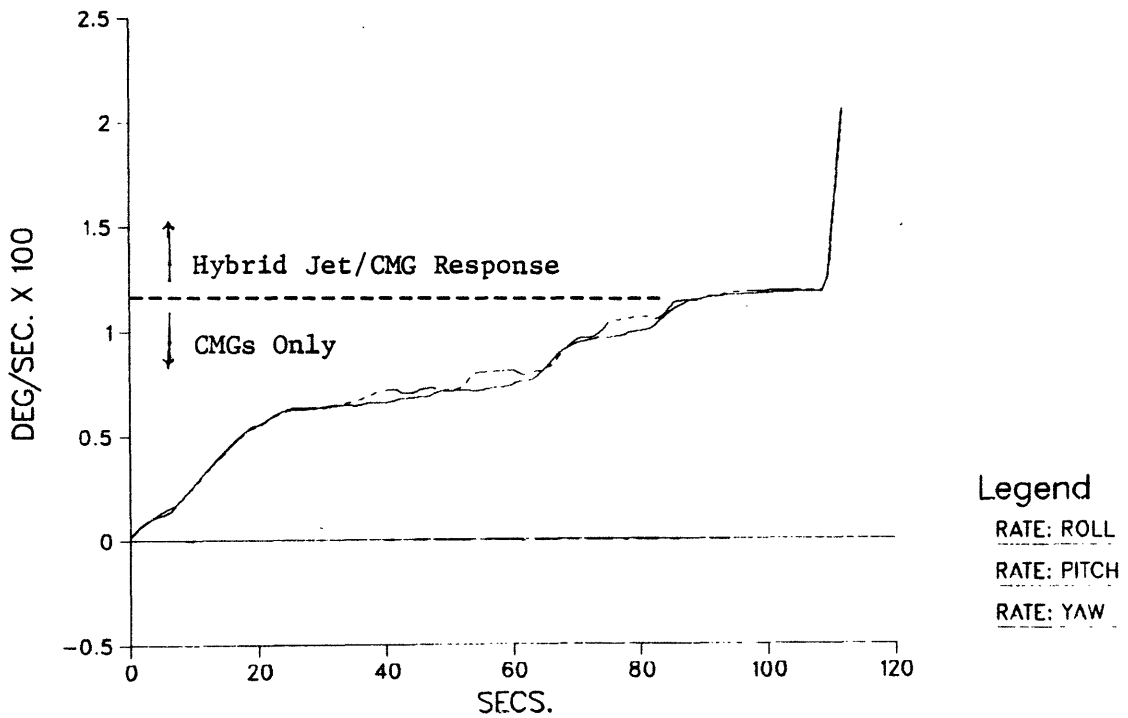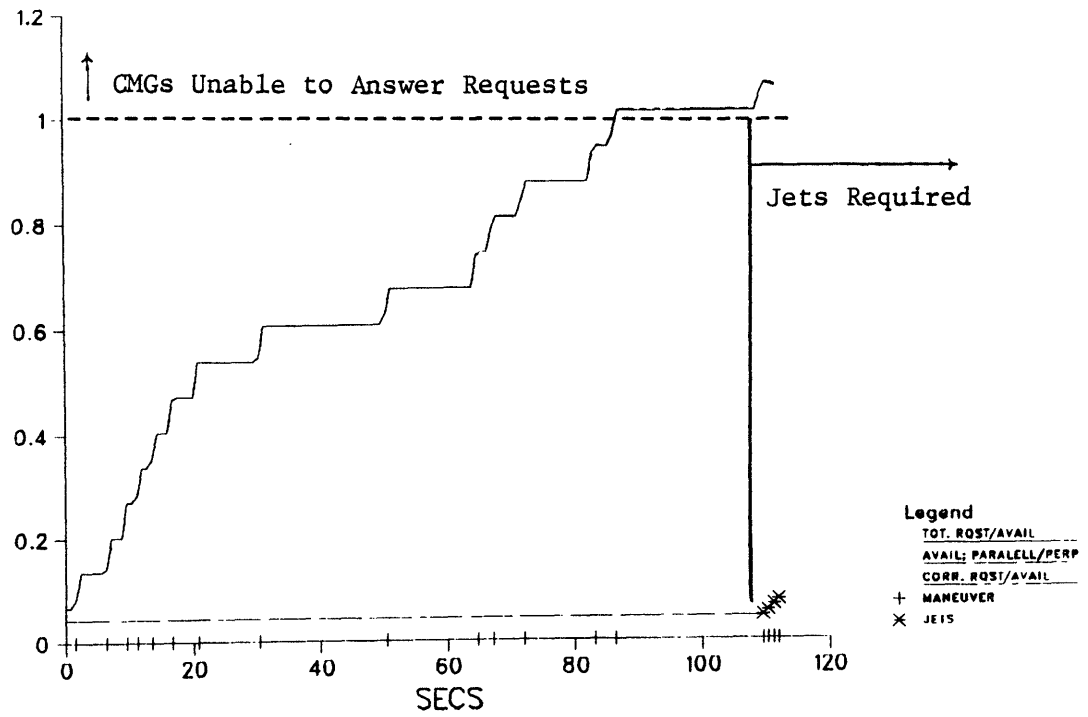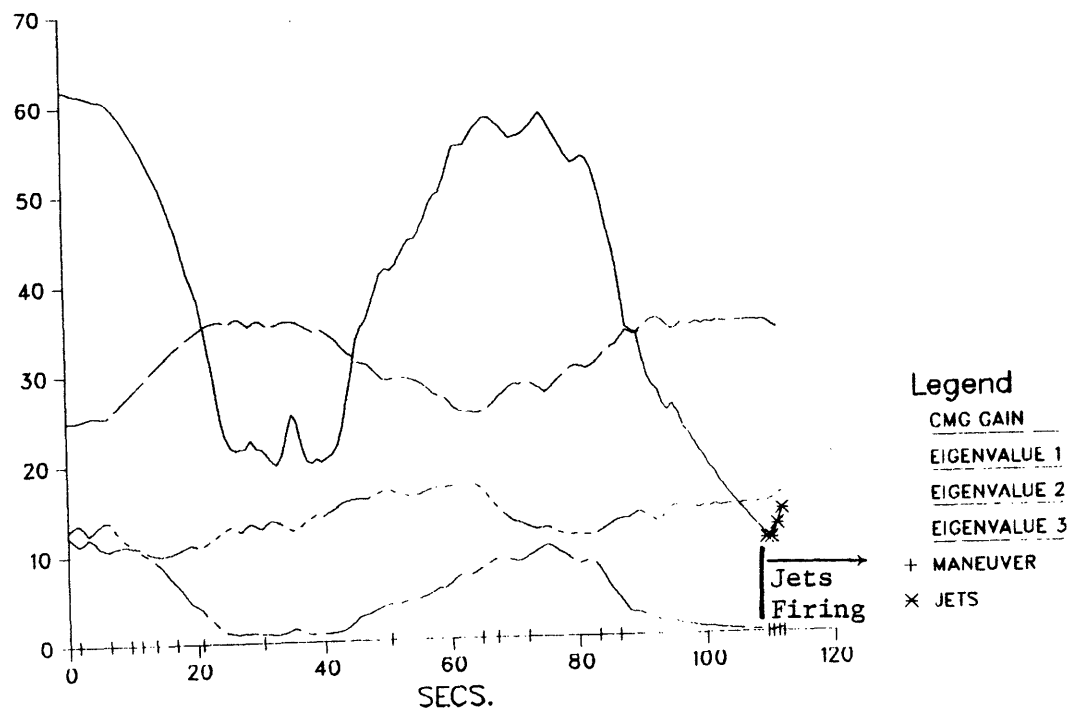
FIGURE 67: Saturate CMGs in Roll/Yaw,
No Singularity Avoidance in Objective

SATURATION DETECT

↑ CMGs Unable to Answer Requests

Jets Required

Legend
TOT. RQST/AVAIL
AVAIL; PARALELL/PERP
CORR. RQST/AVAIL
+ MANEUVER
× JETS

SECS

CMG CONTROLLABILITY

Jets
Firing

Legend
CMG GAIN
EIGENVALUE 1
EIGENVALUE 2
EIGENVALUE 3
+ MANEUVER
× JETS

SECS.

FIGURE 68: Saturate CMGs in Roll/Yaw,
No Singularity Avoidance in Objective

166

(gain steering is applied). After the CMGs are initially driven into saturation, however, the jet-assisted desaturation procedure (Sec. 4.5) is invoked.

The gimbal angles and saturation index for this run are shown in Fig. 69. Shortly after momentum saturation is reached at t = 55 sec., jet-assisted desaturation is requested. The resulting CMG/RCS maneuvers have the effect of removing the system from saturation and pulling the CMG gimbals away from the vicinity of stops (to the point where the stops avoidance function doesn't contribute heavily to the objective evaluation). After the desaturation process is halted, CMGs again respond to input requests until they are pushed back into saturation, and RCS assistance is once more required.

Controllability parameters and total CMG cost (which now contains a component proportional to the negative square root of CMG gain) are plotted in Fig. 70. As the CMGs march toward saturation, the CMG gain is seen to progressively decrease, until 3-axis control is lost at t = 55 secs. (saturation), and jets are introduced. Jet-assisted desaturation, however, is seen to sharply raise the CMG gain and restore controllability to the level prevailing at the start of the test. This is reflected in the plot of net CMG system cost (which the desaturation process works to minimize). The relatively high cost created at saturation is alleviated nearly completely by the desaturation process (indicated by asterisks drawn over the cost curve). After desaturation, the cost again rises and gain drops as the CMGs are pushed once more into momentum saturation.

Vehicle rates are plotted in Fig. 71, where the characteristic acceleration due to the constant pitch/roll request is noted (the increased authority of RCS jets is evident). The pitch/roll rates are held constant during the desaturation process, yielding the plateau in the rising rate curve. Some disturbance is created about the yaw axis (which has approx. a factor of ten lower inertia) during the RCS firings, but yaw rates are nonetheless held close to zero.
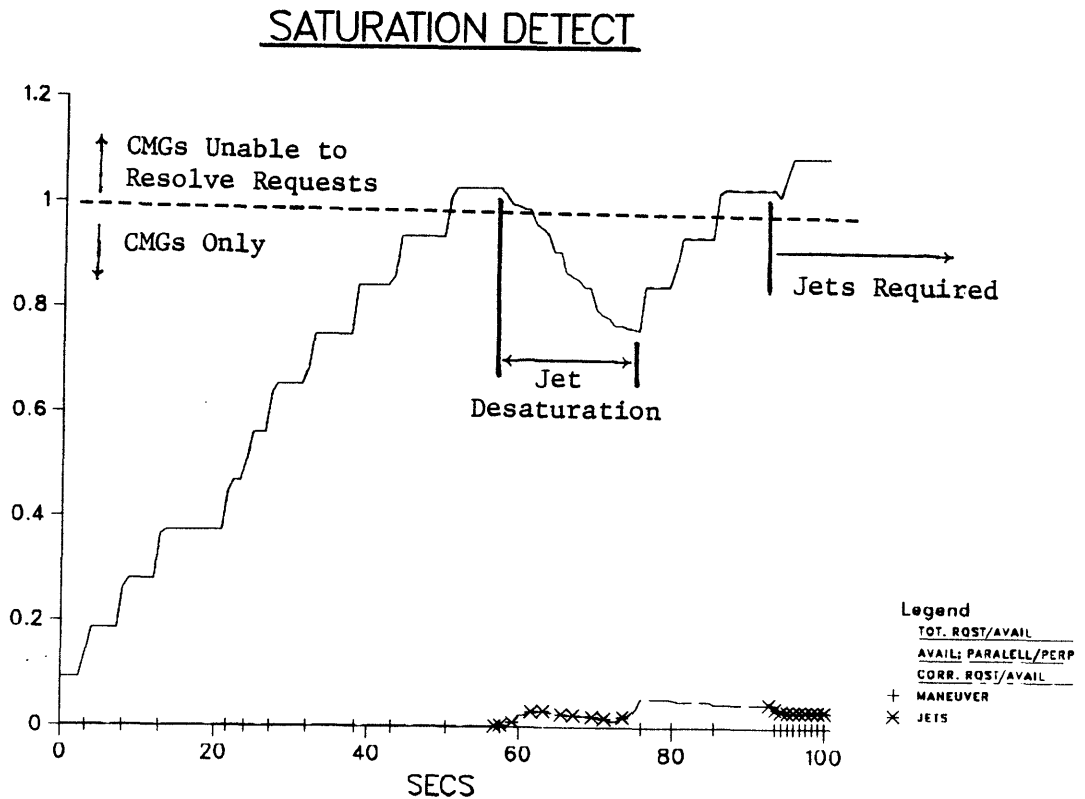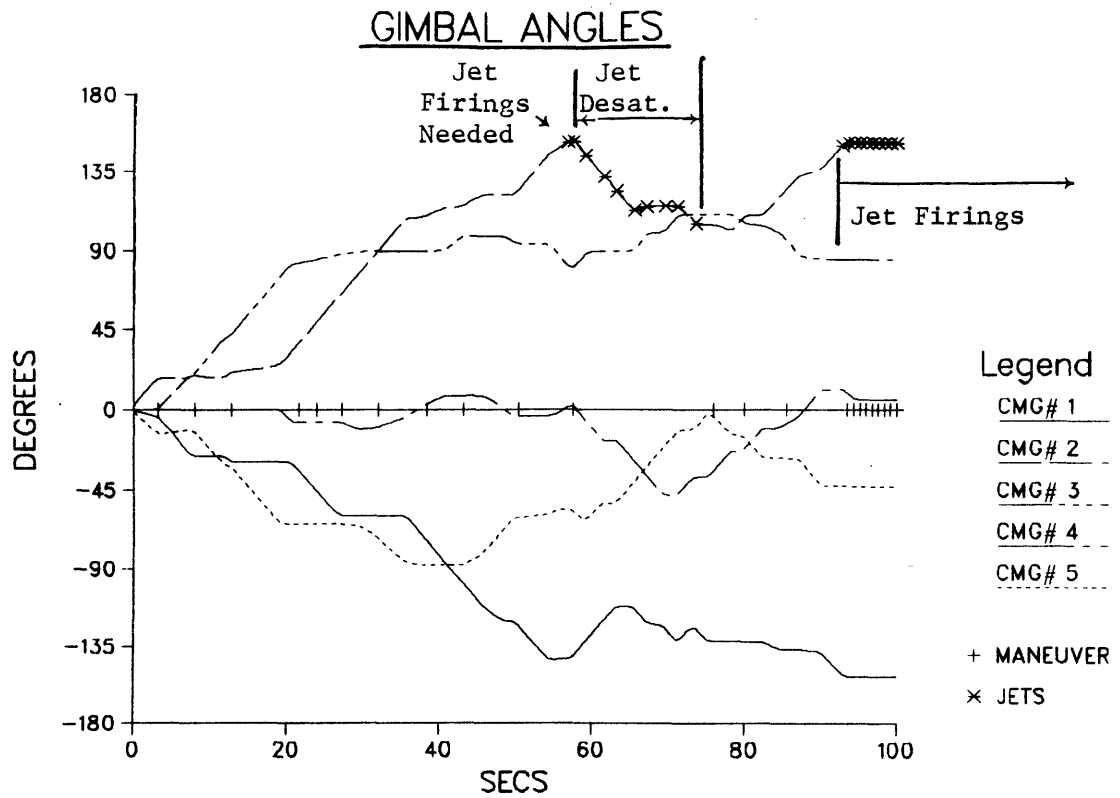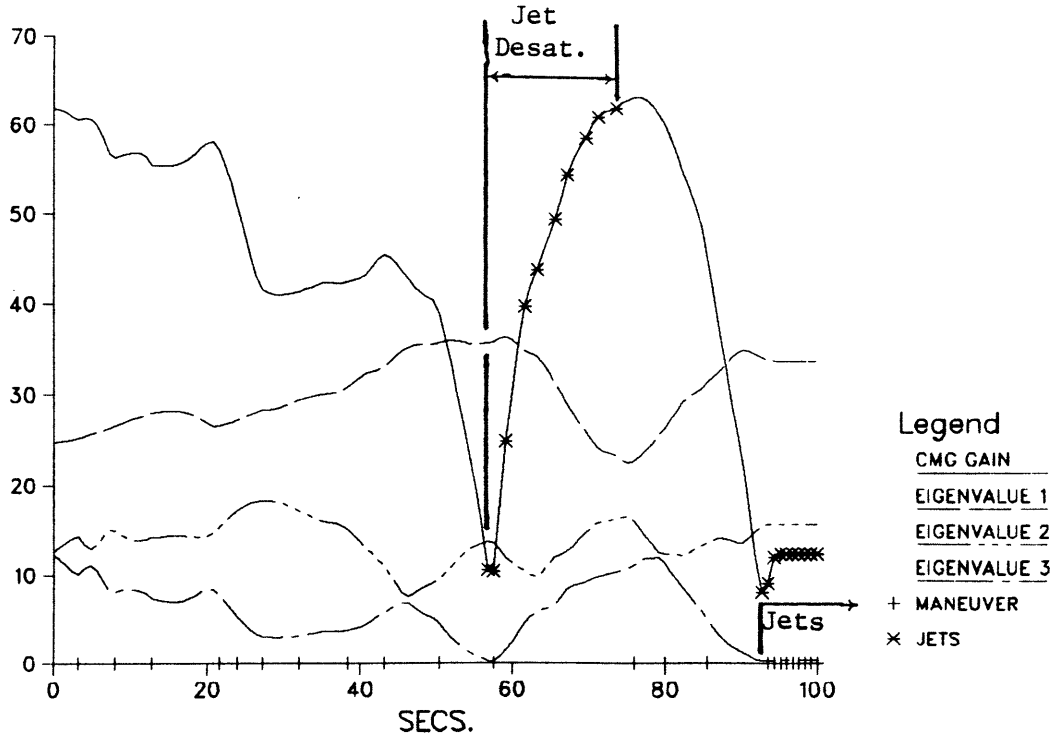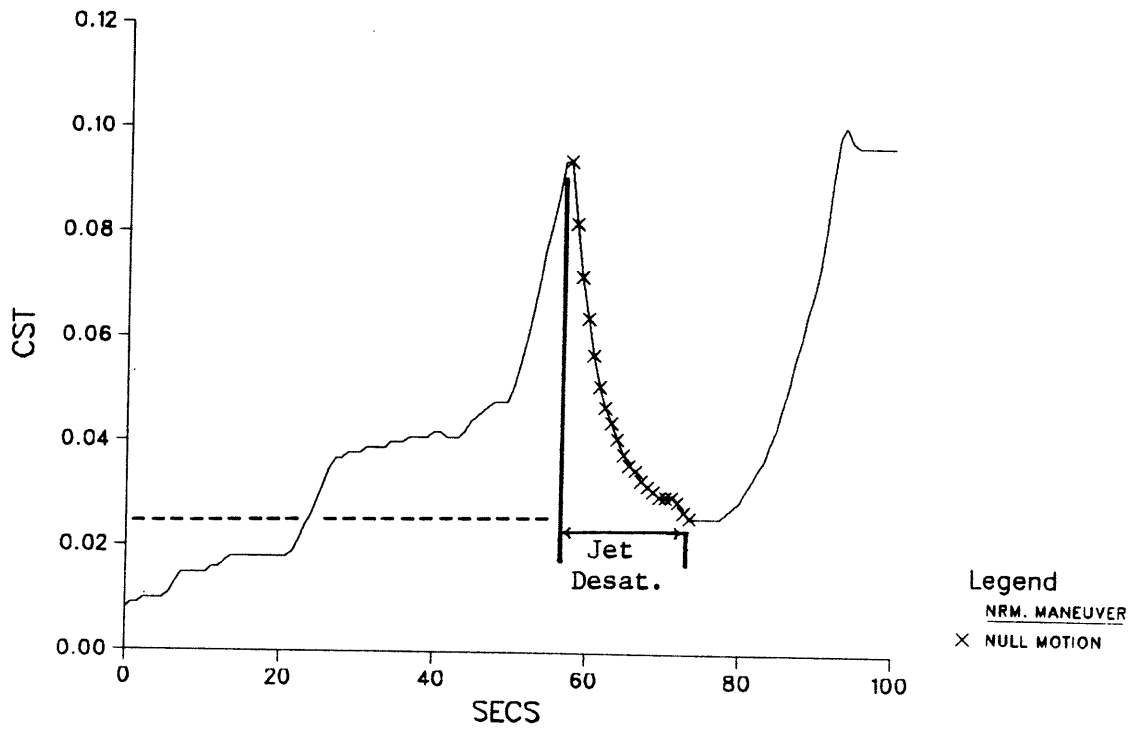
GIMBAL ANGLES

Legend

| CMG# 1 |
| CMG# 2 |
| CMG# 3 |
| CMG# 4 |
| CMG# 5 |

+ MANEUVER
× JETS

SATURATION DETECT

CMGs Unable to Resolve Requests

CMGs Only

Jets Required

Jet Desaturation

Legend
TOT. RQST/AVAIL
AVAIL: PARALELL/PERP
CORR. RQST/AVAIL
+ MANEUVER
× JETS

FIGURE 69: Saturate CMGs in Roll/Yaw, Jet-Assisted Desaturation Commanded

CMG CONTROLLABILITY

Jet Desat.

70

60

50

40

30

20

10

0

0   20   40   60   80   100

SECS.

Legend

CMG GAIN

EIGENVALUE 1

EIGENVALUE 2

EIGENVALUE 3

+ MANEUVER

× JETS

Jets

TOTAL CMG COST

0.12

0.10

0.08

CST

0.06

0.04

0.02

0.00

0   20   40   60   80   100

SECS

Jet Desat.

Legend

NRM. MANEUVER

× NULL MOTION

FIGURE 70: Saturate CMGs in Roll/Yaw, Jet-Assisted Desaturation Commanded

VEHICLE RATES

Legend
RATE: ROLL
RATE: PITCH
RATE: YAW

Jet Desat.

Hybrid Jet/CMG Response

DEG/SEC. X 100

SECS.
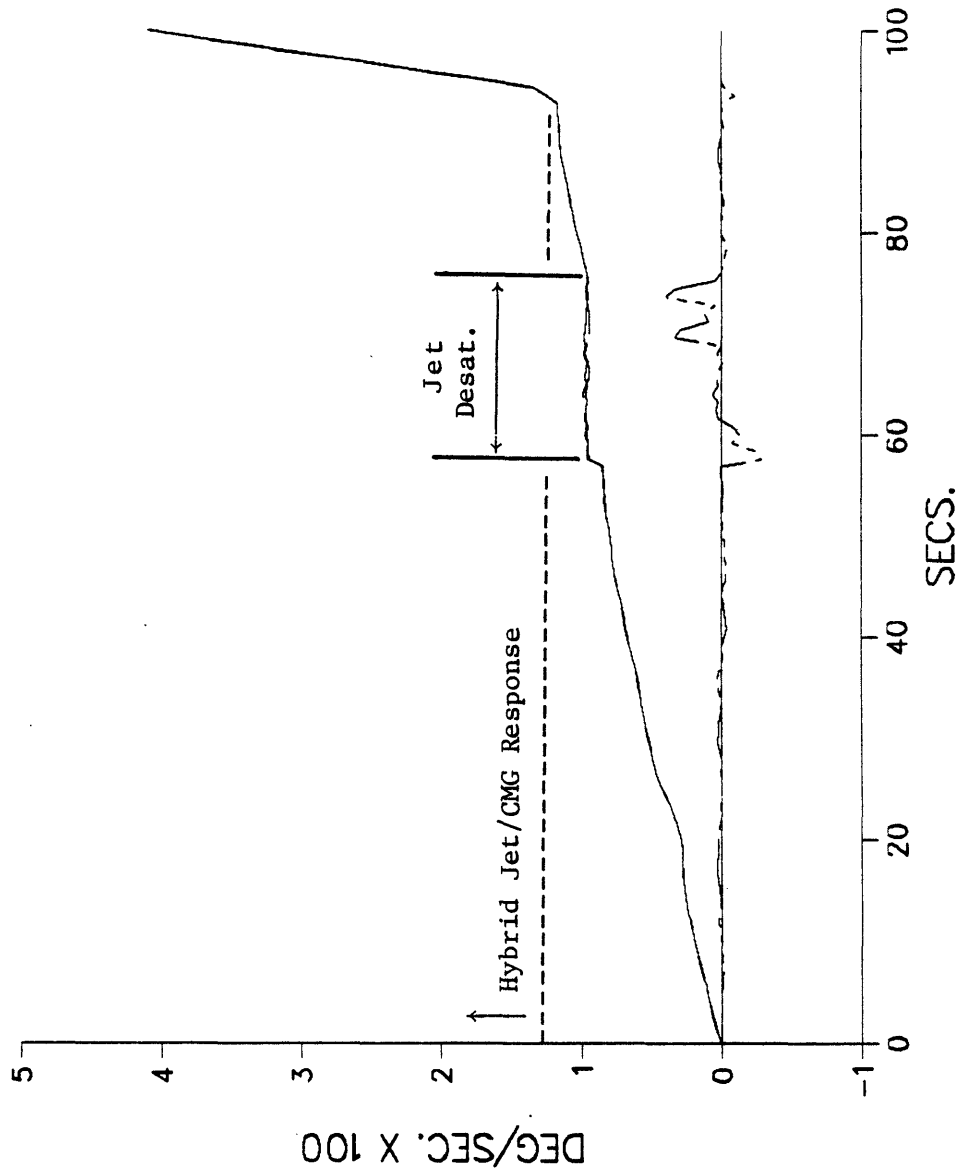
FIGURE 71: Saturate CMGs in Roll/Yaw, Jet−Assisted Desaturation Commanded

As it is currently construed, the desaturation process works to decrease the mean CMG costs, which now depend on CMG gain and distances from gimbal stops. As seen in the above examples, desaturation indeed pulled CMGs sufficently away from stops to cut objective contributions, and restored the system to full gain. It thus provides a direct means of relieving singular orientations and problem CMG states. Momentum saturation is not directly incorporated into the objective function; the desaturation process was seen to remove the system somewhat from saturation, but the dominant result was the restoration of CMG controllability. In order to place more emphasis on momentum desaturation, the objective would have to be modified to account directly for the degree of system saturation (ie. the rotor alignment cost contribution related more specifically to momentum saturation in double gimballed CMG systems).

The next test run uses a 5-CMG array in an orthogonal-mount configuration (as sketched in Fig. 16 and also used in the test of Figs. 63 & 64). The input request sequence is dynammically made proportional to the output torque of CMG #2; the quickest means of answering such a request is to advance primarily CMG #2 and leave the remainder of the system untouched, hence this request sequence provides a means of encouraging CMG #2 to move against its stop. The behavior of the stops avoidance function is thus examined for a single-gimballed system. Each request is sized to advance CMG #2 by six degrees.

The resulting gimbal angles and saturation index are plotted in Fig. 72. One sees that requests were answered nearly exclusively by CMG #2 at the beginning of the run (as expected for this type of request). Since the gain-steering objective contribution dominates before CMG #2 approaches its stop, other CMGs are used as the run progresses in order to keep the CMG gain from dropping. At t = 40 sec., the stops cost on CMG #2 rises abruptly (making its further advance prohibitively expensive), and other CMGs are used to resolve requests. By t = 65 secs., the remaining CMGs can no longer satisfy the request inputs, thus CMG #2 is moved against its stop, and RCS firings are required.
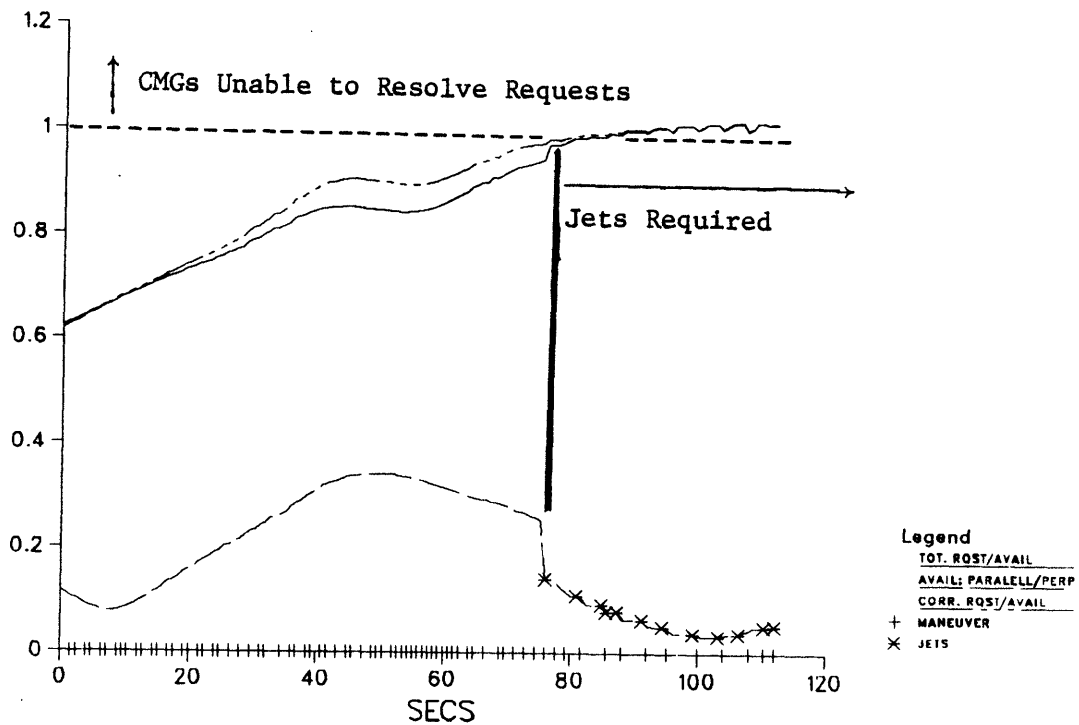
GIMBAL ANGLES

Legend
CMG# 1
CMG# 2
CMG# 3
CMG# 4
CMG# 5

+ MANEUVER
× JETS

CMG #2 Against Stop
Jet Firings

SATURATION DETECT

CMGs Unable to Resolve Requests

Jets Required

Legend
TOT. RQST/AVAIL
AVAIL: PARALELL/PERP
CORR. RQST/AVAIL
+ MANEUVER
× JETS
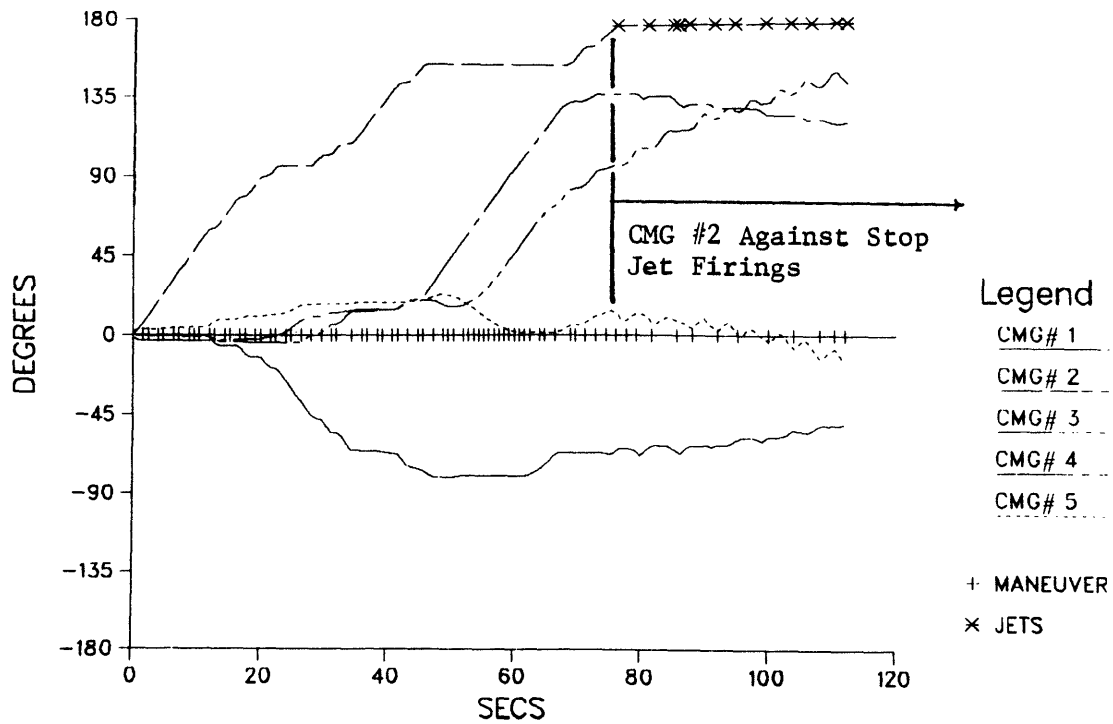
FIGURE 72: Encourage CMG #2 to Move Against Stop

172

CMG CONTROLLABILITY

Legend

__CMG GAIN__

EIGENVALUE 1

EIGENVALUE 2

EIGENVALUE 3

+ MANEUVER

✳ JETS

Jets Required

SECS.
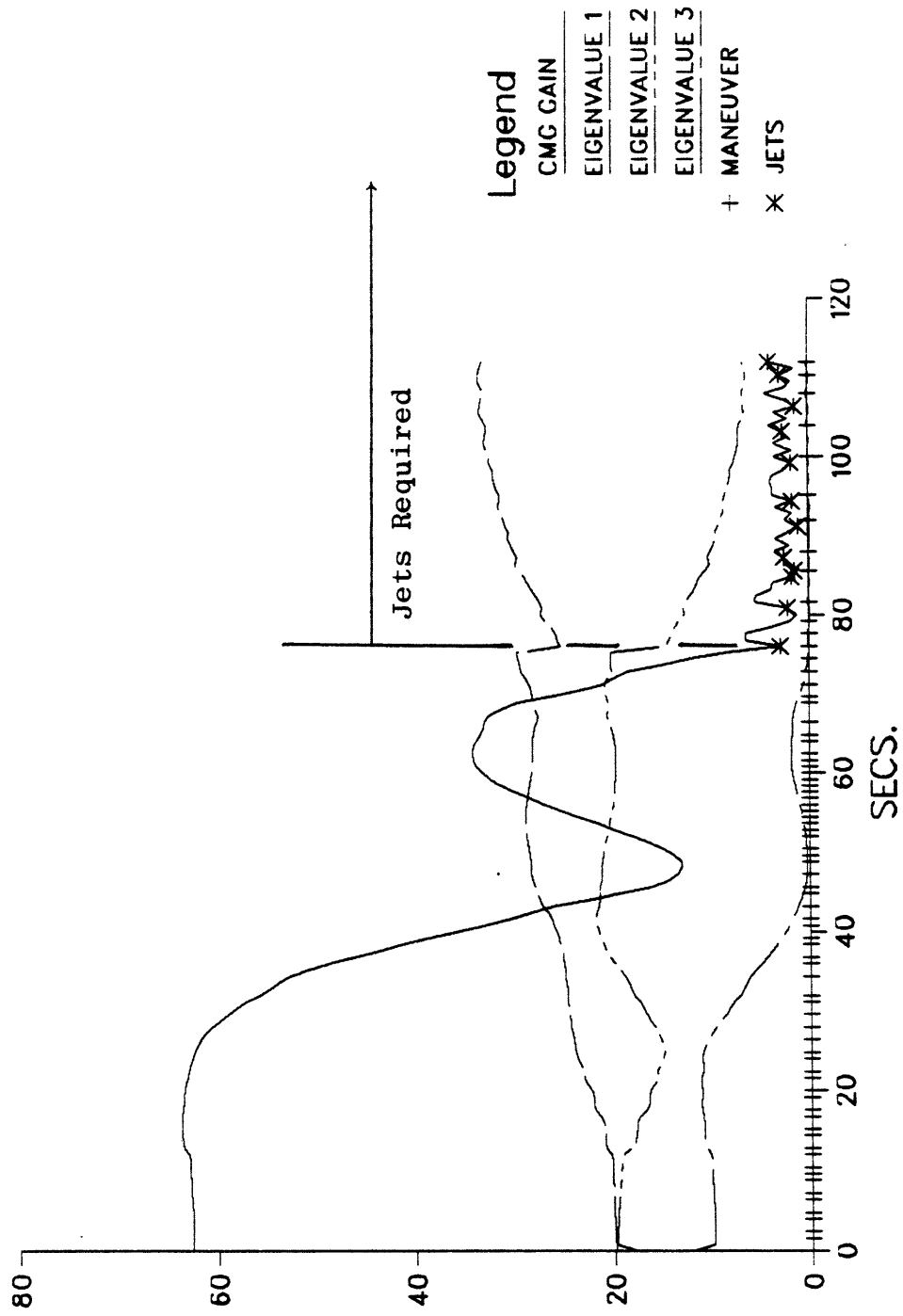
FIGURE 73: Encourage CMG #2 to Move Against Stop

The lower plot in Fig. 72 shows the saturation index (upper curve). The lower curves represent components of the calculation (any CMGs moved against stops are deleted if the request wants to move them further in that direction). The saturation index progressively rises until it hits unity near t = 75 sec., and jets are introduced.

The corresponding CMG controllability curves are plotted in Fig. 73. The initial drop in CMG gain occurs as CMG #2 approaches its stop and other CMGs are used to answer requests. When the system nears saturation and RCS assistance is required, the CMG gain and corresponding eigenvalue are seen to approach zero (CMG #2 is deleted from the calculations if it is against its stop and the input requests favor continued motion in that direction), indicating loss of 3-axis control.

As mentioned at the close of Sec. 6.2, the process of steering a CMG system to instantaneously maximize CMG gain delivers no guarantee that all singular states can be avoided. The final test run of this chapter illustrates this point.

A 4-CMG pyramid-mounted configuration is assumed. This consists of four single gimballed CMGs with rotors constrained to gimbal on the faces of a pyramid (inclined at 45° to the vertical); a cross-section through this mounting arrangement produces a square. In order to avoid starting the system in a singular state, the rotors are initially displaced by 30 degrees. The cyclic request sequence is input, again with a magnitude of 0.0008 deg/sec. per axis for each request. Full costs are assumed; maximum gain steering is used.

Gimbal angles are shown in Fig. 74. One immediately notes that jets were required to complete maneuvers. Vehicle rates are plotted in the lower portion of Fig. 74. One sees the characteristic cyclic velocity profile, but the jet firings created a much quicker vehicle response, causing an asymmetrical rate history.

The reasons for the jet firings can be inferred from the controllability curves given in the upper plot of Fig. 75. Jet firings occured at a point where CMG gain dipped very low and an eigenvalue
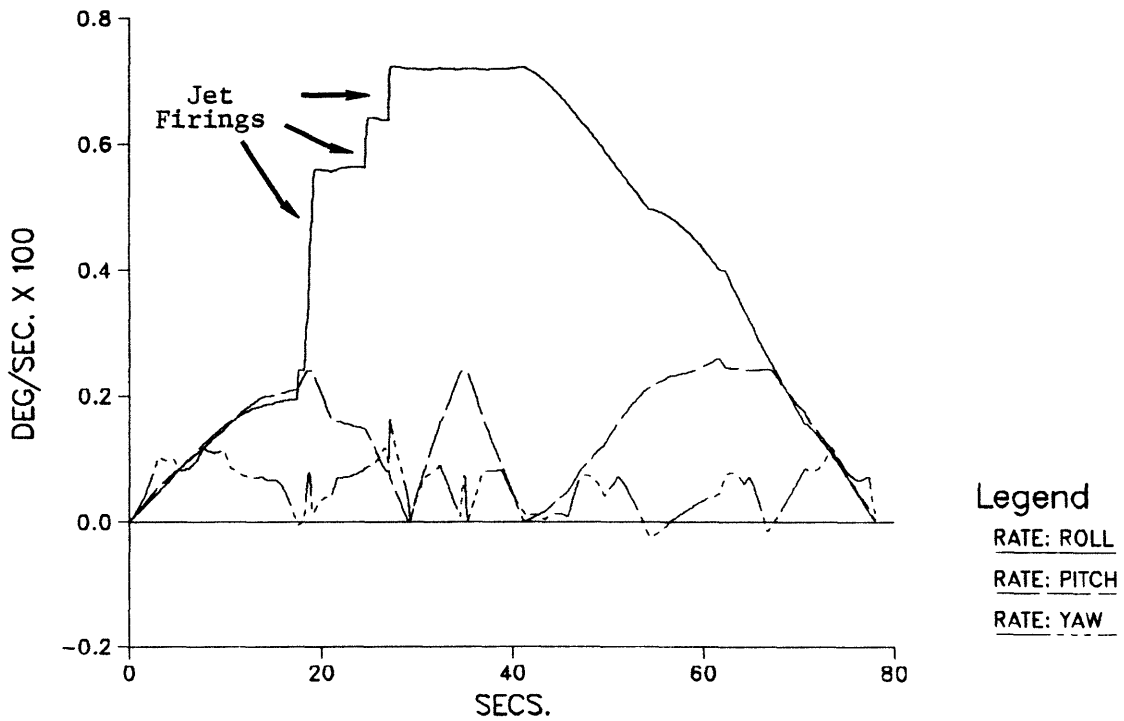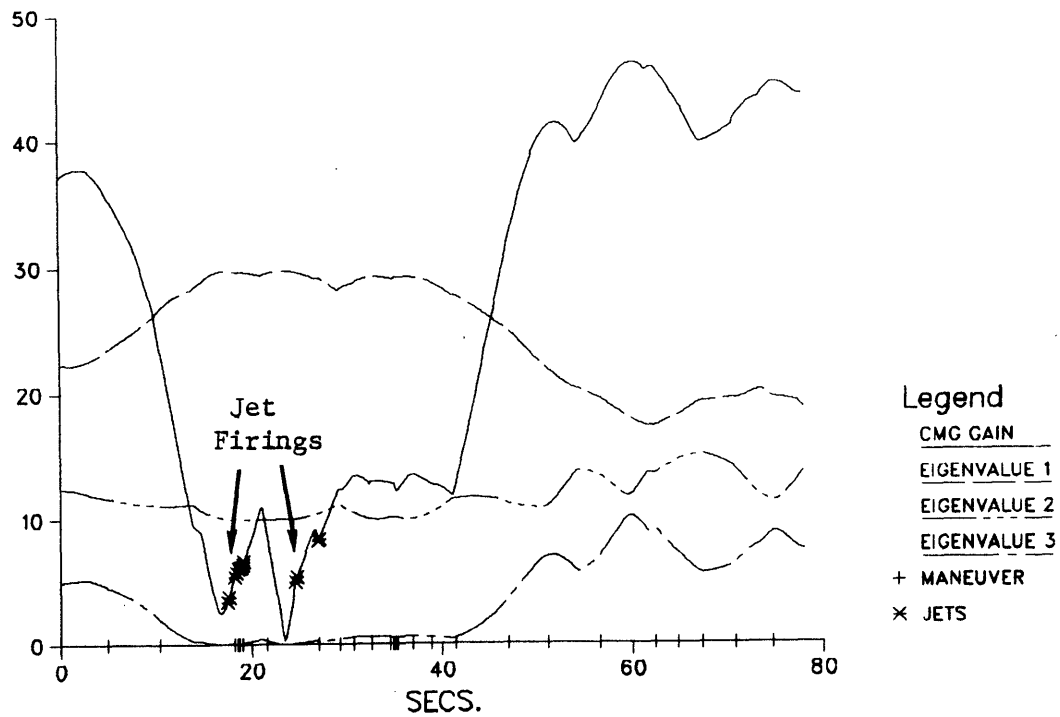
GIMBAL ANGLES

Legend
CMG# 1
CMG# 2
CMG# 3
CMG# 4

+ MANEUVER
✕ JETS

VEHICLE RATES

Legend
RATE: ROLL
RATE: PITCH
RATE: YAW
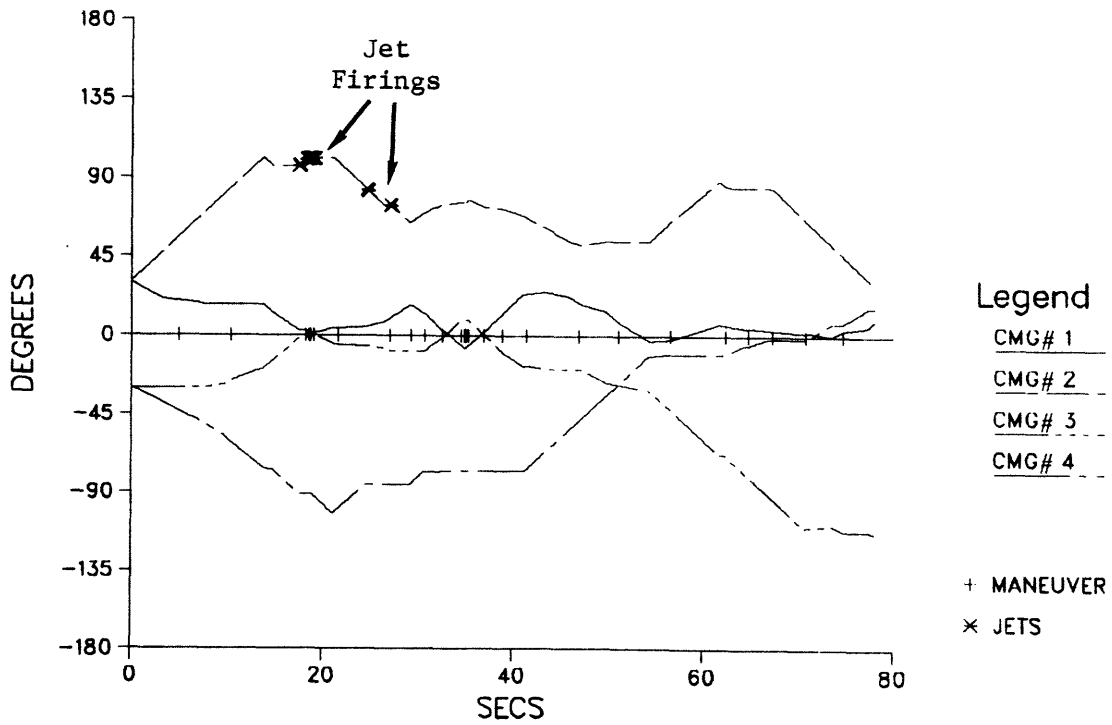
FIGURE 74: Cyclic Maneuver, 4 Single Gimballed CMGs

175

CMG CONTROLLABILITY

Jet
Firings

Legend
CMG GAIN
EIGENVALUE 1
EIGENVALUE 2
EIGENVALUE 3
+ MANEUVER
✕ JETS

SECS.

SATURATION DETECT

Saturation

Jets
Required

Legend
TOT. ROST/AVAIL
AVAIL: PARALELL/PERP
CORR. ROST/AVAIL
+ MANEUVER
✕ JETS

SECS
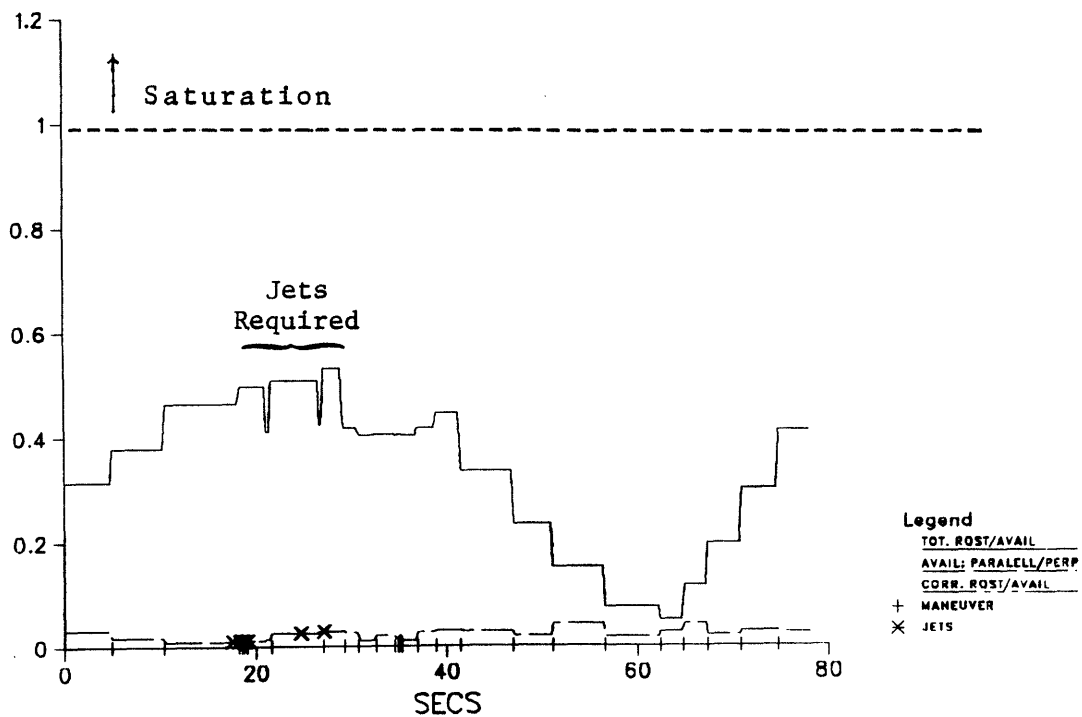
FIGURE 75: Cyclic Maneuver, 4 Single Gimballed CMGs

176

approached zero, indicating loss of 3-axis control. Looking at the saturation index in the lower plot, one sees that the CMG system always remains well below saturation (the index never passes 0.5), indicating that the loss of control occured at an internal singular state. In spite of the objective amplitude working to maximize gain, the system was led into a singular orientation.

As mentioned in Sec. 6.2, this method of linearized gain steering is a compromise which offers considerable flexibility at the cost of less than guaranteed singularity avoidance. This process was able to satisfactorily manage a 5-CMG system to avoid singular states, yet problems arose when a degree of freedom was removed, and the system was truncated to four CMGs. Complex strategies (which incorporate nonlinear aspects of CMG behavior) may acquire superior singularity avoidance characteristics.

CHAPTER 7

SIMULATION EXAMPLES: HYBRID SELECTION DRIVEN BY
PHASE SPACE AUTOPILOT

7.1)   The Phase Space Controller

The test runs of the previous sections were all driven by the
rate-feedback controller, which only directs the steering/selection logic
to attain a commanded vehicle rate-change sequence; vehicle attitude is
ignored. This controller was developed as a straightforward and
economical means of exercising and testing the selection/steering
software, and was not intended to function as an actual vehicle control
law.

In order to to perform a more relevant series of tests, a
phase-space control law (which coordinates control of vehicle attitudes
and rates) was adapted to drive the steering/selection package. It is
based upon the controller used in the OEX autopilot,[23,38] which has
recently completed successful testing on the Shuttle orbiter. The hybrid
selection/steering process has been designed such that it readily
interfaces with the OEX phase-space controller without requiring major
alteration.

Refs. 23 and 38 should be consulted for details concerning the OEX
phase-space controller. The OEX has the capability of exercising
simultaneous control over both vehicle attitude and translational
position. The vehicle state is described by a six-dimensional vector $\underline{x}$,
and the state error $\underline{x}_d - \underline{x}$ (desired minus current state) is denoted

by $\underline{x}_\varepsilon$. Under the original OEX controller, two concentric spheres partition state space into three regions (I, II, and III, as defined by the 2-dimensional slice shown in Fig. 76). The state space origin is defined as the desired vehicle state, and the current state is displaced from the origin by the normalized state error $x'_{\varepsilon_j} = x_{\varepsilon_j}/r_j$, where r_j is the deadband limit for the j'th state coordinate. By scaling the coordinates of $\underline{x}_\varepsilon$ independently by their respective deadbands (which can differ between axes), the radius of the outer sphere is set at unity, and the location of the vehicle state relative to the phase sphere may be directly determined via the magnitude of $\underline{x}'_\varepsilon$ (ie. $\left| \underline{x}'_\varepsilon \right| > 1$ is assumed to indicate a state lying outside deadband limits).

Corrective jet selections are requested whenever the state error is outside of region I and is increasing in magnitude. In this fashion, the state trajectory is intercepted before the deadband limits are reached, and the state error is constrained to limit-cycle within the bounds of region II. In order to slow a potentially rapid approach to the deadzone, revised jet selections are also forced when the vehicle state crosses into the deadband limits (ie. region II) from region III.

To attain the desired target state, the OEX requests a vehicle rate change of the form:

54)
$$\underline{\Delta V} = -c\, \hat{x}_\varepsilon + (\underline{\dot{x}}_d - \underline{\dot{x}})$$

Where: $\hat{x}_\varepsilon =$ Unit vector in direction of state error.

$\underline{\dot{x}}_d =$ Desired vehicle rates.

$\underline{\dot{x}} =$ Current vehicle rates.

$c =$ Magnitude of convergence velocity.

REGION 3

x'_{ϵ_i}

REGION 1

x'_{ϵ_j}
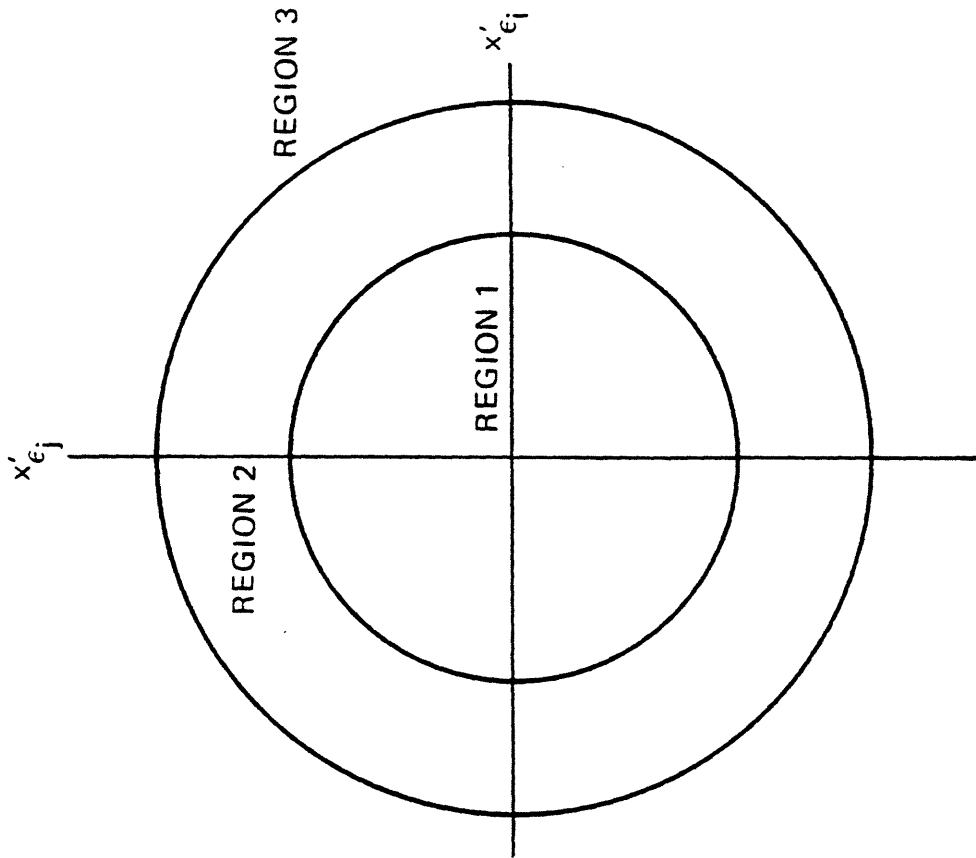
REGION 2

PHASE SPACE REGION DEFINITION (NOTE: THIS IS A 2-DIMENSIONAL PROJECTION OF A 6-DIMENSIONAL FIGURE)

FIGURE 76

The value of c defines a "convergence velocity", which determines how quickly the vehicle state will be returned to the deadzone; its value in region III is larger than its value within the deadband limits in order that vehicle states far removed from the deadzone are restored within a reasonable period. A corrective jet selection is forced if the vehicle rates deviate or drift substantially from their target values after jets (or other actuators) have finished their operation.

The calculation of desired rate is performed differently when the vehicle is subject to a constant disturbance acceleration; in this case, a rate is requested such that the disturbance acceleration will reverse the state trajectory before the opposite deadband is reached, thereby avoiding another limit-cycle firing there.

Little modification was required to adapt the OEX phase-space controller to handle the hybrid selection process and drive CMGs. Because of their much finer control granularity, the CMGs are capable of maintaining the vehicle within a much tighter deadzone boundry than needed with finite RCS firings; state errors and limit-cycling vehicle rates can be damped by replacing the unit vector $\hat{x}_\epsilon$ in Eq. 54 with the actual state error $\underline{x}_\epsilon$. The corrective rate is thus made proportional to the state error magnitude (as opposed to the constant rate requested by Eq. 54).

Hybrid selections are forced whenever the vehicle state is outside a small inner deadzone of tolerated state error and drifting away from its target (ie. state error is increasing). The magnitude of the state error has decreased before each such selection, hence the magnitude of the requested rate becomes smaller and the vehicle trajectory tends to exhibit a damped second-order response; projected onto a phase plane, it is seen to "spiral" into the desired state (this is illustrated in examples presented in the next section). The rapidity of system response (thus the amount of damping) is determined by selecting the gain "c" in Eq. 54. In order to avoid requesting excessive rates in cases where the vehicle is far removed from the desired state (ie. the state error lies

182

in region III), the form of Eq. 54 may be applied to saturate requests (i.e. the unit vector $\hat{x}_\epsilon$ is used) after they exceed a maximum threshold.

Because the logic discussed above waits until the state error begins to increase before requesting an updated hybrid selection, the vehicle will exhibit a damped oscillation as the state error converges to zero. The logic may easily be modified to avoid these effects by requesting a hybrid selection to remove the convergance rate before the state error begins to increase in magnitude. The CMG response required to null the convergence rate $(\underline{\omega}_c)$ may be obtained by performing a hybrid selection for $-\underline{\omega}_c$ after $\underline{\omega}_c$ is attained and the vehicle is coasting. The resulting CMG on-times determine the interval (Δt) required to attain zero vehicle rates; by applying these CMG commands when the magnitude of the state error has has reached a value of $\frac{1}{2} \omega_c \Delta T$, the vehicle rates and state error will reach zero simultaneously, resulting in a "critically damped" response with no overshoot.

A "CMG Monitor" routine has been appended to the logic of the OEX controller in order to address the necessary interaction of CMGs with the control package. The structure of the CMG monitor is similar to the rate-feedback controller as diagrammed in Fig. 15. It is invoked during each pass through the controller executed while CMGs are moving. Since the original software was written for the Shuttle orbiter, 80 msec. cycles are assumed. The CMG monitor recommends an updated hybrid selection whenever the CMGs are in motion and at least one of the conditions apply as listed below:

1) Any CMG gimbal is moved past a preset threshold (θ_{max}) since the previous selection.

2) No jets are firing, and the vehicle rate residual is increasing appreciably.

3) The stops or singularity avoidance objective values have increased significantly since the previous selection.

4) CMGs and jets have completed their commands, but the vehicle rate residual is still significant.

183

A capability has also been integrated into the controller to perform null motion (Sec. 4.4) and jet-assisted desaturation (Sec. 4.5). Most required modifications to the controller software reside in a "Null Monitor" routine which is executed once per cycle. Null motion is requested upon operator command or automatically (when enabled) after net CMG singularity or stops costs have risen significantly since the previous null attempt. The null monitor oversees the null process; the cost filter (Eq. 41) is updated, and null motion is suspended (the nominal hybrid selection is re-established) if no consistant decrease in CMG costs can be established, or an abort is indicated from the hybrid selection (jets or no CMG displacement detected in the solution). Null motion is also suspended if the controller has requested a significantly large rate change. This differs significantly from the rate-feedback controller, where null motion retains control until it senses completion.

In addition to performing coordinated control of vehicle rates and attitudes, the phase-space controller responds in "real time" to input commands queued to execute at particular instants. These features are not supported by the rate-feedback controller (used in Chapters 5 & 6). The rate-feedback controller accepts requests from an input stack, and pursues each request independently to completion before fetching its successor. The "real-time" nature of the phase-space controller, however, evokes immediate response to commands sequenced to execute at pre-determined instants. If a request is not completed before the next arrives, the new command is added to the current residual; the vehicle rate requests are thus dynamically updated by the commands issued from the phase-space controller (as discussed earlier in this section) and input from the operator. In cases where desired states have been achieved before new commands are input, the vehicle will "coast" at the final state until other commands are queued for execution (as opposed to the rate-feedback controller, which promptly fetches the next sequential request and never enters an "idle" state).

Simultaneous translational & rotational control is not enabled in the tests summarized in the following section; only control of vehicle attitude is demonstrated. The software, however, is structured to allow coordinated 6 DOF state space control; future tests will address this capability.

7.2) Simulation Examples

This section summarizes test results obtained by controlling a rigid-body model of the Power Tower Space Station[2] via the modified phase-space controller described in Sec. 7.1. Mass properties are listed in Table I (Sec. 5.2). The CMGs are used as specified in Table I; the orthogonal-mount quad double-gimballed configuration (Fig. 16) is assumed except where explicitly noted. The CMG model[29] and RCS system[33] used in these tests were introduced in Sec. 5.2. RCS jets are assumed to be discrete devices, and firings are rounded to the nearest 80 msec. increment after the selection has been performed. CMGs are still assumed capable of continuous dynamic range. Vehicle environment was modelled via a modified OFS simulation package.[39] No environmental disturbances (eg. gravity gradient and aerodynamic torques) are assumed.

Most parameters pertaining to the hybrid selection process (ie. objective weights, etc.) are set to the values specified in Table I. Update selections are now forced whenever a CMG gimbal is rotated over 5 degrees (θ_{max}) since the previous selection. Hybrid selections are not requested by the phase-space controller when the magnitude of the state error is under 1.5×10^{-8} degs. (well under any noise threshold) and the vehicle rate residual is below 5×10^{-5} degs/sec. The state sphere boundries (of the "conventional" OEX controller) are placed at 0.015 deg. (Region 2/3) and 0.0128 deg. (Region 1/2). The gain "c" in Eq. 54 is set at 0.1. Tests involving double gimballed CMGs steer to avoid rotor alignments, excessive inner gimbal swings, and gimbal stops (Eq. 30), while tests involving single gimballed CMGs steer to maximize CMG gain and avoid gimbal stops (Eq. 52). CMG gimbal rates are normalized to

185

their peak values (via Eq. 27) such that input rate changes are realized promptly. The logic discussed in Sec. 7.1 to attain a critically damped response is not applied in these tests (it is currently being integrated into the software); the vehicle is allowed to coast at the convergence rate until the state error increases.

The first tests to be presented examine the response of the hybrid package to a commanded change in vehicle attitude (ie. commanded step in vehicle rate, followed by an attitude hold). The initial example commands a rate of 0.01 deg/sec. about the pitch axis at the beginning of the run (vehicle rates are initialized to zero), followed by an attitude hold at t = 100 sec.

Resulting vehicle rates are presented in the upper plot of Fig. 77 (dotted lines denote desired rates, solid lines are the simulated vehicle response). The commanded rate was achieved at approx. 25 sec. into the test. After receipt of the attitude hold command at t = 100 sec., the pitch rate was reversed to a desired convergence value (at t = 125 sec.), and all vehicle rates were damped to zero after t = 200 sec. Disturbances about other axes were kept minimal.

Corresponding vehicle attitude is plotted in the lower portion of Fig. 77. The pitch inclination is seen to increase until attitude hold is commanded at t = 100 sec. The desired vehicle attitude is established after the attitude overshoot is removed via the commanded convergence rate; by t = 200 sec., all vehicle rates are zeroed and attitude remains constant.

The CMG gimbal angles are plotted in Fig. 78. The upper plot shows the inner gimbal angles (excessive gimbal swings are avoided), and outer gimbal angles are shown in the lower plot. Jets were not needed to complete these maneuvers; all requests were answered solely via the CMGs. Tick marks drawn on the horizontal axis of plots created under the phase space controller indicate the execution of hybrid selections.

A set of rotor alignment plots are shown in Fig. 79; rotor lineups are seen to be avoided throughout the run.

VEHICLE RATES

Rate
Achieved

Attitude Hold Commanded

Attitude
Restored

DEG/SEC. X 100

SECS.

Legend
RATE: ROLL
RATE: PITCH
RATE: YAW
DESIRED RATE: ROLL
DESIRED RATE: PITCH
DESIRED RATE: YAW

VEHICLE ATTITUDE

Attitude Hold
Commanded

Attitude
Restored

Rate
Achieved

DEGREES.

SECS.

Legend
ATTITUDE: ROLL
ATTITUDE: PITCH
ATTITUDE: YAW
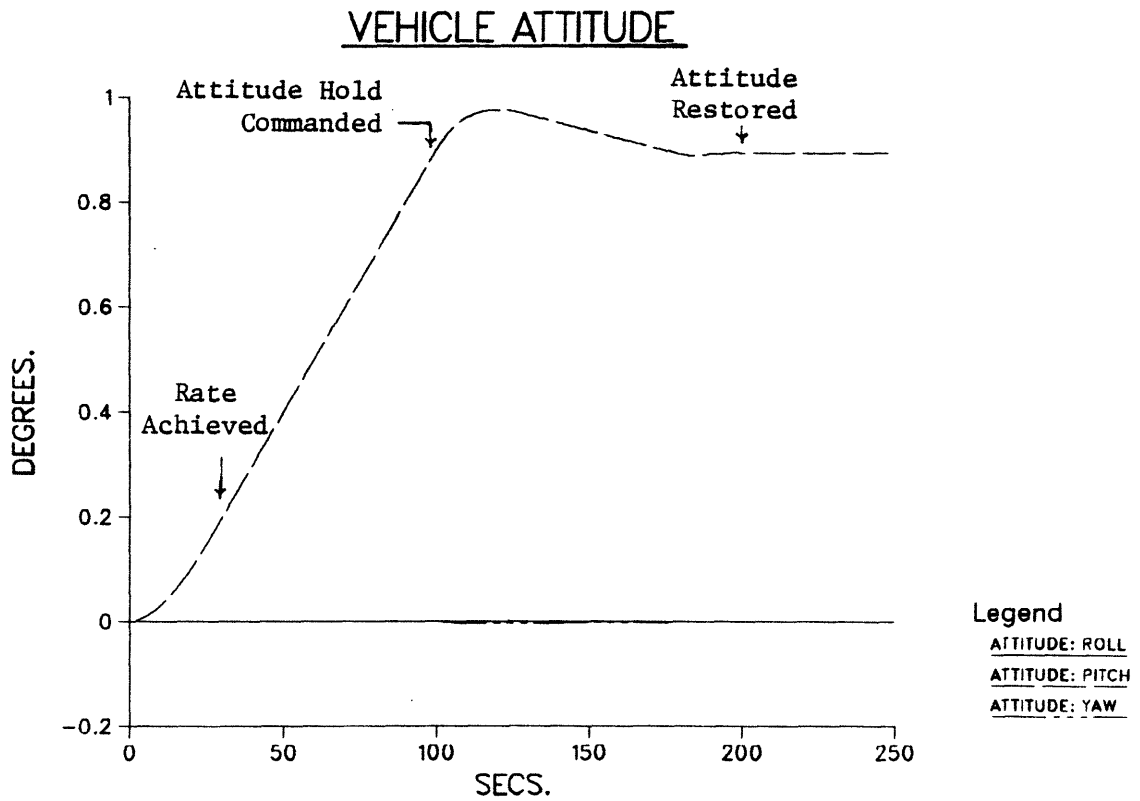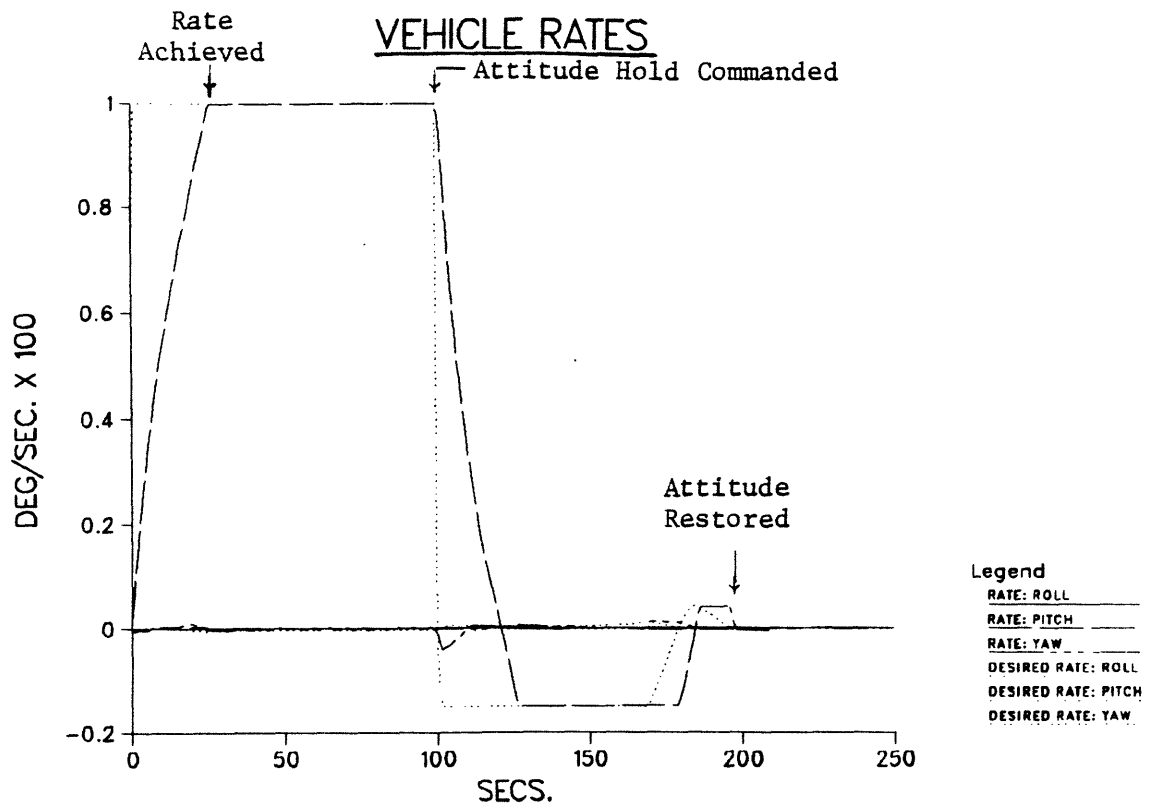
FIGURE 77: Command 0.01°/sec. in Pitch, Attitude Hold

INNER GIMBAL ANGLES

Legend
CMG# 1
CMG# 2
CMG# 3
CMG# 4

+ MANEUVER
✕ JETS

OUTER GIMBAL ANGLES

Legend
CMG# 1
CMG# 2
CMG# 3
CMG# 4
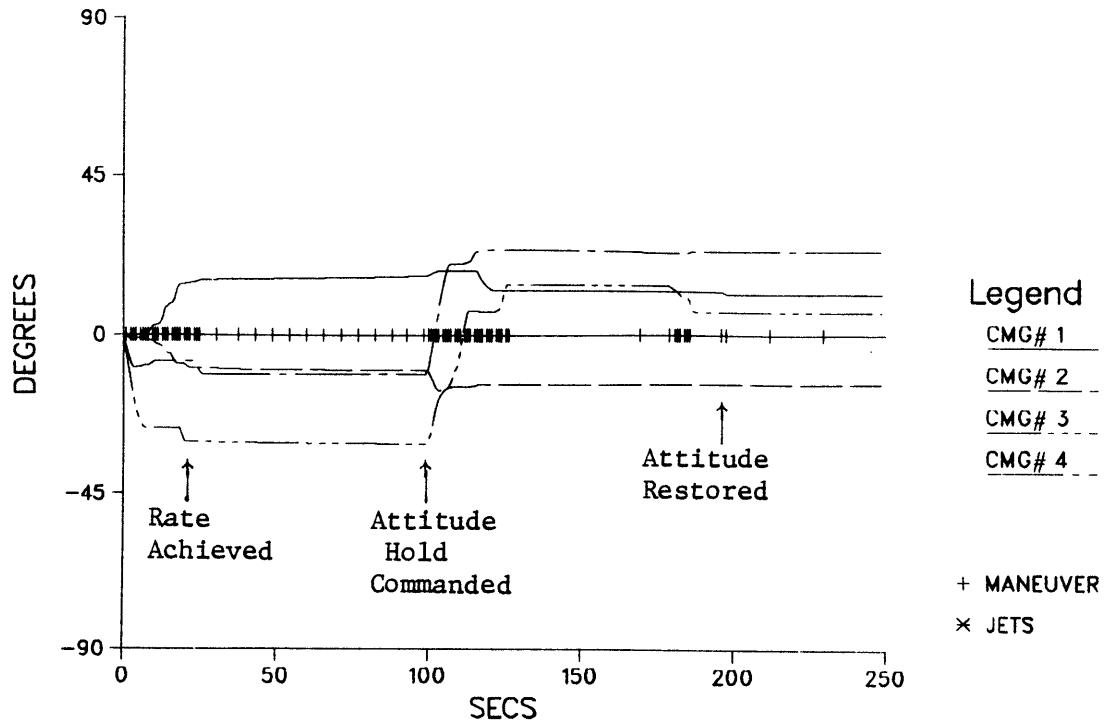
+ MANEUVER
✕ JETS
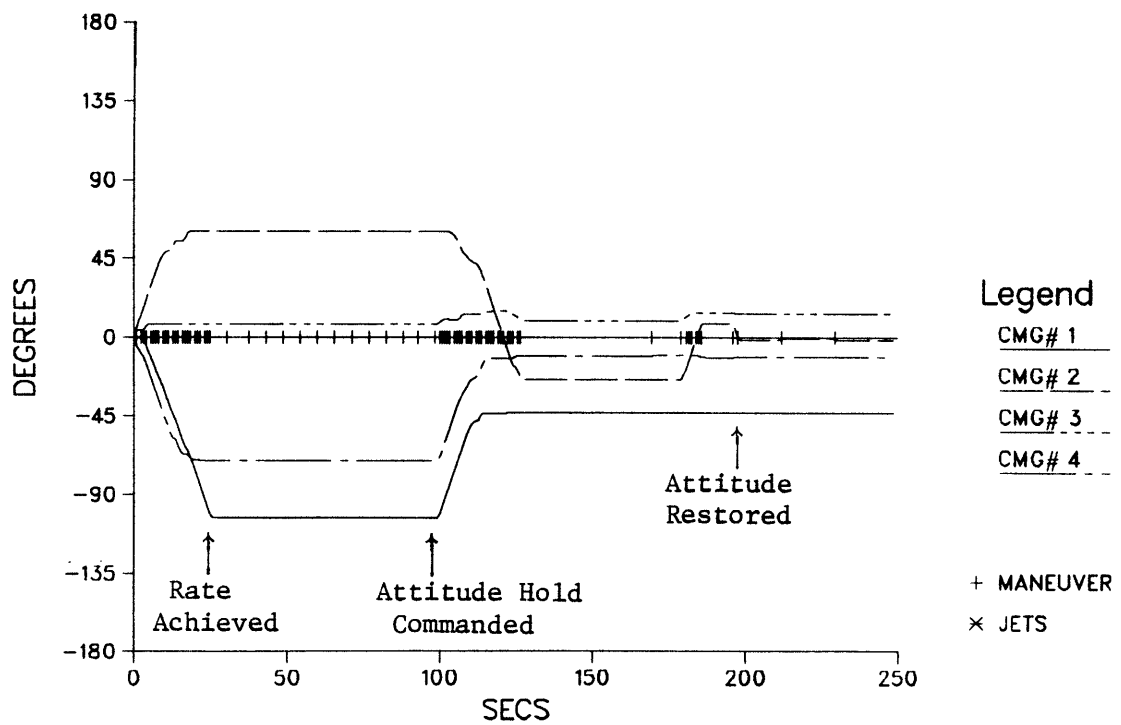
FIGURE 78: Command 0.01°/sec. in Pitch, Attitude Hold

188

RELATIVE ANGLES BETWEEN CMG PAIRS PLT#1

Legend
1.2 ———
1.3 — —
2.3 - - - -
+ MANEUVER
× JETS

RELATIVE ANGLES BETWEEN CMG PAIRS PLT#2

Legend
1.4 ———
2.4 — —
3.4 - - - -
+ MANEUVER
× JETS
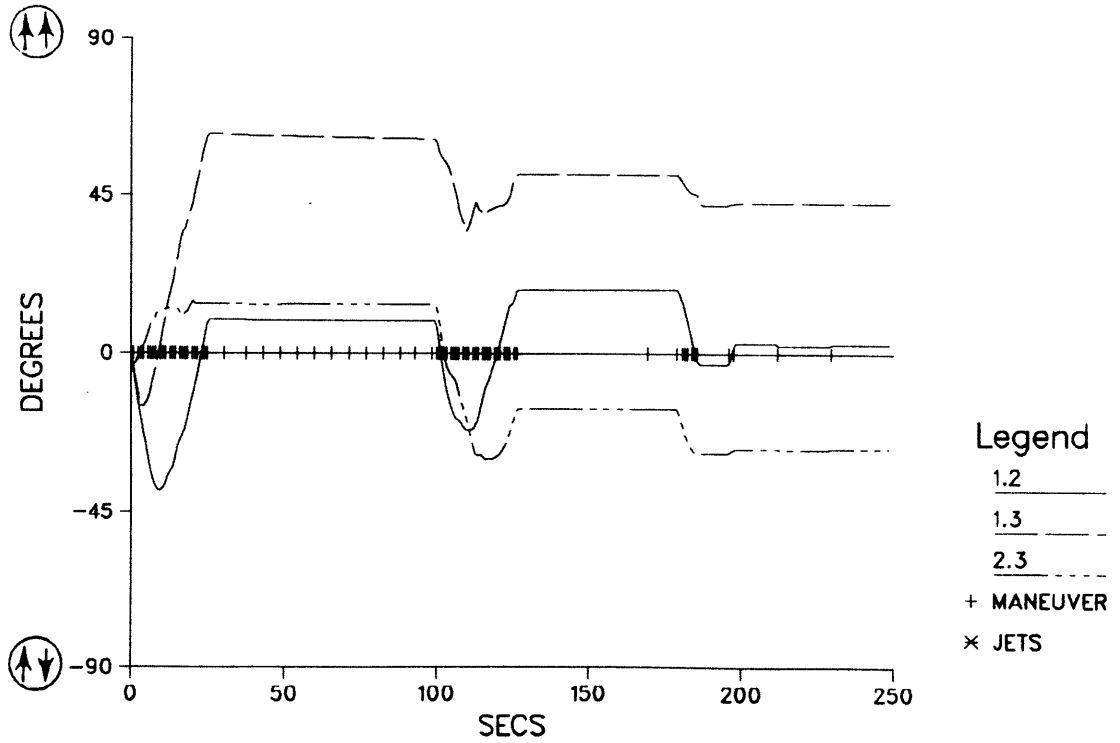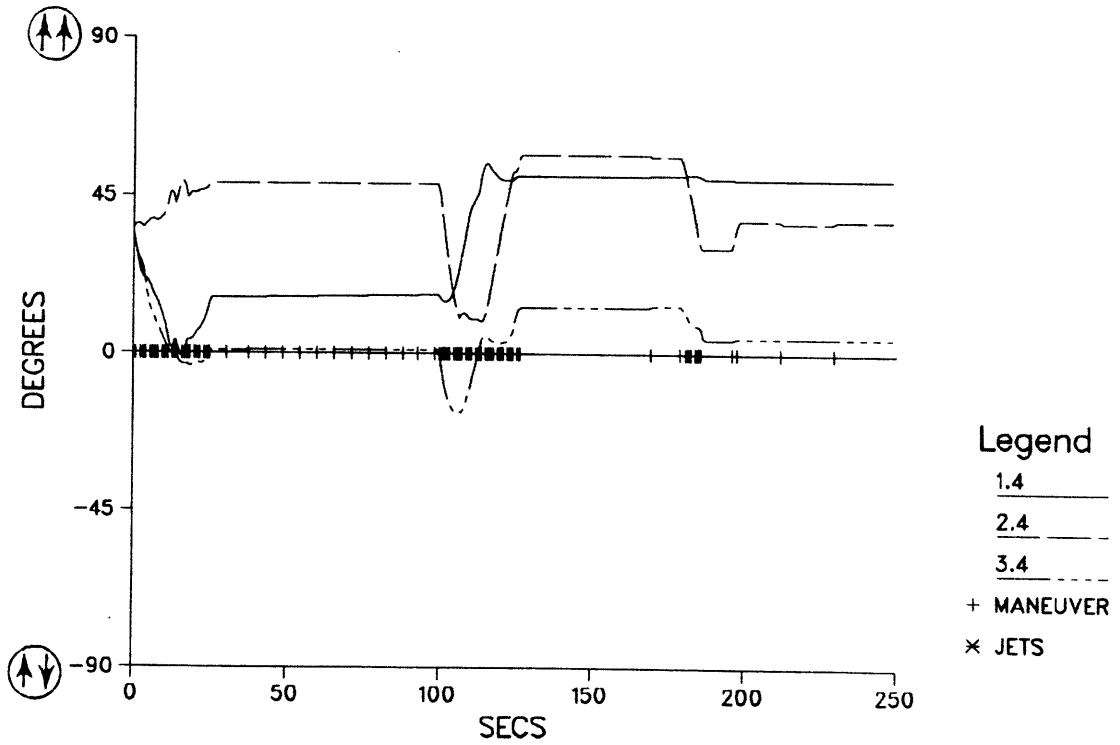
FIGURE 79: Command 0.01º/sec. in Pitch, Attitude Hold

189
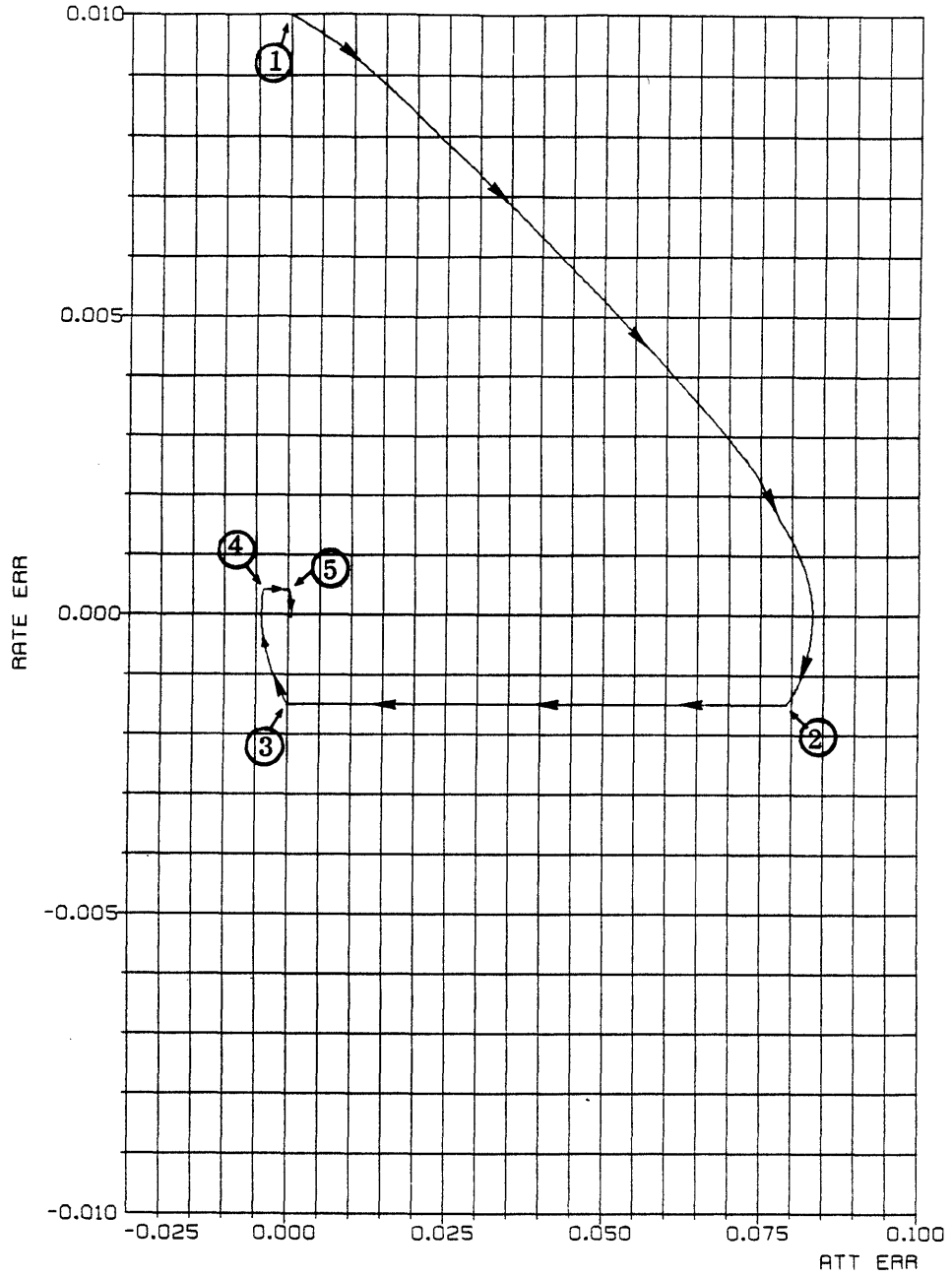
PITCH PHASE PLANE

FIGURE 80: Command 0.01°/sec. in Pitch, Attitude Hold

The resulting pitch axis phase-plane trajectory is plotted in Fig. 80. Arrows are drawn to emphasize the sense of traversal. The vertical axis denotes errors in vehicle rate, while the horizontal axis shows attitude (ie. "state") error. Attitude error begins to accumulate when the attitude hold is commanded at t = 100 sec. (point #1), where the vehicle rate is 0.01 deg/sec. CMGs are commanded to drop the vehicle rate to a convergence value (Eq. 54), which is attained by t = 125 sec. (point #2), after which the attitude error steadily decreases. When the attitude error crosses zero and begins to increase, a hybrid selection is requested (point #3), which shifts the sign of vehicle rate (point #4), and attitude error is again made to (more slowly) decrease. When attitude error once more crosses zero and starts to increase, another hybrid selection is forced (point #5), and remaining vehicle attitude and rate errors are nulled. In this fashion, the phase space logic described in Sec. 7.1 is applied to damp vehicle attitude and rate errors; phase plane trajectories are made to "spiral" into the origin. If the alternate "critical damping" strategy of Sec. 7.1 was applied here, the vehicle state would be intercepted and brought to the origin before point #3 was reached, thereby avoiding the overshoot and damped oscillations.

The next test uses the same sort of "step" input request, but the peak pitch rate requested (0.04 deg/sec.) is four times larger. This corresponds to a momentum transfer of approx. 50,000 ft-lb-sec., which can be expected in the event of a shuttle docking[2] (the mass properties used here are always with shuttle undocked, so one must consider this test as simulating a crude "elastic" collision).

Resulting vehicle rates and attitudes are shown in Fig. 81. The desired rate of 0.04 deg/sec. is accumulated quickly. Attitude hold is commanded at t = 30 sec., at which point the convergence rate is rapidly established, and vehicle rates are returned to zero when attitude is restored after t = 100 sec.

Looking at the CMG gimbal angles plotted in Fig. 82, we see much less CMG usage than in the previous example. The asterisks plotted over
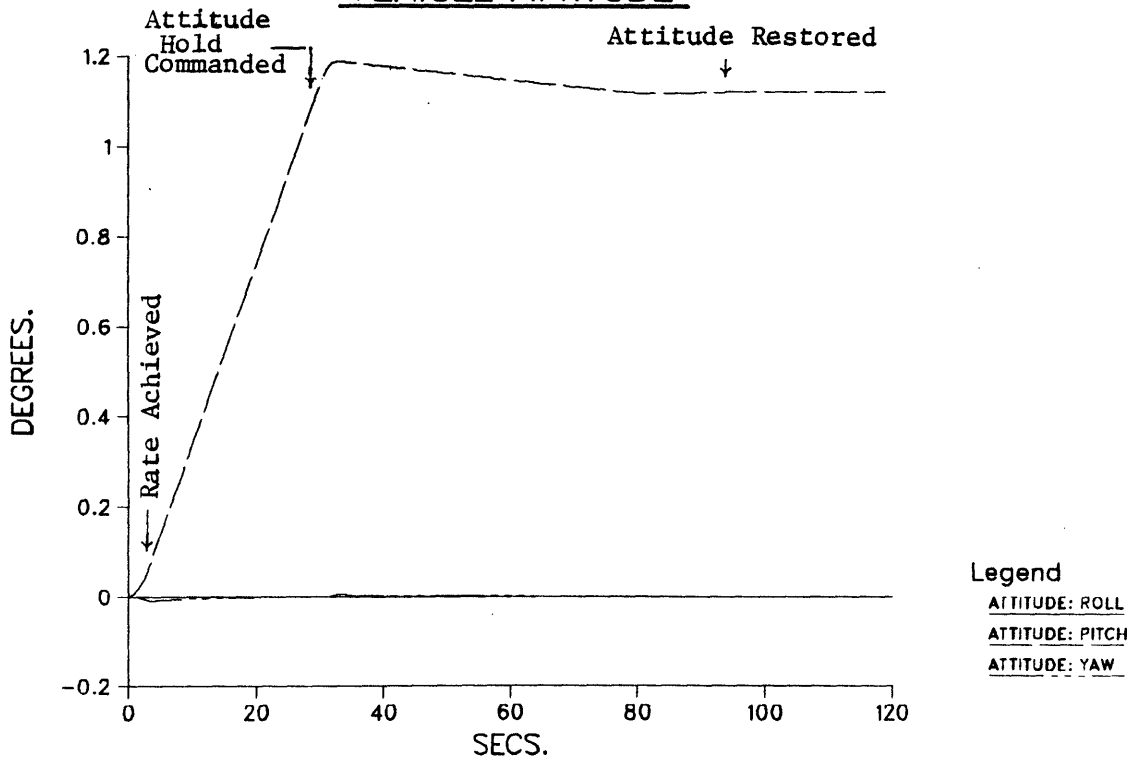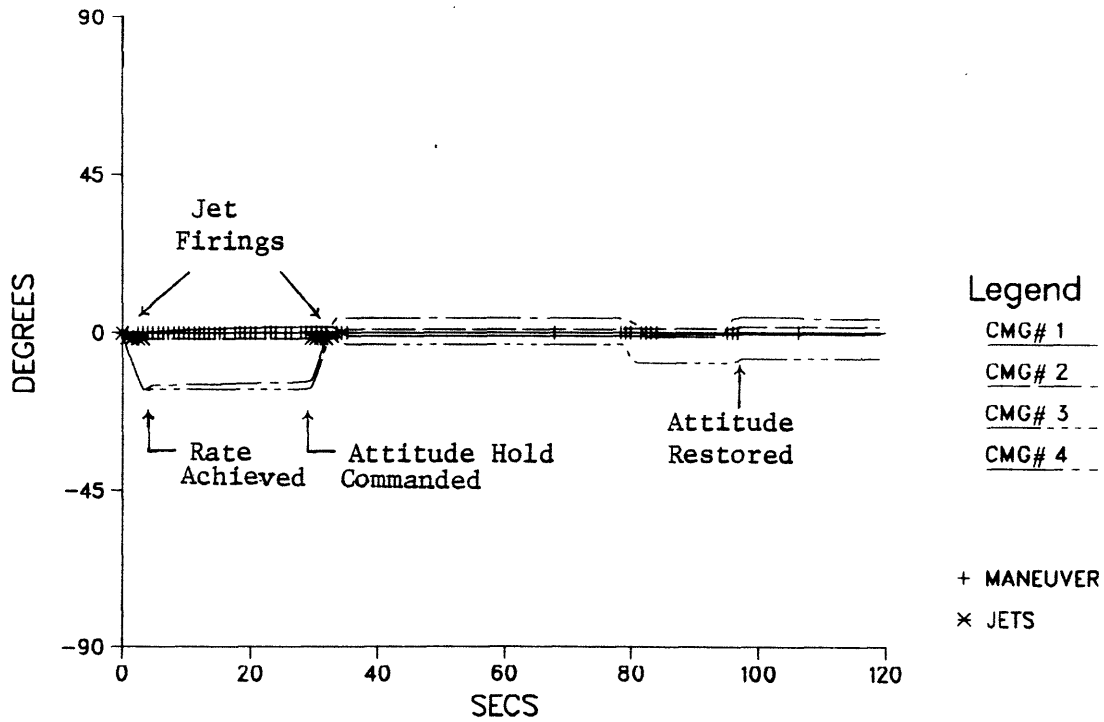
II

VEHICLE RATES
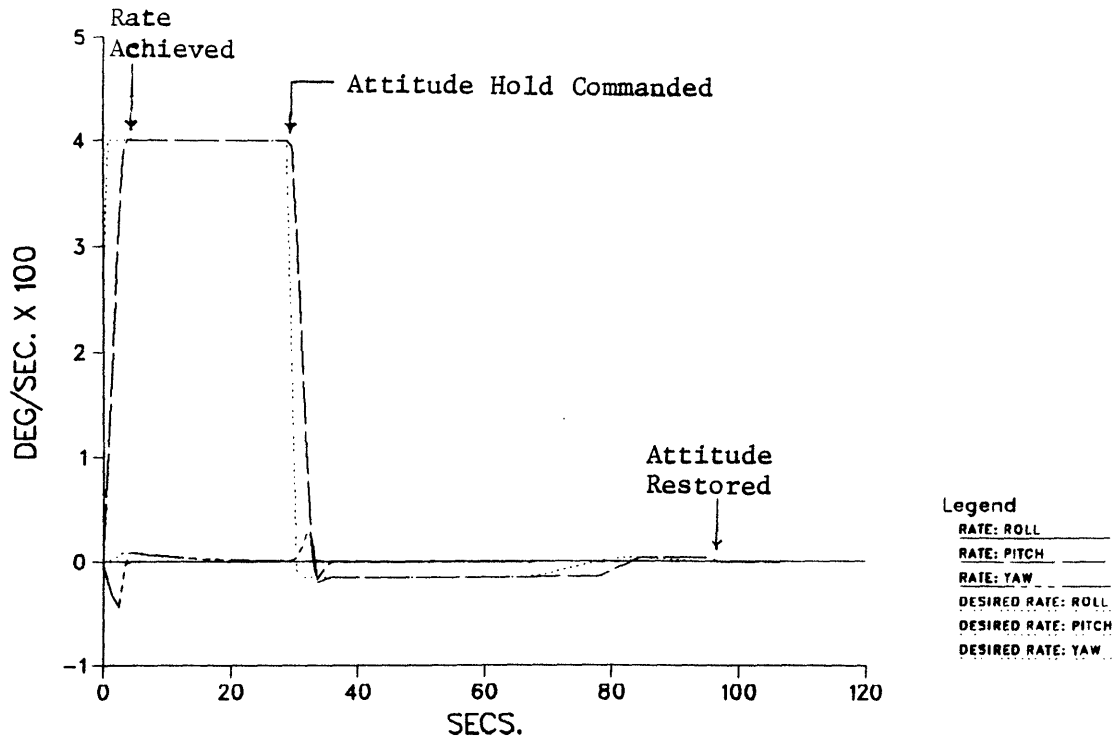
VEHICLE ATTITUDE

FIGURE 81: Command 0.04°/sec. in Pitch, Attitude Hold

192

INNER GIMBAL ANGLES

OUTER GIMBAL ANGLES
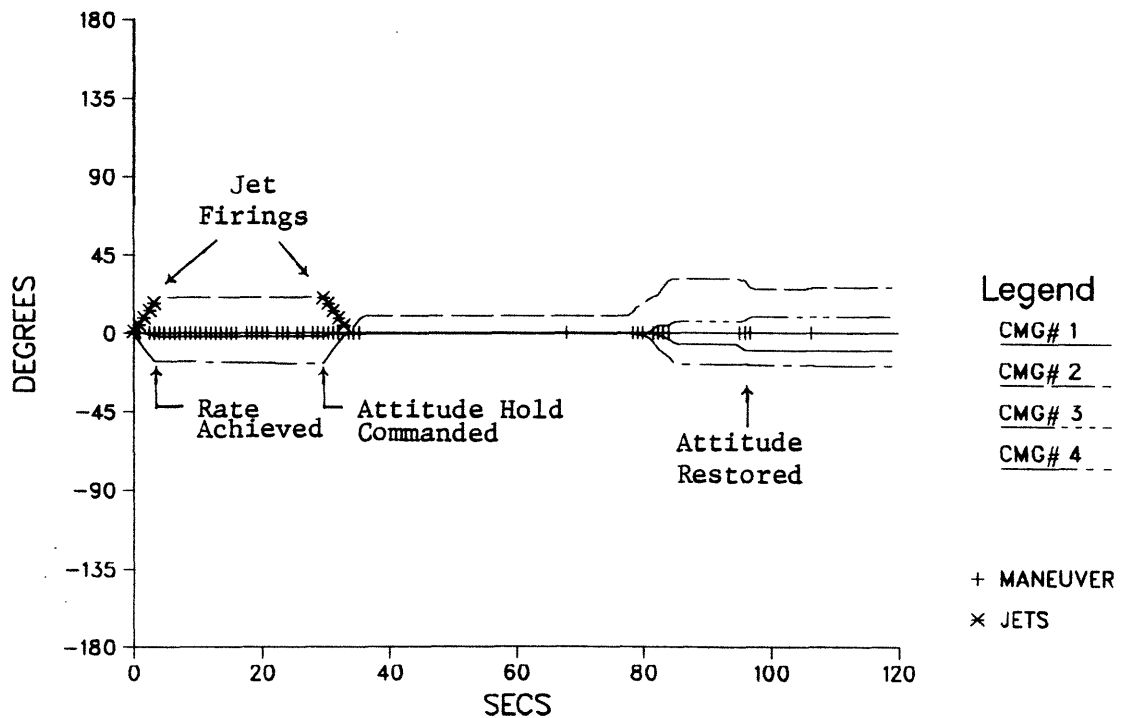

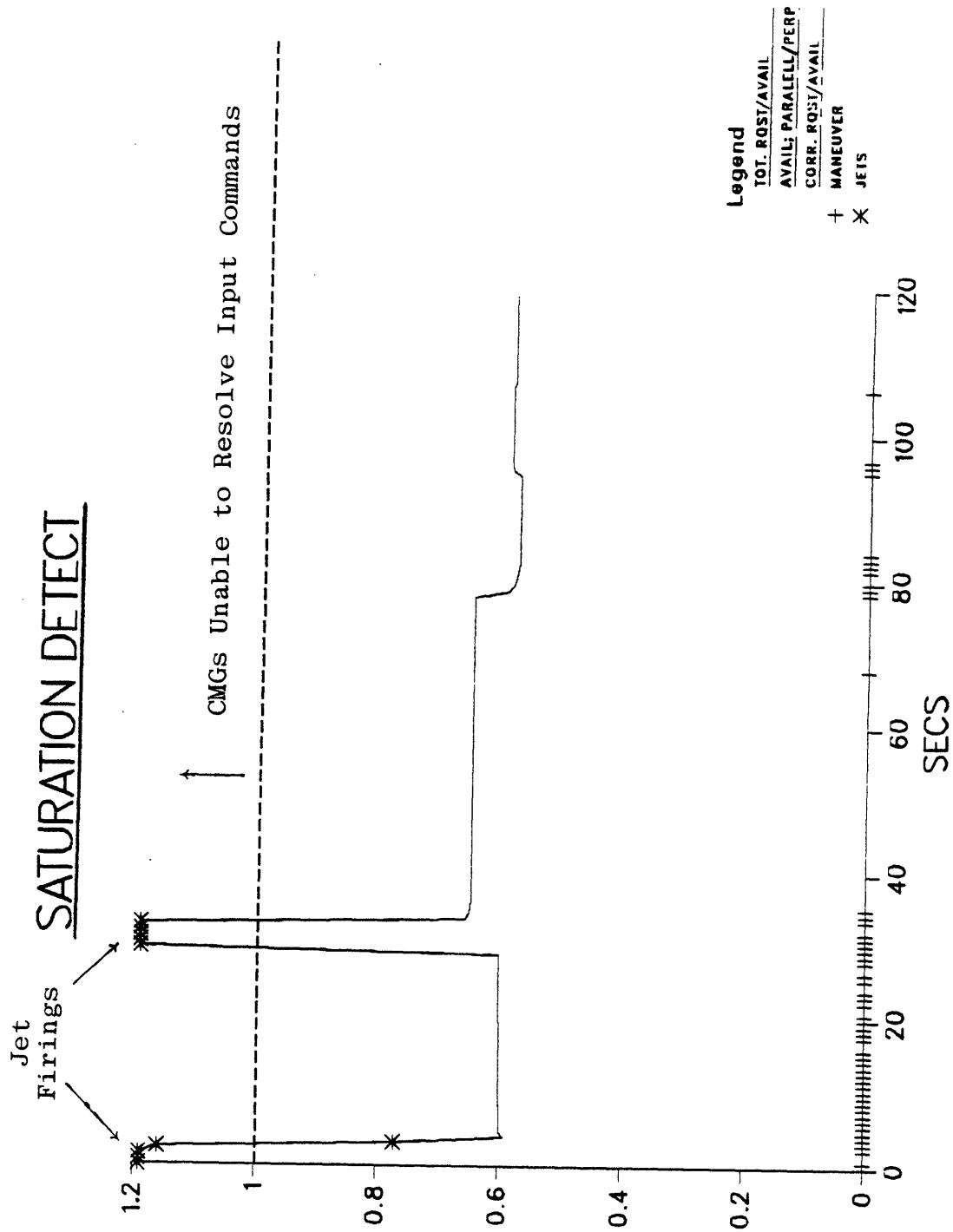
FIGURE 82: Command 0.04°/sec. in Pitch, Attitude Hold

193

FIGURE 83: Command 0.04°/sec. in Pitch, Attitude Hold

the curves at the beginning of the run and circa t = 30 sec. indicate jet firings required to establish and remove the 0.04 deg/sec. requested vehicle rate. CMGs were used exclusively to remove the much smaller convergence rate after t = 90 sec.; no jets were introduced. Fig. 83 shows the saturation index; indeed we see that the requests to establish and remove the 0.04 deg/sec. vehicle rate raised the saturation index well above unity, indicating that the CMGs were unable to provide the requested momentum transfer unaided. The upper bounds placed on CMG gimbal excursion prevent the CMGs from responding to a large request which can drive them into saturation; rather than moving the CMGs into saturation and then firing jets to complete the rate change (leaving the CMGs saturated after the maneuver), jets fulfill the bulk of the request, and CMGs are limited to a "trimming" role (see Sec. 4.3). The CMGs were able to supply the momentum needed to remove the smaller convergence rate without requiring assistance.

The next test run is identical to the first test of this section (0.01 deg/sec. commanded in pitch), except we now use an array of six single gimballed CMGs (as in Sec. 6.3), mounted in the "pyramid" fashion (ie. Fig. 54). Vehicle rates and attitude are plotted in Fig. 84. The commanded rate of 0.01 deg/sec. is achieved without difficulty; the convergence rate is established upon receipt of the attitude hold command, and attitude is completely restored by t = 220 sec (these CMGs operate at the same peak gimbal rate as the double gimballed devices assumed in the earlier tests). The gimbal motion which achieved these results is shown in Fig. 85; no RCS firings were required, and no CMGs are seen to be pushed against gimbal stops (the CMGs were initialized with 30 degs. of deflection to avoid starting the run in a singular state). The lower plot of Fig. 85 shows the CMG controllability parameters; the CMG gain (which was incorporated into the objective function) was kept at a consistantly high level throughout the test.

The following tests demonstrate the performance of null motion and jet-assisted desaturation under the phase space controller. These
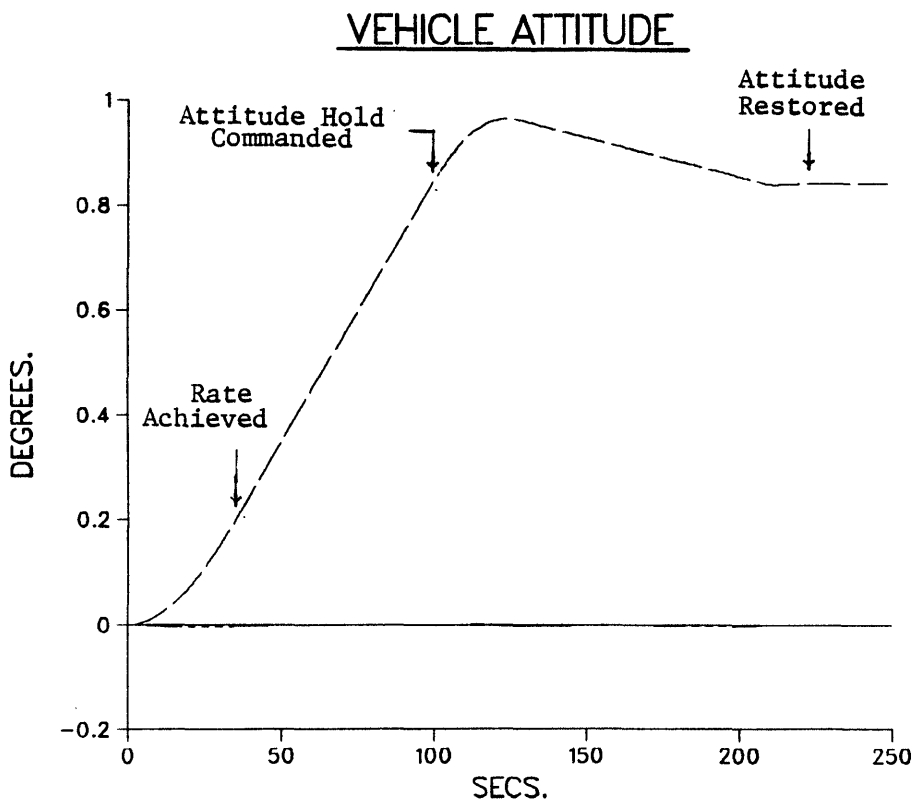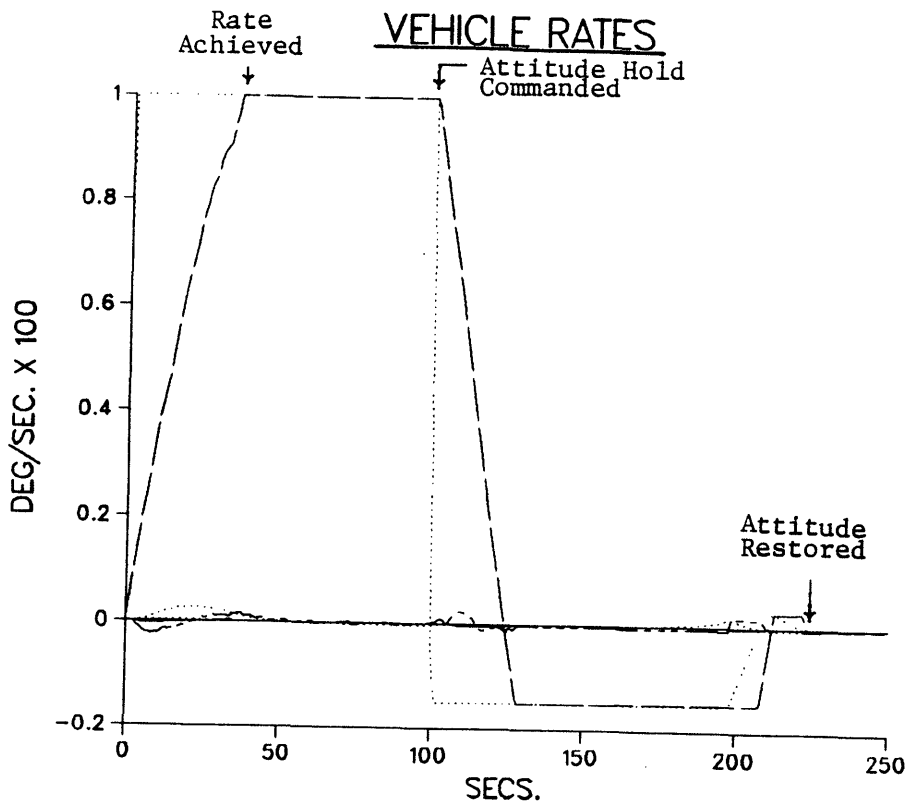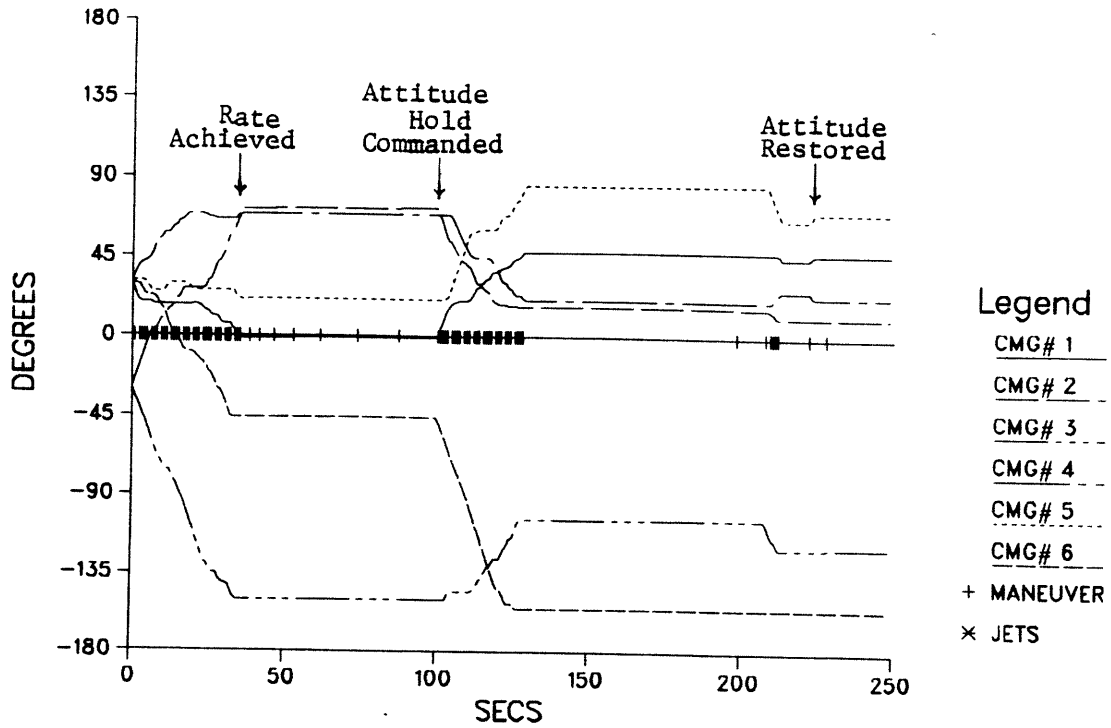
195

VEHICLE RATES

VEHICLE ATTITUDE

FIGURE 84: Command 0.01°/sec. in Pitch, Attitude Hold
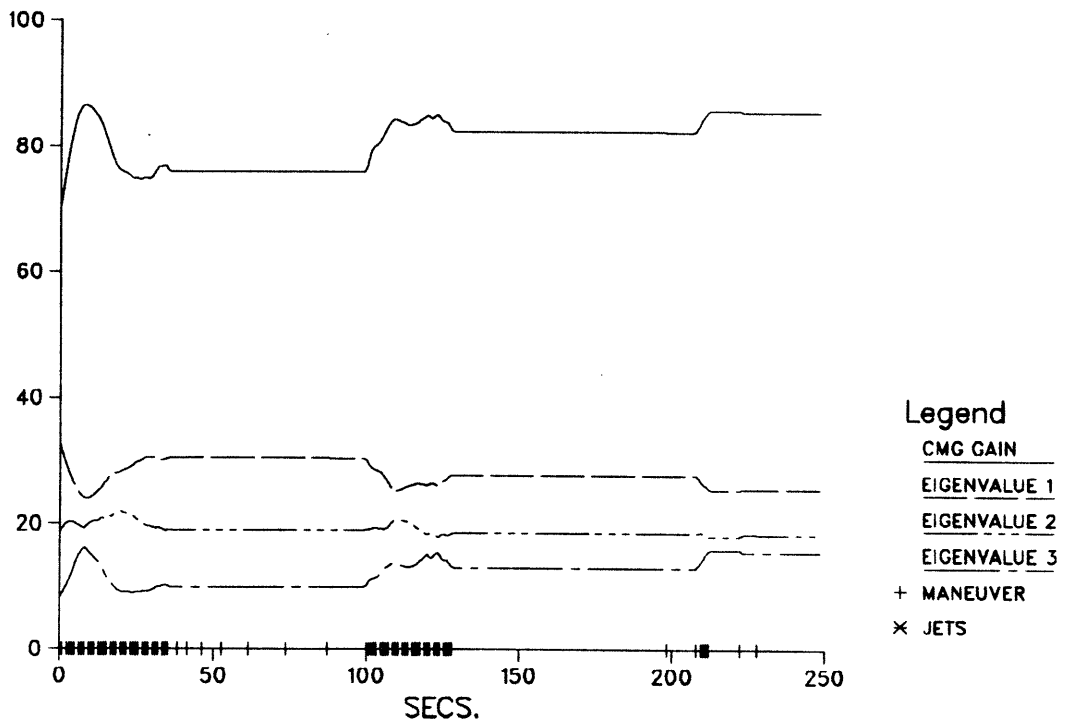(6 Single Gimballed CMGs)

196

GIMBAL ANGLES

CMG CONTROLLABILITY

FIGURE 85: Command 0.01°/sec. in Pitch, Attitude Hold (6 Single Gimballed CMGs)

197

capabilities were introduced in Secs. 4.4 & 4.5 and demonstrated via the rate feedback controller in Sec. 5.5. As mentioned in Sec. 7.1, these procedures were modified to execute in a real-time fashion when used with the phase space controller; the following tests illustrate the resulting performance.

The first test of this sequence uses again the standard quad double-gimballed CMG array (Fig. 16), and commands a series of requests which increase the vehicle rate along the pitch axis until momentum saturation is reached. The CMGs are initialized in a "sub-optimal" orientation (with finite inner gimbal angles and rotor lineups), and null motion (as discussed in Sec. 7.1) now attempts to move the CMGs into a better orientation before the receipt of each input request.

Gimbal angles are shown in Fig. 86. The upper plot shows inner gimbal angles; all are at a minimum by t = 20 sec. (as indicated). Excessive inner gimbal swings are otherwise seen to be avoided until a jet firing is required at t = 135 sec.

Rotor alignment plots are given in Fig. 87; the alignments are brought to a minimum by t = 20 sec. (as indicated). RCS assistance is required after the CMG rotors line up in saturation at the end of the run.

The saturation index is shown in Fig. 88; it exceeds unity at the points where jets were introduced, indicating a momentum saturation condition.

CMG controllability curves have only been shown previously for single gimballed systems; as a point of interest, the controllability parameters for this run have been plotted in the lower portion of Fig. 88. The low value of CMG gain at the start of the run (due to the initial suboptimal orientation) is restored to a maximum value by t = 20 sec. (as indicated). We see that the anti-lineup objective contribution has indeed been able to maintain a high value of CMG gain until saturation was reached and RCS assistance was required.

The upper plot in Fig. 89 shows the net CMG cost (re. Eq. 40); asterisks are plotted over the curve where null motion was attempted. Its effect is plainly to decrease the CMG cost (thus achieve a superior
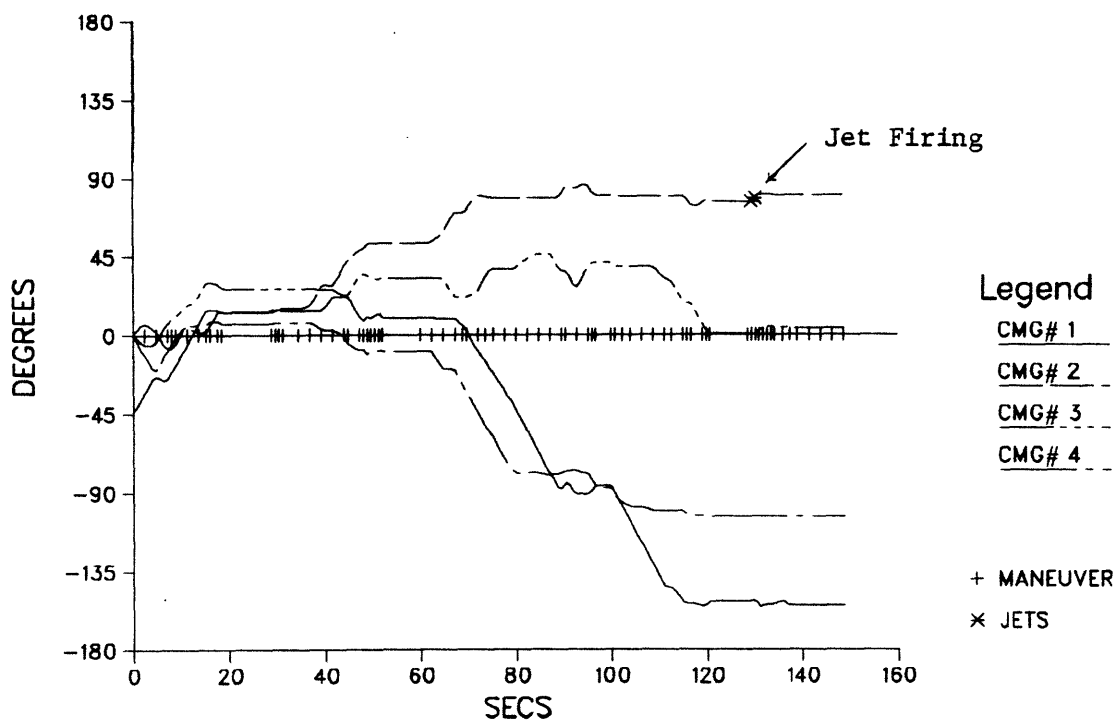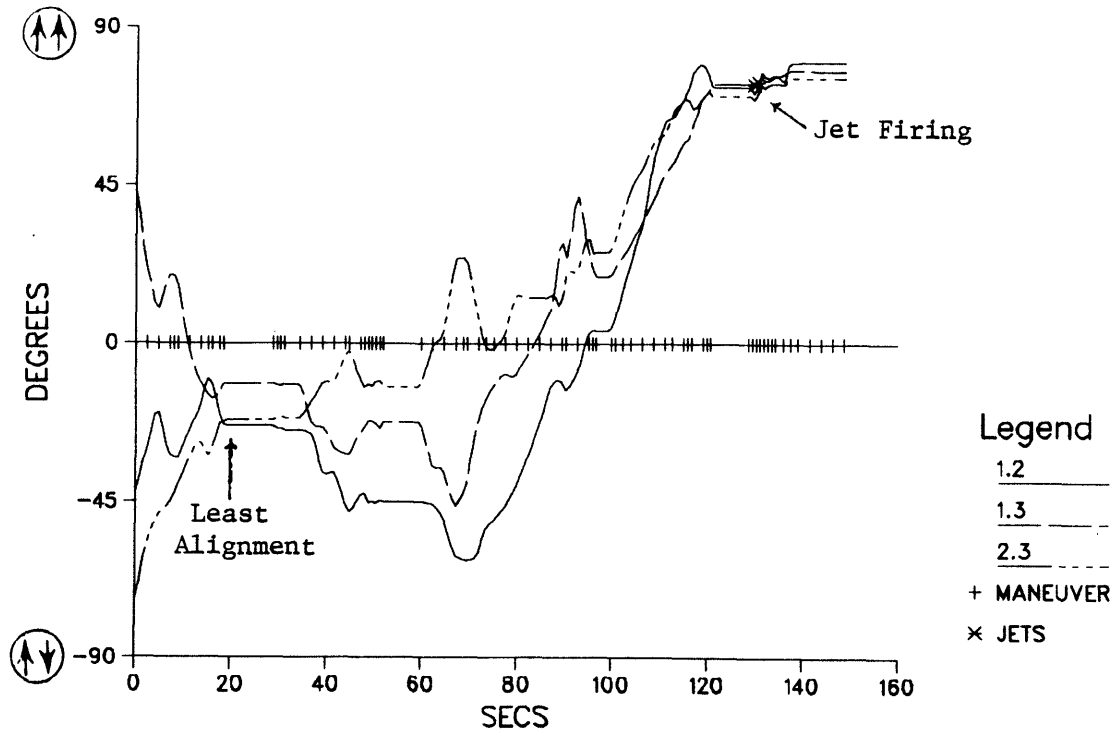
198

INNER GIMBAL ANGLES

Jet Firing

Legend
CMG# 1 ___
CMG# 2 _ _
CMG# 3 _._._
CMG# 4 _ _ _

+ MANEUVER
✕ JETS

Minimum
Inner Gimbal
Angles

OUTER GIMBAL ANGLES

Jet Firing

Legend
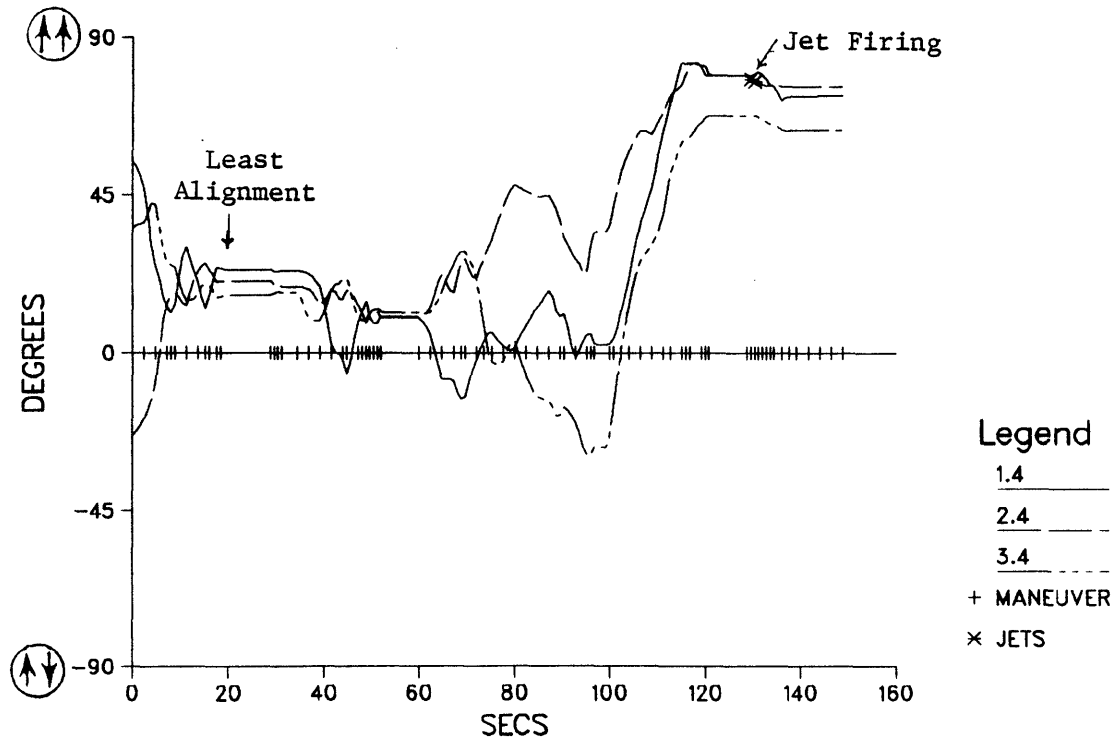CMG# 1 ___
CMG# 2 _ _
CMG# 3 _._._
CMG# 4 _ _ _
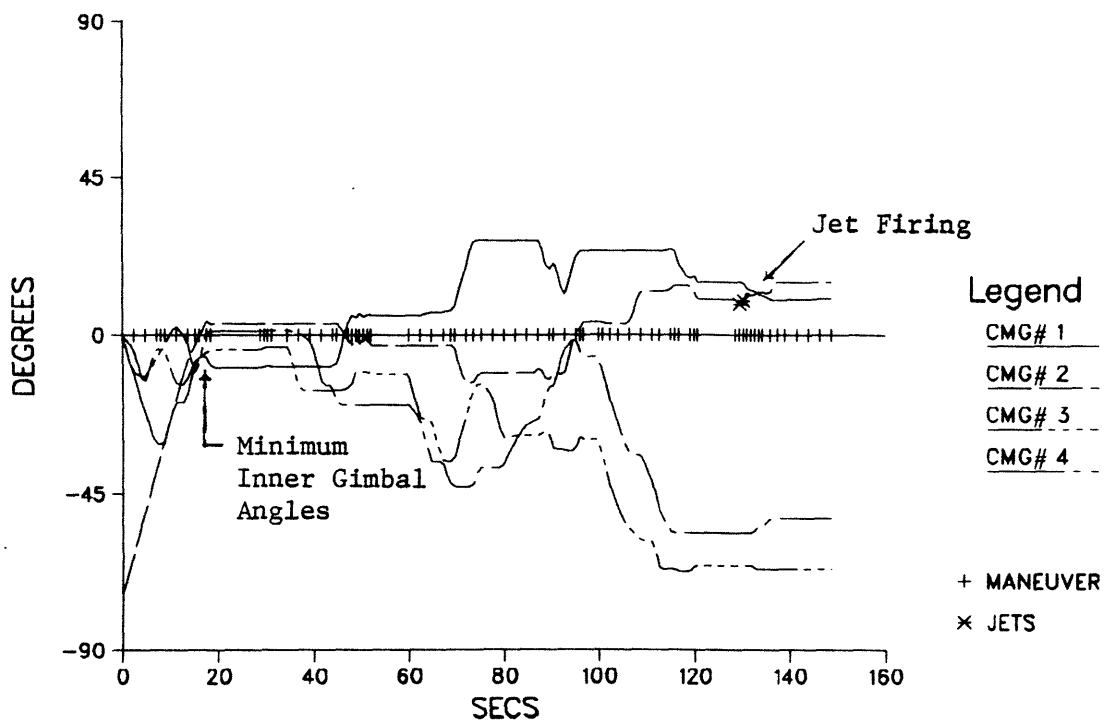
+ MANEUVER
✕ JETS

FIGURE 86: Saturate CMGs in Pitch,
Suboptimal Initialization & Null Motion

199

RELATIVE ANGLES BETWEEN CMG PAIRS PLT#1

Jet Firing

Least
Alignment

Legend
1.2
1.3
2.3
+ MANEUVER
✕ JETS

RELATIVE ANGLES BETWEEN CMG PAIRS PLT#2

Jet Firing

Least
Alignment

Legend
1.4
2.4
3.4
+ MANEUVER
✕ JETS

FIGURE 87: Saturate CMGs in Pitch,
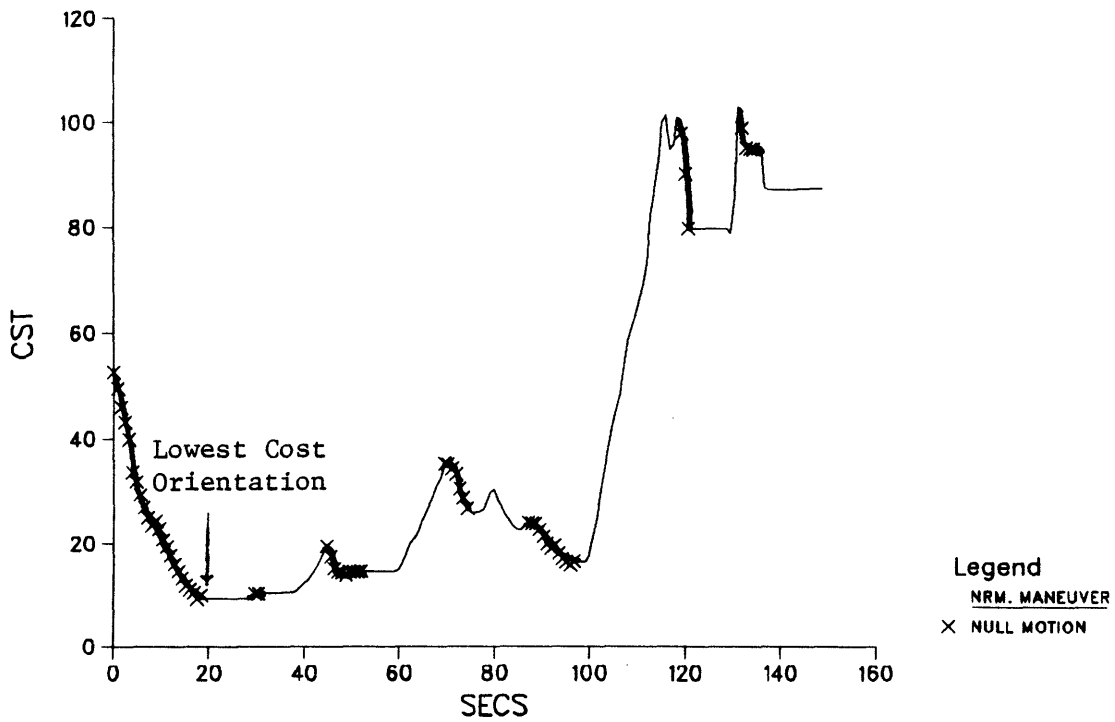Suboptimal Initialization & Null Motion

200

SATURATION DETECT
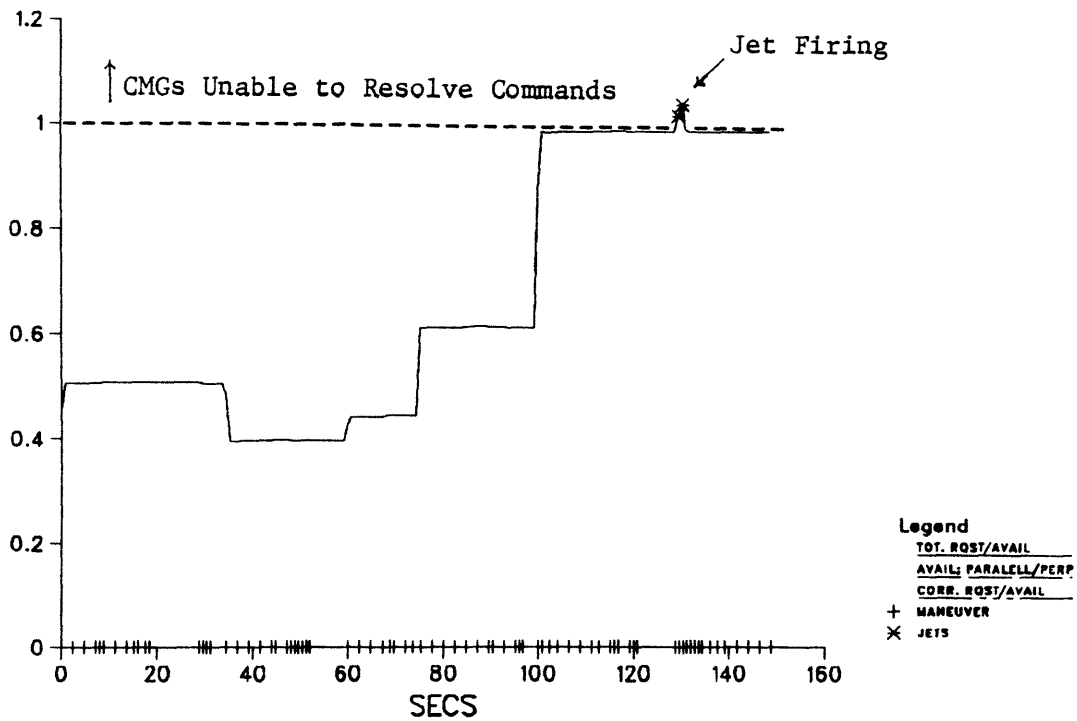
CMG CONTROLLABILITY
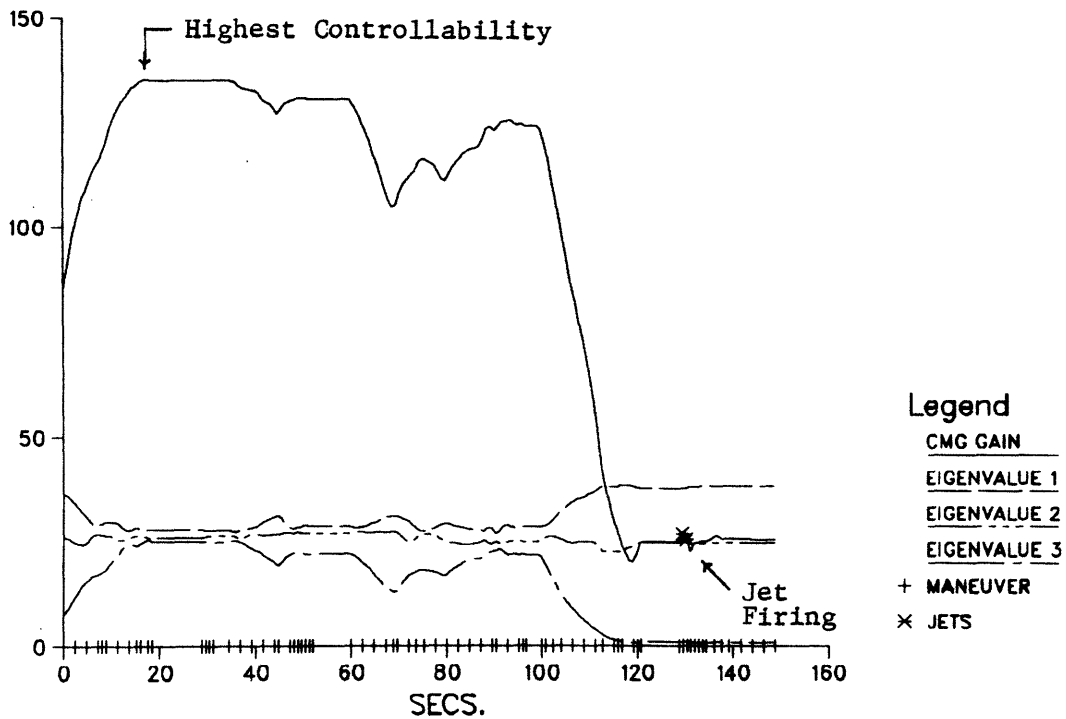
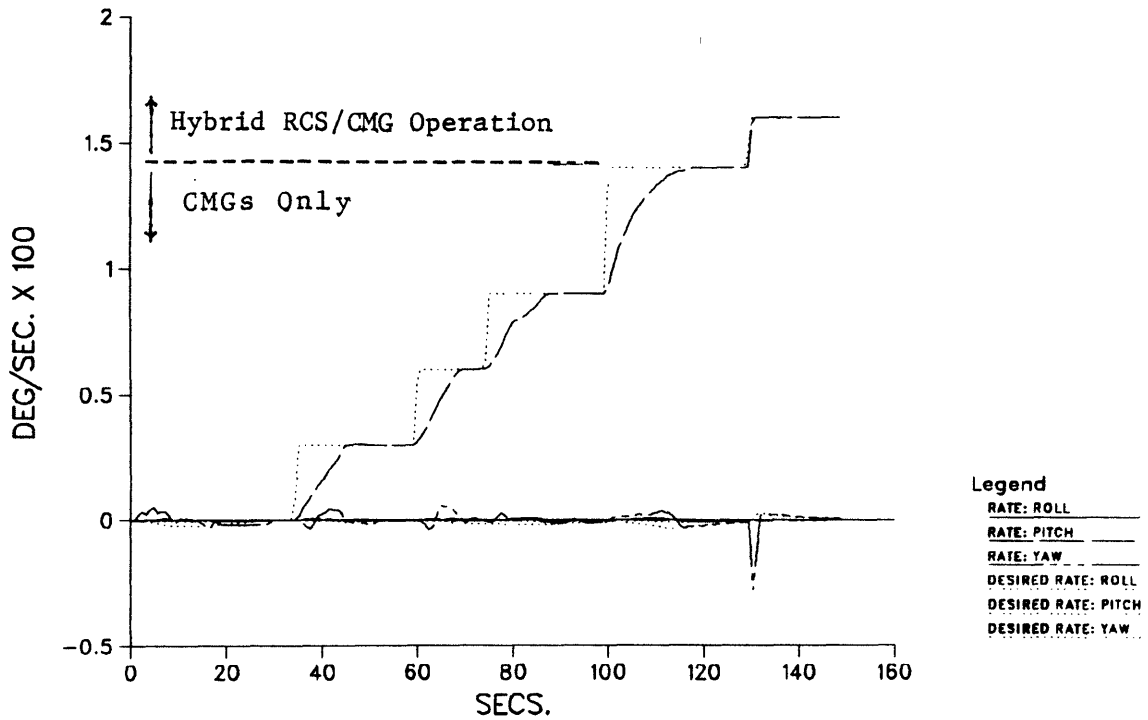FIGURE 88: Saturate CMGs in Pitch,
Suboptimal Initialization & Null Motion

201

TOTAL CMG COST

CST

120 —

100 —

80 —

60 —

40 — Lowest Cost
Orientation

20 —

0 —

| 0 | 20 | 40 | 60 | 80 | 100 | 120 | 140 | 160 |

SECS

Legend
NRM. MANEUVER
✕ **NULL MOTION**

VEHICLE RATES

DEG/SEC. X 100

2 —

1.5 — Hybrid RCS/CMG Operation

CMGs Only

1 —

0.5 —

0 —

-0.5 —

| 0 | 20 | 40 | 60 | 80 | 100 | 120 | 140 | 160 |

SECS.

Legend
RATE: ROLL
RATE: PITCH
RATE: YAW
DESIRED RATE: ROLL
DESIRED RATE: PITCH
DESIRED RATE: YAW

FIGURE 89: Saturate CMGs in Pitch,
Suboptimal Initialization & Null Motion

202

orientation). One sees that the relatively high cost of the initial sub-optimal orientation was reduced drastically by null motion which was performed at the start of the test; the minimum cost thus achieved is at t = 20 sec. (as indicated), which corresponds to the "best" physical orientation noted on the previous figures. Null motion is suspended when it can no longer achieve any further decrease in the system cost, or a significant rate change is requested by the operator or phase-space controller.

Vehicle rates are plotted in the lower portion of Fig. 89. The dotted curve represents the desired vehicle rate profile (which is commanded to increase in a series of discrete steps); the actual vehicle response is plotted in a heavier curve, and is seen to follow the input commands (note that the vehicle responds much more quickly at the last step, where jets were introduced). One sees that vehicle rates were indeed held constant while null motion was being performed. All rate-change commands were applied about the pitch axis; residual roll and yaw rates are seen to remain minimal (the vehicle attitude is commanded to hold at zero about these axes).

The final test presented in this section uses a similar sequence of rate change commands to again drive the CMG array into saturation about the pitch axis. Null motion is not enabled; instead, the jet-assisted desaturation procedure (Sec. 4.5) is requested after the CMGs near saturation at t = 90 sec.

Gimbal angles are plotted in Fig. 90. The upper plot shows inner gimbal angles, which are seen to gradually increase while responding to input commands (this run was initialized in the standard CMG orientation). The jet desaturation process is seen to dramatically decrease inner gimbal angles (which are included in the objective calculation); when the desaturation is completed after t = 100 sec., most inner gimbal excursions are again minimal

A set of rotor lineup plots is shown in Fig. 91, where the total rotor alignment approached at saturation is seen to be almost entirely
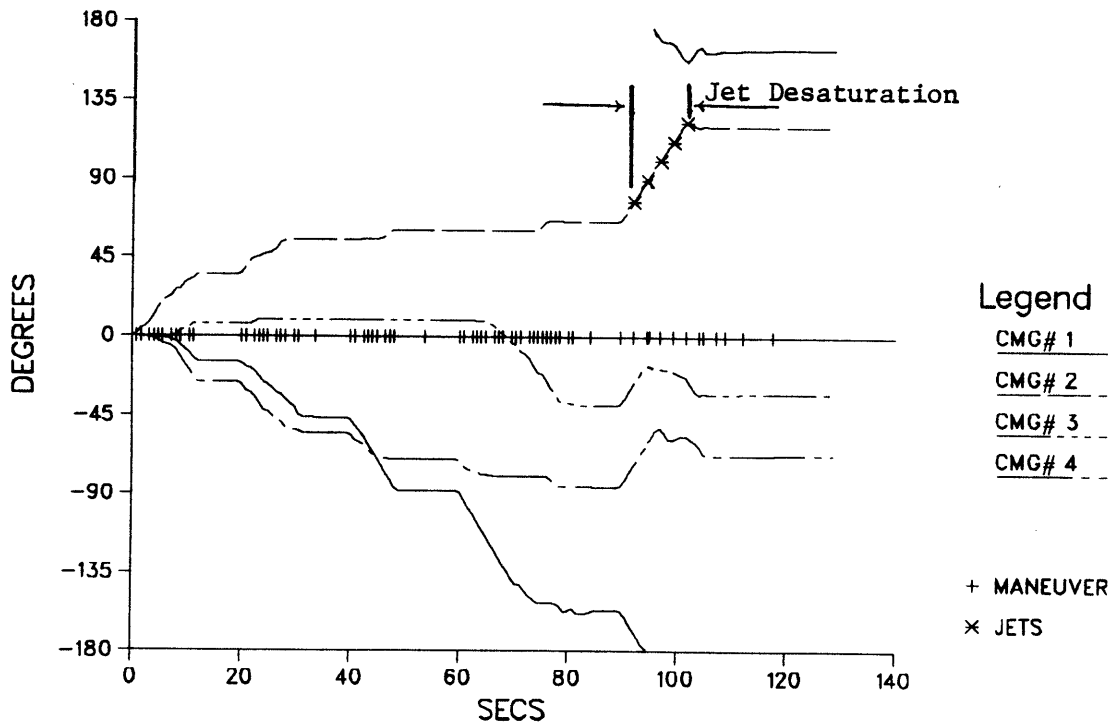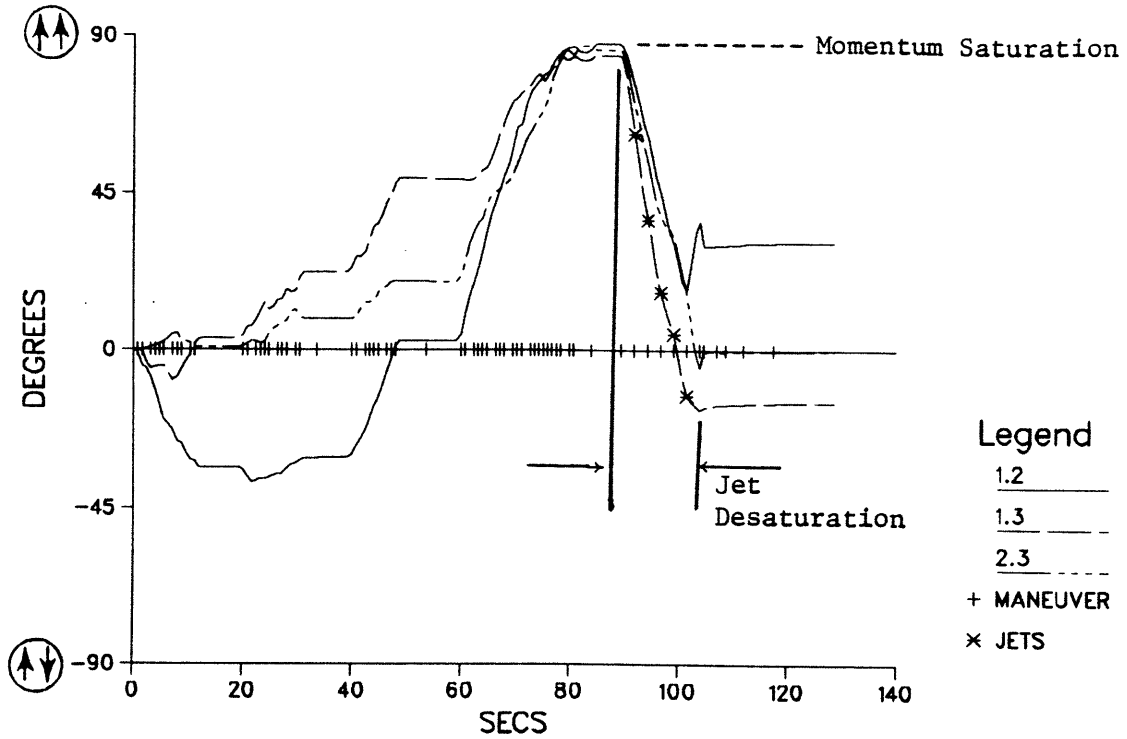
INNER GIMBAL ANGLES
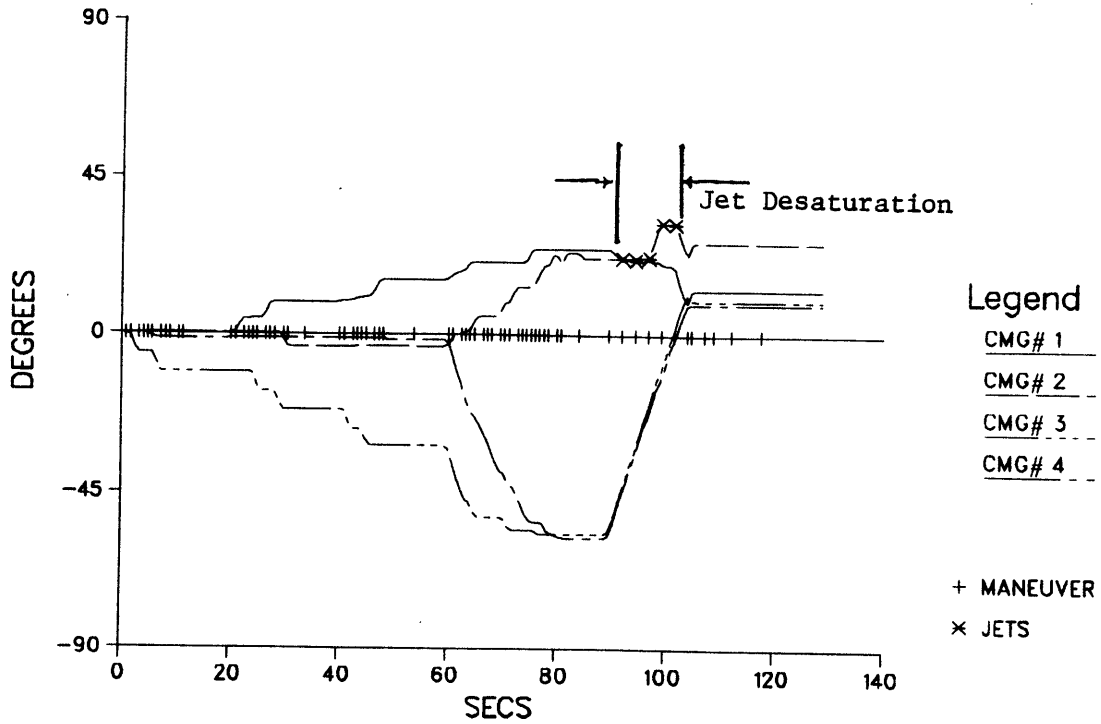
OUTER GIMBAL ANGLES

FIGURE 90: Saturate CMGs in Pitch,
Command Jet-Assisted Desaturation

RELATIVE ANGLES BETWEEN CMG PAIRS PLT#1

Legend
1.2
1.3
2.3
+ MANEUVER
× JETS

RELATIVE ANGLES BETWEEN CMG PAIRS PLT#2

Legend
1.4
2.4
3.4
+ MANEUVER
× JETS
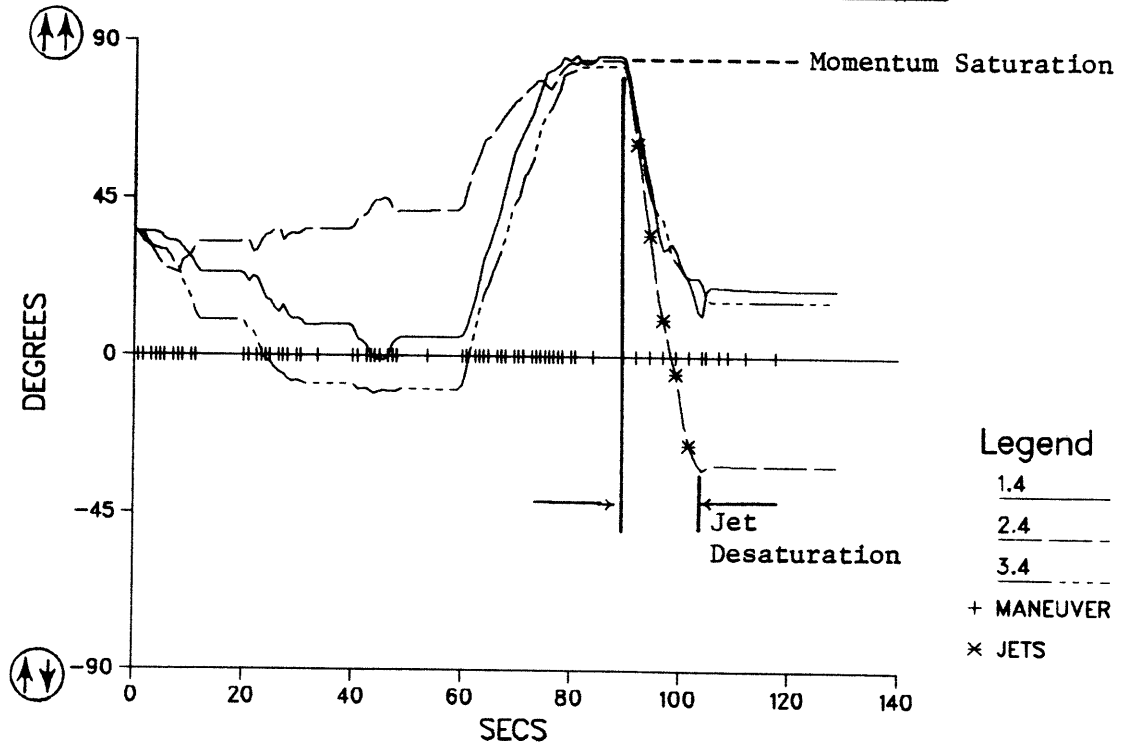
FIGURE 91: Saturate CMGs in Pitch,
Command Jet–Assisted Desaturation

205

SATURATION DETECT

CMGs Unable to Resolve Commands

Jet
Desaturation

Legend
TOT. RQST/AVAIL
AVAIL: PARALELL/PERP
CORR. RQST/AVAIL
+ MANEUVER
✕ JETS

SECS

CMG CONTROLLABILITY

Jet
Desaturation

Legend
CMG GAIN
EIGENVALUE 1
EIGENVALUE 2
EIGENVALUE 3
+ MANEUVER
✕ JETS

SECS.
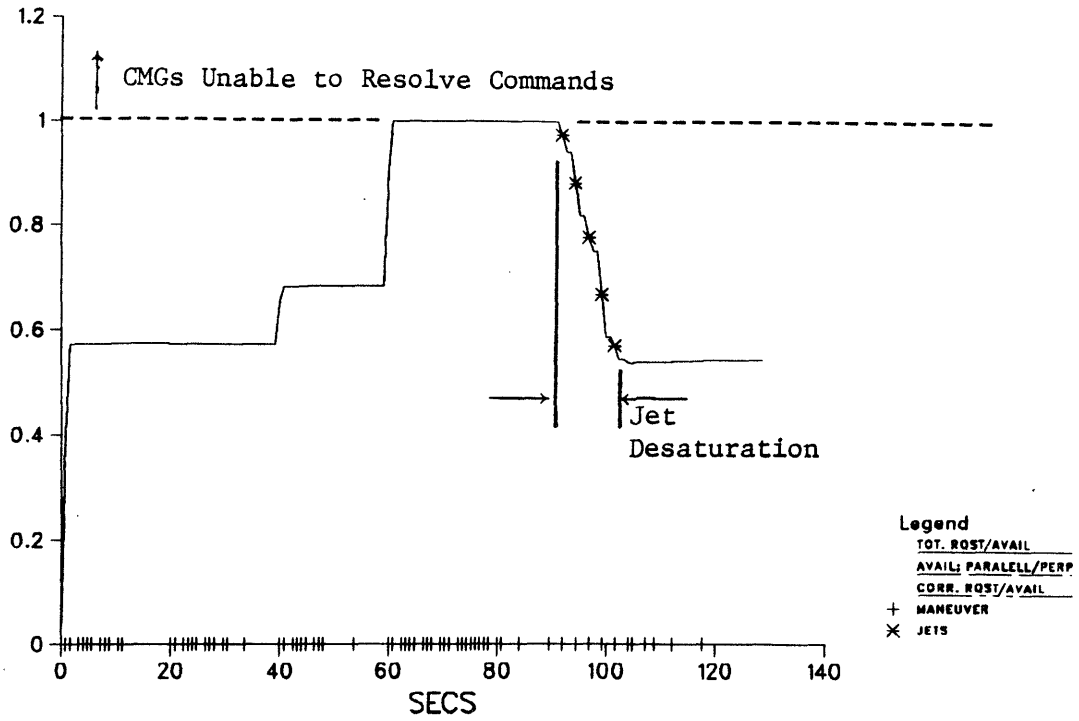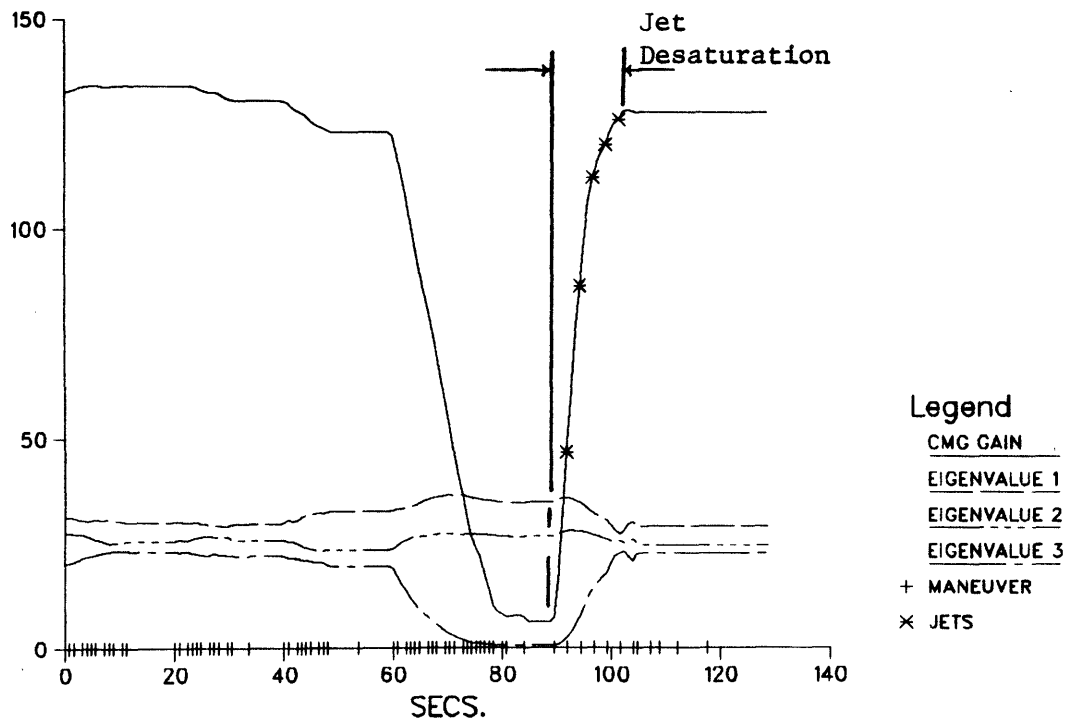
FIGURE 92: Saturate CMGs in Pitch,
Command Jet—Assisted Desaturation

TOTAL CMG COST

Legend
NRM. MANEUVER
X NULL MOTION

VEHICLE RATES

Legend
RATE: ROLL
RATE: PITCH
RATE: YAW
DESIRED RATE: ROLL
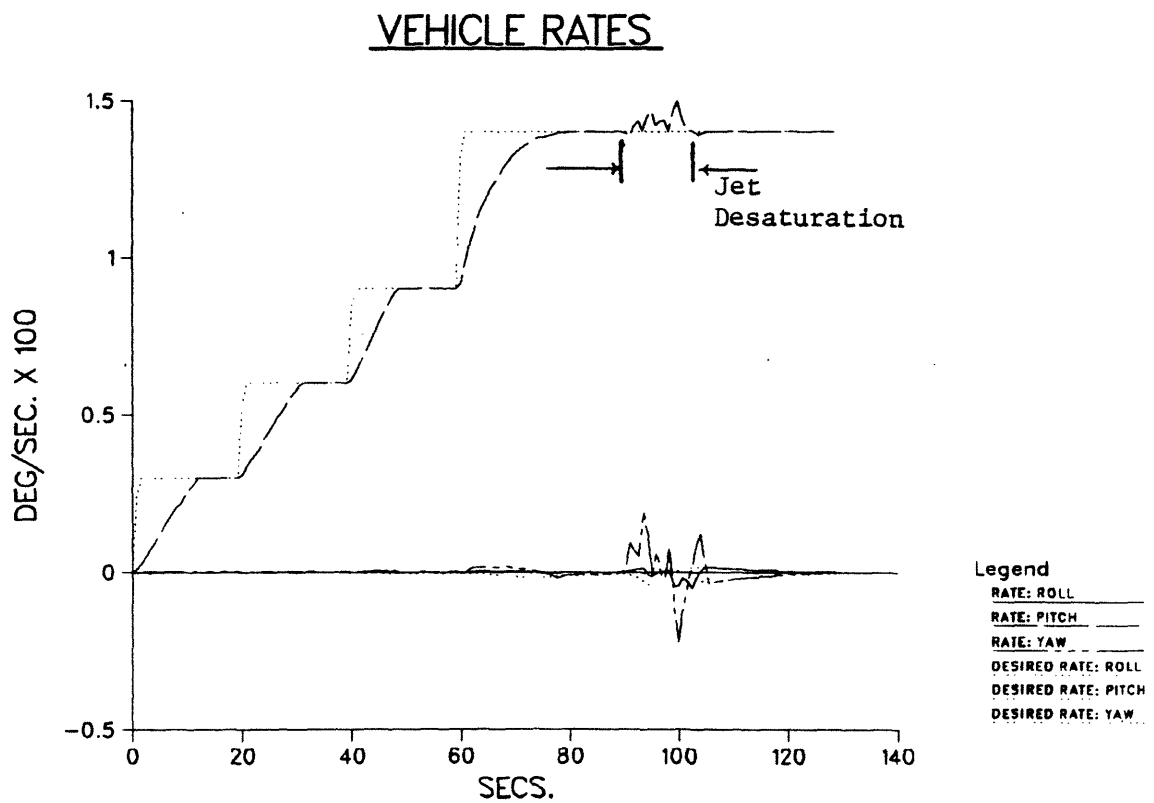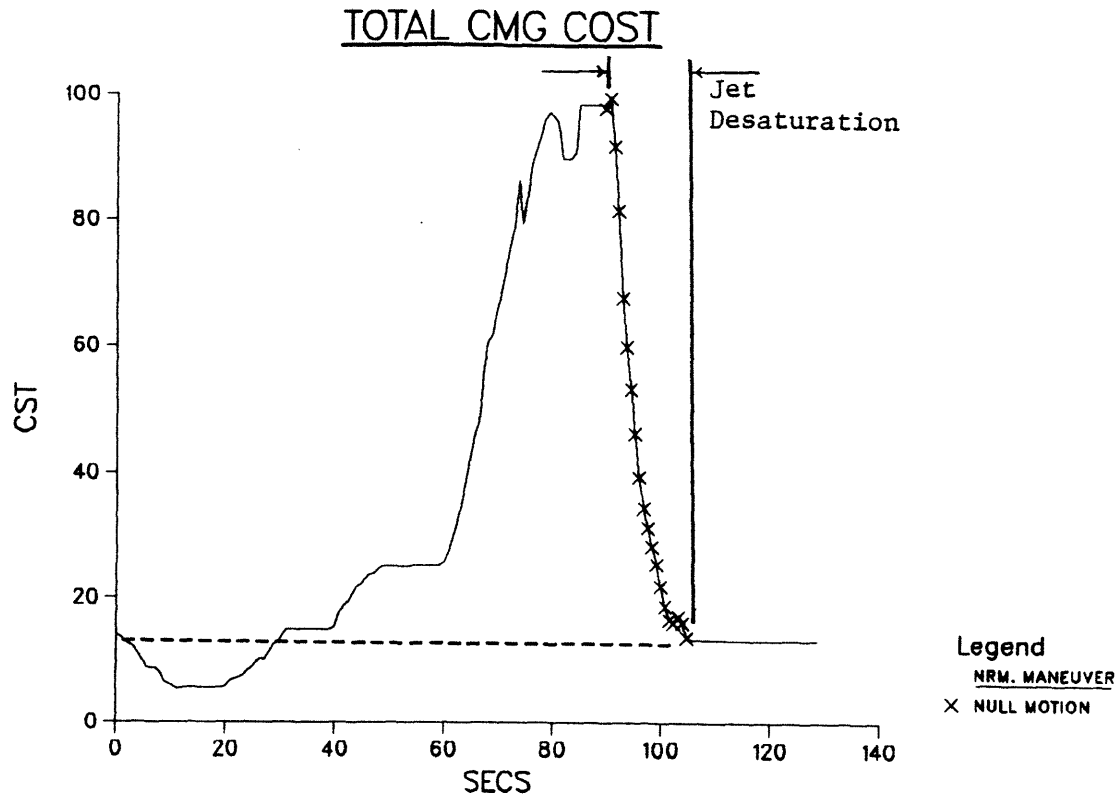DESIRED RATE: PITCH
DESIRED RATE: YAW

FIGURE 93: Saturate CMGs in Pitch,
Command Jet-Assisted Desaturation

207

relieved by the desaturation process. The upper plot of Fig. 92 shows the saturation index; the hybrid jet/CMG maneuvering taking place during desaturation is seen to remove the CMG array considerably from saturation. CMG controllability parameters are plotted in the lower portion of Fig. 92; the jet desaturation is seen to restore net CMG controllability (ie. CMG gain) to the level existing prior to saturation.

The operation of the jet desaturation process is evident from the plot of net CMG cost, which is shown in the upper portion of Fig. 93. The jet/CMG maneuvers during desaturation successfully reduced the net CMG cost in this case to the nearly ideal value existing at the start of the run.

The lower plot of Fig. 93 shows the vehicle rates; the input requests command the CMGs to increase the rate about the pitch axis to 0.014 deg/sec., thereby driving the CMGs into momentum saturation. This rate was held throughout the desaturation process; disturbances about all axes during jet/CMG activity were dynamically compensated and kept minimal (vehicle attitudes about roll and yaw were commanded to remain zero throughout the test).

CHAPTER 8

CONCLUSIONS

This document has described the structure and initial testing of
the hybrid CMG/RCS selection/steering procedure. The hybrid selection
functions as an extremely flexible CMG steering law; it has been seen to
successfully establish control using an array of double gimballed CMGs
mounted in different orientations, and effectively manage truncated CMG
systems resulting from various failure modes. The composite objective
function has been shown to encourage CMG selections that avoid gimbal
stops, excessive inner gimbal swings, and rotor alignments. Modifying
the objective function to maximize CMG gain has been shown to aid in
controlling single gimballed CMG systems. A null motion capability has
been established in order to bring the CMGs into a superior orientation
without transferring momentum to the vehicle.

The hybrid procedure has also performed optimal jet selections,
and has been shown to be effective in addressing mixed CMG/RCS
maneuvers. The adoption of upper bounds in the CMG selection process
directly accounts for gimbal stops, and places an effective limit upon
allowed CMG control authority; RCS jets have been seen to be
automatically introduced in response to requests which can not be
answered via CMGs alone. The incorporation of RCS jets into the null
motion process has produced a "desaturation" procedure which coordinates
CMG motion and jet firings to achieve a superior CMG orientation while
holding constant vehicle rates.

The hybrid selection has been successfully integrated into a
phase-space autopilot; coordinated attitude and rate control has been
demonstrated using both RCS jets and CMGs.

209

CHAPTER 9

ACKNOWLEDGEMENTS

CHAPTER 10

REFERENCES

1) J.F. Applegate, J.M. McMillion, R.E. Smith, "Design and Operation of
   the Skylab Attitude and Pointing Control System," Proc. of the AAS
   Meeting at UCLA, Aug. 20-22 1974, AAS74-126, Adv. Ast. Sci., p. 467.

2) "Space Station Reference Configuration Description," NASA/JSC,
   JSC-19989, August 1984.

3) M.S. Weinberg, "Momentum Exchange Effectors for Space Applications,"
   CSDL-P-1532, May 1982.

4) L. Flook, "Control Moment Gyro Applications to Spacecraft Attitude
   Control and Stabilization," ESRO-CR-23, 1970.

5) S.M. Seltzer, "CMG-Induced LST Dynamics," NASA/MSFC TM-X-64833,
   Feb. 21, 1974.

6) R. Mangoubi, C.S. Draper Lab., personal communication.

7) B.R. Colburn, L.R. White, "Computational Considerations for a
   Spacecraft Attitude Control System Employing Control Moment Gyros,"
   J. Spacecraft and Rockets, Vol. 14, No. 1, Jan. 1977, p. 45.

8) E.D. Scott, JJ. Rodden, "Performance of Gravity Gradient VCMG
   Systems," AIAA Paper 69-831, AIAA Guidance, Control, and Flight
   Mechanics Conference, Aug. 18-20, 1969.

9) J.E. DeLisle, E.G. Ogletree, B.M. Hildebrandt, "Applications of
   Gyrostabilizers to Satellite Attitude Control," Progress in
   Astronautics, Vol. 13, Academic Press, 1964, p. 149.

10) "Astronaut Maneuvering Equipment (Experiment 509) Attitude Control
    System Flight Test Analysis Plan," Project Technical Report (TRW)
    Task E-38D, NAS 9-8166, Nov. 9, 1970.

11) D.A. Liska, "A Two-Degree-of-Freedom Control Moment Gyro for
    High-Accuracy Attitude Control," J. Spacecraft and Rockets, Vol. 5
    No. 1, Jan. 1968, p. 74.

12) J.W. Crenshaw, "2-SPEED, a Single-Gimbal Control Moment Gyro Attitude Control System," AIAA Guidance and Control Conf., Key Biscane Fla., Aug. 20-22, 1973, AIAA Paper 73-895.

13) H.F. Kennel, "A Control Law For Double-Gimballed Control Moment Gyros Used For Space Vehicle Attitude Control," NASA TM X-64536, Aug. 7, 1970.

14) "Study to Define Logic Associated with CMGs to Maneuver and Stabilize an Orbiting Spacecraft, Final Report," Bendix Corp., NASA-CR-134307, Sept. 4, 1973.

15) B.J. O'Connor, L.A. Morine, "A Description of the CMG and its Application to Space Vehicle Control," J. Spacecraft and Rockets, Vol. 6, No. 3, p. 225, March, 1969.

16) H.F. Kennel, "Steering Law For Parallel Mounted Double-Gimballed Control Moment Gyros - Revision A," NASA TM-82390, Jan. 1981.

17) T. Yoshikawa, "A Steering Law For Three Double-Gimballed Control Moment Gyro Systems," NASA TM X-64926, March 1975.

18) B.K. Colburn, L.R. White, J.S. Boland, "Some Simple Steering Laws For Spacecraft Attitude Control Systems," 9'th Annual Asilomar Conf. on Circuits, Systems, and Computers, Pacific Grove, CA., Nov. 3-5, 1975.

19) D.E. Cornick, "Singularity Avoidance Control Laws for Single Gimbal Control Moment Gyros," 1979 AIAA Guidance and Control Conf., Boulder, CO. AIAA 79-1968, p. 20-23, Aug., 1979.

20) "Space Shuttle Orbiter Operational Level C Functional Subsystem Software Requirements; Guidance, Navigation, and Control, Part C, Flight Control Orbit DAP," Rockwell International, STS 83-0009A, June 30, 1985.

21) K. Kurokawa, N. Yajima, S. Usui, "A New Steering Law of a Single-Gimbal CMG System of Pyramid Configuration," Proc. of the X'th IFAC Symposium on Automatic Control in Space, Toulouse, France, 25-28 June, 1985, p. 249.

22) M.A. Floyd, "Single-Step Optimal Control of Large Space Structures," ScD Thesis, MIT/C.S. Draper Lab., CSDL-T-840, April, 1984.
C.R. Johnson Jr., "Adaptive Single-Stage Control of a Broad Class of Nonlinear Multivariable Plants," Automatic Control Theory and Applications, Vol. 6, May 1978, p. 41.
N.R. Tomlinson, "Equivalance of Single-Stage and N-Stage Optimum Digital Control Systems," Electronics Letters, Vol. 4, No. 6, March, 1968, p. 110.

23) E.V. Bergmann, P.S. Weissman, "Conceptual Description of the OEX Advanced Autopilot," C.S. Draper Lab. Report R-1479, July 1981.

24) The OEX Autopilot was flight-tested on Space Shuttle missions STS 51G (June, 1985) and STS 61B (Nov., 1985).

25) E.V. Bergmann, P.S. Weiler, "Accomodation of Pratical Constraints by Linear Programming Jet Select," C.S. Draper Lab. Report CSDL-P-1704, June 1983.

26) A. Chung, Linear Programming, Charles E. Merrill Books, Inc., Columbus Ohio, 1966.

27) S.P. Bradley, A.C. Hax, T.L. Magnanti, Applied Mathematical Programming, Addison-Wesley Publishing Co., Reading, MA, 1977.

28) B.S. Crawford, "Operation and Design of Multi-jet Spacecraft Control Systems," ScD Thesis, MIT/C.S. Draper Lab., T-509, Sept. 13, 1968.

29) J.A. Paradiso, "An Efficient OFS-Compatible Kinematic Model for Generalized CMGs," C.S. Draper Lab. Dept. 10C Space Station Memo 85-9, March 25, 1985.

30) P.D. Hattis, "Predicitve Momentum Management for the Space Station," to be published in AIAA Journ. of Guidance, Control, and Dynamics.

31) Skylab Program: Operational Data Book Vols. II and IV, NASA MSC-01549, 1971.

32) "Space Station Advanced Development Control Moment Gyro (CMG) Data," NASA MSFC memo ED15-85-43, July, 1985.

33) R. Vaughan, "Space Station Control Using RCS Jets," C.S. Draper Lab. Dept. 10C Space Station Memo 84-11, August, 1984.

34) G. Margulies, J.N. Aubrun, "Geometric Theory of Single-Gimbal Control Moment Gyro Systems," Journ. Ast. Sci., Vol. 26, No. 2, April/June 1978, p. 159.

35) W. O. Schiehlen, "Two Different Approaches for a Control Law of Single Gimbal Control Moment Gyro Systems," NASA TM X-64693, Aug. 2, 1972.

36) T. Yoshikawa, "Steering Law for Roof Type Configuration Control Moment Gyro System," Automatica, Vol. 13, 1977, p. 359.

37) P.C. Muller, H.I. Weber, "Analysis and Optimization of Certain Qualities of Cotrollability and Observability for Linear Dynamical Systems," 2'nd IFAC Symposium in Multivariable Control Systems, 1971.

38) E.V. Bergmann, S.R. Croopnick, J.J. Turkovich, C.C. Work, "An Advanced Spacecraft Autopilot Concept," Journ. of Guidance and Control, Vol. 2, No. 3, May/June 1979, p. 161.

39) J. Higgins, P. Kachmar, S. Shepperd et. al, On-Orbit Functional Simulator (OFS), C.S. Draper Laboratory.